THE PALAEOMAGNETIC SIGNIFICANCE OF THE BUSHVELD COMPLEX AND RELATED 2 GA MAGMATIC ROCKS IN ANCIENT CONTINENTAL ENTITIES

Shawn Andrew Letts

A thesis submitted to the Faculty of Science,
University of the Witwatersrand, Johannesburg,
in fulfilment of the requirements for the degree of Doctor of Philosophy.

Johannesburg, 2007

DECLARATION

I declare that this thesis is my own, unaided work. It is being submitted for the Degree of Doctor of Philosophy in the University of the Witwatersrand, Johannesburg. It has not been submitted before for any degree or examination in any other University.

Signed

____

Shawn Andrew Letts

___________ day of _________________2007

ABSTRACT

The Kaapvaal Craton was the scene of two major magmatic events around 2.0 Ga, namely the Bushveld Complex and the Phalaborwa Complex. Both complexes have been the subject of numerous palaeomagnetic studies during and prior to the 1980s. Despite these studies, systematic inconstancies for emplacement ages, in particular for the Bushveld Complex, have been found between the palaeomagnetic findings and well constrained ages. The greatest concern with the Bushveld Complex results are the large spread in pole positions previously determined for the different zones. This has been interpreted in prior studies to indicate that the Bushveld Complex was emplaced and cooled below the Curie temperature of magnetite over a time span of 50 my. The results obtained previously for the Phalaborwa Complex appear to be out of position (~16°) with respect to those for the Bushveld Complex. This is of concern because new geochronological data show that the Rustenburg Layered Suite of the Bushveld Complex was emplaced approximately 1 my after the Phalaborwa Complex. These inconsistencies have prompted the current re-investigation of the palaeomagnetic results for both the Bushveld Complex and the Phalaborwa Complex.

New palaeomagnetic data collected from all zones of the Rustenburg Layered Suite from the Eastern, Northern and Western Lobes of the Bushveld Complex, yielded palaeomagnetic poles that eliminated the spread in the apparent polar wander path. This observation is in agreement with precise age data, constraining the time period of emplacement of the complex to ~ 6 my. Resulting bedding-corrected high blocking components from all zones produced better groupings, thereby supporting a primary magnetic signature and indicating that the complex was intruded in a near-horizontal position. Dual polarities identified within each zone of the complex and positive reversal tests have identified one of the oldest known reversals of the Earth's magnetic field.

Palaeomagnetic data from the Phalaborwa Complex have produced a pole position that is in close proximity to those obtained from the coeval Bushveld Complex.

In an attempt to achieve a better understanding of tectonic events occurring in the Kaapvaal Craton a number of dual polarity dykes within the Bushvled and Phalaborwa Complexes were palaeomagnetic analysed. Results revealed that the acquired pole positions are in agreement with ~1.9 Ga dykes, indicating the possibility that the dykes occurring in both complexes are part of the same magmatic event.

Palaeopoles generated during this study were used in refining the Kaapvaal Craton apparent polar wander path around 2.0 Ga, and in conjunction with other well-defined 2.0 Ga poles for the Kaapvaal Craton, a robust cratonic pole was produced that was used in Precambrian palaeographic reconstructions with emphasis on the postulated Vaalbara continent and the Columbia supercontinent. Palaeomagnetic reconstruction derived in this study has cast doubt on the existence of the Vaalbara continent at 2.0 Ga. Although, some support is given to the existence of the Columbia supercontinent at the same period.

In memory of my younger sister

Kerry Ann Letts

1979-1990

ACKNOWLEDGEMENTS

The author wishes to thank the following organisations and individuals for their assistance and support.

- Mr. Gordon Chunnett and Anglo Platinum, for financial support and the use of aeromagnetic data.
- Professor Trond Torsvik and the Norwegian Geological Survey, for financial support and the use of the laboratories.
- Ms. Sue Webb, Professor Trond Torsvik and Professor Lew Ashwal, for their valuable input into the project and constructive criticism.
- Dr. Edgar Stettler and the Council for Geoscience for the use of regional aeromagnetic data.
- Mr. Arthur Letts and Mrs. Margaret Letts, for their love and support.
- National Research Foundation, for financial support.
- Dr. Andy Rompel and Anglo American, for kindly allowing me to work on my thesis during working hours.

LIST OF FIGURES

LIST OF TABLES

TABLE OF CONTENT

CONTENT **PAGE**

CHAPTER 1: INTRODUCTION

This palaeomagnetic study provides a comprehensive re-investigation of the Bushveld Complex as well as the similar-aged Phalaborwa Complex in an attempt to clarify certain inconstancies that had arisen during earlier studies. An additional palaeomagnetic investigation was conducted on dykes that intruded both the Bushveld and Phalaborwa Complexes. In light of the newly-determined pole positions, a refined apparent polar wander path for the Kaapvaal Craton was constructed. The palaeopoles generated during this study were also used in conjunction with other well-defined poles for the Kaapvaal Craton in producing a robust cratonic pole around 2.0 Ga. This was used in Precambrian palaeographic reconstruction with emphasis on the postulated Vaalbara and Columbia supercontinents.

1.1 Basic Objectives

The Kaapvaal Craton has recently been linked to the postulated Columbia supercontinent formed between 2.1 and 1.8 Ga (Zhao et al., 2002). Palaeomagnetism offers a quantitative reconstruction tool that provides the latitude and rotation for a continent, which can be used to examine the time of growth and dispersal of supercontinents. In order to test the Columbia hypothesis with respect to the Kaapvaal Craton, reliable palaeopole positions from South Africa are required.

The Bushveld and Phalaborwa Complexes represent a keystone in the understanding of the ca. 2.0 Ga tectonic assemblage of Columbia. Both complexes have been the subject of numerous palaeomagnetic studies that stem from the 1960-1970s. Despite these studies, systematic inconstancies have been found that cannot be clarified by a simple re-evaluation of the existing data. Based on the observed discrepancies and the fact that palaeomagnetic equipment and data analysis have improved over the past 30 years, a new study on both the Bushveld and Phalaborwa Complexes was conducted to produce reliable palaeopoles that will be used in the Precambrian palaeographic reconstructions.

1.2 Previous Palaeomagnetic Studies on the Bushveld Complex

The 2,058 ± 5 Ma Bushveld Complex (Buick et al., 2001), has been the subject of a number of palaeomagnetic investigations (Table 1.1). The first study was completed by Gough and Van Niekerk (1959) on five sites located in the Main Zone of the Eastern and Western Lobes of Bushveld Complex. The study produced a single palaeomagnetic pole for the Bushveld Complex. Later studies by Hattingh (1986a; 1986b; 1986c; 1989) analysed samples from 88 sites, located in the Eastern and Western Lobes of the complex. He obtained four palaeomagnetic pole positions: one for the Critical Zone (seven sites from the Western Lobe and one site from the Eastern Lobe), two for the Main Zone (one for the Eastern and the other for the Western Lobe) and one for the Upper Zone (six sites in the Eastern Lobe and two sites in the Western Lobe). The latest study by Hattingh and Pauls (1994) sampled 17 sites in the Main and Upper Zones of the Northern Lobe of the Bushveld Complex, yielding one palaeomagnetic pole position for the Main Zone and a virtual palaeomagnetic pole position for the Upper Zone (calculated from a single observation). A simplified geological map of the Bushveld Complex with the locations of the palaeomagnetic sites used by Hattingh (1986a; 1986b; 1986c; 1989), and Hattingh and Pauls (1994) is shown in Figure 1.1.

Table 1.1 Palaeomagnetic pole positions and associated errors dp and dm from the palaeomagnetic studies conducted on the Bushveld Complex.

Study and Zone	Pole Longitude	Pole Latitude	dp	dm
Gough and Van Niekerk (1959): Main Zone (Eastern and Western Lobes)	23°N	36°E	12°	12°
Hattingh (1986c): Critical Zone (Eastern and Western Lobes)	39.5°N	47°E	7.8°	13.1°
Hattingh (1986b): Main Zone Eastern Lobe	17.3°N	35.7°E	5.4°	6.4°
Hattingh (1986a): Main Zone Western Lobe	9.2°N	27.3°E	4.2°	4.9°
Hattingh (1989): Upper Zone (Eastern and Western Lobes)	16.1°N	31.5°E	14.7°	18°
Hattingh and Pauls (1994): Main Zone of Northern Lobe	1.6°N	22.3°E	14.7°	15.9°
Hattingh and Pauls (1994): Upper Zone of Northern Lobe	7.9°N	359.3°E	44.4°	54.6°

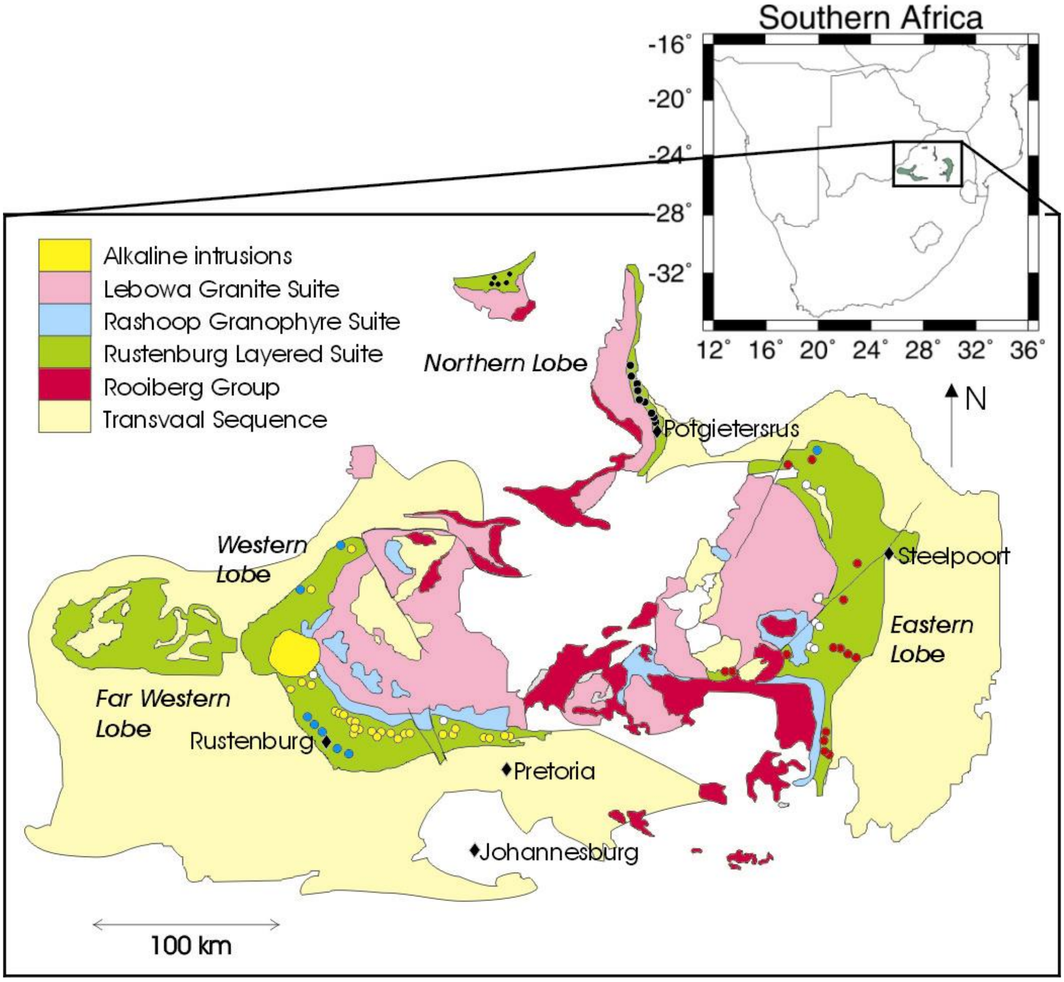

Figure 1.1 Geological map of the Bushveld Complex after Cairncross and Dixon (1995), indicating the locations of the palaeomagnetic samples taken by Hattingh (1983), and Hattingh and Pauls (1994). Black circles indicate Northern Lobe samples, yellow circles indicate samples from the Main Zone of Western Lobe, red circles indicate samples from the Main Zone of Eastern Lobe, white circles indicate samples from the Upper Zone and blue circles indicate samples from the Critical Zone.

The following inconstancies have been found in the palaeomagnetic findings:

- The Rustenberg Layered Suite (RLS) was assumed to have been formed in a horizontal attitude (Hattingh, 1986a; 1986b; 1986c; 1989; 1995; 1998; Hattingh and Pauls, 1994) and that the present attitude was only acquired after the igneous layering had cooled below the Curie temperature for magnetite (580°C). From the five studies conducted, only one (that of the Eastern Main Zone) has passed the fold test of McElhinny (1964a) (i.e. the data have a significant increase in pole clustering at the 95% confidence level). The other four studies are not significant at the 95% confidence level after restoring the igneous layering to the horizontal. Therefore the assumption that the complex was horizontal at the Curie temperature of magnetite has not been statistically shown by most previous studies.

- Based on apparent polar wander paths for the Bushveld Complex (Figure 1.2), it was assumed that the different zones of the RLS were emplaced and cooled to below the Curie temperature of magnetite over a time span of ~50 my (age was determined on pole spread of different zones and average plate motion). This is in contradiction to newly determined precise geochronological data obtained from the felsic rocks associated with the Bushveld Complex, which bracket the Rustenburg Layered Suite between 2,060 ± 2 Ma (Walraven, 1997) and 2,054.4 ± 1.8 Ma (Walraven and Hattingh, 1993a). These ages were obtained from pre-RLS granophyric sills, which intrude the 2,061 ± 2 Ma felsic volcanics of the Rooiberg Group (Walraven 1997), and from the Lebowa Granite Suite, which succeed the RLS (Walraven and Hattingh, 1993). The RLS itself has been dated at 2,058.9 ± 0.8 Ma using U-Pb isotopes from newly-grown titanite found in calc-silicate xenoliths (Buick et al., 2001). The 50 my emplacement span is also in contradiction to a thermal model proposed by Cawthorn and Walraven (1998), which indicates that the Bushveld Complex crystallized in about 200,000 years. Although the model does not give a cooling time for the Curie temperature of magnetite, 50 my seems an excesive length of time.

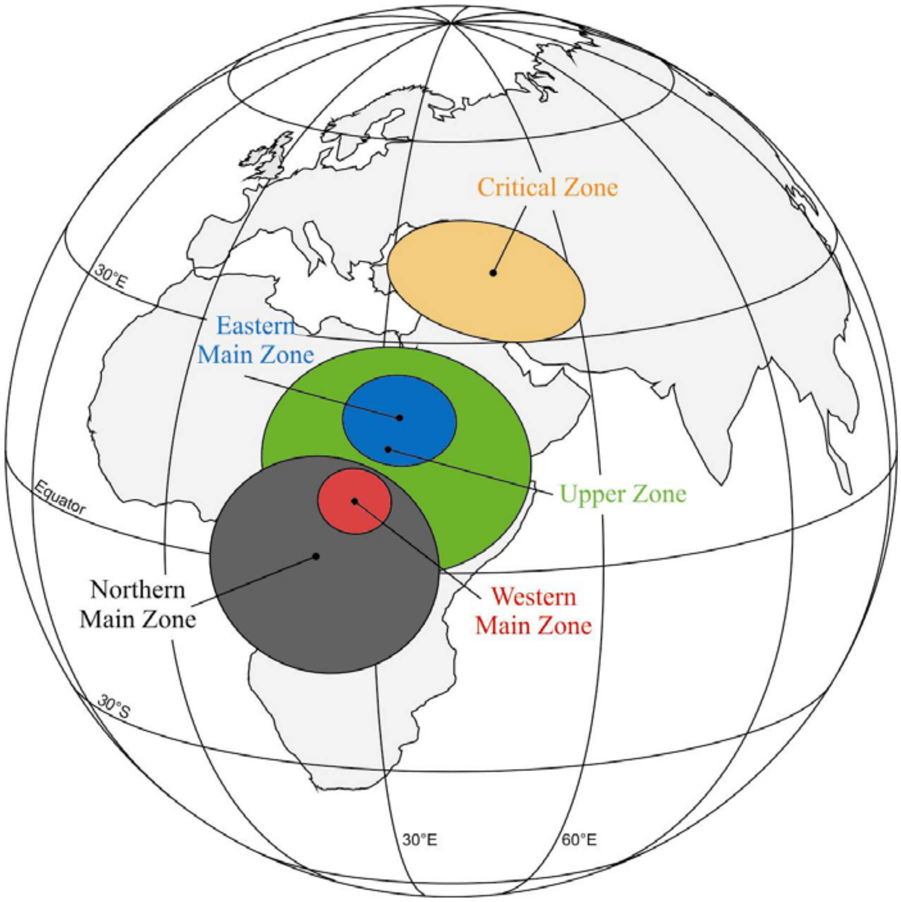

Figure 1.2 Equal-area projection of paleopole positions determined by Hattingh (1986a; 1986b; 1986c; 1989), and Hattingh and Pauls (1994). The resulting spread in pole position was interpreted to represent a 50 my emplacement period for the different zones of the complex.

1.3 Previous Palaeomagnetic Studies on the Phalaborwa Complex:

The Phalaborwa Complex 2,060.6 ± 0.5 Ma (Reischmann, 1995), located in the Limpopo Province (formerly known as the Northern Province), is a carbonatite-pyroxenite-fenite central complex. A palaeomagnetic study of the Phalaborwa Complex (Morgan and Briden, 1981) obtained two poles from two groups of rocks (Table 1.2). Group 1 samples were derived from pyroxenites, which form one of the oldest phases of the central complex, while Group 2 samples were derived from synetites and dolerite dykes (Figure 1.3). The palaeomagnetic poles from Group 1 are associated with the main intrusive event while Group 2 is believed to be associated with the NE-trending Mashonaland dolerite dyke swarm (~1,800 - 1,900 Ma), based on similarity in pole positions (Morgan and Briden, 1981). This relatively old study requires a re-investigation to pinpoint the relative magmatic events occurring at the complex.

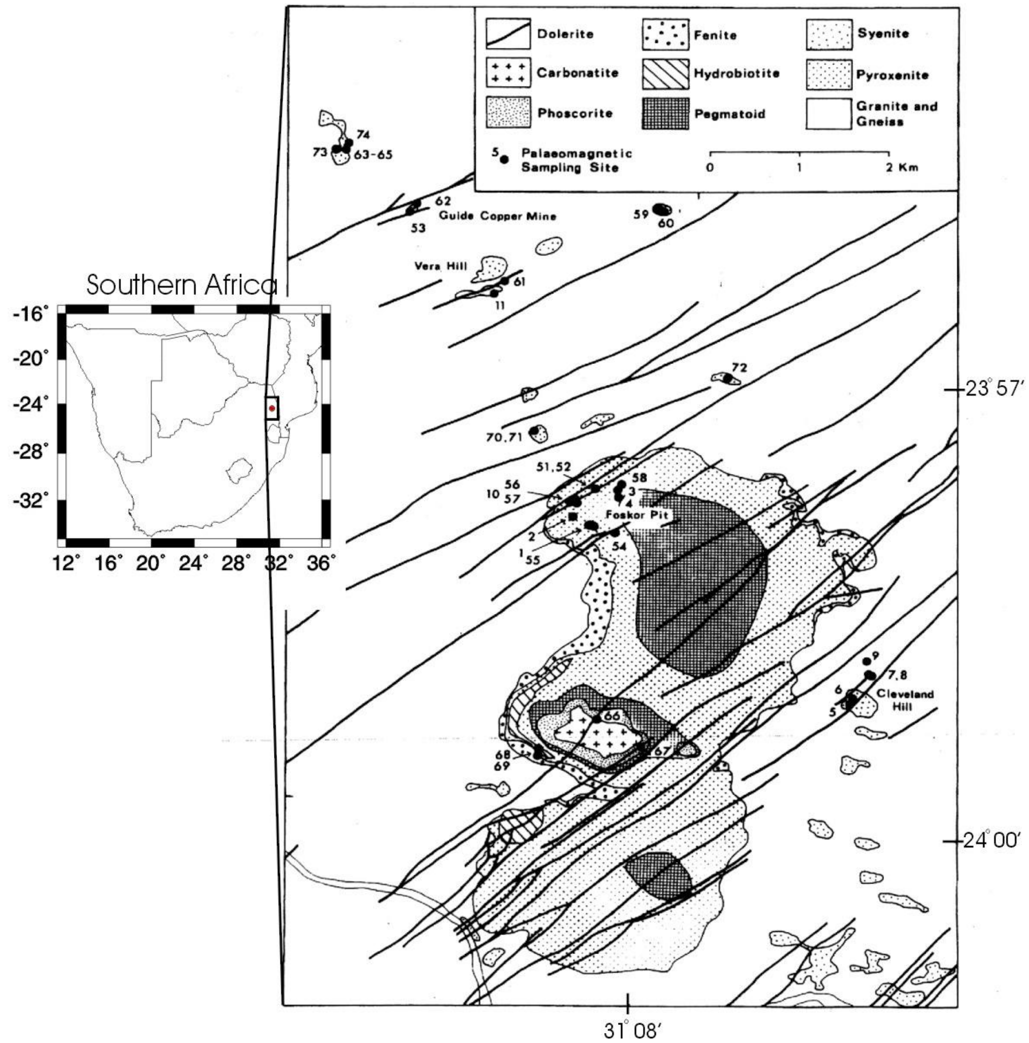

Figure 1.3 A simplified geological map of the Phalaborwa Complex showing palaeomagnetic sampling sites of Morgan and Briden (1981).

Table 1.2 Palaeomagnetic pole positions and associated errors dp and dm from the palaeomagnetic studies conducted on the Phalaborwa Complex (Morgan and Briden, 1981).

Group and Lithology	Pole Latitude	Pole Longitude	dp	dm
Group 1: Pyroxenites from central intrusive complex	35.9°N	44.8°E	6.9°	10.5°
Group 2: Synetites and dolerite dykes	4.2°N	357.8°E	9°	11°

1.4 Thesis Structure

This thesis includes a brief description of basic palaeomagnetic principles, including the main types of rock magnetism, mineralogy responsible for magnetic properties in rocks, procedures carried out in the acquisition of palaeomagnetic core samples, procedures in laboratory work and theory of palaeomagnetic analysis.

Palaeomagnetic results are presented on the basis of their geographical distributions within the three main study areas. Results from the Bushveld Complex are presented first. Due to the extensive amount of samples analysed on the Bushveld Complex (915) it is dealt with in three chapters: the first chapter deals with the geology and sampling of the complex, the second provides all the data and findings, classified according to the different zones of the complex, while the final chapter deals with the interpretation of all the results from the complex.

Results from the Phalaborwa Complex are presented next with the geology, sampling, data and interpretation of results grouped into one chapter. Similarly, the palaeomagnetic investigations of dykes occurring in both the Bushveld and Phalaborwa Complexes are presented in a single chapter.

The final part of the thesis is dedicated to palaeographic analysis of the Kaapvaal Craton and the Precambrian palaeographic reconstruction of the postulated Vaalbara and Columbia supercontinents.

CHAPTER 2: METHODS IN PALAEOMAGNETICS

2.1 Palaeomagnetic Theory

2.1.1 Earth's magnetic field

The Earth's magnetic field at any given point can be represented by three components (Figure 2.1):

- The total intensity of the magnetic field ***H***,
- Declination ***D***: the angle from magnetic north to geographic north, ranging in value from 0º to 360º in a clockwise direction,
- Inclination ***I***: the vertical angle (dip) from the horizontal component H_h to the total intensity of *H*, ranging from +90º at the North Pole, 0º at the equator through to –90º at the South Pole.

The declination and inclination are used to describe the direction of the magnetic field.

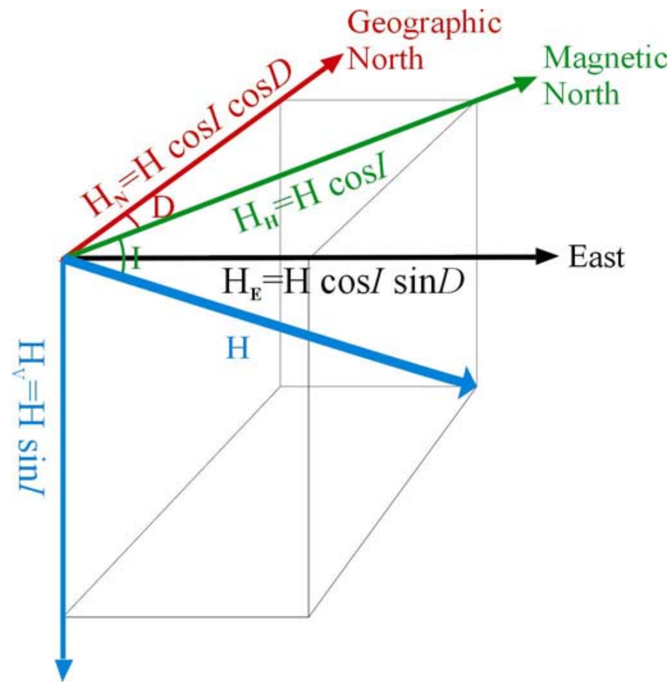

Figure 2.1 The main elements of the geomagnetic field. The magnetic field is defined by the total intensity *H*, declination *D*, and inclination *I*. The total intensity *H*, can be broken down into a vertical H_v and horizontal component H_H. The geographic and magnetic North directions are both represented in the diagram (Merrill et al., 1983).

The total intensity of the magnetic field H can be broken down into a number of components. The vertical component H_v, is defined as positive downwards and is given by

$$H_V = H \sin I \tag{2.1}$$

The horizontal component, H_H, is defined as

$$H_H = H \cos I \tag{2.2}$$

and can be further broken down into a geographical north H_N and east H_E component,

$$H_N = H \cos I \cos D \tag{2.3}$$

$$H_E = H \cos I \sin D \tag{2.4}$$

The Earth's magnetic field varies around the world in direction and magnitude. Such variations can be viewed in isomagnetic charts (Figure 2.2 & 2.3), in which the figures only indicate inclination and intensity of the magnetic field. However, there are other charts that can be constructed that show the other components of the magnetic field. The charts shown below are based on the International Geomagnetic Reference Field (IGRF) 2005 model. This model represents the main magnetic field of the Earth without external sources, utilizing spherical harmonics of the scalar potential of the field in geocentric coordinates. Due to the Earth's magnetic field changing with time, the model has to be revised every few years. To keep up-to-date, the IGRF model coefficients are updated every five years from geomagnetic measurements obtained from magnetic observatories, ships, aircraft and satellites.

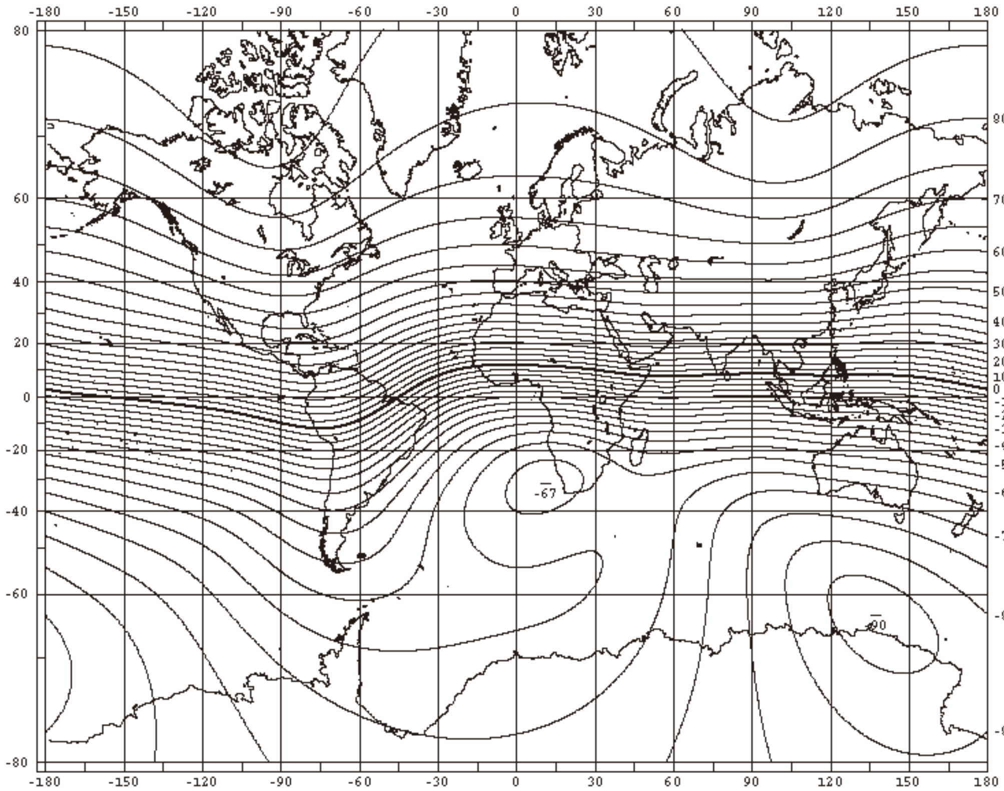

Figure 2.2 An isoclinic chart illustrating the observed inclination of the Earth's magnetic field; contour intervals are in 5º increments. The map is based on the IGRF 2005 model (Toshihiko, 2007).

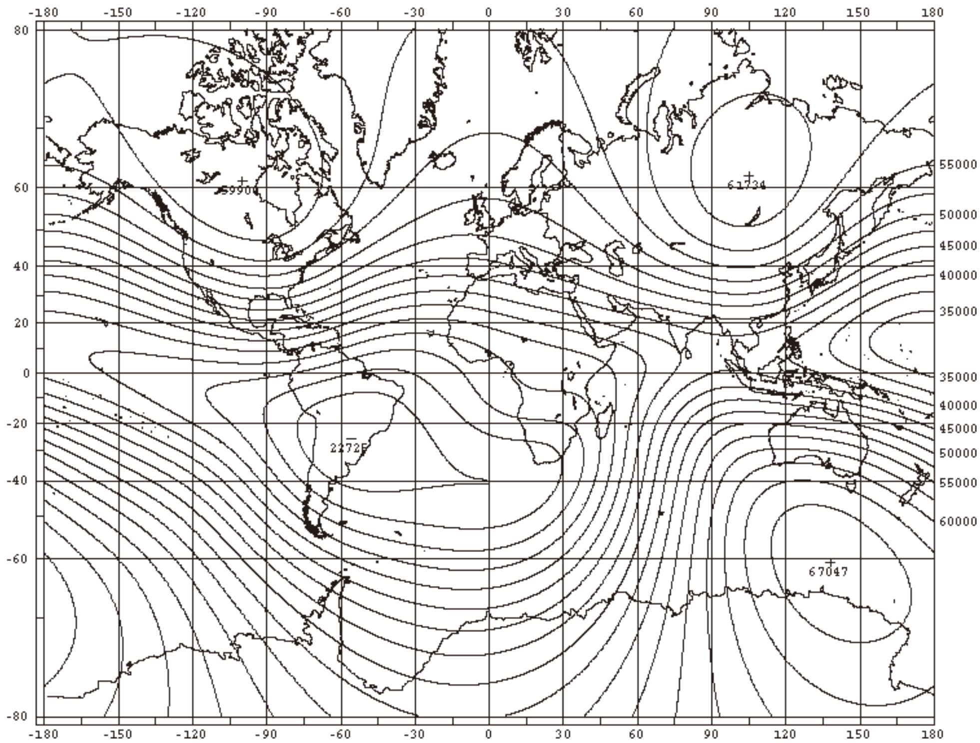

Figure 2.3 An isomagnetic chart of the world indicating the total intensity of the Earth's magnetic field; contour increments are 2,500 nT. Based on the IGRF 2005 model (Toshihiko, 2007).

A first order approximation of the Earth's magnetic field is that of a bar magnet located at the centre of the Earth (geocentric axial dipole) (McElhinny, 1973). However, the Earth's magnetic poles do not coincide with those of the geographic poles. Therefore, a better approximation of the field is that of an inclined geocentric dipole, where the magnetic poles would be at the geomagnetic poles (Figure 2.4). The dipole is inclined at 11.5º to the Earth's rotational axis. Unfortunately this model only accounts for 90% of the Earth's field. The remaining 10% is due to nondipolar fields from within the Earth, remanent magnetisation on the surface and external fields from solar and planetary magnetic fields. These nondipolar fields cause the magnetic poles to be observed slightly off the geomagnetic poles.

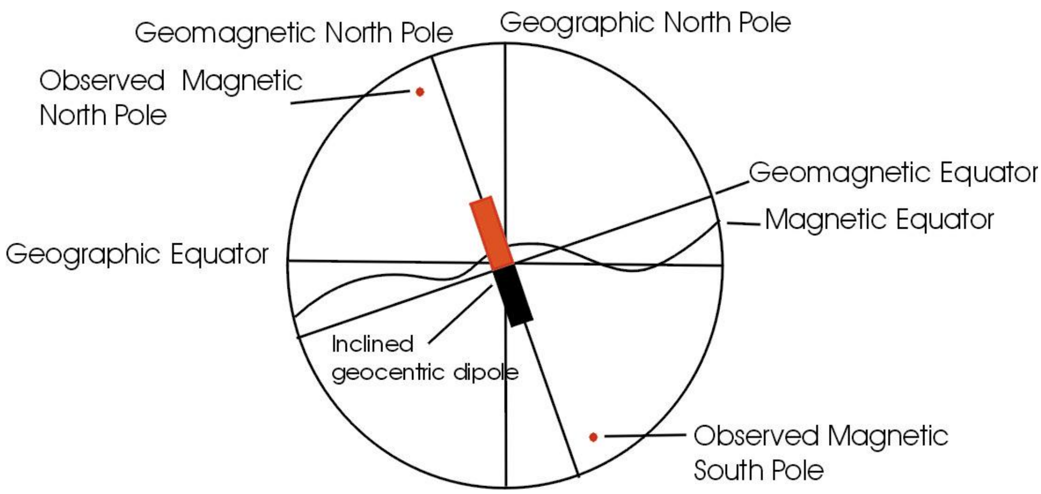

Figure 2.4 A schematic representation of the Earth's Magnetic field (observed poles) and an inclined geocentric dipole (geomagnetic) relative to the Earth's coordinate system (geographic). From (McElhinny, 1973).

The magnitude and direction of the magnetic field slowly changes with time; these variations are referred to as secular variations. Such secular variations have been recorded since 1576 in London and since 1617 in Paris (McElhinny, 1973) (Figure 2.5). Secular variations are different in magnitude and direction from place to place through out the world. London and Paris show similar changes; however, a more pronounced change would occur between points from different continents. Secular variations are believed to originate from nondipolar sources during the generation of the Earth's magnetic field (Merrill et al., 1983).

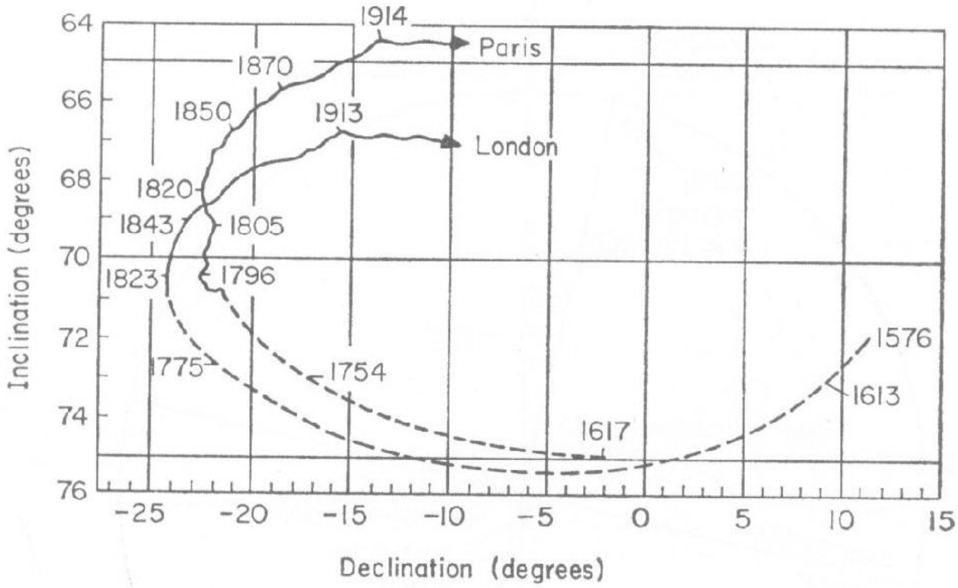

Figure 2.5 Secular variations observed in London from 1576 to 1913 and in Paris from 1617 to 1914 (McElhinny, 1973).

Origin of the Earth's magnetic field

The origin of the Earth's magnetic field is not completely understood. A number of key properties have been identified through the study of the magnetic field over time, and a number of theories have been proposed. A key property of the main field was determined in 1839 when Gauss concluded by spherical harmonic analysis that the field was solely produced by an internal source. A number of models based on permanent magnetisation of the Earth's crust had been developed, although these models fail to account for the reversal of the Earth's field (Irving, 1964). Due to this reversibility of the Earth's magnetic field it was concluded that the Earth must be able to generate and maintain its own magnetic field; the latest model based on this is the dynamo theory.

The dynamo theory was initially suggested by Larmor in 1919. He suggested that the Solar magnetic field might be maintained by a self-exciting dynamo. Elsasser (1946) and Bullard (1949) followed up Larmor's idea by suggesting that the electrically conducting core of the Earth could produce electrical currents necessary to maintain a self-exciting dynamo and therefore a geomagnetic field. It is believed that the mechanism behind the generation of the Earth's magnetic field occurs in the electrically conducting liquid outer core. Where an east-west fluid flow shears poloidal magnetic field and in the process generates new toroidal (east-west) fields. This results in helical fluid flows that twists toroidal magnetic fields and generates new poloidal field (Parker, 1955).

The Glatzmaier-Roberts model (1995a) was the first three dimensional, time-dependent, self-consistent numerical solutions of the magnetohydrodynamic equations that describe thermal convection and magnetic field generation in a rapidly rotating spherical fluid shell with a solid conducting inner core. The model uses similar properties of dimensions, rotation rate, heat flow and the material properties of the Earth's core (Glatzmaier and Roberts, 1995a). The inner core was modeled as rotating between 2 and 3 degrees longitude per year faster than the solid mantle and surface (Glatzmaier and Roberts, 1995a).

Evidence of this increased rotation has been found by investigating seismic waves that traverse the Earth's inner core (Song and Richards, 1996; Su et al., 1996). The magnetohydrodynamic equations that describe this model are solved using spherical harmonic and Chebyshev polynomial expansions that treat all linear terms implicitly, and nonlinear terms explicitly. A more detailed description of the model is given in Glatzmaier and Roberts (1996).

The resulting three-dimensional numerical simulation of the geodynamo spans more than 300,000 years in calculation. The simulated magnetic field has a dipole dominated structure that is very similar to that of the Earth (Figure 2.6) and the surface westward drift of the non-dipolar structures is essentially the same as the 0.2 degrees per year measured on the Earth (Glatzmaier and Roberts, 1995a). The magnetic field underwent a reversal of its dipole moment 36,000 years into the simulation, the period of reversal occurring in little more than a thousand years. The intensity of the magnetic dipole moment decreased by about a factor of ten during the reversal and recovered immediately afterwards (Glatzmaier and Roberts, 1995b). The solution obtained illustrates how the influence of the Earth's rotation on convection in the fluid outer core is responsible for this magnetic field structure and time dependence (Glatzmaier and Roberts, 1995a).

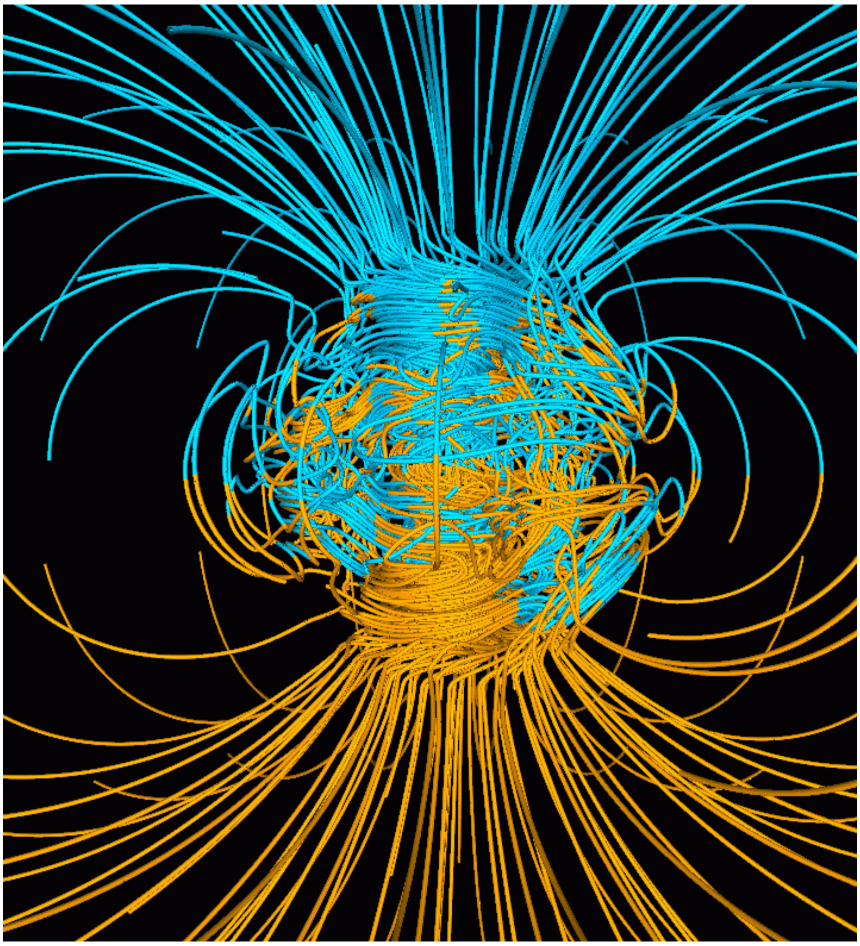

Figure 2.6 The 3D magnetic field structure simulated with the Glatzmaier-Roberts geodynamo model. Magnetic field lines are blue where the field is directed inward and yellow where directed outward. The field lines are drawn out to two Earth radii (Glatzmaier, 1997).

Axial geocentric dipole hypothesis

In order to analyse palaeomagnetic results around the world, a stable model of the Earth's magnetic field is required. The long-term average behaviour of the field should be used in the modelling in order to reduce the effect of the nondipolar field. However, measurements of the average magnetic field have been short (300 years) in terms of geological time. In order to determine this long-term average behaviour, archeomagnetic and palaeomagnetic records over the past 2,000 years were analysed from eight volcanic rock regions located around the globe (Butler, 1992). The mean directions of the geomagnetic field were determined at 100 year intervals and a global average was then determined from the magnetic poles for each interval (Figure 2.7). The variation in the geomagnetic pole position indicates a random walk around the geographic North Pole and it is assumed that after the Earth's magnetic field settled down that on average the position of the geomagnetic pole is that of the North Pole (for this study we assume that the magnetic field had settled down at 2.0Ga). The axial geocentric dipole hypothesis is what makes it possible to model the time-averaged Earth's magnetic field as a geocentric axial dipole. All palaeomagnetic studies rely on this hypothesis to calculate palaeomagnetic poles.

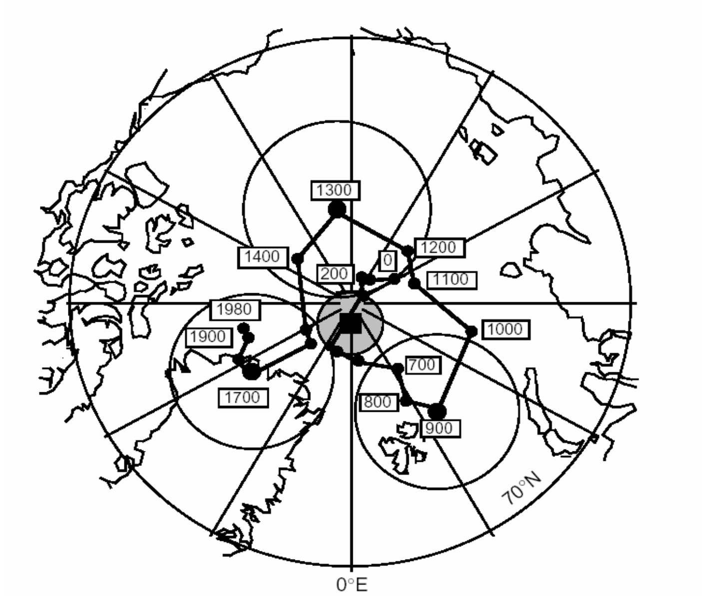

Figure 2.7 A schematic representation of the position of the North Pole over 2 000 years. Each point represents a mean polar position, calculated from eight regions of the globe. The large unfilled circles around 900, 1,300 and 1,700 are the α_{95} (a 95% confidence level that the pole falls within the circle, discussed later) values for each of the respective points. The mean geomagnetic pole is indicated by the square in the centre (Butler, 1992).

2.1.2 Rock magnetism

Magnetism of minerals and rocks

Magnetic properties in a solid are created by atomic magnetic moments caused by electrons orbiting around their nucleus (orbital magnetic moment) and by the electrons spinning about their own axis (spin magnetic moment). The magnetic dipole moment of an atom as a whole is the result of all the orbital and spin moments of its electrons (Butler, 1992).

Magnetic minerals can be divided into different categories based on their behaviour when placed in an external field. There are several types of magnetism that exist in minerals. Minerals that only have magnetisation in the presence of an applied field are known as diamagnetic and paramagnetic; the magnetic effect of these minerals is weak.

- Diamagnetism: When placed in a magnetic field the orbital motions of the electrons are altered to produce a small induced magnetisation opposite to that of the applied field. The level of magnetisation *(J)* is linearly dependent on the applied field *(H)* and is reduced to zero when the applied field is removed (Figure 2.8). Diamagnetism is a property of all matter, although it will only prevail if the net magnetic moment of all atoms is zero when there is no magnetic field. Diamagnetic materials have negative and temperature-independent magnetic susceptibility, χ (Figure 2.8). Examples of some diamagnetic minerals are: quartz, gold, galena, graphite and salt (Butler, 1992).

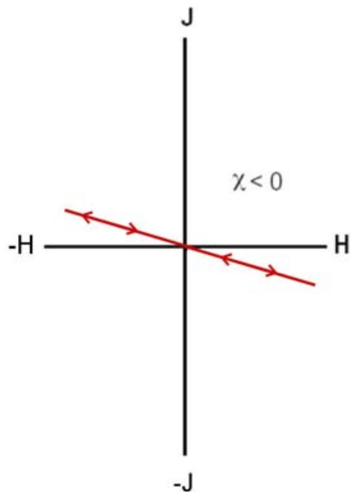

Figure 2.8 The effect an applied field *(H)* has on the magnetisation *(J)* on a diamagnetic mineral. Magnetic susceptibility (χ) is a negative constant.

- Paramagnetism: This type of magnetisation occurs in minerals that contain atoms with atomic magnetic moments equally distributed in all directions (randomised), with a resultant magnetisation of zero, and with no interaction between adjacent atomic moments. When placed in a magnetic field the magnetic moments of the atoms tend to align themselves with the applied field. The level of magnetisation is linearly dependent on the applied field. When the field is removed the magnetisation returns to zero (Figure 2.9). Paramagnetic materials have positive magnetic susceptibility, χ. Examples of some paramagnetic minerals are: pyroxenes, biotite, amphiboles, ilmenite and garnet (Butler, 1992).

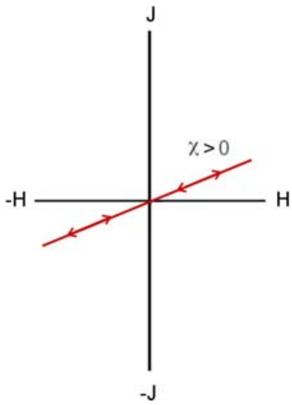

Figure 2.9 The effect an applied field *(H)* has on the magnetisation *(J)* on a paramagnetic mineral. Magnetic susceptibility (χ) is a positive constant.

The last type of magnetism occurs when there is a strong magnetic field interacting between magnetic moments, causing alignment of moments in fairly large regions (domains). This effect is referred to as ferromagnetism. The general term ferromagnetism is used to indicate materials that have coupling of adjacent atomic magnetic moments. There are three types of ferromagnetism; antiferromagnetism, ferromagnetism, and ferrimagnetism (Butler, 1992).

- Ferromagnetism: Spin moments are parallel to each other in order to reduce the exchange energy to a minimum within the crystal. This is an idealised case and does not occur in most minerals in nature.
- Antiferromagnetism: An equal number of magnetic moments are in opposite directions and thus there is no net magnetisation. In same cases the spin moments are canted resulting in a small net remanence (Figure 2.10), referred to as canted antiferromagnetism. The most common example is hematite.

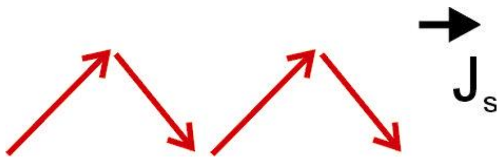

Figure 2.10 A sketch illustrating the resulting net remanence from canted antiferromagnetism.

- Ferrimagnetism: Occurs when an unequal number of magnetic moments are in opposite direction, or moments are tilted with respect to each other, or the magnetic moments have different amplitudes, resulting in a net magnetisation. Ferrimagnetism is most common type of magnetisation in magnetic minerals. The most common examples are magnetite, titanomagnetite, titanium and pyrrhotite.

Ferromagnetic and ferrimagnetic minerals acquire spontaneous magnetisation due to the electron spins of the atoms aligned with each other. At a specific temperature, referred to as the Curie temperature or Curie point, the alignment of the electron spins is destroyed and the spontaneous magnetisation is reduced to zero. Above this temperature the mineral is paramagnetic (McElhinny, 1973).

Antiferromagnetic minerals do not have Curie temperatures because there is no net ferromagnetism. The ordering of atomic moments of these minerals is destroyed at the Nėel temperature. Above this temperature the mineral is paramagnetic (Irving, 1964).

Magnetic domains

The basic principle in the formation of magnetisation and magnetic domains within a grain is how various energies interact. No matter how complex or simple the combinations of energies are, the grain seeks the configuration of magnetisation that minimizes its total field.

In a mineral, atomic magnetic moments are modelled as pairs of magnetic charges. Adjacent atoms cancel internally, but produce a magnetic charge distribution at the surface. For a spherical particle, one hemisphere has positive charge and the other a negative charge, resulting in energy being stored in this charge distribution because of repulsion between adjacent charges. This is magnetostatic energy, e_m.

The formation of magnetic domains within a grain decreases the percentage of surface covered by magnetic charges, and thereby decreases the magnetostatic energy. In a uniformly magnetised grain (with magnetisation $j = j_s$), e_m is proportional to j^2. With the formation of magnetic domains, the magnetisation internal to any individual domain is j_s. However, the entire grain has net magnetisation $j << j_s$ (Butler, 1992).

Grains containing numerous domains are referred to as multidomain (MD) grains, and the region separating domains is referred to as a domain wall. With decreasing grain size, the number of magnetic domains decreases. At a specific size, the energy required to make a domain wall is larger than the decrease in magnetostatic energy resulting from the formation of the two domains. When this occurs a grain will only contain one domain, and these grains are referred to as single-domain (SD) grains.

The size of the grain is not the only factor responsible for whether a grain is single or multiple domain. The shape and saturation magnetisation (j_s) are also of importance. Ferromagnetic grains with low j_s are generally SD grains due to the magnetostatic energy being too low to form magnetic domains. On the other hand, high j_s allows smaller grains to be MD. The shape of a grain is a more complicated component (Figure 2.11). Elongated grains can be SD with larger sizes than that of cubic grains (Butler, 1992).

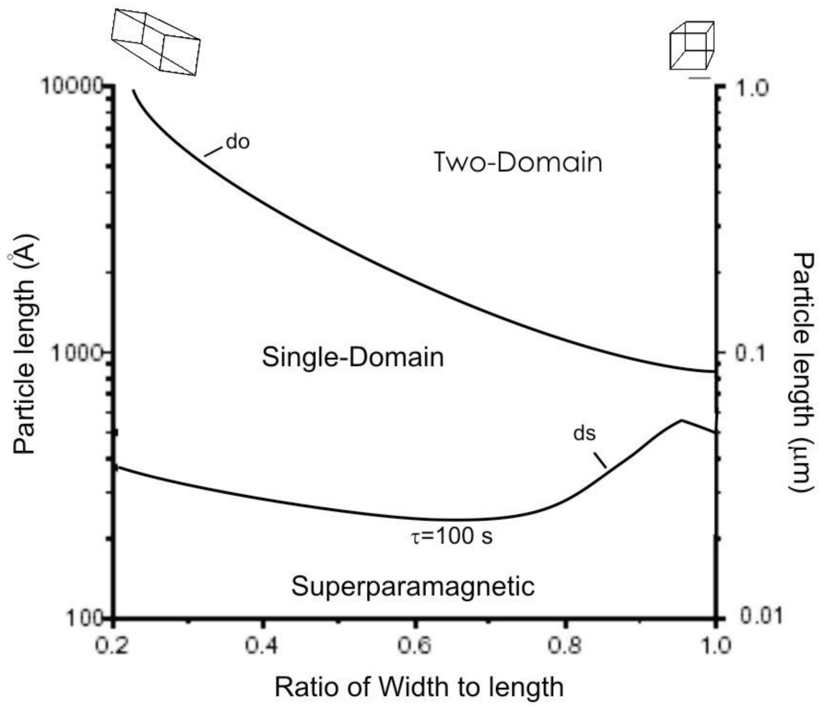

Figure 2.11 The effect of size and shape on the formation of single-domain and two-domain configurations for parallelepipeds of magnetite at 290 Kelvin. The curve labelled d_0 separates the single-domain size and shape field from the size and shape distribution of grains that contain two domains; curves labelled d_S are size and shape distribution of grains that have τ (characteristic relaxation time) = 100 s; grains with sizes below d_S curves are superparamagnetic (Butler, 1992).

The magnetic properties of SD and MD grains are dramatically different from each other (Butler, 1992). The behaviour of magnetic grains is governed by the energies that control the direction of magnetisation. Interaction energy (e_H) represents the interaction between the applied magnetic field (H) and the atomic magnetic moments integrated over the volume of the ferromagnetic grain. This energy describes how the magnetisation of a ferromagnetic grain is influenced by an externally applied magnetic field. Magnetostatic energy (e_m), discussed earlier, is another energy responsible for the control of the magnetisation direction.

Hysteresis

A ferromagnetic substance, when placed in an alternating magnetic field, will follow a magnetic curve, known as a hystersis loop (Figure 2.12). On application of an initial magnetizing field, the grains obtain a net magnetisation parallel to that of the field (along the path *a-c*). During the application of the field, the saturation magnetisation (j_S) of individual grains begins to rotate towards the applied magnetic field because of the interaction energy (e_H). If the applied field is increased to a sufficient level, all grains will have their magnetisation aligned with the field. At this point the sample has reached its saturation magnetisation (J_S). Saturation magnetisation is linearly dependent on the concentration of ferromagnetic minerals. On removal of the magnetic field, the magnetisation of the individual grains rotates to the nearest long axis, thus minimizing the magnetostatic energy, e_m. Magnetisation of the sample follows the path *c-d*. After the magnetic field has been removed (point *d*) a remanent magnetisation, J_r, remains. The ratio of remanent to saturation magnetism (J_r/J_s), is generally used as a measure of efficiency in acquiring remanent magnetisation.

In order to force the magnetisation back to zero, an opposing magnetic field is applied. The magnetisation decreases along the path *d-e*, and the magnetic field required to drive the magnetisation back to zero (i.e. rotate the magnetisation) is the bulk coercive force, H_c .The microscopic coercive force, h_c, is the magnetic field required to make irreversible changes within part of a grain, such as the passage of a domain wall over a local energy barrier. The bulk coercive force does not depend on the concentration of ferromagnetic materials, because it depends only on h_c, which in turn depends on the energy balance within the individual grains. Driving the sample to saturation in the negative direction and then returning to saturation in the positive direction completes the hysteresis loop. This hysteresis loop indicates how single domain ferromagnetic grains acquire remanent magnetisation and are resistant to demagnetisation. Rocks generally have a large percentage of MD grains and pseudo-single-grains, which have lower h_c and lower J_r/J_s values (Butler, 1992). This hysteresis loop is the basic principle behind alternating field demagnetisation (discussed in Section 2.3.3).

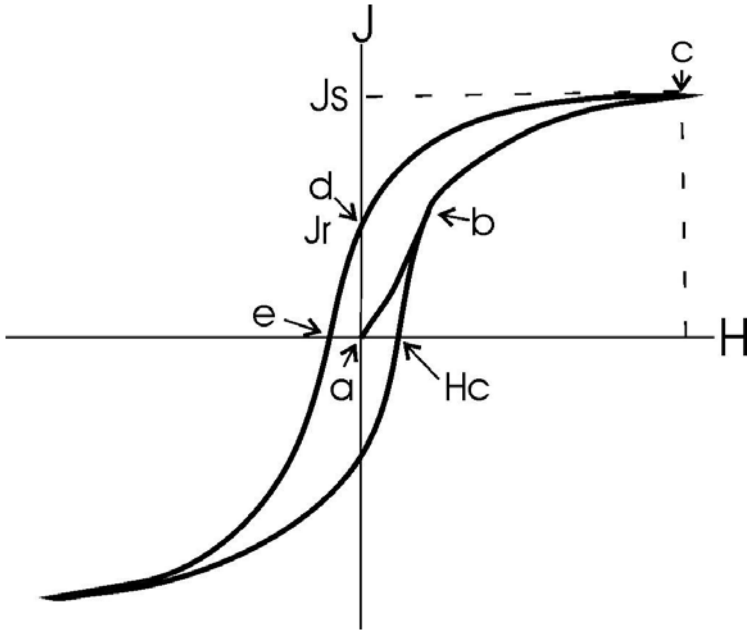

Figure 2.12 Hysteresis loop for a synthetic sample containing 5% by volume elongated SD magnetite grains. J_r is the remanent magnetisation, J_s is the saturation magnetisation and *Hc* is the bulk coercive force (Butler, 1992).

Hysteresis of multidomain grains

On the application of an applied field to a multidomain (MD) grain, domains are produced with magnetisation parallel to the field. If the applied field is sufficiently strong, domain walls are destroyed and magnetisation reaches saturation, i.e. $j = j_S$. Once the field has been removed, domains re-form and move back towards their initial position. However, rather then returning to their initial position, the domain walls settle in energy minima near to their initial position, resulting in a small remanent magnetisation. Only a small magnetic field is required to drive the domain wall back to zero. MD grains are not very effective recorders of palaeomagnetism (McElhinny and McFadden, 2000).

Pseudo-single-domain grains

There is no sharp boundary between SD grains and small MD grains. Instead, there is an interval of grain size exhibiting intermediate J_r/J_S and intermediate coercive forces. These grains are referred to as pseudo-single-domain (PSD) grains, and are important in understanding magnetisation of rocks containing magnetite and titanomagnetite. The PSD grain-size interval for magnetite is approximately 1-10 μm. Grains in this size range contain a small number of domains and can have substantial magnetic moment. In igneous and sedimentary rocks the majority of grains fall within the magnetite PSD field. They exhibit significant coercivity and time stability of remanent magnetisation and are therefore important carriers of palaeomagnetism (McElhinny and McFadden, 2000).

Magnetic relaxation

Thermal activation can also lead to the rotation of j_s over energy barriers. An effect of thermal activation is magnetic relaxation, in which remanent magnetisation of an assemblage of SD grains decays with time. The exponential decay of remanent magnetisation, J_r, after the removal of the magnetizing field is given by

$$J_r = J_{r0} \exp\left(\frac{-t}{\tau}\right), \tag{2.5}$$

where J_{r0} is the initial value of remanent magnetisation, t is the time and τ is the characteristic relaxation time, after which $J_r = J_{r0}/e$.

The characteristic relaxation time is given by

$$\tau = \frac{1}{c}\exp\left(\frac{vh_c j_s}{2kT}\right) \tag{2.6}$$

Where C is the frequency factor, v the colume of the grain, hc is the microscopic coercive force of SD grain, js is the saturation magnetization and kT is the thermal energy. The relaxation time is controlled by the ratio of blocking energy (energy required to rotate j_S) to thermal energy. Values for relaxation time vary over many orders of magnitude. SD grains with short relaxation times are referred to as superparamagnetic. Superparamagnetic grains have strong magnetisation; however, they are unstable and decay to zero very soon after the removal of the magnetizing field (Butler, 1992). Relaxation times for SD grains at a constant temperature are dependent on grain volume, and microscopic coercive force (Figure 2.13). In order to record palaeomagnetism effectively, a grain must have a relaxation time in the order of τ = 4.5 Ga, or equivalent to the age of the rock sampled. The effect of size and shape of an elongated magnetite grain is shown in (Figure 2.13). SD grains with $d_S < d < d_0$, are within the stable SD grain-size range, (i.e. long relaxation times) and they also have high J_r/J_S and h_c, and they are highly effective carriers of palaeomagnetism.

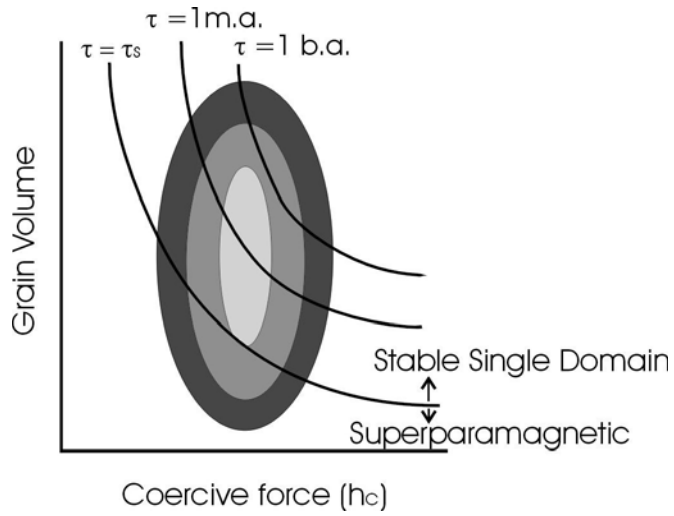

Figure 2.13 A plot of relaxation times of SD grains on a volume (v)-versus-coercive force (h_c). The lines of equal τ are lines of equal product vh_c. Superparamagnetic grains plot below the $\tau = \tau_S$ line. Stable SD grains plot above $\tau = \tau_S$. The shaded regions represents the population of SD grains; increased population is represented by lighter shades (Butler, 1992).

Blocking temperature

Relaxation time has strong temperature dependence. This is because parameters controlling the relaxation time are controlled by temperature, i.e. j_S and h_c. Due to temperature dependences, a SD grain will have different relaxation times at different temperatures (Figure 2.14). This indicates that a SD magnetite grain will have a relaxation time of 100 s at 555°C, while at 510°C the relaxation time is around a billion years. With these changes in relaxation time, a grain can change from superparamagnetic to a stable SD grain at a specific temperature referred to as the blocking temperature (T_B). Between the Curie temperature T_C and T_B, the grain will be ferromagnetic (i.e. remanent magnetisation will decay quickly if the field is removed while at this temperature). Below the blocking temperature (T_B), τ exceeds τ_S and increases rapidly during continued cooling. Remanent magnetism formed at or below the blocking temperature can be stable, especially if temperature is decreased (Butler, 1992).

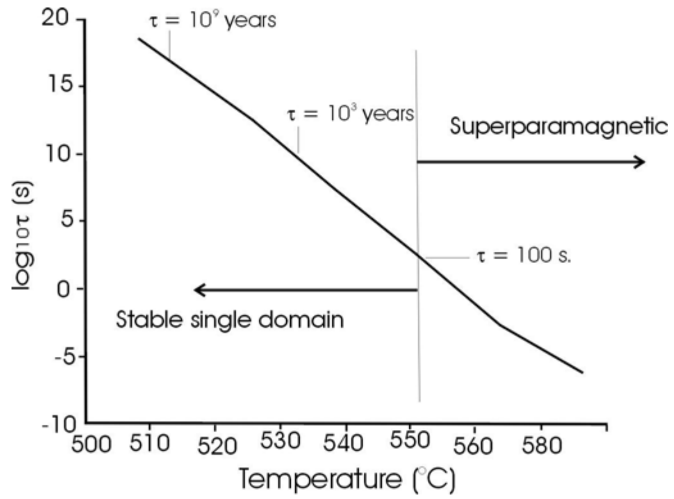

Figure 2.14 Semi-log plot of relaxation time (τ) as a function of temperature for a SD magnetite grain. The separation between superparamagnetic and stable single domain represented by the vertical line indicates the blocking temperature (Butler, 1992).

2.1.3 Mineralogy

The majority of minerals responsible for the magnetic properties of rocks are found within the iron-titanium oxides, (ternary system FeO-TiO_2-Fe_2O_3, Figure 2.15), the oxyhydroxides of iron (e.g. geothite and lepidocrocite) and pyrrhotite ($Fe_{1-x}S$).

Iron-titanium oxides

Iron-titanium (Fe-Ti) oxides are generally opaque and polished sections are required to examine them. Figure 2.15 illustrates the ternary diagram for iron-titanium oxides. The ratio of ferric (Fe^{3+}) to ferrous (Fe^{2+}) iron increases from left to right, while the Ti content increases from bottom to top. Two solid solution series are considered in palaeomagnetism; titanomagnetites and titanohematites (Butler, 1992).

- Titanomagnetite series: The end members are ulvospinel (Fe_2TiO_4) and magnetite (Fe_3O_4). Ulvospinel does not generally occur as a discrete phase, but occurs as intergrowths in magnetite. It is paramagnetic at normal temperatures and antiferromagnetic at low temperatures. The Nėel temperature is –153˚C. Magnetite is the most common magnetic mineral. It is magnetically anisotropic and has a Curie temperature of 578°C (McElhinny, 1973).

- Titanohematite series: The two end members are ilmenite ($FeTiO_3$) and hematite (αFe_2O_3). Single crystals of hematite are paramagnetic in the direction of the triad axis, but exhibit weak ferromagnetic properties in the plane normal to the axis. The Curie temperature is 680°C. Ilmenite is paramagnetic at room temperature and antiferromagnetic at very low temperatures (McElhinny, 1973).

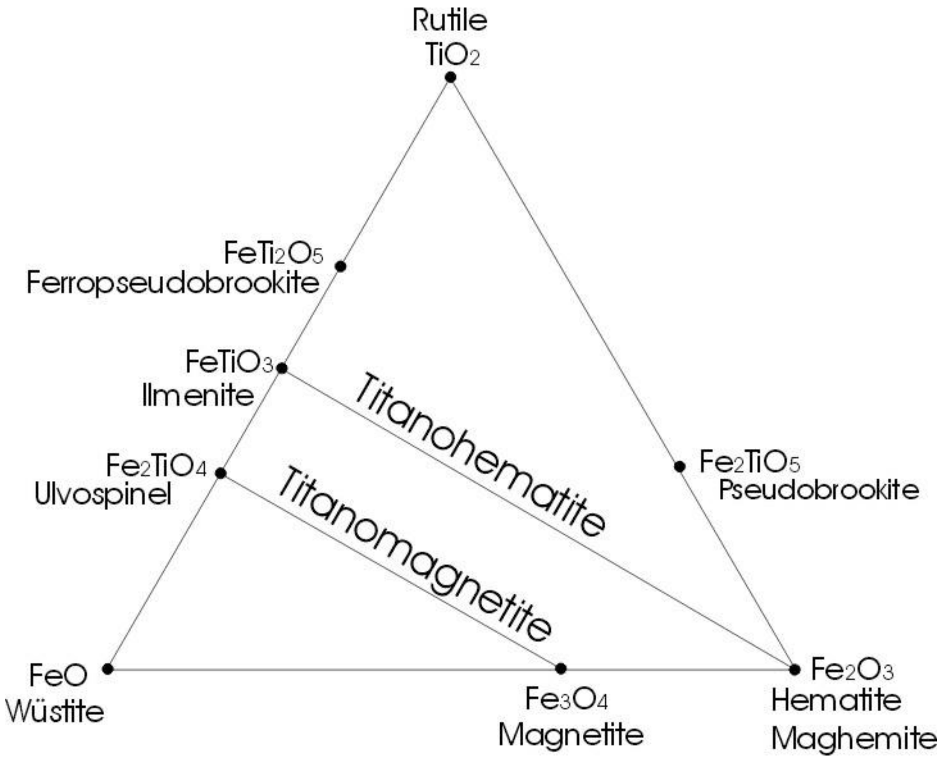

Figure 2.15 FeO-TiO_2-Fe_2O_3 ternary diagram, showing the principal solid solution series (McElhinny, 1973).

Oxyhydroxides of iron

There are two minerals that are important to palaeomagnetism within this group that occur naturally and dehydrate to oxides at 100 to 300°C (McElhinny, 1973).

- Geothite ($\alpha FeOOH$): the oxyhydroxide corresponding to hematite (Irving, 1964).
- Lepidocrocite ($\gamma FeOOH$): the oxyhydroxide corresponding to maghemite (Irving, 1964).

Pyrrhotite ($Fe_{1-x}S$, where $0 < x \leq 0.14$)

Pyrrhotite is the only iron-sulphide that shows remanent magnetisation (i.e. ferromagnetic). Below 300°C it is antiferromagnetic when $0 < x \leq 0.09$, and ferromagnetic when $0.09 < x \leq 0.14$ (McElhinny, 1973).

2.1.4 Magnetisation

The magnetisation of rock *in situ* depends mainly on two components: the present day field (induced magnetisation, lost when removed from field), and the natural remanent magnetism (NRM). The two components add vectorially in amplitude and direction.

The total magnetisation J_t of a rock *in situ* is made up of the vector sum of the two components J_i induced by the Earth's field, and the remanent magnetism J_r (McElhinny, 1973).

$$J_t = J_i + J_r \tag{2.7}$$

Magnetic susceptibility

The intensity of magnetisation (*J)* is related to the strength of the magnetic field (*H)* through a constant of proportionality (χ) known as the magnetic susceptibility.

$$J = \chi H\,. \tag{2.8}$$

Magnetic susceptibility is a dimmensionless constant that is determined by the physical properties of the magnetic material. It can take on either positive or negative values. Positive values imply that the induced magnetic field is in the same direction as the inducing field, *H*. Negative values imply that the induced magnetic field is in the opposite direction as the inducing field (Irving, 1964). Susceptibility can be measured in the SI or the CGS system; the conversion is given by:

$$\chi_{SI} = 4\pi\chi_{CGS}\,. \qquad (2.8)$$

Koenigsberger ratio

The Koenigsberger ratio *(Q)* is defined as the ratio of the remanent to induced magnetisation and is given by

$$Q = \frac{J}{\chi H} \quad . \tag{2.10}$$

J is the remanent magnetisation in the rock (NRM), and H is the induced/local magnetisation. In South Africa the local geomagnetic field is approximately 30,000 nT. In general, the Koenigsberger ratio is used as a measure of the stability in indicating a rock's capability of maintaining a stable remanent magnetisation. A low value of the Koenigsberger ratio indicates that minerals have unstable remanent magnetisation and are more susceptible to an external magnetic field (Irving, 1964).

2.1.5 Remanent magnetisation

Natural remanent magnetisation (NRM) is dependent on the geomagnetic field and the geological processes during the formation and history of the rock. NRM typically is composed of more than one component. The NRM acquired during the formation of the rock is referred to as the primary NRM component and is the component sought in palaeomagnetic investigations. Secondary NRM components can be acquired after rock formation and can alter the primary NRM. The different components of NRM add vectorially to produce the total NRM (Butler, 1992). There are three basic forms of primary NRM:

- Thermoremanent magnetisation (TRM): NRM acquired during the cooling of a rock from above the Curie temperature in the presence of a magnetic field. As the rock cools below its Curie temperature, the direction of the magnetic field is retained or “blocked” when the magnetic-ordering energy becomes greater than the thermal-disordering energy. This temperature is referred to as the blocking temperature. TRM is the most important form of NRM in igneous and many metamorphic rocks (Stacey and Banerjee, 1974).

- Partial thermoremanent magnetisation (PTRM): Occurs when rocks are reheated and subsequently cooled when they are buried and/or metamorphosed.
- Chemical remanent magnetisation (CRM): Formed by the growth of ferromagnetic grains at low temperatures (below the Curie temperature) by chemical or phase change in the presence of an applied field. CRM is generally encountered in sedimentary rocks (McElhinny, 1973).
- Detrital remanent magnetisation (DRM): This process occurs during the deposition and lithification of sedimentary rocks. In order to obtain DRM the sediments need to contain particles with a net magnetic moment. The water conditions need to be non-turbulent and a long period of time is needed to allow magnetic moments to align themselves parallel to the Earth's field as they settle (McElhinny, 1973).

The secondary NRM component can result from chemical changes in ferromagnetic minerals, exposure to lightning strikes (isothermal remanent magnetism (IRM), exposure to strong magnetizing fields at constant temperature), or the long-term exposure to the geomagnetic field (viscous remanent magnetism, VRM) (Butler, 1992).

2.2 Palaeomagnetic Core Sample Collection

Core samples are collected in the field with the use of a portable gasoline powered drill, equipped with a water-cooled non-magnetic diamond drill bit (Figure 2.16). The core samples have a diameter of 2.54 cm (1 inch) and are drilled to a depth of approximately 6 cm; this enables the core to be cut into 2 samples and to remove near surface weathering effects.

Figure 2.16 Portable gasoline-powered drill fitted with a non-magnetic diamond drill bit and water pump used to cool the drill bit during drilling.

Once drilling has been completed, the sample-holder (Figure 2.17) is inserted into the hole and the orientation of the core (i.e. dip and core azimuth) is determined. A sun compass reading is recorded after the magnetic reading. This is done in case the rock being drilled is very magnetic and deviation occurs with the magnetic compass readings (Figure 2.18). When recording the sun compass readings the date, time, latitude and longitude must be taken.

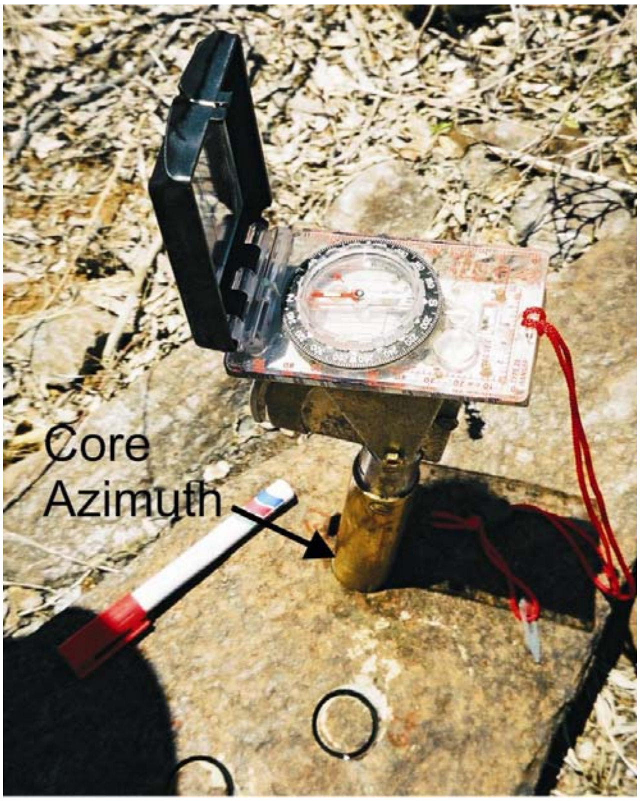

Figure 2.17 Orientation of core; the sample holder is inserted into the drill hole with Silva compass on top. The core azimuth is taken at the front, when using a Silva compass.

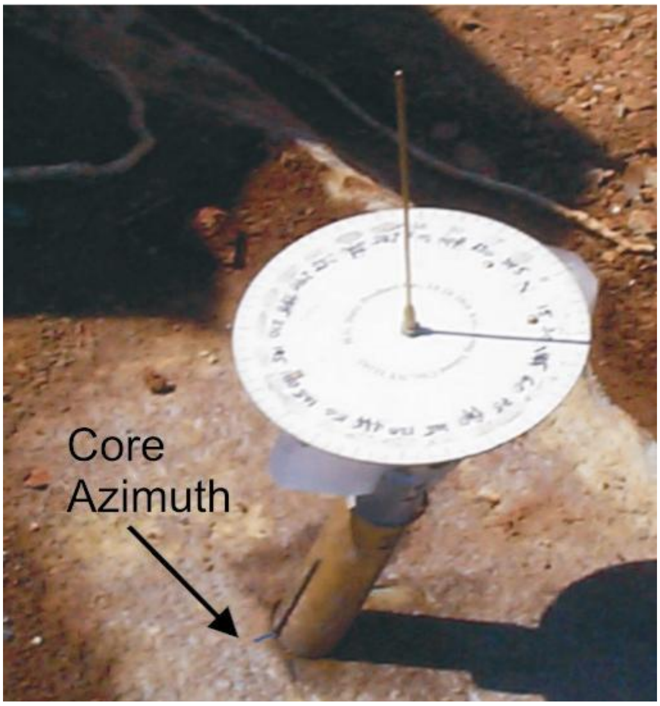

Figure 2.18 Sun compass. The sun compass used has a reading of 180° at the core azimuth and increases clockwise. When taking a sun compass reading the date, time and longitude and latitude must also be taken.

After orientation, the core is marked and broken off from the outcrop. When breaking the core a copper extractor is used (Figure 2.19) to prevent any shock magnetism from occurring when removing the core. During the entire core acquisition the sample does not encounter any magnetic material.

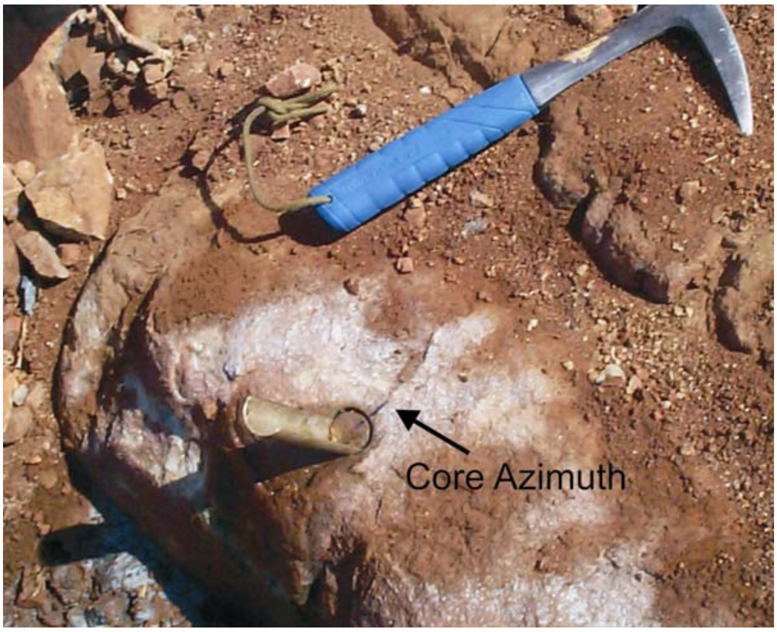

Figure 2.19 Core sample is marked and extracted using a copper extractor.

2.3 Palaeomagnetic Laboratory Procedure

All laboratory procedures and measurements were conducted at the Geological Survey of Norway (NGU) in Trondheim, Norway. In the laboratory, core samples were initially cut into smaller samples measuring 2 cm in length using a copper disk cutter (to prevent introducing magnetisation). The samples were then measured for NRM, susceptibility and finally demagnetised by thermal or alternating field (AF) demagnetisation.

2.3.1 Susceptibility

Susceptibility measurements were carried out on all samples before demagnetisation. The susceptibility was measured using a Bartington MS2 magnetic susceptibility meter (Figure 2.20). The sensor is designed for use with 1-inch diameter core samples. The susceptibility meter operates on the principle of a.c. induction. A low intensity alternating magnetic field (~ 250µT) is produced in the coils surrounding the sample. The influence of this field on the sample produces a change in the oscillator frequency. This change in frequency is then converted to a value of magnetic susceptibility. The susceptibility meter is linked to a computer that uses a program developed by Professor T.H Torsvik to record the measurements. An "air" reading (measurement with no sample) is measured before every sample is analysed. By doing so the instrument is set to zero and an accurate measurement of the sample may be taken. The susceptibility is recorded as volume susceptibility and in SI units x10^{-6}.

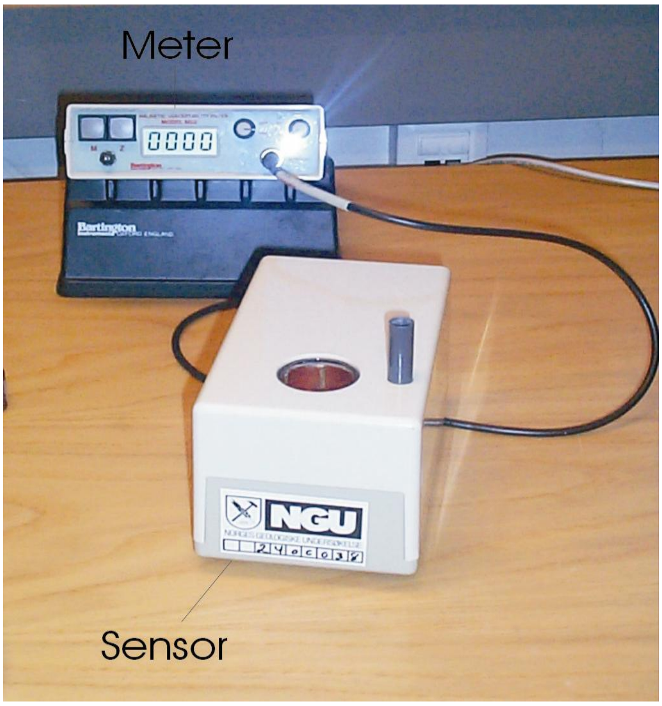

Figure 2.20 The Bartington magnetic susceptibility meter used in the study.

2.3.2 Faraday cage

The Faraday cage is designed so that magnetic measurements and demagnetisations can be performed in a low intensity magnetic field. The three components of the magnetic field are independently adjusted to remove any magnetic anomalies within the cage. The field inside the cage is monitored with the use of a Bartington (Mag-03M) 3-axis magnetometer and is automatically compensated for any changes that occur in magnetic field by a field regulator. The field is kept at around 0.005-0.010 µT, in comparison to the 50,000 nT Earth's field experienced in Norway. The cage offers an alternative to a µ-metal room (a room completely made out of μ-metal) and has the advantage of allowing the magnetic fields due to the equipment to escape and not enhance it. The spinner magnetometer and thermal demagnetiser are both used in the Faraday cage.

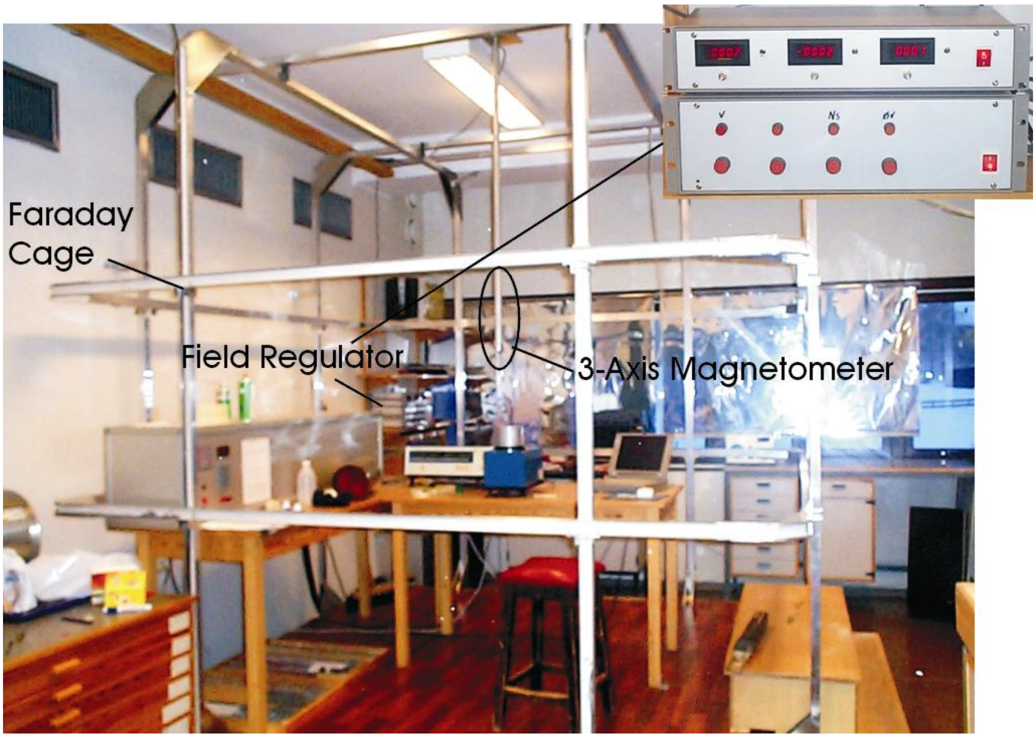

Figure 2.21 Faraday cage, containing the spinner magnetometer and thermal demagnetiser. The field is monitored with the use of a 3-axis magnetometer and is then automatically compensated for any change in magnetic field with the use of a field regulator, (insert top right).

2.3.3 Demagnetisation (magnetic cleaning)

The process of demagnetisation is performed to progressively demagnetise samples and remove components of NRM. Components that are easily removed are referred to as low-stability components. Removal of these low-stability components by partial demagnetisation will allow isolation of the more resistant high-stability components. The high-stability or high temperature blocking (HB) component of NRM, is referred to as the characteristic component (ChRM) of NRM. One cannot determine whether the ChRM is primary; additional information is required (Butler, 1992). In this study demagnetisation was conducted using thermal and alternating field (AF) demagnetisation.

Alternating field demagnetisation

During AF demagnetisation samples are subjected to an alternating magnetic field. While they are rotated, the AF value is increased in progressive steps. The AF demagnetiser is enclosed in its own Faraday cage that is set to zero before demagnetisation occurs. The alternating field used is of sinusoidal nature (400Hz) and has a linear decrease in magnitude with time (Figure 2.22). Samples are rotated in the centre of the field with the use of a tumbler. This enables all the axes of the sample to be aligned with the alternating field. The process of AF demagnetisation progressively removes the magnetisation of magnetic grains with coercivities below the maximum field produced by the peak current (Irving, 1964). This is accomplished by producing VRM in these grains in a zero field and in a random direction. A 2-axis tumbler alternating field demagnetiser was used in this study (Figure 2.23).

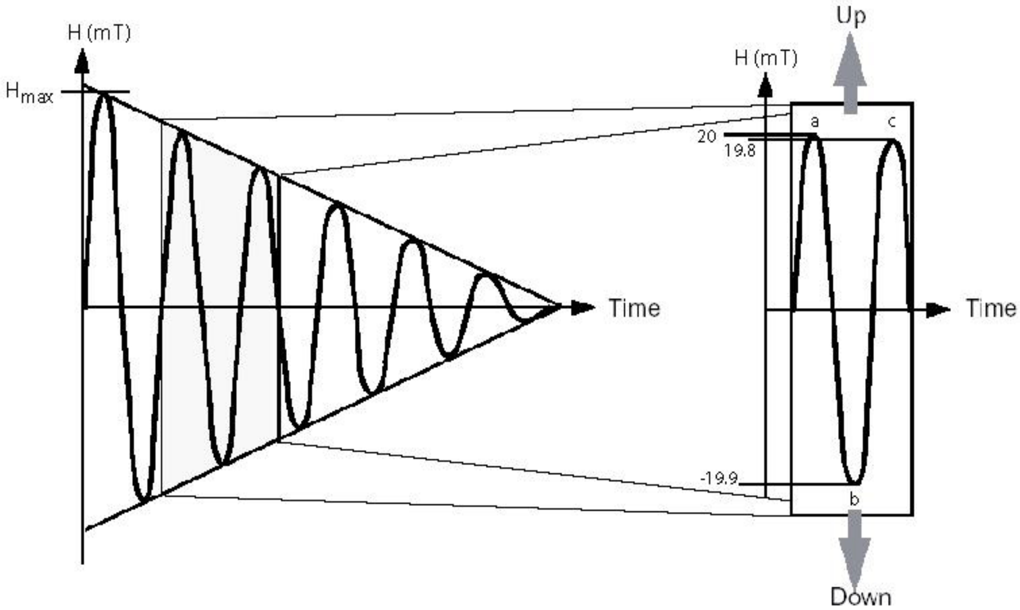

Figure 2.22 A schematic representation of alternating field demagnetisation. During decay of the magnetic field magnetic grains with coercivities lower then the field will acquire the field direction at that time. Grains with coercivities between 20 mT and 19.9 mT will acquire an “up” magnetic field and grains with coercivities between 19,9 mT and 19.98 mT will acquire a “down” magnetic field. The net magnetic moment of the two intervals affectively cancels each other (Butler, 1992).

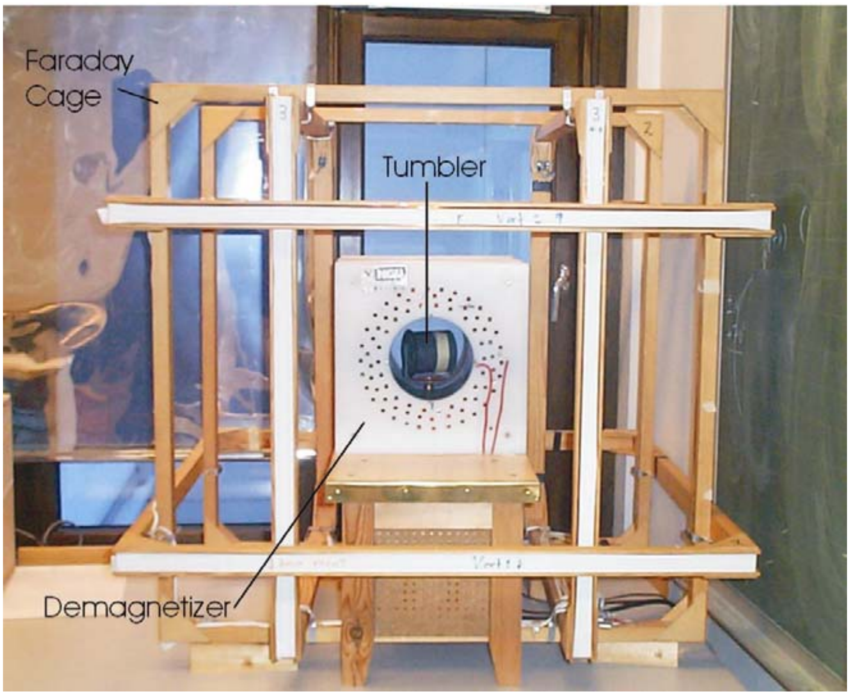

Figure 2.23 The 2-axis tumbler alternating field demagnetiser enclosed in a Faraday cage used in the study.

Thermal demagnetisation

During thermal demagnetisation samples are heated to a specific temperature, which is held constant for 25 minutes (in order to allow for thermal stabilization), and then rapidly cooled (by a fan) in a zero magnetic field. During the cooling period, grains with blocking temperatures less than the heated temperature acquire a thermoremanent magnetisation (TRM) in a zero magnetic field, thereby erasing their NRM at that temperature.

A MMTD60 thermal demagnetiser (Figure 2.24) was used for thermal demagnetisation in this study. The oven is programmable to heat 60 samples at a time, and is surrounded by 4 layers of μ-metal that are automatically degaussed (to remove any electrical charges on the layers). The residual field inside the oven is generally kept below 10 nT in an unshielded environment. However, with the instrument being used in a Faraday cage the internal residual field will be below 1 nT. These low levels in the magnetic field are produced to prevent the samples from acquiring the present day field during cooling.

Figure 2.24 The *MMTD60* thermal demagnetiser used in the study.

Thermal demagnetisation has an advantage over AF demagnetisation, because AF only produces VRM for grains with short relaxation time. Therefore, even if a grain has a low coercivity force, it might have a high relaxation time (due to large volume) and therefore may not be successfully demagnetised during the short demagnetisation process. In the event that this occurs (i.e. AF demagnetization was unsuccessful in completely demagnetising samples) thermal demagnetisation is required after the application of AF demagnetization.

2.3.4 Spinner magnetometer

The measurement of ChRM and secondary magnetisation in this study was acheived with the use of a JR-6A spinner magnetometer (Geofyzik BRND). The JR-6A spinner magnetometer is composed of two parts, a pick-up unit and a measuring unit (Figure 2.25). The pick-up unit includes the sample holder (spinner system), motor, pick-up coils and a triple permalloy (μ metal) shield. The measuring unit incorporates the electronic circuits required for signal processing and motor speed regulation, and a LED display indicating the vector components (Wallace, 2002).

The magnetic vector components of the sample are determined by rotating the sample at a constant rate within the pick-up coils. During rotation an alternating voltage is induced in the pick-up coils; the amplitude and phase of this signal is dependent on the magnitude and direction of the sample's magnetic vector. The voltage is then amplified, filtered and digitised. Fourier analysis is applied to the signal to produce two rectangular components of the magnetic field, and the components are in the plane perpendicular to the rotation axis. The JR-6A has an automatic holder that enables the pick-up unit to rotate the sample into different positions, and therefore determine the three components necessary to determine the magnetic vector of the sample. The three positions of the core are shown in Figure 2.26.

Figure 2.25 JR-6A spinner magnetometer, with μ-metal shield removed to reveal pickup coils and sample holder and spinner system.

.

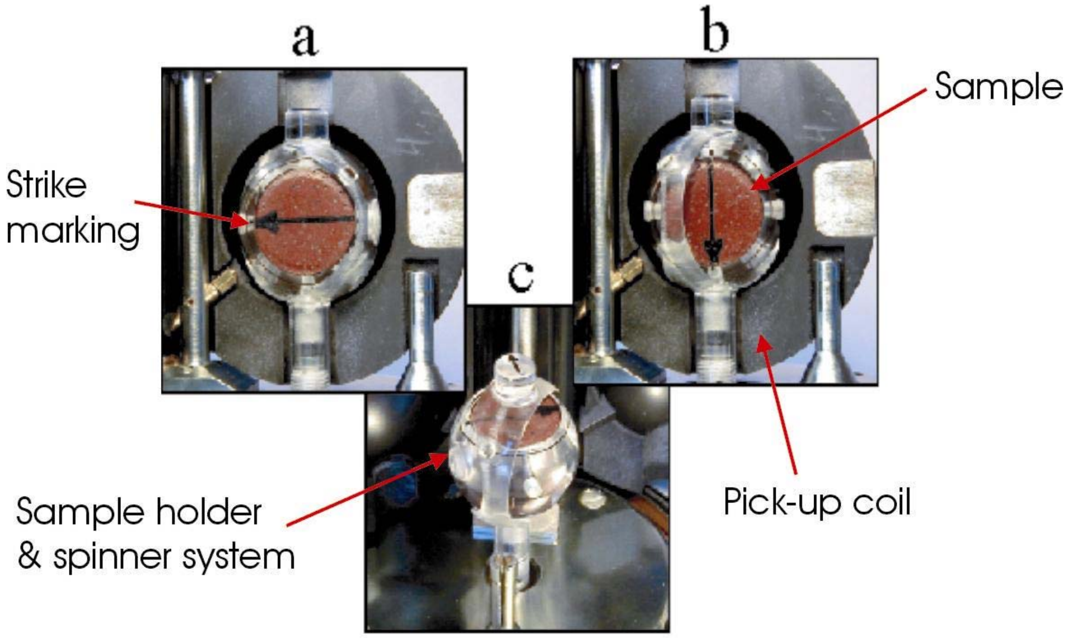

Figure 2.26 The three positions in which the sample is measured in the sensors. A) Initial position, X and Z components are measured, b) second position Y and Z components are measured, c) final position were the X and Y components are measured. The black arrows on the samples indicate the strike.

2.3.5 Thermomagnetic analysis

Thermomagnetic analysis (TMA) was carried out on a horizontal translation balance (Curie Balance, Figure 2.27) in order to determine the Curie temperature of samples and hence the carrier of magnetisation. The analysis involves placing a small piece of the sample into a furnace located inside an electromagnet. The sample is mounted on the end of the balance beam which is supported by quartz wires; the beam has a damper to dampen any vibrations.

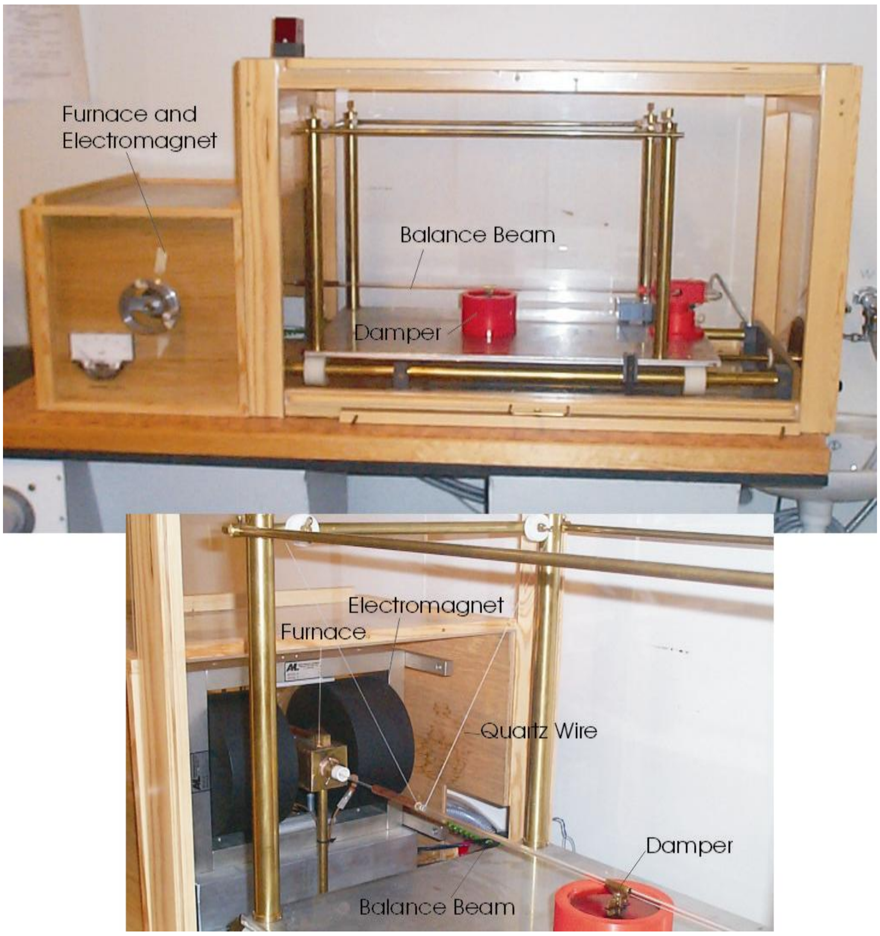

Figure 2.27 Curie Balance, with a close up view (bottom image).

The magnetisation of a sample is determined by exposing it to a strong magnetic field gradient while the temperature is increased. At the start of the experiment the sample is pulled in towards the electromagnet and this initial point is assigned as the saturation magnetisation. As the temperature is increased the sample decreases in magnetisation and moves out of the oven, while the amount of movement relative to the starting point is calculated electronically. Once the magnetisation has reached zero the furnace starts to cool down and the sample is pulled in as before. The results are plotted as a thermomagnetic plot, from which the Curie temperatures of the minerals present in the sample may be determined (by major decrease in magnetisation). During heating, chemical and textural changes commonly occur in magnetic minerals, resulting in different cooling and heating paths.

2.4 Palaeomagnetic Analysis

Once demagnetisation has been successfully completed, the end result is a set of progressively remanent magnetic measurements. In order to analyse the data, a graphical technique is used to show the change in direction and magnitude of a three-dimensional vector on a two-dimensional plot. A number of vector component diagrams have been developed to show such changes. The Zijderveld diagram is the most common (Irving, 1964).

2.4.1 Zijderveld diagram

In order to construct a Zijderveld diagram each NRM vector that was recorded for each sample must be broken down into a north (*N*), east (*E*) and vertical (*Z*) component.

$$N_i = NRM_i \cos I_i \cos D_i, \qquad (2.11)$$

$$E_i = NRM_i \cos I_i \sin D_i, \qquad (2.12)$$

$$Z_i = NRM_i \sin I_i. \qquad (2.13)$$

NRM_i is the intensity of the i^{th} *NRM* measurement, I_i and D_i are the inclination and declination of the i^{th} *NRM* measurement.

Zijderveld diagrams are composed of two projections (horizontal and vertical), projected onto a single (2-dimensional) vector component diagram (Figure 2.28). The horizontal component is projected onto the horizontal plane by plotting N_i versus E_i. When viewing this vector one has to imagine looking down on the diagram as from above (red line in Figure 2.27). The vertical projection is projected onto the vertical plane be plotting Z_i versus N_i (or E_i). During observation one has to imagine the plot as a cross-section (green line in Figure 2.28). Horizontal projections are generally plotted as a solid symbols while vertical projections are plotted as open symbols. Points from each projection represent the end of a vector (Zijderveld, 1967).

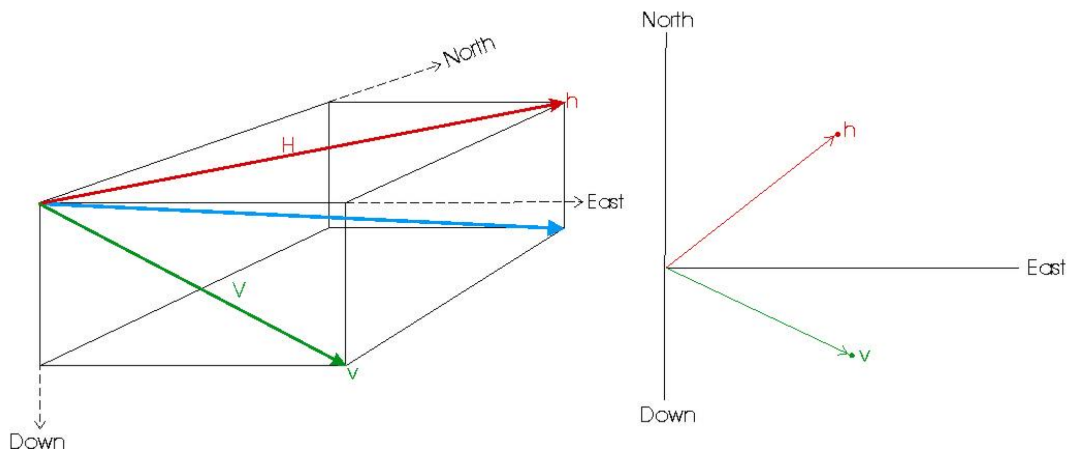

Figure 2.28 A schematic representation of NRM vector on a Zijderveld plot. The diagram to the left indicates the 3-D NRM vector (blue), which is broken down into the horizontal vector (red) and vertical vector (green). The diagram to the right is the Zijderveld plot, with the two end points, horizontal and vertical being plotted in red and green, respectively.

2.4.2 Picking linear components of NRM and ChRM

By plotting the NRM vectors it is possible to recognise different components of NRM, and ultimately determine the ChRM in the samples. In order to pick the NRM and ChRM components, one has to examine the horizontal and vertical plots (Figure 2.29). A component may be identified if the horizontal and vertical projections are co-linear over the same measurements (red lines in Figure 2.29). The ChRM component also has to be collinear but at the same time the points have to project towards the origin (green lines in Figure 2.29). If they do not project towards the origin, they are considered as a younger overprint and not the ChRM components, i.e. not the magnetisation acquired at time of formation.

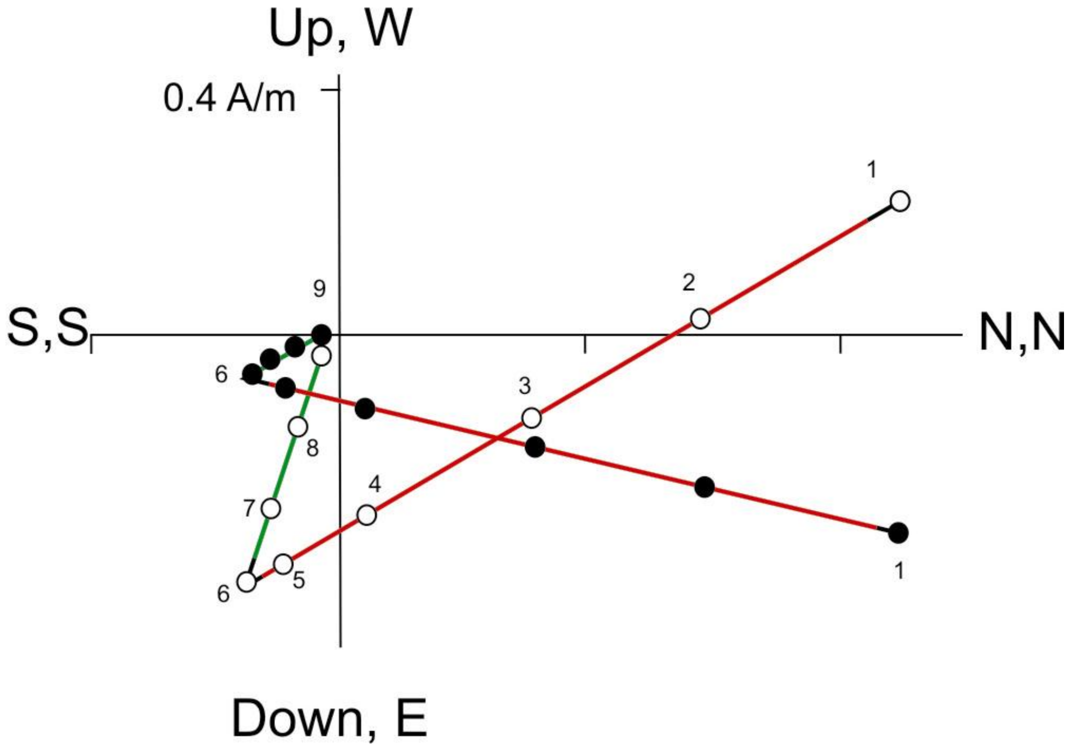

Figure 2.29 A Zijderveld plot for synthetic data, indicating the process of line picking. NRM components may be identified if the horizontal and vertical projections are co-linear over the same measurements/steps. The red lines indicate a secondary magnetisation while the green lines indicate the ChRM magnetisation. Solid circles indicate horizontal components while open circles indicate vertical components.

Once components have been picked it is possible to determine the inclination of both ChRM and the low-stability secondary component. The true inclination can be determined as follows:

$$\tan I = \tan I_{app} \left|\cos D\right|, \tag{2.14}$$

where I_{app} is the apparent inclination.

2.4.3 Blocking temperature and coercivity spectra.

Generally a sharp change in trajectory of the vector end points is not observed but rather a curved trajectory is seen. Overlapping blocking temperature or coercivity spectra of the grains carrying different components of NRM causes the curving in a Zijderveld diagram. The degree of overlap determines the amount of curvature (Figure 2.30). The amount of curvature is also affected by how detailed the demagnetisation steps are.

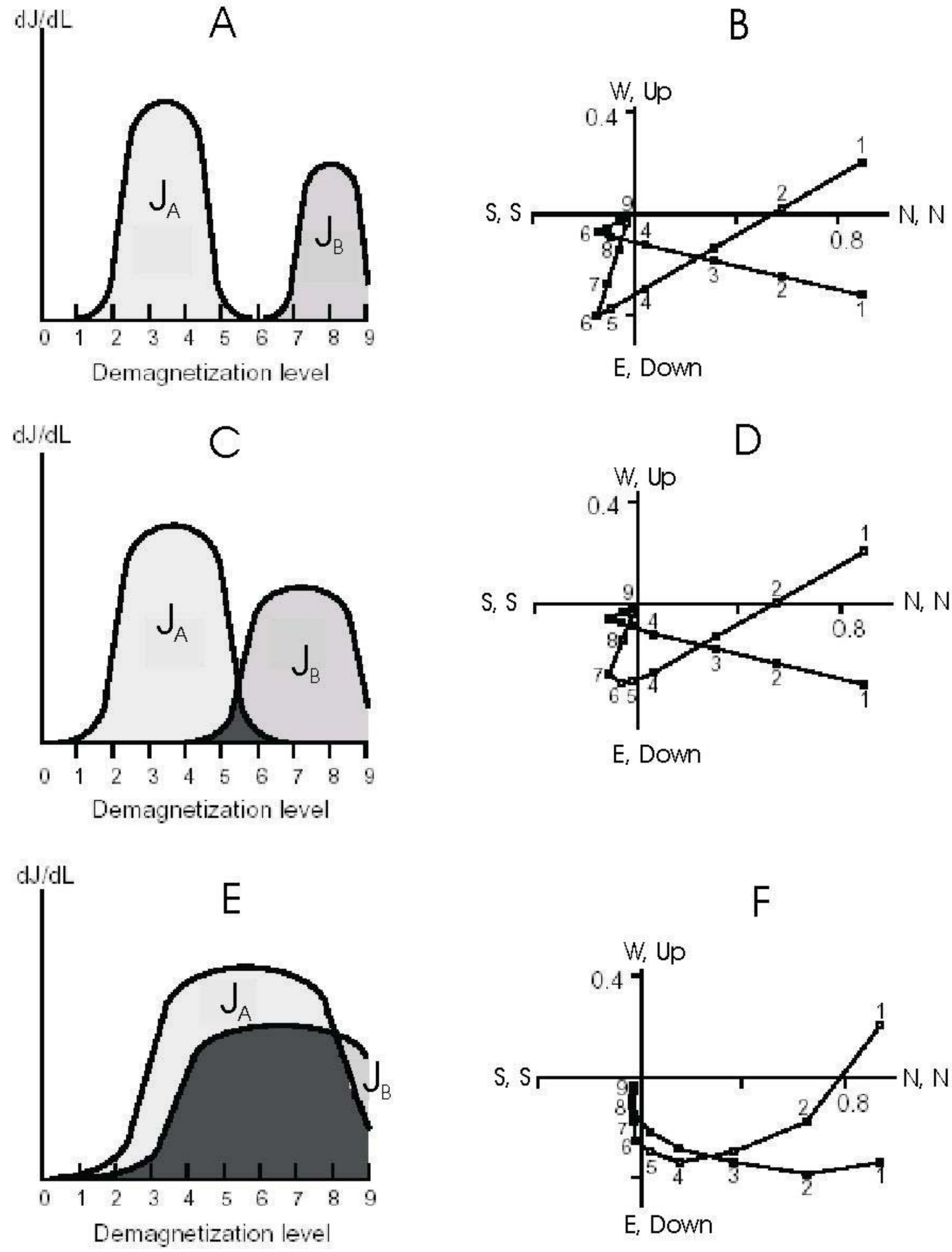

Figure 2.30 A schematic representation of how the overlapping blocking temperature / coercivity spectra can effect a Zijderveld plot after Dunlop (1979).

Figure 2.30 only shows two components of NRM; however, it is possible to have three or more components of NRM.

2.4.4 Principal component analysis

The picking of the best-fit co-linear line in a vector diagrams can be obtained by principal component analysis. This method is used to find and estimate the directions of lines of best least-squared fit along a demagnetisation path. When fitting a line to the data there are three options on how to treat the origin:

- Anchored line fit: the line is forced to pass through the origin,
- Origin line fit: the origin is treated as a separate data point,
- Free line fit: the origin is not considered in calculations.

During the line calculation, data points farthest from the origin are given the maximum weighting. This is because they have a higher signal to noise ratio. The precision at which the best-fit line is fitted is determined by a quantitative measure known as the maximum angular deviation (MAD). MAD is the maximum angular deviation of the direction that a line would have if the fit along each axis were off by one standard deviation (McElhinny and McFadden, 2000). Components were only excepted if they had a MAD of less then 5 for this study.

2.4.5 Field tests

A number of field tests can be applied to the data in order to provide information on the timing of ChRM acquisition and the stability of the magnetisation over all or part of the geological time interval since the rock was formed.

Fold test or bedding-tilt test

The fold test (applied when measurements have been obtained from both ends of a fold) or bedding-tilt test (when only one side of a fold is evaluated) is used to evaluate the relative time of acquisition of remanent magnetism relative to folding. In other words a bed can be evaluated as being horizontal or at an angle at the time of magnetisation. If remanent magnetism was acquired prior to folding, the directions of ChRM (from sites on opposite limbs of a fold) when plotted on a stereo plot would be dispersed but would converge when a bedding correction is applied. The bedding correction restores the bedding to the horizontal position and in the process moves the ChRM by the same amount. Figure 2.31 illustrates a positive fold test (McElhinny, 1973).

One cannot decide that there is an improvement in the overall grouping if there is merely an increase in clustering, as this improvement may only be a consequence of the particular random samples chosen (McFadden and Jones, 1981). In order to determine whether the improvement is "real", a statistical test (McElhinny, 1964b) uses a comparison of estimates for the population precision parameter (κ), before and after unfolding at a specified confidence level (generally at 95%, this value is known as the critical ratio) to determine whether or not the fold test has statistical significance. It should be noted that the fold test of McElhinny (1964b) has a fundamental error in its assumption that the sample population obeys a Fisher distribution in both the in-situ and tilt corrected forms cannot be true for a positive test. However, in practice it is typically conservative (McElhinny and McFadden, 2000) and has therefore been used in this study.

Another statistical procedure is to determine whether the mean direction of a group of sites from one limb may be distinguished from the mean direction of a group from another limb of the fold (McFadden and Jones, 1981). This is a true fold test; the other is a bedding-tilt test.

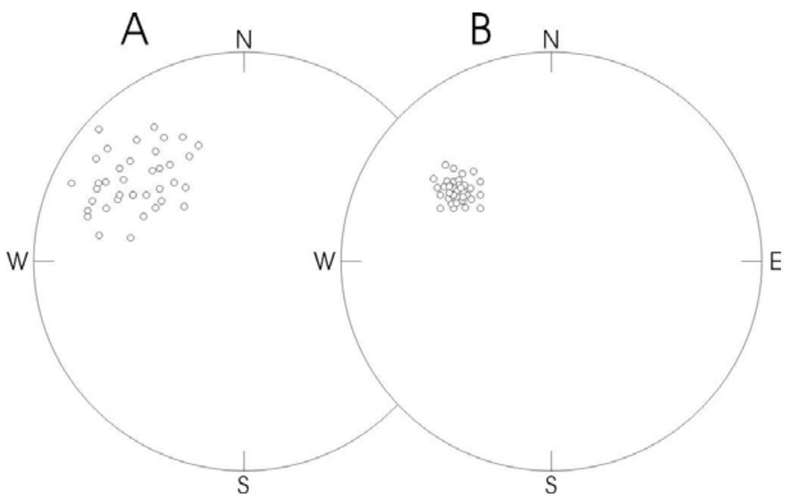

Figure 2.31 A synthetic example of a positive fold test. a) ChRM uncorrected directions. b) ChRM directions after the application of structural correction to restore beds to the horizontal position (McElhinny, 1973).

Reversal test

The time-averaged geocentric axial dipole has both normal and reversed polarity over different time intervals the difference in the two is 180°. Therefore to determine if a sample has a reversal recorded, one has to have a sufficient average of secular variation during both normal and reversed polarity intervals. The average direction of the primary NRM of the normal polarity for the sample is expected to be 180° different in direction to that of the primary NRM of the reversed polarity. However, the acquisition of secondary NRM components will result in the differences being less then 180° (Figure 2.32). ChRM directions are said to "pass" the reversal test if the mean direction computed from the normal-polarity sites is 180° from the direction of the mean reversed-polarity sites. ChRM directions that "fail" the reversal test have an average direction of the normal and reversed polarity that differs by an angle significantly less then 180° (Butler, 1992).

Failure of the reversal test can indicate:

- The acquired magnetisation is not from the same period.
- Inadequate sampling of geomagnetic secular variations during the different polarity intervals
- The presence of an unremoved secondary NRM component.

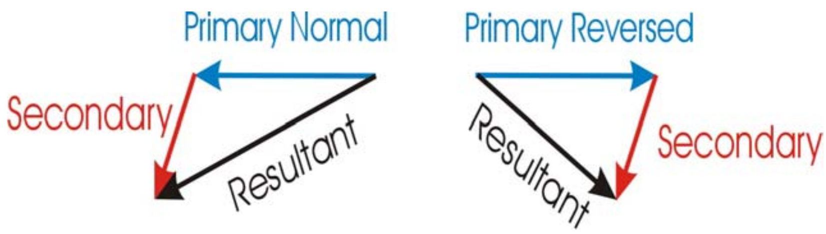

Figure 2.32 A schematic representation of the reversal test of palaeomagnetic stability. Primary fields are antiparallel. However, with the addition of secondary components the normal and reversed polarities are no longer antiparallel.

In practice, the test is performed by inverting the observations from one polarity and testing whether the two sets of observations could have been drawn from distributions sharing a common mean direction. McFadden and Lowes (1981) provide a test that involves the forming of a null hypothesis that the two sets of observations are in fact drawn from distributions that share a common mean direction. Observations are considered at some level of confidence (generally 95%) to determine whether they are inconsistent with this hypothesis. If they are not inconsistent at that level, the null hypothesis is accepted (i.e. that they share a common pole at 95% confidence level). Otherwise, it is rejected in favour of the alternative hypothesis that the distribution does not share a common mean direction. However, it has been found that if only a small amount of information is available then almost without exception the null hypothesis cannot be rejected, irrespective of the validity of this hypothesis. A simple, yet effective measure of the information available is the angle γ_c between the mean directions of the two sets of observations at which the null hypothesis of a common mean direction would be rejected with 95% confidence. A new classification of the fold test (McFadden and McElhinny, 1990) uses this angle. This test is only conducted if there are fewer than five but more then one observation in either polarity. The test involves the calculation of the critical angle between the two mean directions γ_c. If the observed angle between the two polarities γ_o is less then γ_c, then the reversal test is considered to be positive and is classified further by considering the angle γ_c. A positive reversal test is then further categorized into four different classes:

- *'A'* if $\gamma_c \leq 5°$,
- *'B'* if $5° < \gamma_c \leq 10°$,
- *'C'* if $10° \leq \gamma_c \leq 20°$
- *' indeterminate'* if $\gamma_c > 20°$,

In other words an "A" classification has an angle of 180° - 175° between the two polarities, a "B" classification 175° - 170°, etc.

2.4.6 Statistics

Statistical analysis of palaeomagnetic data is required in determining a mean direction from a set of observed directions (NRM and ChRM), based on a probability density function. This function describes the distribution of data for a hypothetical, infinite set of data called a population. In palaeomagnetic investigation the Fisher distribution is commonly used.

The Fisher distribution

The Fisher distribution developed by R.A. Fisher (1953) applies a probability density function to palaeomagnetic directions. Each direction is given unit weight and is represented by a point on a sphere of unit radius. The Fisher distribution function $P_{dA}(\theta)$ gives the probability per unit angular area of finding a direction within an angular area, dA, centred at an angle θ from the true mean. Directions are distributed according to the probability density function

$$P_{dA}(\theta) = \frac{\kappa}{4\pi \sinh(\kappa)} e^{\kappa \cos\theta}, \tag{2.15}$$

where θ is the angle from true direction (0 at true mean), and κ is the precision parameter. The notation $P_{dA}(\theta)$ is used to emphasize that this is a probability per unit angular area.

The distribution of directions is azimuthally symmetric about the true mean. κ is a measure of the concentration of the distribution about the true mean direction. κ is 0 for a distribution of directions that are uniform over the sphere (random) and approaches ∞ for directions concentrated at a point.

The angle from the true mean within which a chosen percentage of directions lie can also be calculated from the Fisher distribution (Butler, 1992). The angle within which 50% of directions lie is analogous to the interquartile of the normal distribution and is:

$$\theta_{50} = \frac{67.5°}{\sqrt{\kappa}}. \tag{2.16}$$

The angle analogous to the standard deviation of the normal distribution, which is commonly called the angular standard deviation, is given by:

$$\theta_{80} = \frac{81°}{\sqrt{\kappa}}. \tag{2.17}$$

The final critical angle of interest is that containing 95% of directions and is given by:

$$\theta_{95} = \frac{140°}{\sqrt{\kappa}}. \tag{2.18}$$

Computing a mean direction

The above equations (2.16 - 2.18) apply to a population of directions that are distributed according to the Fisher probability density function. However, we only have a small sample of directions for which we must calculate:

- A mean direction,
- A statistic indicating the amount of scatter of the directions,
- A confidence limit for the calculated mean direction.

By employing the Fisher distribution, the following calculation scheme can provide the desired quantities (Butler, 1992). The mean of a set of directions is found by vector addition. To compute the mean direction from a set of *N* unit vectors, the direction cosines of the individual vectors are first determined by

$$l_i = \cos I_i \cos D_i \tag{2.19}$$

$$m_i = \cos I_i \sin D_i \tag{2.20}$$

$$n_i = \sin I_i \tag{2.21}$$

Where D_i is the declination of the i^{th} vector; I_i is the inclination of the i^{th} vector; and l_i, m_i, and n_i are the direction cosines of the i^{th} vector with respect to north, east, and vertical direction. The mean direction cosines, *l, m*, and *n*, of the mean direction are then given by

$$l = \frac{\sum_{i=1}^{N} l_i}{R}, \tag{2.22}$$

$$m = \frac{\sum_{i=1}^{N} m_i}{R}, \tag{2.23}$$

$$n = \frac{\sum_{i=1}^{N} n_i}{R}, \tag{2.24}$$

where *R* is the resultant vector with length *R* given by

$$R^2 = \left(\sum_{i=1}^{N} l_i\right)^2 + \left(\sum_{i=1}^{N} m_i\right)^2 + \left(\sum_{i=1}^{N} n_i\right)^2. \tag{2.25}$$

The declination and inclination of the mean direction can therefore be computed by:

$$D_m = \tan^{-1}\left(\frac{m}{l}\right) \tag{2.26}$$

and

$$I_m = \sin^{-1}(n). \tag{2.27}$$

Dispersion estimates

A measure of the dispersion of the population of directions from which the sample dataset was calculated can be determined from a precision parameter (κ). From a finite set of directions, κ is unknown, but a best estimate of κ can be calculated from

$$\kappa = \frac{N-1}{N-R}, \tag{2.28}$$

where N is the number of vectors and R is the resultant vector length. As R approaches N for a tightly clustered set of directions, k increases.

The confidence level of the mean direction may be defined as an angular radius (α) from the calculated mean direction, with a specified probability level (p). For a set of data containing N directions, the angle $\alpha_{(1-p)}$ within which the unknown true mean lies at confidence level (1-p) is given by

$$\cos\alpha_{(1-p)} = 1 - \frac{N-R}{R}\left[\left(\frac{1}{p}\right)^{\frac{1}{N-1}} - 1\right]. \tag{2.29}$$

In palaeomagnetic studies, the probability level, *(1-p),* is 0.95 (95%) used and is noted as α_{95}. An approximation of equation 2.29 can be given by

$$\alpha_{95} \approx \frac{140°}{\sqrt{\kappa N}}, \tag{2.30}$$

α_{95} is a measure of the precision with which the true mean direction has been estimated. This implies that the true mean direction has a 95% confidence level of occuring within the α_{95} value (Butler, 1992).

Calculation of the palaeomagnetic pole position

The declination and inclination of the dipolar magnetic field varies with position on the globe, although the position of the magnetic pole of the geocentric dipole is independent of position. The pole position is the geographic location of the projection of the negative end of the geocentric dipole onto the Earth's surface (point *P* in Figure 2.33). The calculation of a pole position is the best way to compare results from various global positions.

Before one can calculate a pole position, a sign convention needs to be defined for geographic locations:

- Latitude: -90° at the geographic South Pole, 0° at the equator and +90° at the geographic North Pole.
- Longitude: Coordinates to the east of the Greenwich meridian are positive and to the west are negative.

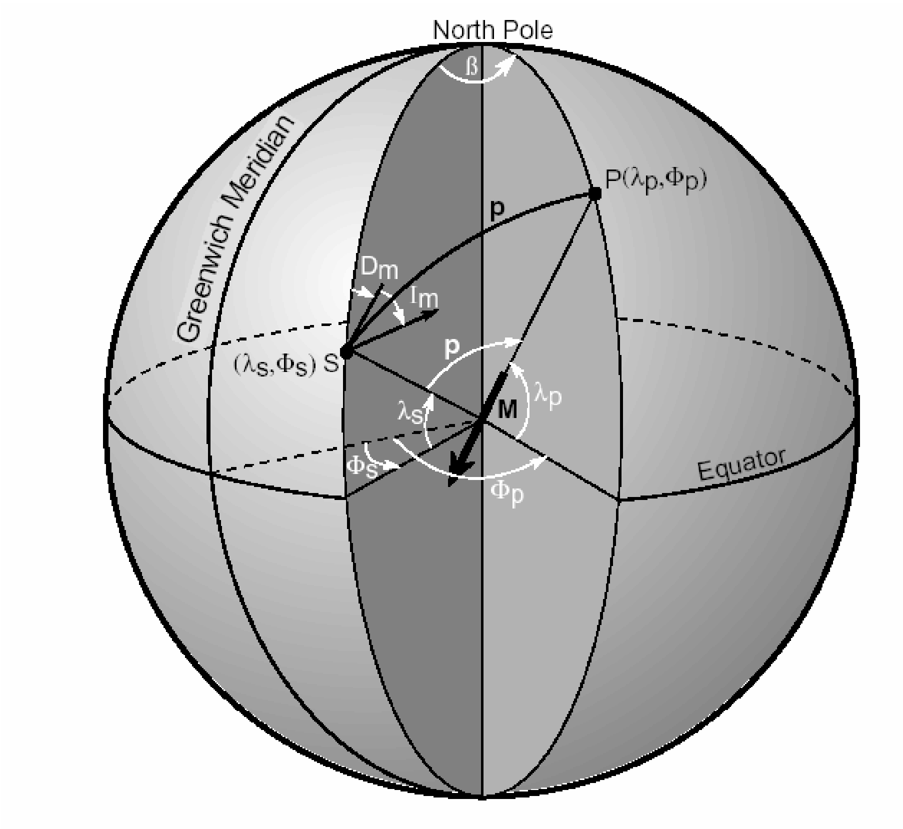

Figure 2.33 The essential angles needed to determine the pole position for point S (Butler, 1992).

The pole position (λ_p,ϕ_p) can be calculated from a site-mean direction (I_m, D_m) measured at a particular site (λ_s,ϕ_s). Firstly the magnetic colatitude, p - the great-circle distance from site to pole, must be determined. From the dipole equation

$$\tan I = \left(\frac{H_v}{H_h}\right) = \left(\frac{2\sin\lambda}{\cos\lambda}\right) = 2\tan\lambda\,, \tag{2.31}$$

we can derive:

$$p = \cot^{-1}\left(\frac{\tan I_m}{2}\right) = \tan^{-1}\left(\frac{2}{\tan I_m}\right). \tag{2.32}$$

The pole latitude is given by:

$$\lambda_p = \sin^{-1}(\sin\lambda_s \cos\lambda_p + \cos\lambda_s \sin p \cos D_m). \tag{2.33}$$

The longitudinal difference between the pole and site, β, is positive towards the east, and is given by

$$\beta = \sin^{-1}\left(\frac{\sin p \sin D_m}{\cos\lambda_p}\right). \tag{2.34}$$

There are two possibilities for pole longitude, ϕ:

- If $\cos p \geq \sin\lambda_S \sin\lambda_p$ then

$$\phi_p = \phi_s + \beta. \tag{2.35}$$

- Or, if $\cos p < \sin\lambda_s \sin\lambda_p$ then

$$\phi_p = \phi_s + 180° - \beta. \tag{2.36}$$

The site-mean directions I_m and D_m have an associated confidence limit α_{95}. The circular confidence limit about the site-mean direction is transformed into an ellipse of confidence about the calculated pole position (Butler, 1992). The semi-axis of the ellipse of confidence has an angular length along the site-to-pole great circle given by:

$$dp = \alpha_{95}\left(\frac{1+3\cos^2 p}{2}\right), \tag{2.37}$$

and the semi-axis perpendicular to the great circle is given by

$$dm = \alpha_{95}\left(\frac{\sin p}{\cos I_m}\right). \tag{2.38}$$

CHAPTER 3: GEOLOGY AND SAMPLING OF THE BUSHVELD COMPLEX

Over the past 40 years the Bushveld Complex has been the subject of numerous studies, including an initial palaeomagnetic investigation in 1959 followed by five in the early 1980s, as discussed in Chapter 1. Based on previous palaeomagnetic studies (Chapter 1) and the fact palaeomagnetic equipment and data analysis have improved over the past 20 years, a simple re-evaluation of the existing data was not sufficient to accurately evaluate the palaeomagnetism of the Bushveld Complex. Thus, in order to take advantage of new laboratory and data analysis techniques in palaeomagnetic methods, a new study was conducted. The following chapter gives a brief description of the basic geology of the Bushveld Complex and the sampling strategy used.

3.1 General Geology of the Bushveld Complex

The 2,058 ± 0.8 Ma Bushveld Complex (BC) (Buick et al., 2001) , covering an area of ~ 65,000 km^2 in northern South Africa, is the world's largest known layered intrusion and contains the majority of the world's resources of platinum group elements (PGE), chromium and vanadium (Lee, 1996). The complex as a whole is composed of five major magmatic suites: the Rooiberg Volcanic Suite (Buchanan et al., 2002); the Rustenburg Layered Suite (mafic component of the complex and the subject of study for this project); marginal pre- and syn-Bushveld sills and intrusions (Frick, 1973; Sharpe, 1981); the Roshoop Granophyre Suite (Walraven, 1985) and the Lebowa Granite Suite (Walraven and Hattingh, 1993b).

The Rustenburg Layered Suite (RLS), also known as the mafic rocks of the Bushveld Complex occurs in four discrete regions or Lobes (Figure 3.1): The Western Lobe, which extends from near Pretoria westwards to Rustenburg and around the Pilanesberg alkaline complex, to and along the southern flank of the Makoppa Dome of the Archaean granitiods and gneisses; a south-eastern (Bethal) Lobe, which is largely covered by Mesozoic rocks (not shown in Figure 3.1); an

Eastern Lobe that extends in a northwards arc west of Belfast up to Atok, and a northern Lobe that extends south of Mokopane to Villa Nora (Tankard et al., 1982).

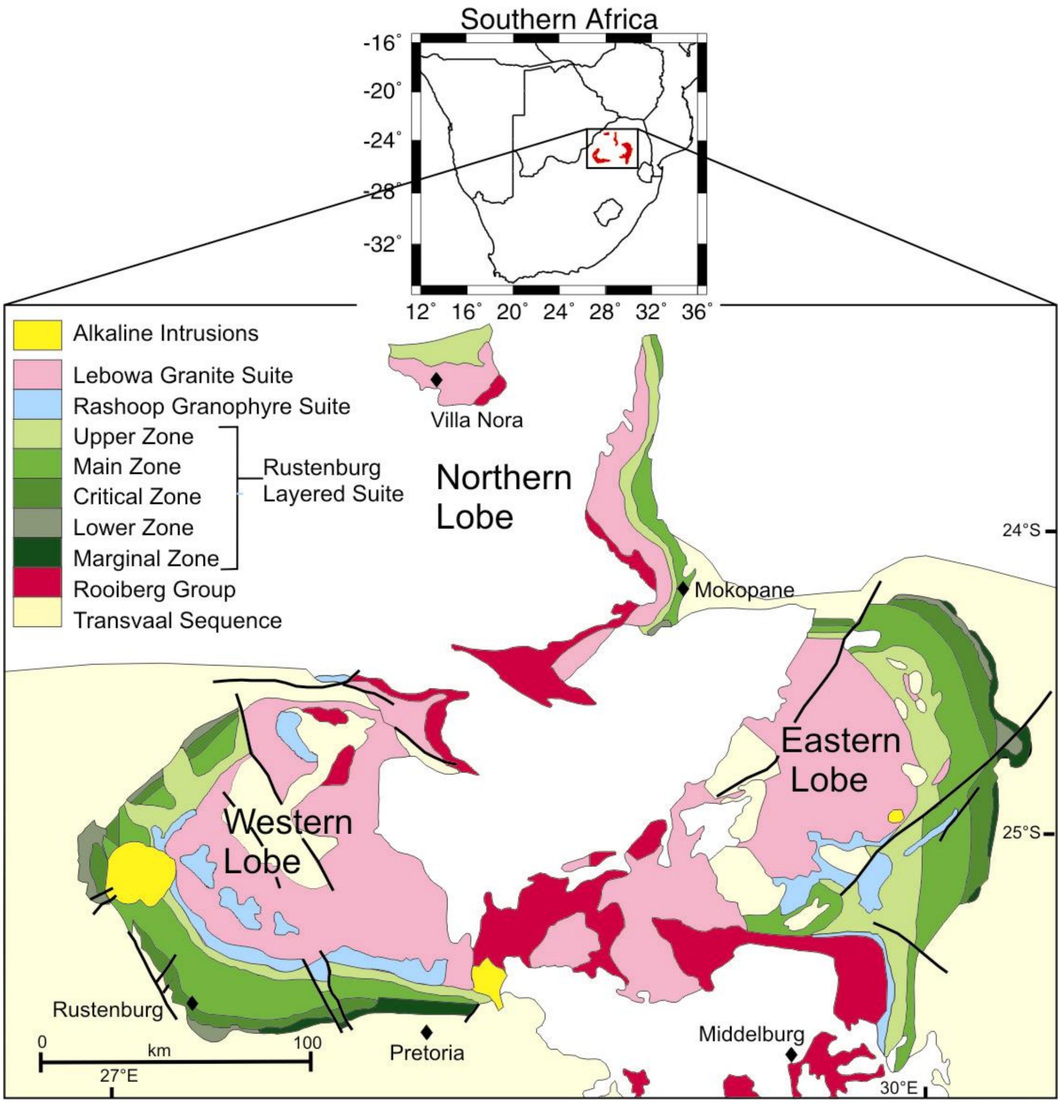

Figure 3.1 Simplified geological map of the Bushveld Complex, including the mafic zones (Rustenburg Layered Suite) and felsic phases (Lebowa Granite Suite, Rooiberg group and Rashoop Granophyre Suite) after Cairncross and Dixon (1995).

The RLS has been stratigraphically subdivided by SACS (1980) into five zones based on cumulus mineral assemblages:

- The Marginal Zone comprises fine grained plagioclase-orthopyroxene cumulates, forming a thin layer (0 to 800 m thick in one extreme case) in between the country rock and the rest of the RLS.

- The Lower Zone approximately 1.9 km thick is dominated by olivine-rich cumulates (harzburgite, dunite) and orthopyroxenite.
- The Critical Zone approximately 1.3 km thick is characterized by the regular layering of dunites, harzburgites, pyroxenites, chromitites, norites and anorthosites. It is the carrier of two of the world's largest platinum-bearing ore bodies, the Upper Group 2 Chromitite (UG2) and the Merensky Reef, as well as a number of chromite reserves within the Lower (LG), Middle (MG) and Upper (UG) Group chromittite layers (Hatton and Von Gruenewaldt, 1987).
- The Main Zone comprises approximately 2.5 km thick succession of dominantly gabbronoritic rocks.
- The Upper Zone approximately 1.5 km thick consists of magnetite gabbro (and olivine diorite in the Eastern Lobe); the base had been defined at the appearance of cumulus magnetite according to SACS (1980).

In recent years there has been much debate on the position of the Upper and Main Zone boundaries by Kruger (1990), and Mitchell & Scoon (1991). Kruger (1990) produced Sr isotopic arguments for capping the Main Zone (Figure 3.2) at the base of the Pyroxenite Marker and hence redefining both the Main and Upper Zones.

Based on his initial isotopic findings, Kruger (1994) divided the RLS into four major zones that correlated with major unconformities that are associated with major magma influxes. They are:

- "harzburgitic" Lower Zone with the "orthopyroxenitic" Lower Critical Zone forms the ultramafic part of the intrusion (BvLz magma influx);
- "noritic" Upper Critical Zone (BvCz),
- the "gabbronoritic" Main Zone (BvMz)
- and the differentiated "ferro-gabbronoritic" Upper Zone (BvUz).

A summary of the different zones and magma influxes are shown in Figure 3.2; a more detailed description of the subdivisions can be found in Kruger (2005).

For this study the boundary between the Upper and Main Zone has been adopted according to the SACS (1980) classification and has been made at the first appearance of cumulus magnetite.

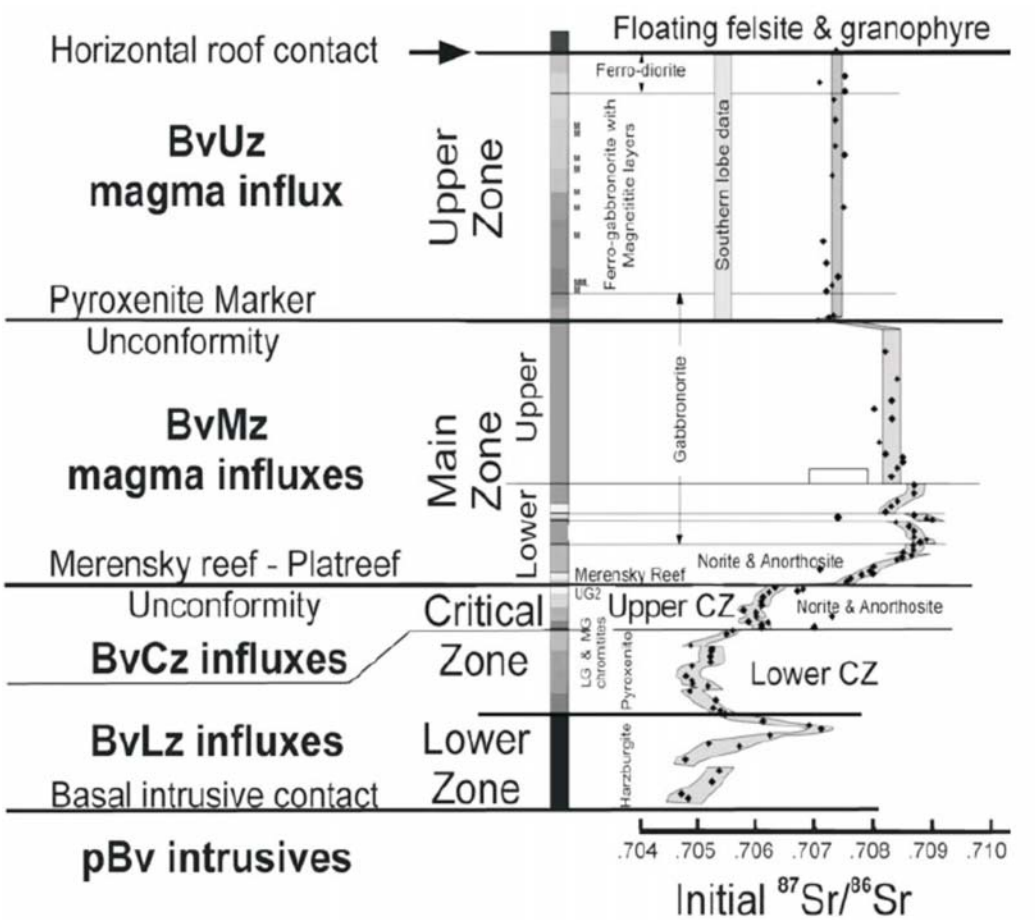

Figure 3.2 Stratigraphic and isotope summary showing the variation in isotope compositions and the location of major unconformities of the Rustenburg Layered Suite (Kruger, 2005). The isotope profile is from Kruger (1994).

The dips of the RLS for the Eastern and Western Lobes are towards the centre of the complex, usually at low angles between 10° and 25°. In the northern Lobe, rocks dip towards the west and can display dips as steep as 60° in the vicinity of Villa Nora (Tankard et al., 1982).

Precise geochronological data obtained from the felsic rocks associated with the Bushveld Complex, have bracketed the age of the Rustenburg Layered Suite between 2,060 ± 2 Ma (Walraven, 1997) and 2,054.4 ± 1.8 Ma (Walraven and

Hattingh, 1993b). These ages were obtained from pre-RLS granophyric sills which intrude the 2,061 ± 2 Ma felsic volcanics of the Rooiberg Group (Walraven, 1997), and from the Lebowa Granite Suite (which succeed the RLS). The RLS itself has been dated at 2,058.9 ± 0.8 Ma using U-Pb isotopes from newly grown titanite found in calc-silicate xenoliths (Buick et al., 2001). Another geochronological study reported an $^{40}Ar/^{39}Ar$ age on biotite crystals from the UG2 layer as 2,044.1 ± 2.9 Ma (Nomade et al., 2004). However upon examination these authors concluded that the age reported was due to a miscalibration of the $^{40}Ar/^{39}Ar$ system. By applying an *ad hoc* correction, they obtained the same age determined by Buick et al. (2001) and thereby concluded that the RLS experienced a very rapid cooling (1000°C/m.y.) from 700° to <500°C.

3.2 Sampling of the Bushveld Complex

Large areas of the Bushveld Complex are covered by considerably thick soil layers (5 to 15 meters), and due to lack of positive topography, exposures and hence sampling localities are generally isolated. This resulted in samples for this study being obtained from dimension stone quarries, road cuttings and limited stream sections; in a few instances samples were obtained from low-lying hill outcrops in the northern Lobe. Topographic highs were not considered due to these areas being prone to lightning strikes (lightning can produce high IRM values that can mask or destroy primary NRM). With the scarcity of suitable sampling locations and the limited number of road and river exposures in the Bushveld Complex, a number of sites sampled in this study are identical to those of Hattingh (1983). This has enabled a direct comparison of new and old data.

A total of 101 sites were sampled throughout the Bushveld Complex (Figure 3.3), with the majority of them being obtained from dimension stone quarries (42), river sections (23), road exposures (20), low lying hills (14) and one from a railroad cutting. Stratigraphic locations of sites within the complex are shown in Figure 3.4 and Figure 3.5. A grand total of 915 core samples were obtained and subjected to palaeomagnetic analysis, the results of which are discussed in Chapter 4.

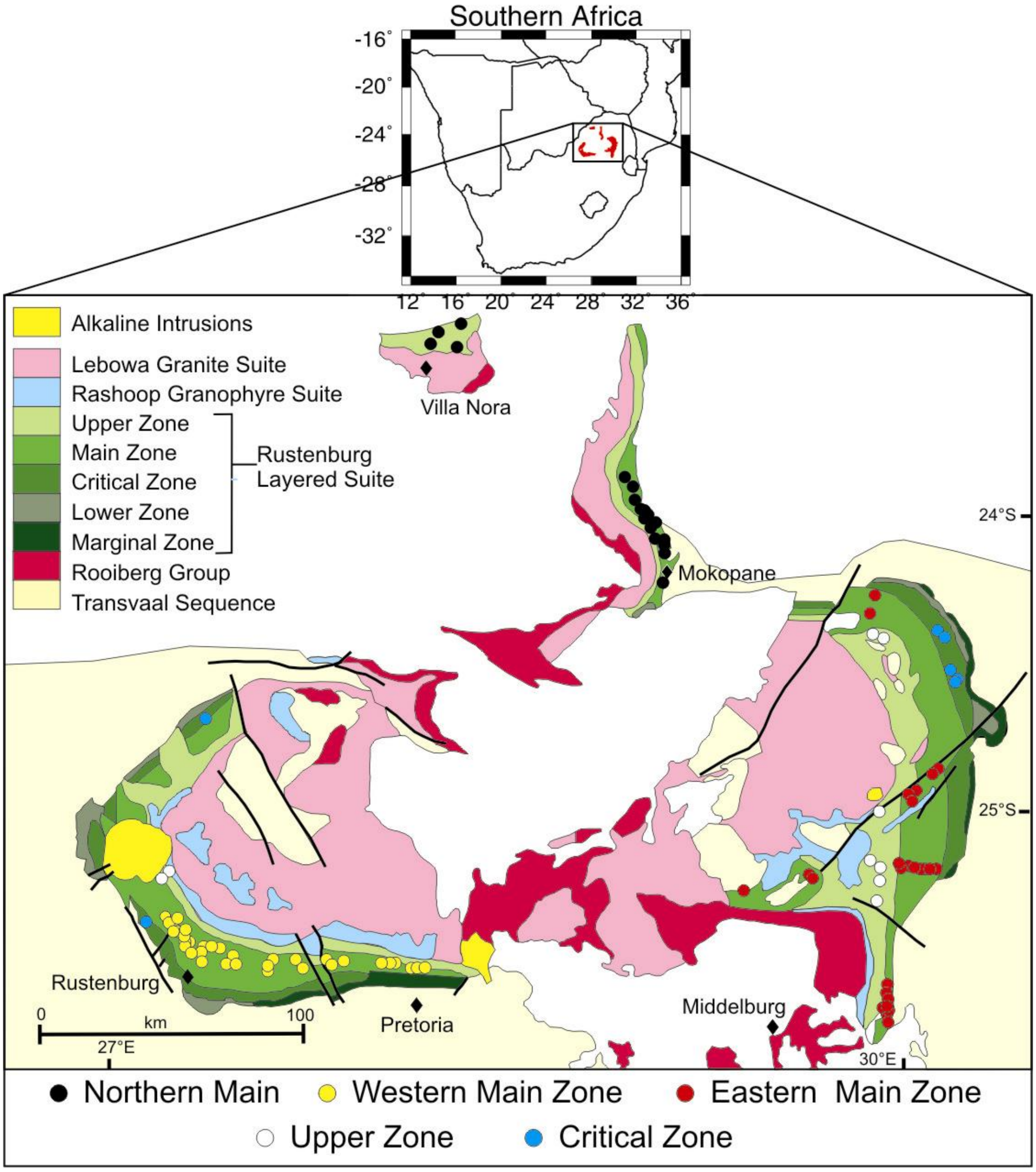

Figure 3.3 Simplified geological map of the Bushveld Complex, indicating site locations after Cairncross and Dixon (1995).

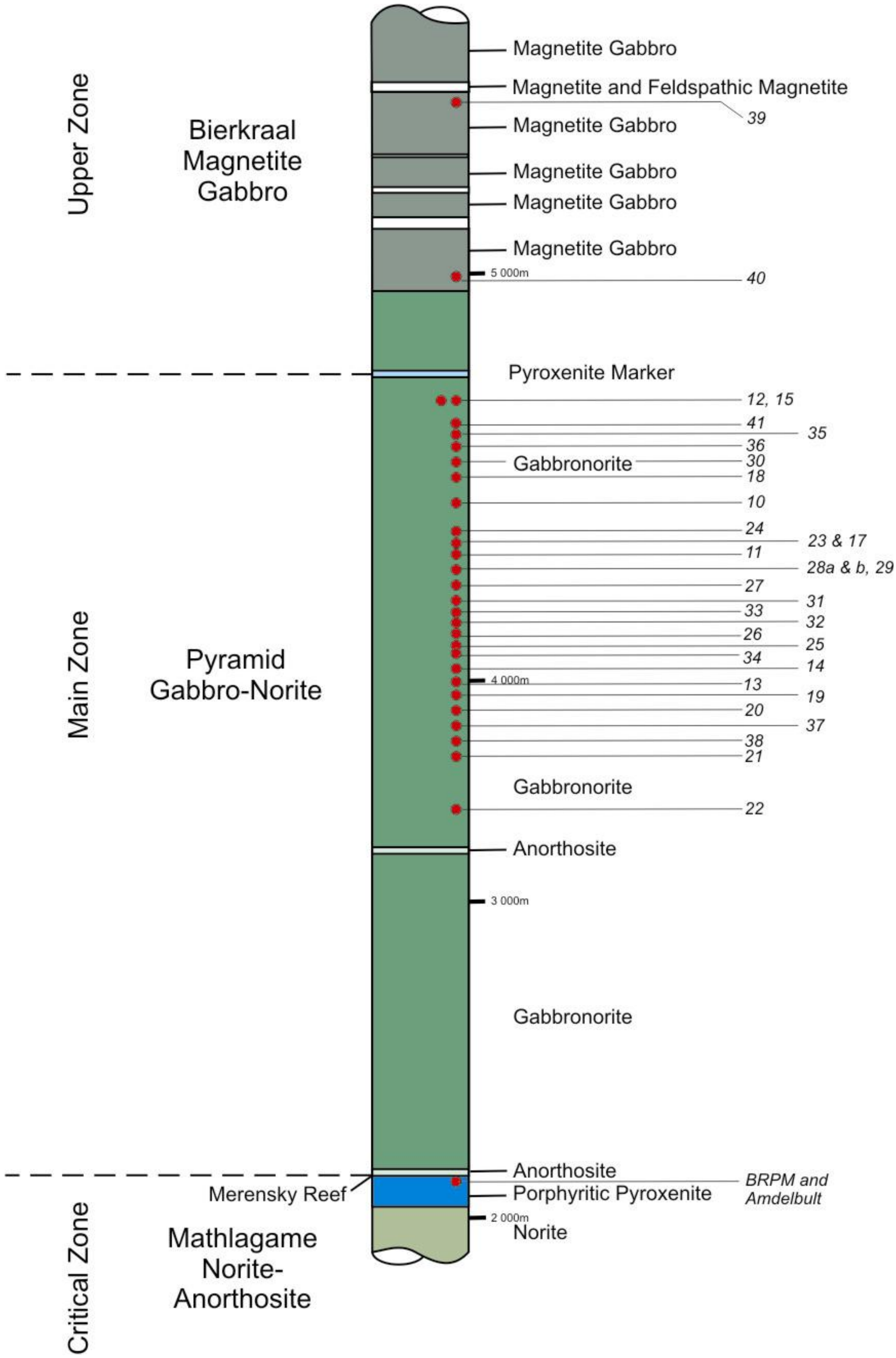

Figure 3.4 Lithostratigraphic column of the Rustenburg Layered Suite in the Western Bushveld with site locations (modified after SACS, 1980) stratigraphic positions are based on Hattingh (1983) site locations.

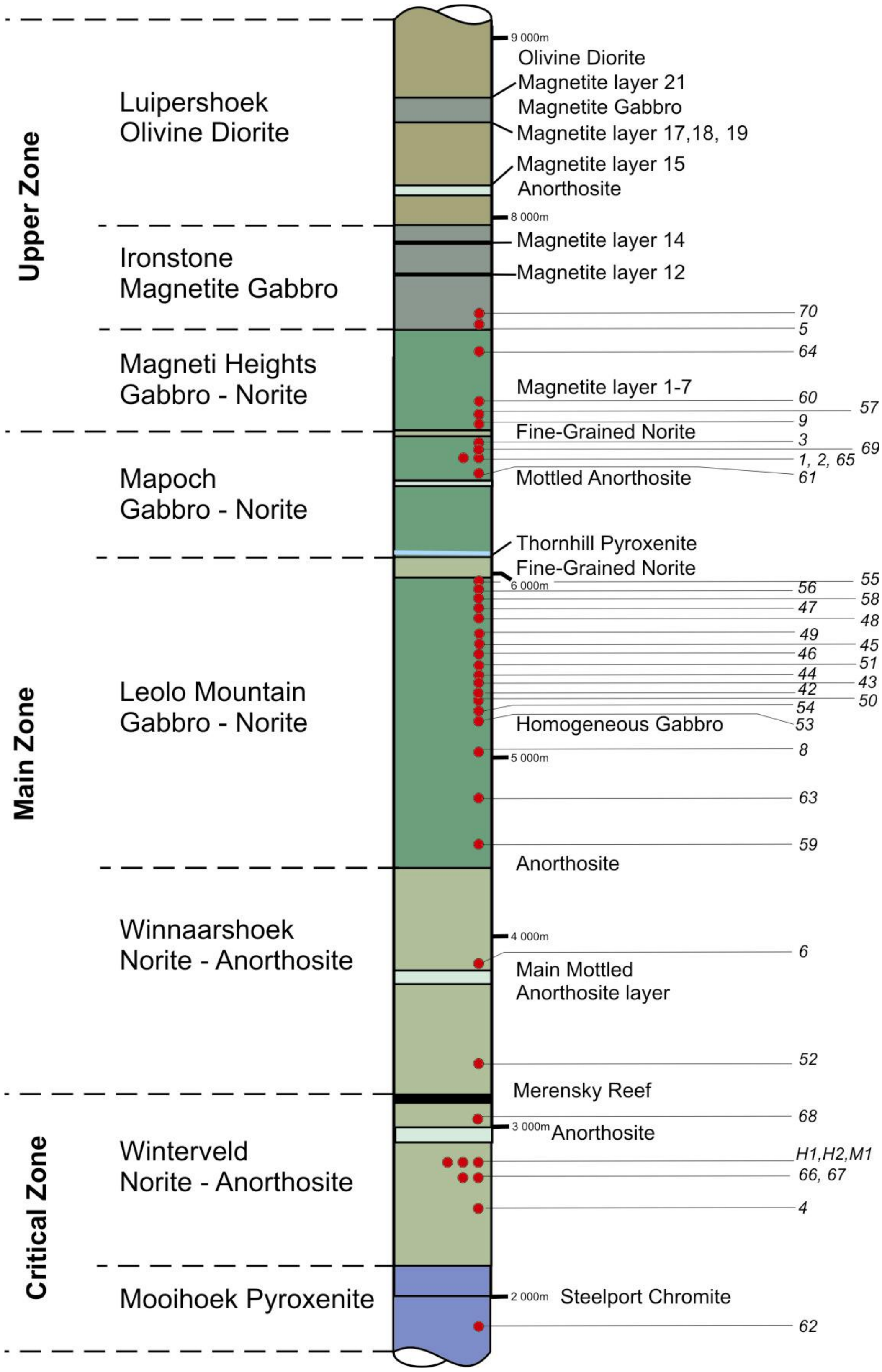

Figure 3.5 Lithostratigraphic column of the Rustenburg Layered Suite in the Eastern Bushveld with site locations (modified after SACS, 1980) stratigraphic positions are based on Hattingh (1983) site locations.

CHAPTER 4: PALAEOMAGNETIC STUDY ON THE RUSTENBURG LAYERED SUITE OF THE BUSHVELD COMPLEX

The sections that follow give a detailed account of the results obtained from a new palaeomagnetic study conducted on the Rustenburg Layered Suite (RLS) from the Bushveld Complex over 2004 and 2005. Palaeomagnetic results have been broken down into 5 groups: western Main Zone, eastern Main Zone, Upper Zone, Critical Zone and Northern Main Zone.

4.1 Main Zone, Western Lobe

Palaeomagnetic drill locations in the Western Lobe of the Main Zone were limited to the lower portion, extending from Pretoria westwards towards the Pilanesburg Complex (Figure 4.1). The area to the north of the Pilanesburg Complex was not included as no suitable sampling sites could be located due to the highly weathered nature of rock outcrops

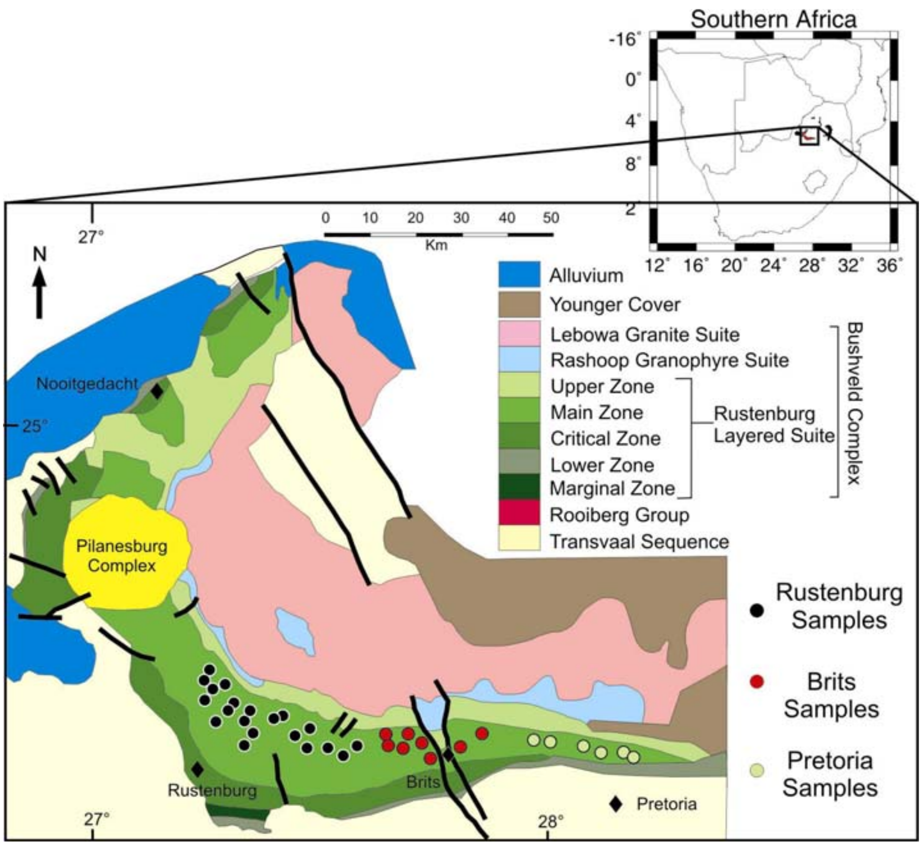

Figure 4.1 Simplified geological map of the Western Bushveld Complex, indicating the locations of sites.

A total of 32 sites were drilled in the Main Zone of the Western Lobe of the Bushveld Complex, with each site containing 9 samples. The majority of sites were located in dimension stone quarries (30 sites) as genuine outcrop in the area was rare. The remaining two sites were located in a riverbed and a railway cutting (Figure 4.2). Sampling localities consisted of gabbronorites and were situated at different stratigraphic heights within the Pyramid Gabbro-Norite sections of the western Main Zone (Figure 4.3).

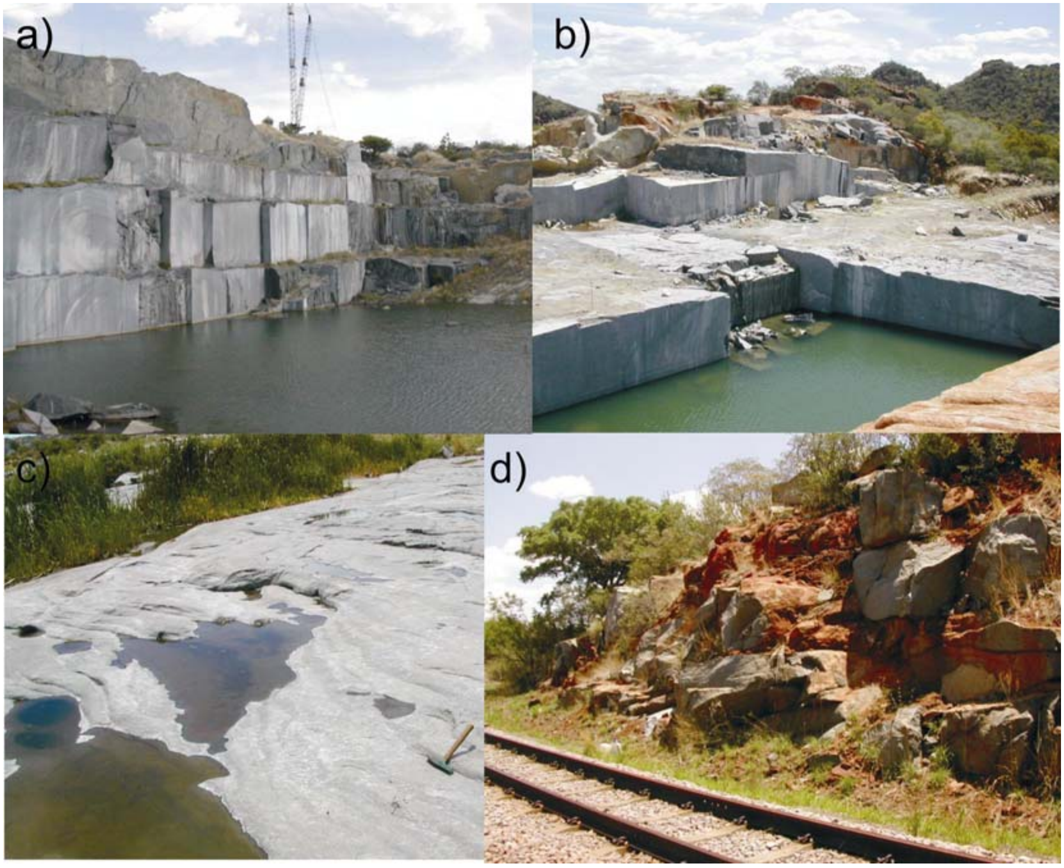

Figure 4.2 Examples of various sites for the Main Zone in the Western Lobe, a) and b) are two from dimension stone quarries, sites 13 and 34 respectively c) river exposure, site 27 and d) a rail road exposure, site 17.

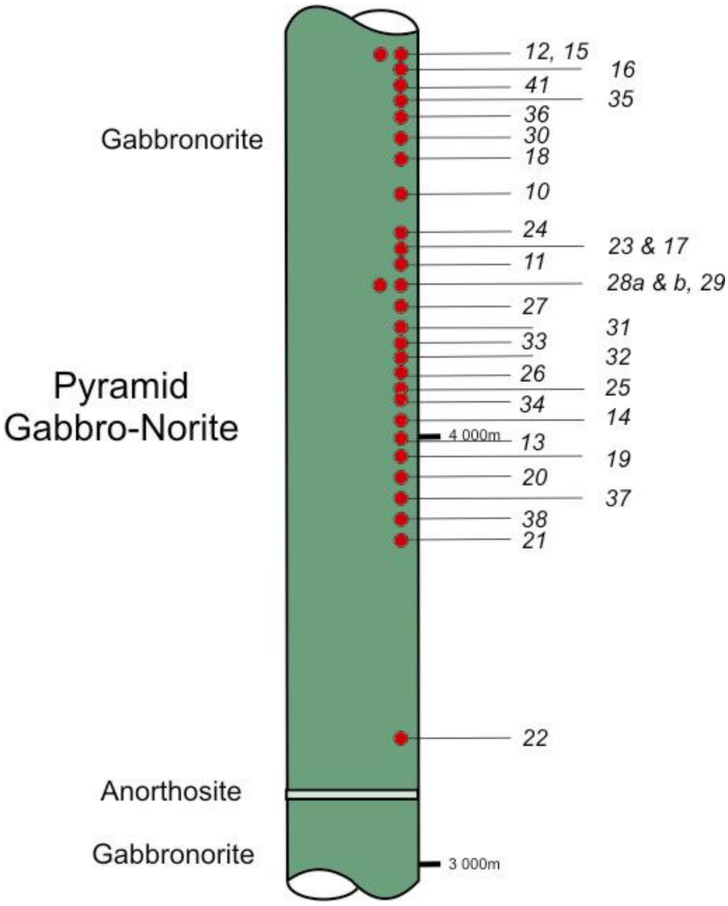

Figure 4.3 Simplified stratigraphic column of the western Main Zone, indicating locations of sites (modified after SACS, 1980).

4.1.1 NRM

A total of 270 cores were initially measured for NRM and bulk susceptibility before being subjected to progressive demagnetisation. With the exception of the first 3 sites from the top of the Main Zone (12, 15 &16) and site 33, which all had exceptionally high mean site values, the NRM intensities varied from 0.416 to 2.502 A/m with an average NRM intensity value for the western Main Zone of 1.311 A/m. With the exception of the first three sites and site 36, susceptibility values had site-averages varying between 475 to 1498 $\times 10^{-6}$ SI units with an average value of 825 $\times 10^{-6}$ SI units for the entire western Main Zone. The variations in susceptibility and NRM intensity values based on stratigraphic locations are shown in Figure 4.4. Mean NRM values and bulk susceptibility values with errors for all sites are shown in Table 4.1

Table 4.1 Mean NRM, mean bulk susceptibility and Q ratio of all sites. *Dec.* = declination, *Inc.* = inclination, α_{95} = 95 percent confidence circle around mean direction, N= number of samples, +/- = 1 σ error and Susc. = Susceptibility.

Site	NRM Dec.	NRM Inc.	α_{95}	N	Intensity Average (A/m)	+/- (mA/m)	Susc. Average ($\times 10^{-6}$ SI units)	+/- ($\times 10^{-6}$)	Q Ratio
10	46.8	88.8	2.3	9	1.69	104.1	1278.0	71.5	55
11	248.4	77.2	6.8	9	0.54	151.7	787.4	206.1	28
12	14.8	87.1	1.5	9	8.38	555.6	2705.6	285.8	130
13	5.2	63.7	9.8	9	1.54	175.6	1127.7	152.0	57
14	10.7	70.9	2.8	9	1.54	58.7	912.8	41.3	71
15	39.1	81.6	2.6	9	8.38	1568.7	4947.5	1182.7	71
16	20.5	82.9	2.2	9	5.32	1017.3	3974.4	945.5	56
17	47.0	89.2	1.4	9	0.66	74.1	661.4	54.8	42
18	124.2	85.3	2	9	0.42	33.7	520.8	30.5	34
19	90.0	68.5	18.9	9	0.68	130.3	683.7	67.8	42
20	36.2	64.6	7.1	9	0.79	114.3	577.6	18.2	58
21	27.4	72	3.8	9	0.39	32.1	525.1	51.0	31
22	35.7	62.2	2.5	9	1.50	87.2	1031.7	133.9	61
23	339.0	75.4	1.3	9	1.55	128.6	904.4	101.1	72
24	29.9	66.1	7.6	9	2.37	446.1	919.7	60.6	108
25	334.6	72.5	3.8	9	1.04	78.7	877.2	103.9	50
26	324.3	73.1	1.2	9	1.75	89.2	899.5	92.0	82
27	256.9	83	22.1	9	2.43	404.7	551.5	14.9	185
28	315.0	70.1	25.9	9	1.17	505.5	491.0	82.0	100
29	335.0	78.4	6.9	9	0.96	59.2	492.3	47.7	81
30	323.0	74.8	9.1	9	1.87	176.5	742.8	97.1	105
31	327.0	75	1.5	9	1.13	72.8	610.6	39.4	77
32	327.0	79.9	1.2	9	1.62	145.5	702.3	91.0	97
33	338.2	75.4	2.9	9	3.62	242.3	1194.6	144.8	127
34	342.7	75.9	2.8	9	1.25	51.6	869.3	54.5	60
35	333.2	70.4	2.6	11	2.41	319.5	1553.4	275.9	65
36	184.2	-18.3	4	11	0.90	62.0	2376.5	184.2	16
37	348.1	69.9	5.3	9	1.33	133.4	799.5	39.1	70
38	41.3	68.5	8.8	5	1.14	68.5	595.8	33.0	80
41	4.1	72.3	2.2	9	1.46	123.5	1312.2	163.5	47

Individual samples from each site show good clustering in direction, represented by α_{95} in Table 4.1 and Figure 4.5.b, with the exception of sites 19, 27 and 28 were there is a very scattered population in both direction and position. The distribution of NRM directions illustrated in Figure 4.5 shows a distinctive correlation with geographic location. Sites have been coloured in Figure 4.5 to illustrate this (red represents samples from the Brits area, green from Pretoria area, black from the Rustenburg area). Mean NRM directions of samples from the Rustenburg area yielded a steep north-westerly direction. The Brits area indicates a steep north-easterly direction and the Pretoria area yields an extremely steep northerly direction. In general, mean results from all sites produce a crescent in NRM directions between steep NW directions to steep NE directions.

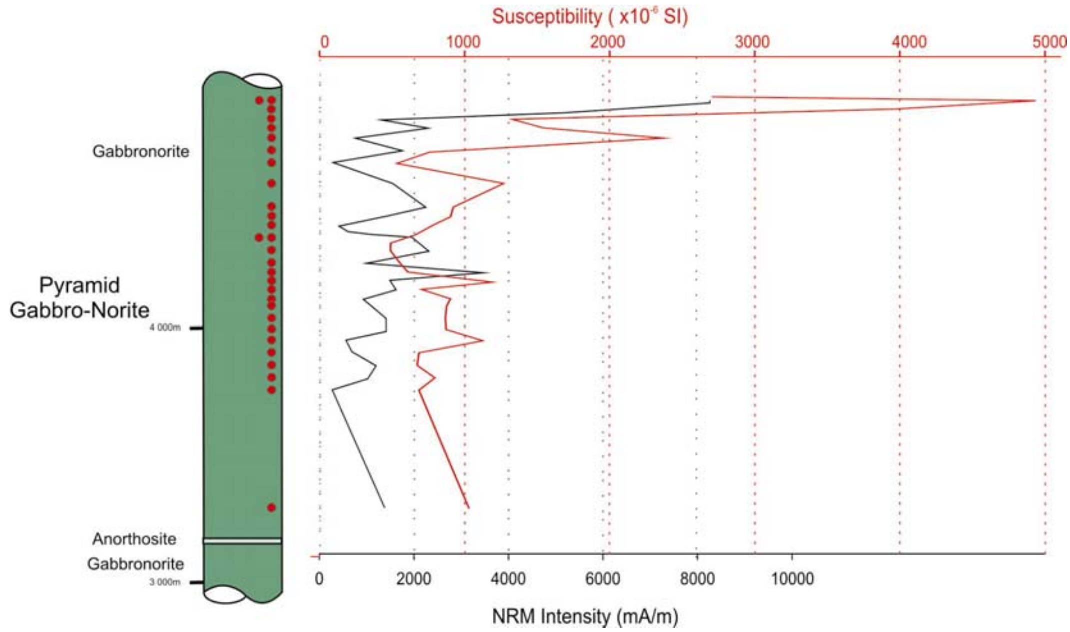

Figure 4.4 Variation in NRM intensity and susceptibility for the Main Zone.

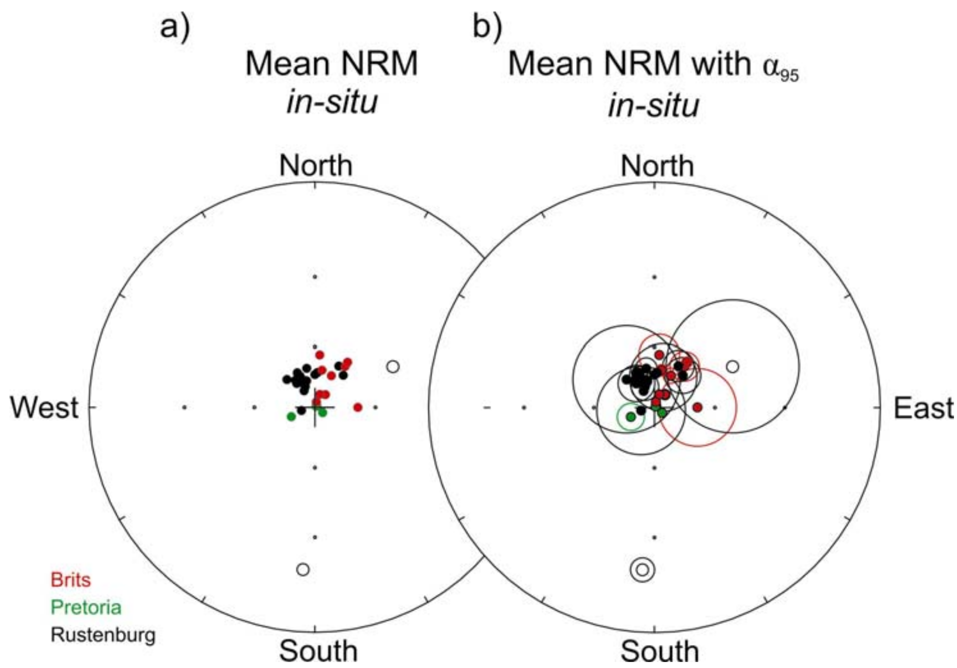

Figure 4.5 a) Site mean NRM results from the Main Zone of the Western Lobe of the Bushveld Complex. b) The same mean NRM results but this time with α_{95} values. Results have been coloured based on geographic location, red results are from the Brits area, green from Pretoria area, black from the Rustenburg Area.

4.1.2 Demagnetisation

In order to reveal the magnetic history of the samples and hence determine the primary magnetisation of the Main Zone of the Western Lobe of the Bushveld Complex, samples were subjected to progressive demagnetisation. Demagnetisation was completed with the use of AF demagnetisation on 124 samples, and thermal demagnetisation on the remaining 150 samples. The levels of demagnetisation for AF demagnetisation were: 2, 4, 6, 8, 10, 15, 20, 30, 40, 50, 70 and 95 mT. For thermal demagnetisation, the levels were: 100, 200, 300, 400, 450, 500, 520, 540, 560, 580 and 595°C. Some variations in the above values occurred due to different levels of magnetisation being present in different samples. Once demagnetisation was completed, data were plotted on Zijderveld diagrams and subjected to principal component analysis to determine low temperature blocking components and high-stability components of NRM (a MAD value of 5 was used for rejection of components).

4.1.3 Components of magnetisation

On completion of demagnetisation it was found that samples were composed of two components of magnetisation, a low coercivity or low unblocking (LB) component and a high unblocking (HB) component. In the majority of cases the LB component was poorly defined and could not be identified using principal component analysis. However, in a small number of samples LB components were identified. Figure 4.6a shows the variation in LB components obtained in one site (site 37), the resulting mean direction from site 37 is highlighted in blue in Figure 4.6b along with other mean NRM directions. LB components are randomly scattered and were typically demagnetised below 300-400ºC or 30 mT (Figure 4.7) Mean directions for each site are listed in Table 4.2.

Table 4.2 Mean LB component directions. *Dec.* = declination, *Inc.* = inclination, N_o = original number of samples per site, N = number of samples analysed per site.

Site	Dec	Inc	α_{95}	N_o/N
10	322.1	75.5	15.3	9/5
11	87	35.9	180	9/3
12	45.5	60.3	107.7	9/2
13	345	40.8	30.6	9/3
14	353.8	47.1	74.5	9/2
15	33.7	34.1	180	9/2
16	35.9	15.4	180	9/3
17	357.8	52.4	51.3	9/4
18	24.9	7.1	130.9	9/4
19	145.2	12.6	130.9	9/2
20	63.8	52.7	180	9/2
21	318.5	23.9	132.4	9/3
22	15.1	65.4	48	9/5
24	46.5	11.4	180	9/3
25	322.9	24.3	118	9/4
26	323.6	22.1	31.6	9/3
27	105	-23.9	180	9/3
28a	116.9	-5.5	180	9/3
28b	28.9	13.7	18.6	9/4
29	213.7	23.1	180	9/3
30	275.3	25.3	180	9/3
31	122.1	13.9	0	9/1
32	231.4	1.9	88.4	9/3
33	253.2	7	35.7	9/2
34	359.4	60	89.1	9/4
35	252.9	-4.5	0	11/1
36	234.4	-35.6	88.3	11/4
37	287.1	49.1	180	9/4
38	67.7	55.8	63.8	9/2
41	323.2	22.1	115.5	9/3

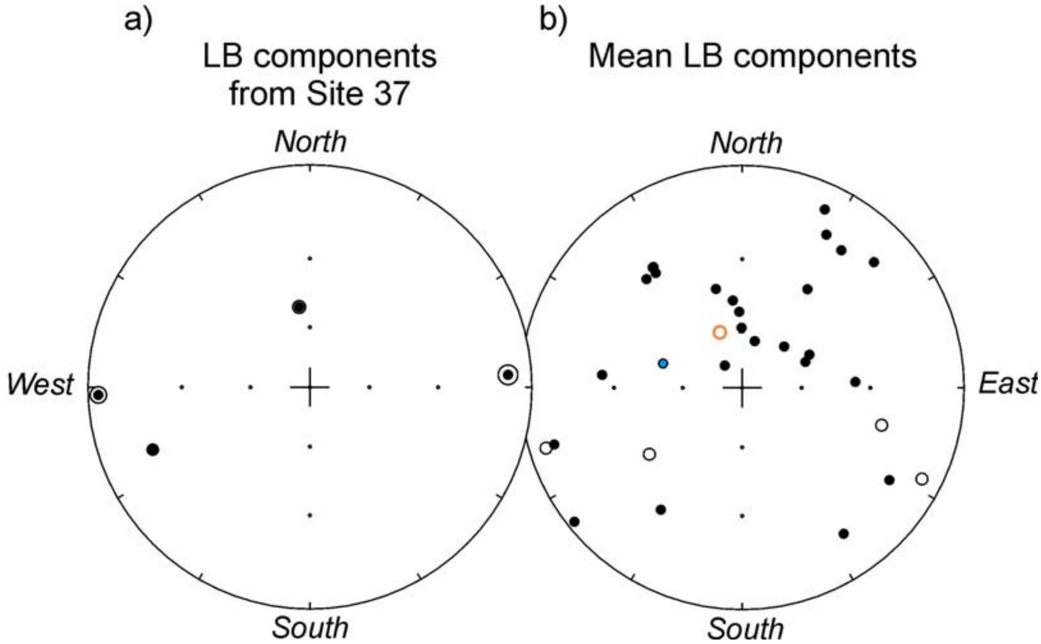

Figure 4.6 a) LB components from site 37 b) mean L components from main western Lobe, α_{95} circles are not shown as most values are greater then 90°. Blue circle represents the mean direction for site 37. The orange open circle in a NW steep direction represents the current magnetic direction in South Africa.

With the removal of LB components, well-defined HB components were identified at ≈ 560-580°C and above 50 mT. Although the maximum AF demagnetisation field of 95 mT did not completely demagnetise all samples, NRM intensities were reduced to 35 - 19 %, and showed the same behaviour as thermal demagnetisation with clear decay towards the origin. Resulting HB components show good clustering, and produce well grouped results within sites. The resulting HB components are shown and listed in Figure 4.8 and Table 4.3.

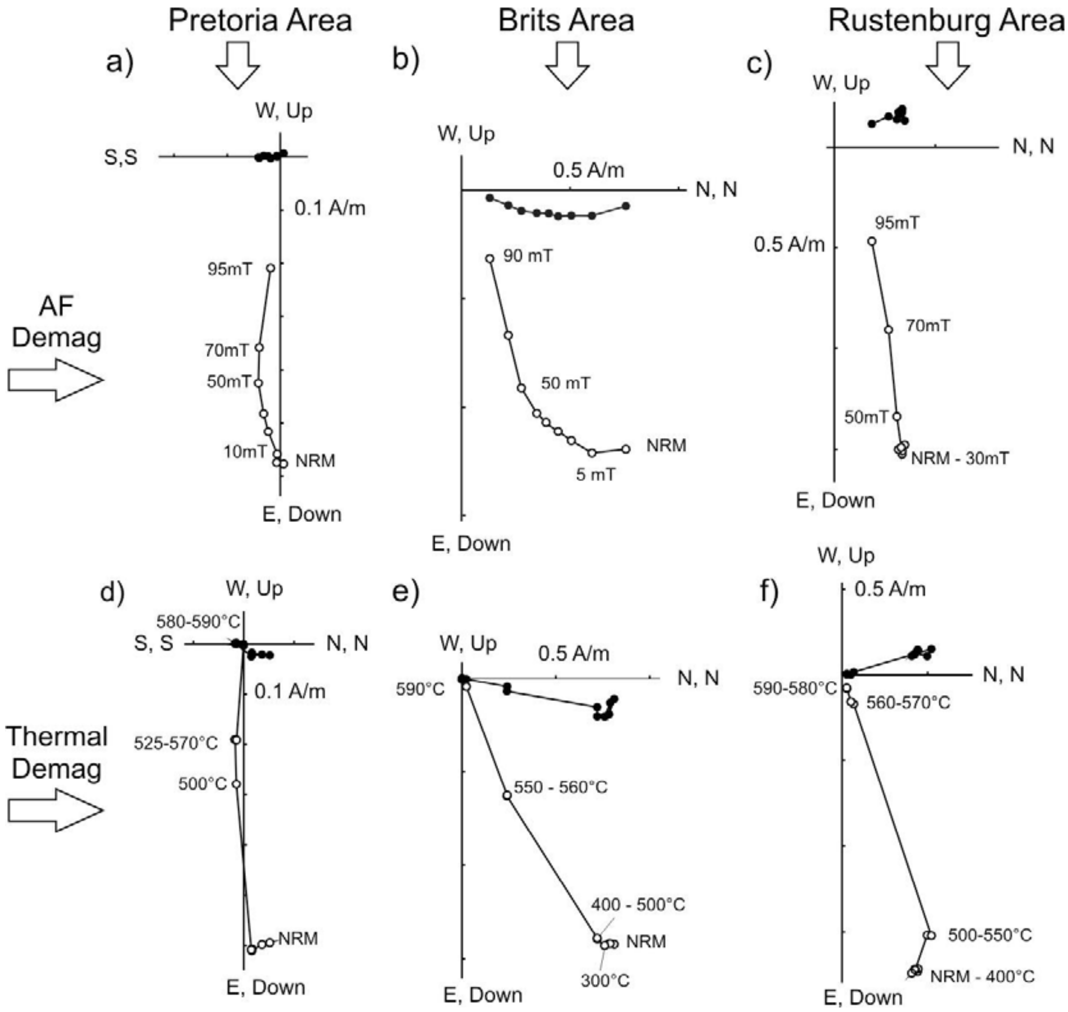

Figure 4.7 Typical examples of AF (a, b & c) and thermal demagnetisation (d, e & f) of Main Zone samples from the three different geographical groups; Pretoria (a & d), Brits (b & e) and Rustenburg (c & f). Open (solid) symbols represent projections onto the vertical (horizontal) planes, respectively.

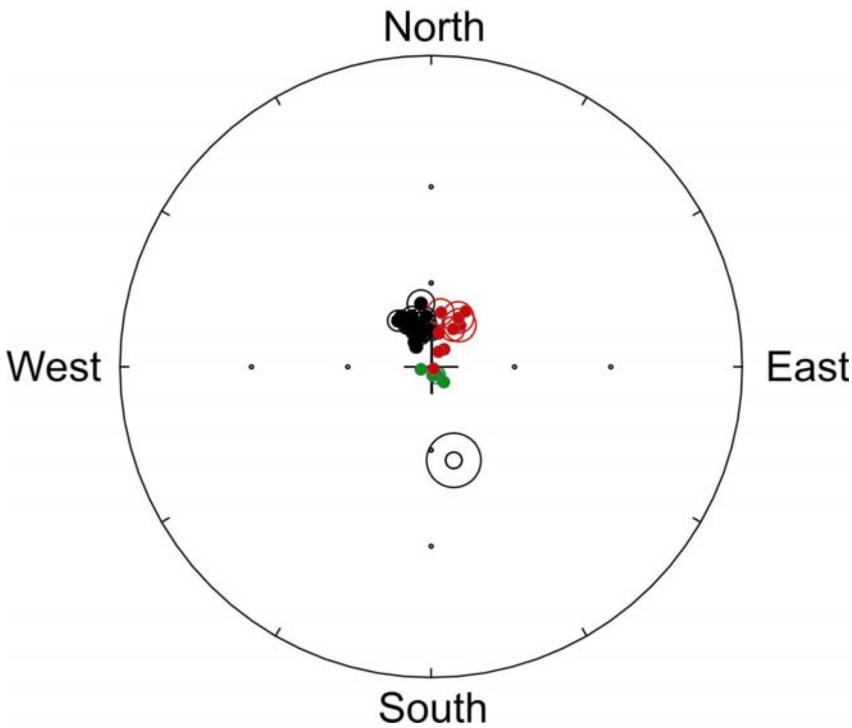

Figure 4.8 Site mean direction for Main Zone sites from the Western Lobe *in situ.,* Showing distinctive grouping based on geographic location. Results have been coloured based on geographic location. Red symbols are from Brits area, green from Pretoria area, black from Rustenburg Area.

Upon completion of demagnetisation the grouping in NRM directions (based on geographical location of sites, i.e. Rustenburg, Brits and Pretoria) was strengthened to form tighter clusters. Sites located near Pretoria produced HB components with extremely-steep positive inclination and southern to south-westerly declination (Figure 4.7 a,d & Figure 4.9). Sites in the vicinity of Brits have steep to very-steep positive inclinations with north-easterly declinations (Figure 4.7 b,e & Figure 4.9), while sites located around Rustenburg have steep positive inclinations with north westerly declinations (Figure 4.7 e,f & Figure 4.9).

Table 4.3 Mean HB component of magnetisation directions of each site *in situ*. N_o = original number of samples per site, N = number of samples analysed per site; α_{95} = 95 percent confidence circle around mean direction; κ = precision parameter.

Site	Dec	Inc	Strike	dip	N_o/N	α_{95}	κ
10	146.2	86.3	268	25	9/9	3.1	271.37
11	258.5	85.8	279	26	9/9	2.8	298.13
12	126.6	89.1	273	16	9/9	2.2	537.21
13	9.9	69.9	268	12	9/9	4.7	199.97
14	12.2	77.2	266	10	9/9	2.1	604.36
15	35.1	81.9	275	12	9/8	1.6	1170.89
16	24.2	83.7	275	12	9/8	2.2	662.70
17	177.7	87	275	26	9/9	2.4	459.51
18	142.2	83	268	27	9/9	2.5	410.17
19	34.6	71.6	250	10	9/8	5.8	135.50
20	28.9	69.7	252	11	9/9	5.6	85.19
21	29.9	74.1	269	15	9/9	4.3	144.63
22	31.5	66.4	250	14	9/9	2.6	386.19
23	342.3	77.7	300	6	9/8	3.4	269.27
24	350.8	66.9	315	7	9/9	4.8	185.24
25	338.7	70.4	311	11	9/9	3.5	222.52
26	329.5	69.2	310	11	9/9	2.2	545.75
27	344.3	75	300	8	9/8	5.2	170.07
28a	330.8	70.8	354	10	9/9	5.9	171.57
28b	345.1	74.4	354	10	9/9	9.1	71.23
29	328.9	72.8	312	11	9/8	2.9	369.55
30	329.2	69.1	312	10	9/8	2.4	658.06
31	332.5	73.6	306	11	9/8	2.2	645.67
32	325.9	79.1	307	11	9/8	1.5	1375.97
33	334.5	75.1	305	11	9/9	3.1	277.45
34	331.9	75	307	10	9/8	2.2	652.97
35	331.7	72.9	296	11	11/10	2.9	288.13
36	324	69.5	310	10	11/8	3.7	220.17
37	354.5	71.7	290	8	9/8	3.2	348.77
38	323.4	80.8	290	10	9/9	3.5	222.58
41	2.2	77.1	298	11	9/9	3	286.67

Thermal and AF demagnetisation yielded similar directional results from sites, with the exception of site 36. It was observed that at the end of AF demagnetisation (95mT,) site 36 had a shallow negative inclination in a southerly direction, while thermal demagnetisation on the same site had removed this direction, with high temperatures around 550-560°C. Cores from site 36 that were initially subjected to AF demagnetisation were then further demagnetised using thermal methods, in order to completely demagnetise samples. Upon thermal demagnetisation the persistent LB component was successfully removed to reveal a HB component similar to the other sites in the Rustenburg area (Figure 4.9).

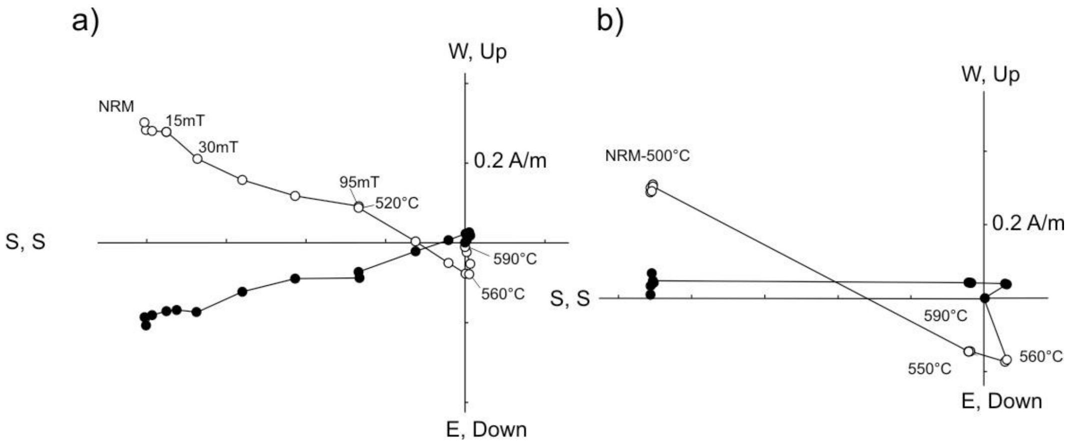

Figure 4.9 Examples of AF (a) and thermal (b) demagnetisation of samples from site 36. The maximum AF demagnetisation field of 95mT was not successful in demagnetising the samples, and samples were further demagnetised thermally. Note that if there was no comparison to thermal demagnetisation it would appear that the AF demagnetisation was decaying towards the centre. Open (solid) symbols represent projections onto the vertical (horizontal) planes, respectively.

4.1.4 Thermomagnetic and petrographic analysis

Thermomagnetic analysis (TMA) results illustrated in Figure 4.10 shown Curie curves to be almost reversible, with a Curie temperature indicated at ≈ 580°C.

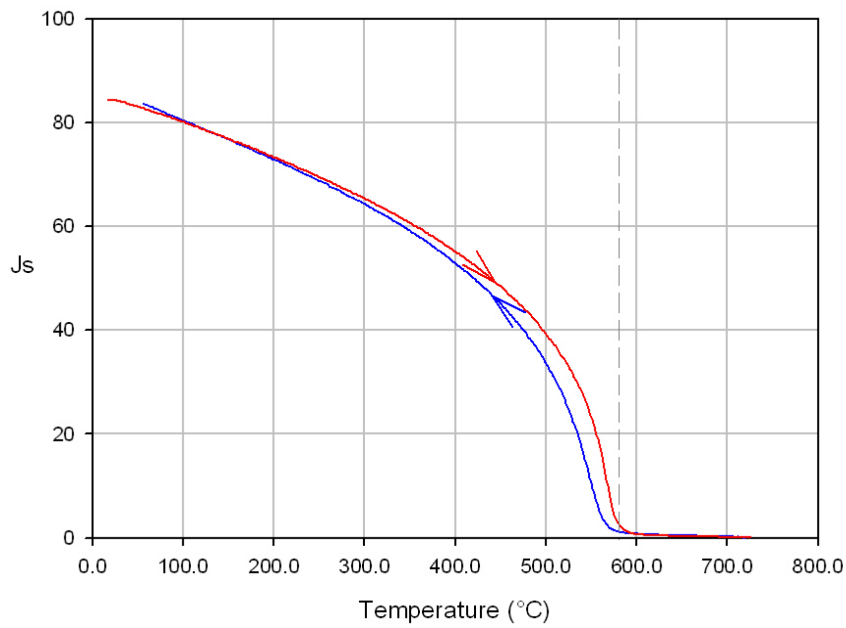

Figure 4.10 Typical thermomagnetic analysis response from site 12 occurring in the Main Zone of the Western Lobe. Red line and arrow indicate heating phase while blue line and arrow indicate cooling phase. Curie temperature for magnetite at ≈ 580°C observed (dashed line).

Petrographic analysis was undertaken to determine the opaque mineralogy for samples from the Main Zone of the Western Lobe, i.e. to determine the carrier of magnetisation. Samples throughout the western Main Zone contained similar mineralogy. It was found that magnetite was the dominant mineral that occurred as lamellae or needles in both plagioclase and pyroxene and in rare occasions as discrete grains. A number of large needles of magnetite were discovered by reflected light microscopy (Figure 4.11), however the smaller lamellae could not be accurately identified as magnetite due to their small size. Previous petrographic analyses of Main Zone rocks have successfully identified the occurrence of magnetite as needles in both plagioclase (Groeneveld, 1970; Hattingh, 1983; Scharlau, 1972), and pyroxene (Hattingh, 1983 and Scharlau, 1972). On average, the needles were 4.5 μm long and 1.5 μm wide for pyroxene and 10μm long and 1μm wide for plagioclase. Based on the observed Curie temperature of 580°C from TMA, it was concluded that the lamellae observed by transmitted light microscopy (Figure 4.12 and Figure 4.13) are magnetite. Discrete ilmenite and pyrrhotite grains were also found to a minor extent.

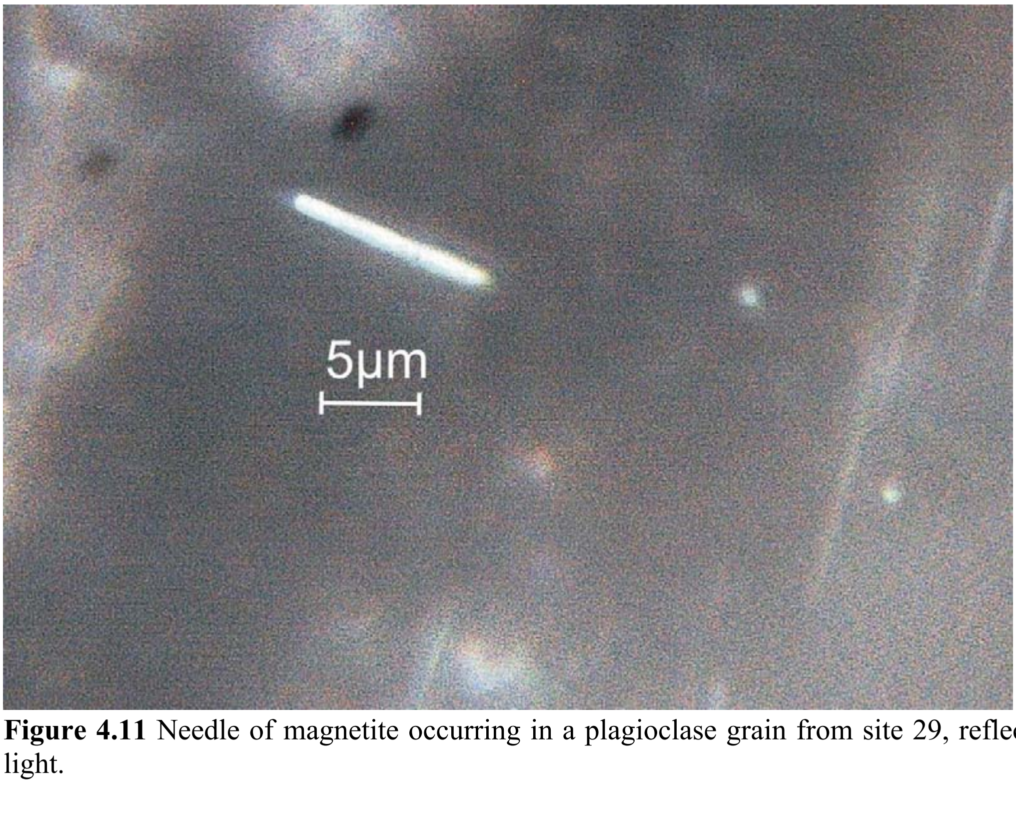

Figure 4.11 Needle of magnetite occurring in a plagioclase grain from site 29, reflected light.

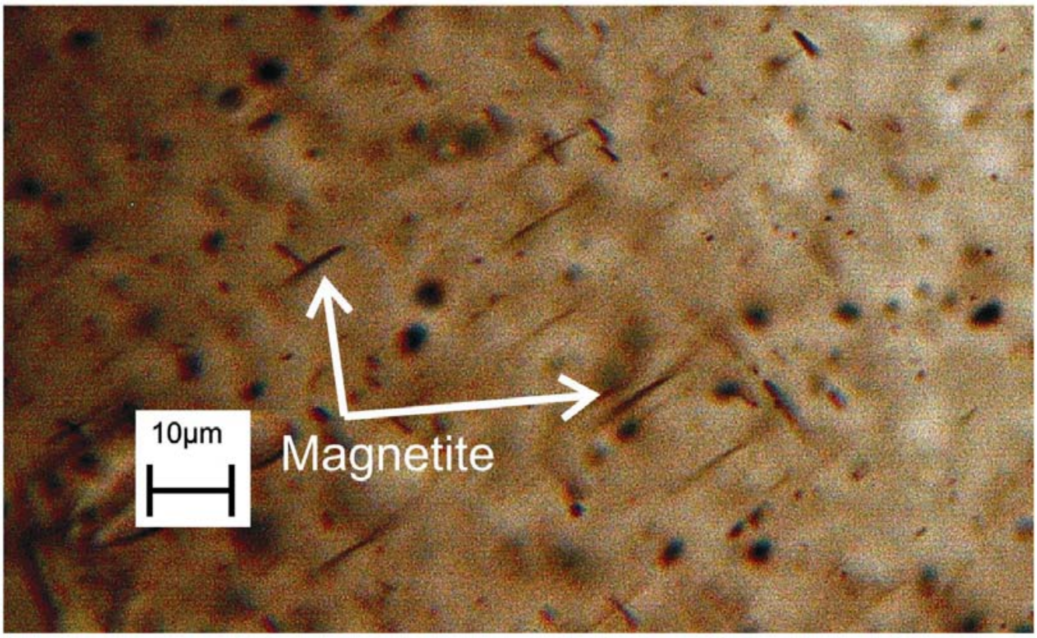

Figure 4.12 Needles or lamellae of magnetite occurring in a pyroxene from site 24, transmitted light.

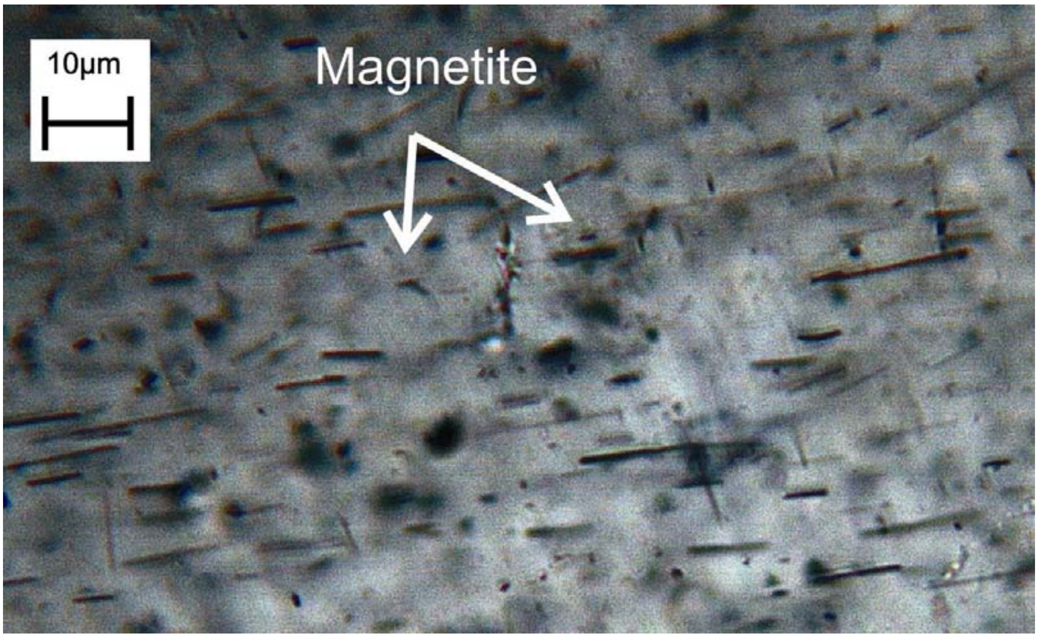

Figure 4.13 Needle of magnetite occurring in a plagioclase from site 37, transmitted light.

4.1.5 Field stability tests

Fold Test

Rocks from the Western Lobe form an arc from Pretoria through to the Pilanesburg Complex, dipping towards the centre of the complex at angles of between 10° and 25°. In order to reveal whether the distinctive grouping experienced by sites based on their geographic location is due to the current attitude of the rock, samples were subjected to a fold test.

Bedding corrections were applied to all HB components to restore the layers to a horizontal attitude; the dips and strikes used in the bedding correction are listed in Table 4.3. Upon stepwise unfolding, a uniform increase in statistical precision parameter κ was observed from 58.49 to 169.27 (Figure 4.14c). This can be seen noticeably in graphical representation by the increase in clustering (Figure 4.14b) and hence the removal of geographical grouping (Figure 4.14a). The classical fold test of McElhinny (1964b) produced a positive fold test at the 95% confidence level.

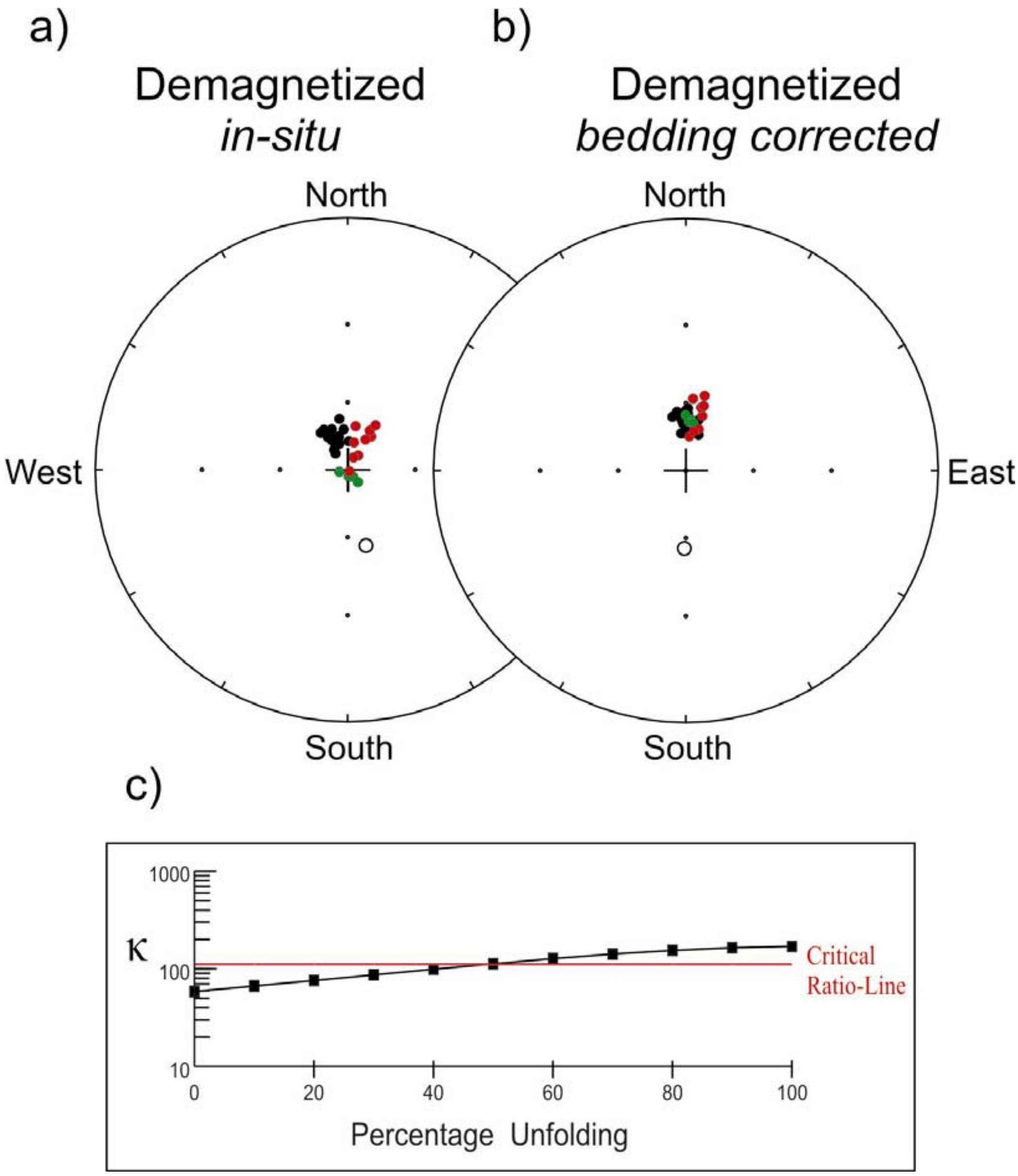

Figure 4.14 Site mean direction for Main Zone sites from the Western Lobe in both *in situ* (a) showing geographical location of sites, and bedding-corrected co-ordinates (b). Closed symbols denote positive inclination. Once again results have been coloured based on geographic location, red symbols are from the Brits area, green from Pretoria area, black from the Rustenburg Area, (c) shows variation in precision parameter κ as a function of stepwise unfolding. The red line is the 'critical ratio-line' indicating the 95% statistically significant level.

Reversal Test

All mean site directions posses a positive inclination with the exception of site 28b. In order to determine if the magnetisation is of similar age to the others, the reversal test of McFadden and Lowes (1981) was implemented. It was found that the site shared a common mean at 95% confidence. The more recent reversal test of McFadden & McElhinny (1990) could not be implemented due to only one site possessing a different direction in magnetisation.

4.1.6 Interpretation of palaeomagnetic data from the Western Lobe Main Zone

Complete progressive demagnetisation of samples has successfully removed minor low temperature components and identified high temperature components, which produce extremely well clustered results for sites.

Thermal demagnetisation spectra and thermomagnetic analysis suggest that titanium-poor magnetite or nearly pure magnetite (maximum unblocking temperatures of 565-580°C and Curie temperatures at ≈ 580°C) is the bulk remanence carrier. Petrographic analysis further strengthens these observations, revealing that the opaque mineralogy of the samples is dominated by magnetite.

A fold test applied to the samples yielded a statistically positive result, supporting a primary magnetic signature from HB components, and indicates that at the time the western Main Zone passed through the Curie temperature of magnetite it was in a near horizontal position. The positive reversal test also indicates that the HB components are primary and all sites were emplaced over the same time span.

The high-temperature components of all the samples, with site 28b inverted to the same polarity, yield a mean remanence direction with declination = 1.1°, inclination = 66.9° (α_{95} = 2º, N =32 sites) and a pole position with latitude =15.5° and longitude = 28.2°, dp/dm = 2.7°/3.3° (palaeopole calculated at mean sampling co-ordinates of 25°S and 27.5°E).

4.2 Eastern Main Lobe

A number of "natural" outcrops occur in the eastern Main Zone. However, they are either extremely weathered and jointed (making them impossible to drill) or they occur on hill tops where they have been prone to lightning strikes over prolonged periods of time (thereby increasing the chance of induced IRM and removal of primary magnetisation), making them unsatisfactory for palaeomagnetic sampling. The lack of desirable sampling locations leads to a rather uneven site distribution in which sites were limited to road cuttings (14), dimension stone quarries (12) and a river bed. A total of 26 sites were sampled in the Main Zone of the Eastern Lobe of the Bushveld Complex (Figure 4.15) with an average of 9 cores per site. Even though sampling was limited to specific localities, a reasonable coverage was obtained throughout the Main Zone in which the SACS (1980) classification of the sub zones A, B and C (also known as Winnaarshoek Norite-Anorthosite, Leolo Mountain Gabbro-Norite and Mapoch Gabbro-Norite) were sampled (Figure 4.16).

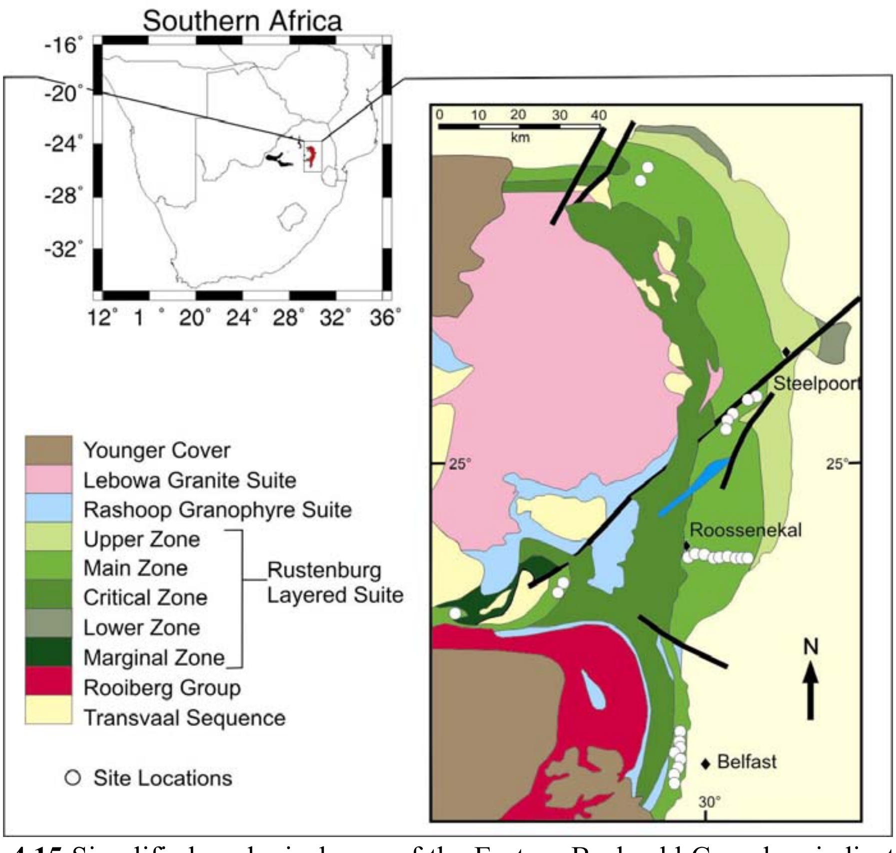

Figure 4.15 Simplified geological map of the Eastern Bushveld Complex, indicating the locations of sites.

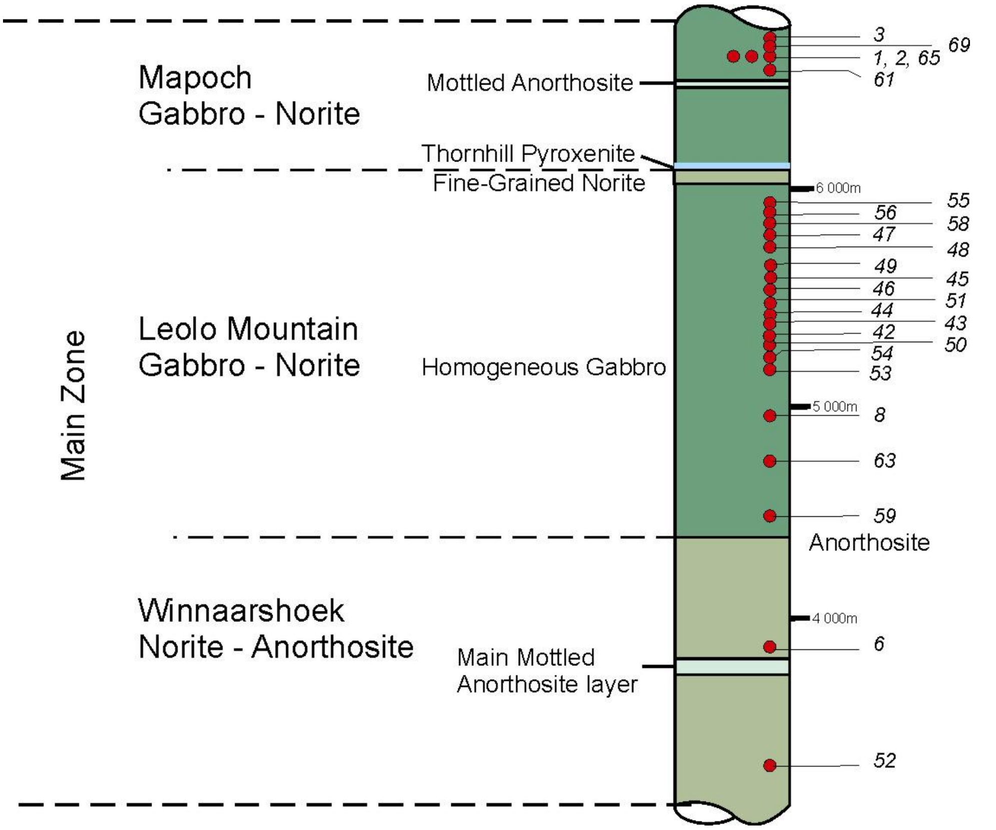

Figure 4.16 Simplified stratigraphic column of the eastern Main Zone, indicating locations of sites (modified after SACS, 1980).

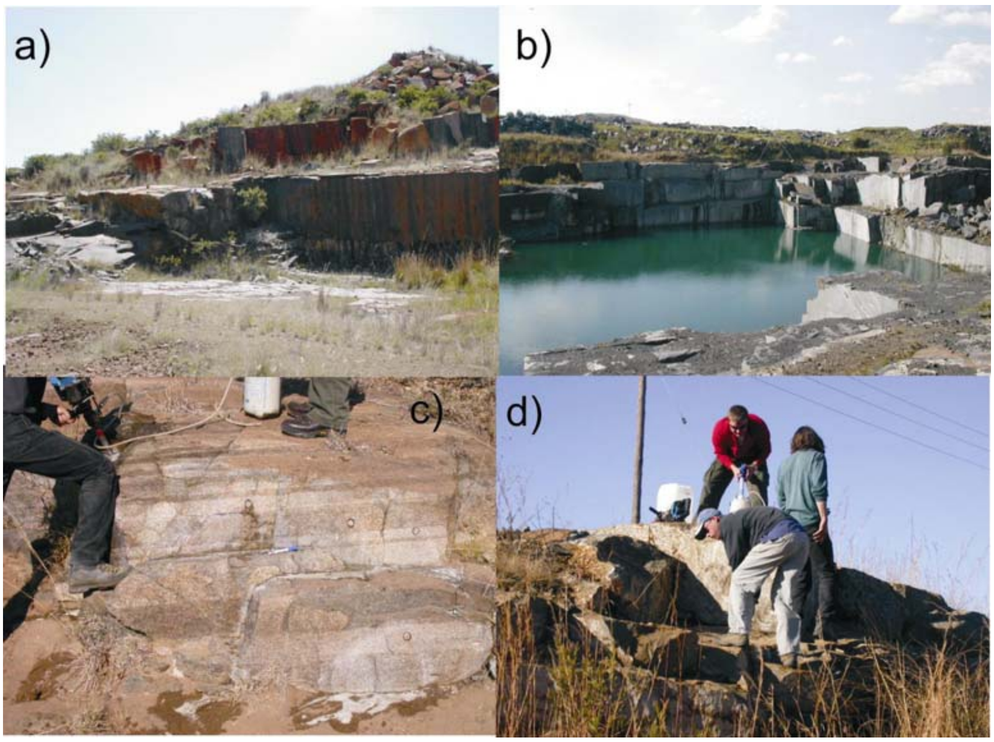

Figure 4.17 Typical rock outcrops of Main Zone rocks in the Eastern Lobe. A) and b) are examples of dimension stone quarry sites (sites 42 and 51, respectively), while c) and d) are from road exposures, sites 2 and 6, respectively.

4.2.1 NRM

From the 26 sites a total of 222 core samples were analysed initially for NRM and bulk susceptibility before demagnetisation took place. A wide range in NRM intensities were observed in the Main Zone of the Eastern Lobe and was rather dependent on stratigraphic location. Samples obtained from subzone C (Mapoch Gabbro Norite) have values ranging from 0.02 to 0.64 A/m, with the average value being 0.28A/m, and susceptibility from 391 to 1511 $\times10^{-6}$ SI units, with an average of 970 $\times10^{-6}$ SI units. Samples located in subzone B (Leolo Mountain Gabbro-Norite) have values from 0.17 to 28.29 A/m, with the average value being 10.48 A/m, while the susceptibility ranges from 495 to 12843 $\times10^{-6}$ SI units with an average of 4466 $\times10^{-6}$ SI units. The Winnarshoek Norite-anorthosite section only contains 2 sites and has values of 4129 and 7458 A/m and susceptibility of 744 and 8205 $\times10^{-6}$ SI units. Variation in susceptibility and NRM intensity with stratigraphic location is shown in Figure 4.18. Site mean NRM values and bulk susceptibility values for all sites with errors are shown in Table 4.4.

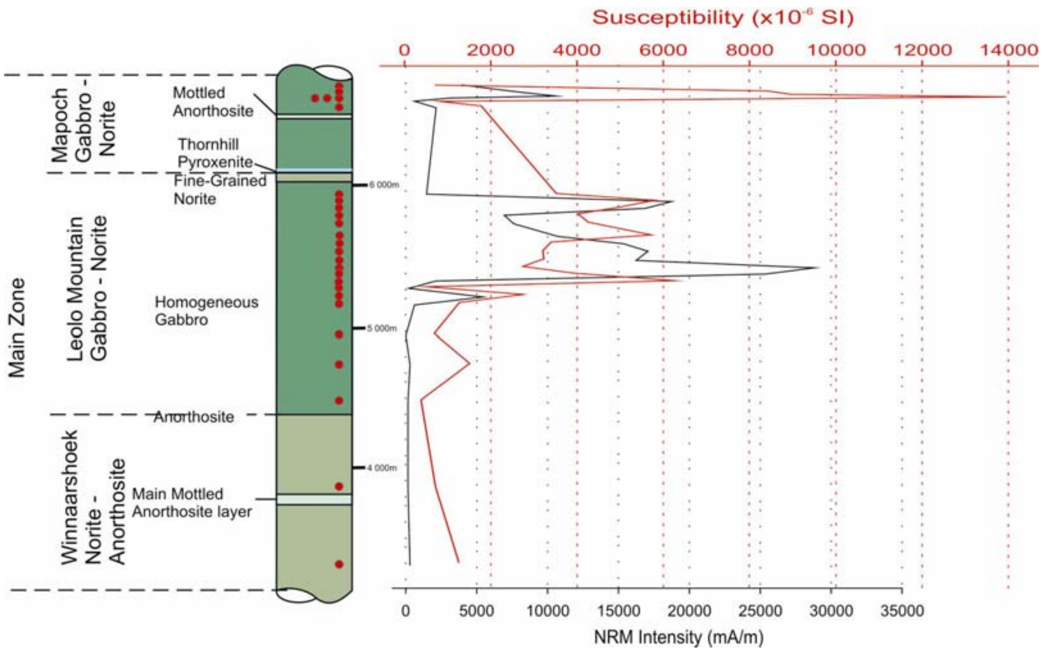

Figure 4.18 Variation in NRM intensity and susceptibility for the eastern Main Zone

Table 4.4 Site mean NRM, mean bulk susceptibility and Q ratio of all sites. *Dec.* = declination, *Inc.* = inclination, α_{95} = 95 percent confidence circle around mean direction, N= number of samples, +/- = 1 σ error and Susc. = Susceptibility.

Site	NRM Dec.	NRM Inc.	α_{95}	N	Intensity Average (A/m)	+/- (mA/m)	Susc. Average ($\times10^{-6}$ SI units)	+/- ($\times10^{-6}$)	Q Ratio
1	220.0	-66.6	4.5	9	0.21	68.72	691.95	53.83	13
2a	220.5	-59.4	4.5	7	0.16	79.22	391.00	108.10	17
2b	209.2	-56.3	2.8	7	0.19	85.21	483.00	95.21	17
3	201.2	-47.7	6.4	14	0.29	172.79	1511.71	488.83	8
8	36.2	61.9	2.8	8	0.61	32.54	784.38	43.85	33
42	35.9	64.8	2.4	9	16.89	561.77	4979.83	317.16	142
43	30.8	61.4	2.4	10	6.95	677.46	4027.01	234.05	72
44	48.5	61.4	2.8	8	7.56	569.66	4260.68	304.61	74
45	30.2	67.9	1.6	9	17.08	638.88	3206.57	165.34	223
46	35.8	62.5	1.5	10	15.39	1596.73	3394.95	129.94	190
47	39.5	62.7	1.1	9	25.31	762.31	3936.42	183.84	269
48	35.7	64.1	1.4	7	28.87	729.23	2744.13	159.28	441
49	32.8	66.7	0.9	8	16.28	517.97	3231.45	198.12	211
50	31.1	57.2	2.7	9	18.77	2071.53	5812.99	445.83	135
51	46.4	59.3	1.9	9	10.73	1039.60	5724.38	849.27	79
52	14.3	33.9	8.7	8	3.93	1323.82	704.78	120.73	234
53	14.6	62.7	7.1	8	2.14	622.14	1810.91	604.03	50
54	1.2	66.2	2.4	9	1.54	153.01	3520.69	332.47	18
55	45.5	60.8	3.3	8	6.49	2651.42	7503.73	362.31	36
56	32.9	57.7	7.5	9	0.18	43.17	495.27	56.31	15
58	45.5	60.8	3.3	8	3.16	1211.59	6260.26	718.48	21
59	358.2	75.1	4.4	6	10.63	3765.73	8947.39	2760.22	50
61	203.0	-62.3	5.0	8	0.67	105.26	1271.74	290.22	22
63	19.5	54.8	3.8	9	2.99	613.04	16490.38	3788.26	8
65	20.8	27.9	3.6	8	0.02	2.51	691.97	114.05	1
69	218.2	-71.1	4.0	8	0.31	85.05	1262.31	607.92	10

The resulting NRM directions (Figure 4.19 and Table 4.4) obtained from the eastern Main Zone can be divided into two assemblages based on their outcrop type. The first assemblage is composed of sites obtained in dimension stone quarries where extremely fresh and unweathered rock produced well clustered NRM directions with a steep northeasterly direction (red samples in Figure 4.19). The exception to this grouping is site 53, in which the quarry sampled was exceptionally small and outcrop was not as pristine as in the others. The second assemblage consists of sites from road cuttings and the one river cutting site. Their resulting mean site NRM directions produce a scattered distribution (when inverted to normal magnetisation, Figure 4.19b) around those from group 1 and α_{95} values per site are considerably higher then those from group 1 (Figure 4.19a).

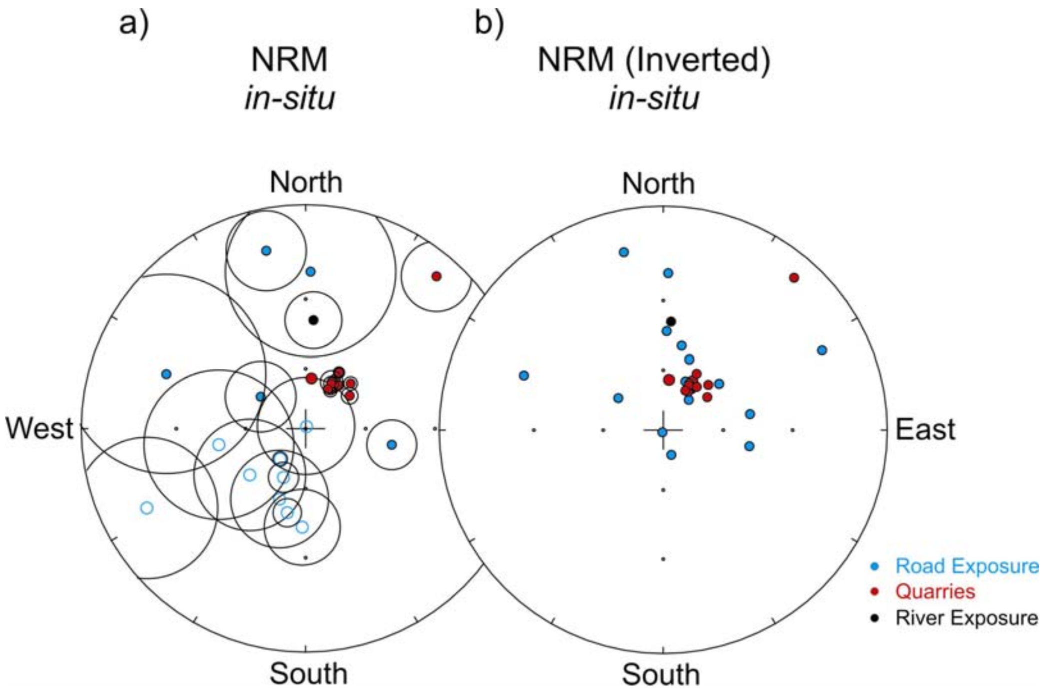

Figure 4.19 a) Site mean NRM directions from the eastern Main Zone with α_{95} circles. b) Site mean NRM directions with negative inclinations inverted to positive inclinations. α_{95} circles have been removed to reduce confusion. Results shown in red represent sites from dimension stone quarries, blue results from road exposures, and the one black result is from a river exposure. Results from dimension stone quarries (red) show a good grouping with a NE and steep directions, with the exception of site 53 which has a NE shallow direction.

4.2.2 Demagnetisation

To determine the different components of magnetisation and therefore determine the primary magnetisation of the Main Zone of the Eastern Lobe of the Bushveld Complex, samples were subjected to progressive demagnetisation. Demagnetisation was completed with the use of AF demagnetisation on 106 samples, and thermal demagnetisation on the remaining 116 samples. Demagnetisation was carried out using between 10 and 16 steps up to 620° C (but generally 600°C) or 95mT (maximum level obtained from AF machine). Upon completion, data were plotted on Zijderveld diagrams and subjected to principal component analysis to determine the ChRM and low temperature blocking components.

4.2.3 Components of magnetisation

Typical behaviour of Eastern Lobe Main Zone rocks upon demagnetisation is indicated in Figure 4.20. The majority of samples obtained from road cuttings were composed of two components of magnetisation: a low coercivity or low unblocking (LB) component and a well defined high-stability or high temperature blocking (HB) component. On the other hand, samples from dimension stone quarries (Figure 4.20 a & d) reflected almost univectorial demagnetisation behaviour (i.e. single component of NRM) and in the rare instance where LB components were present they were often removed after only two or three treatment steps and are consequently directionally ill-defined.

Although LB components are present in road cutting samples, they are randomly scattered within site (denoted by exceptionally large α_{95} values, around 68 and some as high as 127) and from site to site. These random overprints are more persistent then those present in the Western Lobe, and are typically removed at around 500ºC or 30-40mT. Mean LB components for sites are shown in Figure 4.21 and listed in Table 4.5. They show no correlation with any known remanence direction for the region or that of the present day magnetic field. Results for LB components have been shown to indicate their presence and effect on NRM results, but due to their random distribution and lack of significant geological meaning, they are not considered further.

Removal of low coercivity remanence isolates well-defined HB components that are identified above 550°C and 50mT. Both thermal and AF demagnetisation yielded similar directional results. As in the Western Lobe, a few sites were not completely demagnetised by AF demagnetisation and required thermal demagnetisation (Figure 4.22) to determine primary magnetisation.

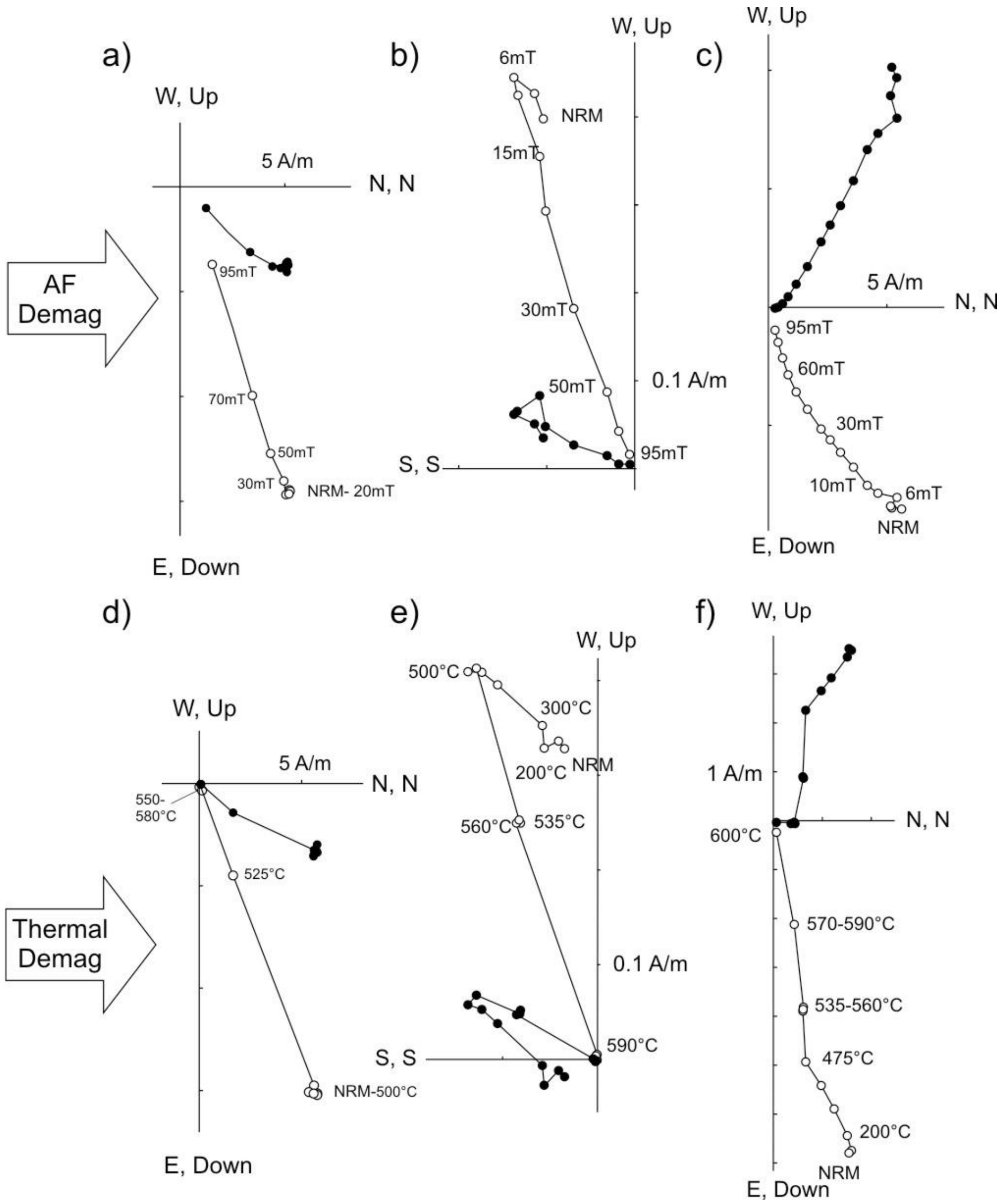

Figure 4.20 Characteristic examples of AF (a, b & c) and thermal (d, e & f) demagnetisation of Eastern Lobe Main Zone samples. Samples from (a) and (d) have been acquired from dimension stone quarries and possess near univectorial demagnetisation (i.e. single component of NRM) behaviour. Samples represented in (b), (c), (e) and (f) are from road cuttings and possess both LB and HB components. Open (solid) symbols represent projections onto the vertical (horizontal) planes, respectively.

Table 4.5 Site mean LB component directions. *Dec.* = declination, *Inc.* = inclination, α_{95} = 95 percent confidence circle around mean direction, N_o = original number of samples per site, N = number of samples analysed per site and κ = precision parameter.

Site	Dec	Inc	α_{95}	N_o/N	κ
1	82.8	-81.3	76	9/6	1.73
2a	114	-8.6	70.6	7/5	2.13
2b	201.5	-42.8	63	7/6	2.09
3	182.2	-52.5	42.3	14/5	4.22
8	112.3	68.2	80.5	8/6	1.65
42	254.5	11.4	180	9/3	1.02
43	315.3	49.5	180	10/2	0.85
44	85.7	36	52.4	8/4	4.05
45	63.9	49.8	94.3	9/3	2.82
46	325.5	52	85.6	10/3	3.17
47	325.5	52	85.6	9/3	3.17
48	308.4	54	109.1	7/3	2.41
49	288.6	22	0	8/1	n/a
50	55.2	43.4	127.2	9/3	2.11
51	56.4	53.2	29.3	9/2	74.87
52	344.1	11.3	13.6	8/4	20.52
53	40.6	11.4	11.9	8/8	8.15
54	29.5	54.4	56	9/4	3.67
55	286.1	42.5	19.2	8/6	4.23
56	345.6	-76.5	119.8	9/5	1.23
58	122.2	-22.4	44.6	8/8	1.76
59	277.3	1.4	30.5	6/6	2.99
61	181	-32.8	35.2	8/8	3.43
63	2.8	30.9	65.9	9/5	2.31
65	313.5	-11.1	60.1	8/8	1.7
69	40.5	19.7	60.8	8/5	2.54

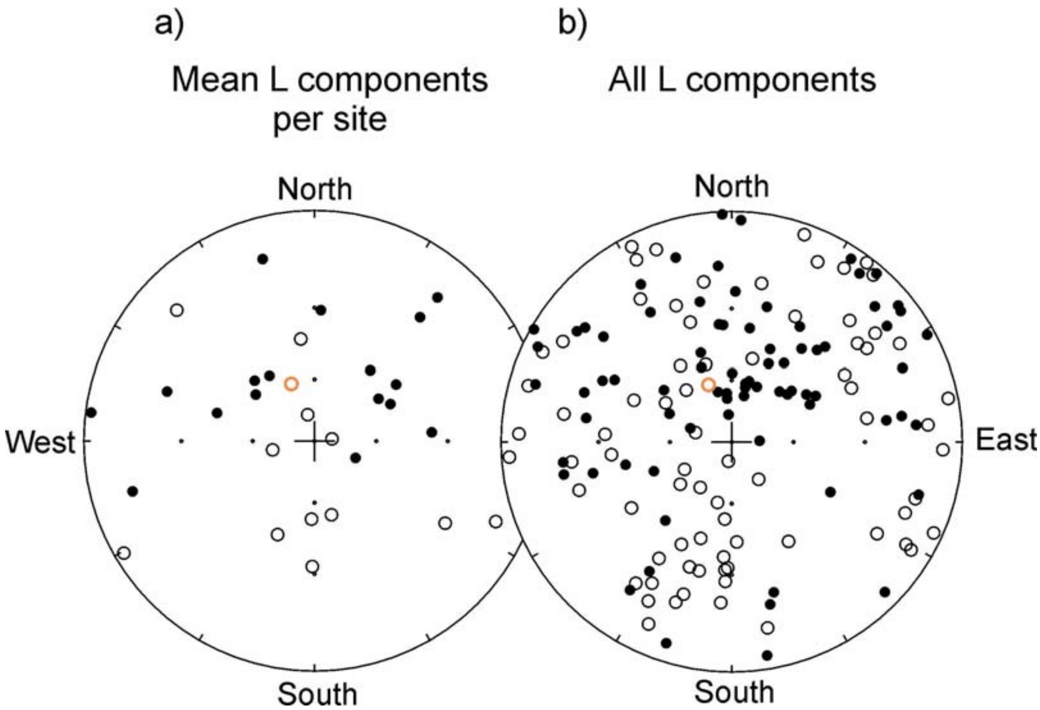

Figure 4.21 a) Site mean LB components from main Eastern Lobe sites, α_{95} circles are not shown as most values are greater then 90° b) All LB components from Western Lobe. The orange open circle in a NW steep direction represents the current magnetic direction in South Africa.

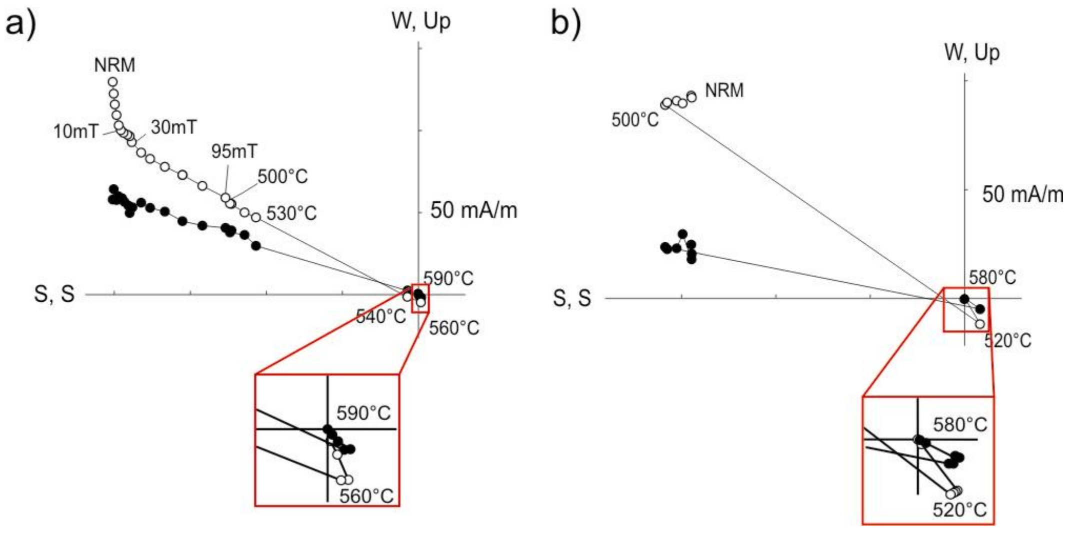

Figure 4.22 Examples of AF (a) and thermal (b) demagnetisation of samples from site 36. The maximum AF demagnetisation field of 95mT was not successful in demagnetising samples (a) and were further demagnetised thermally. Note that if there was no comparison to thermal demagnetisation (b) it would appear that the path defined by AF demagnetisation was decaying towards the centre and therefore be identified as the primary component.

HB components show extremely good grouping within sites, with α_{95} often <4° (Figure 4.23), and the resulting mean directions for sites show a remarkable increase in clustering from NRM directions. HB directions for sites show both positive and negative inclination, with the majority of the sites possessing HB components with steep positive inclinations and northeasterly declinations, while the remaining six sites have steep negative inclinations with southwesterly declinations. The resulting HB components are listed in Table 4.6.

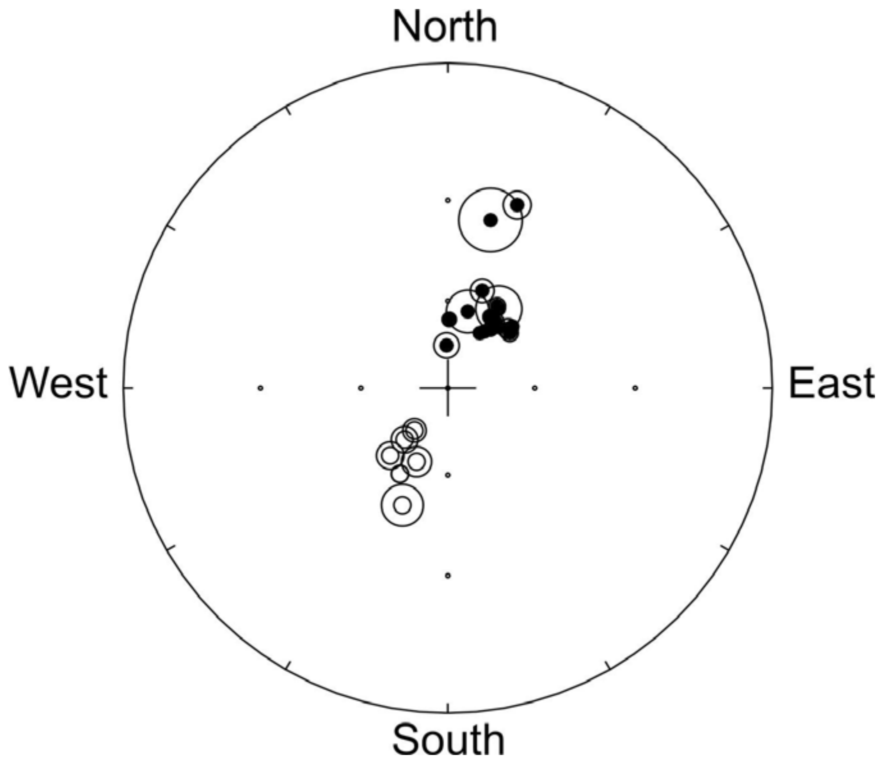

Figure 4.23 Site mean direction for Main Zone sites from the Eastern Lobe *in situ.* Mean site directions have drastically increased in clustering with the removal of secondary components. Sites possess both normal and reversed magnetisation, which are anti-polar to each other. Solid symbols indicate a positive inclination, while open symbols indicate a negative inclination.

Table 4.6 Site mean HB component of magnetisation directions of each site *in situ*. N_o = original number of samples per site, N = number of samples analysed per site; α_{95} = 95 percent confidence circle around mean direction; κ = precision parameter.

Site	Dec	Inc	strike	Dip	N_o/N	α_{95}	κ
1	220.1	-69.9	220	11	9/9	4.5	133.45
2a	230.3	-54.1	218	14	7/7	4.5	181.93
2b	204.4	-63.1	216	14	7/7	2.8	479.85
3	200.3	-52.9	210	15	14/14	6.4	39.15
8	36.2	61.9	169	10	8/8	2.8	405.98
42	34.6	64.8	195	12	9/9	2.4	477.92
43	30.8	61.4	190	11	10/10	2.4	420.08
44	53.1	62.4	194	10	8/8	2.8	389.93
45	32.8	67	205	10	9/9	1.6	1014.69
46	28.9	63	199	11	10/10	1.5	1099.84
47	37.7	62.5	193	11	9/9	1.1	2086.86
48	29.5	64	195	11	7/7	1.4	1910.6
49	29.2	67.1	197	10	8/8	0.9	4021.26
50	30.6	57.4	187	12	9/9	2.7	366.44
51	44.8	58.2	192	11	9/9	1.9	762.04
52	347.5	11.8	90	40	8/4	8.7	112.49
53	40.7	6.3	36	10	8/8	7.1	61.65
54	6.6	64.5	36	10	9/9	2.4	474.89
55	305.5	62.3	195	11	8/8	3.3	5550
56	182	-42.4	181	10	9/5	7.5	104.64
58	100.6	47.3	181	12	8/8	3.3	8
59	291.4	22.5	160	10	6/6	4.4	236.6
61	192.3	-47.9	210	11	8/8	5	124.77
63	4.1	38.3	134	15	9/9	3.8	188.67
65	1.8	20	134	15	8/8	3.6	243.51
69	21.9	-88.8	216	14	8/8	4	195.24

4.2.4 Thermomagnetic and petrographic analysis

Typical response to TMA is shown in Figure 4.24 in which curves are almost reversible, except for a small increase in saturation magnetisation upon cooling. Samples indicate a Curie temperature of ≈ 580°C.

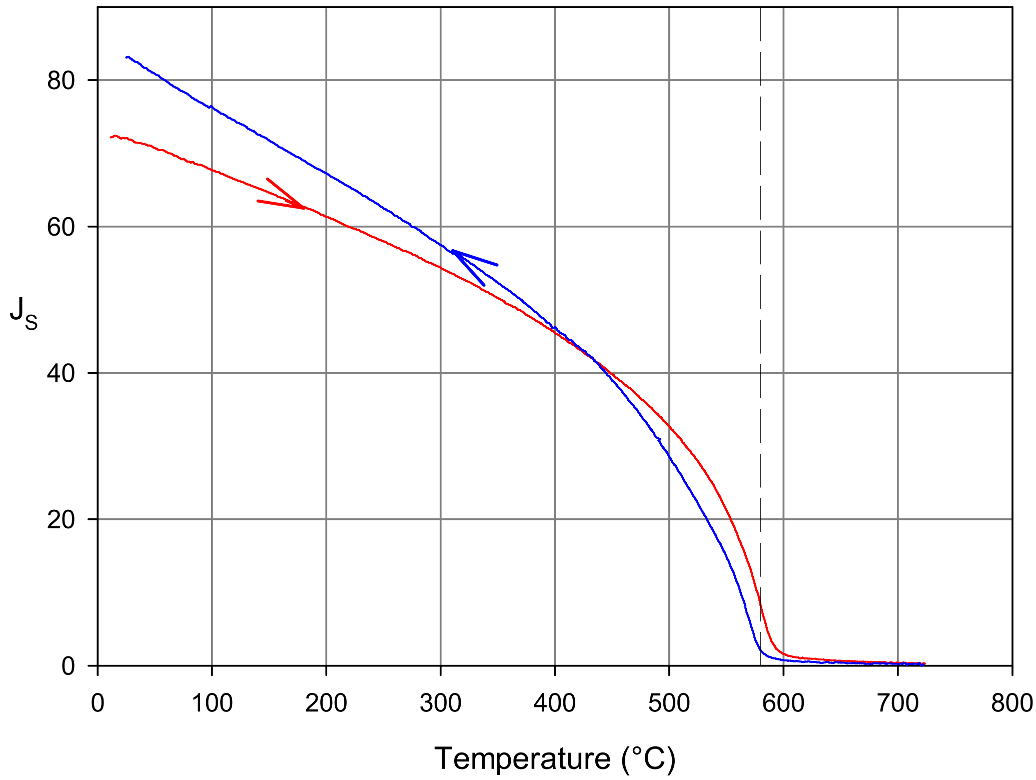

Figure 4.24 Typical thermomagnetic analysis response from Eastern Main Zone sites, this example is from site 52. Red line and arrow indicate heating phase while blue line and arrow indicates cooling phase. Curie temperature for magnetite at ≈ 580°C observed (dashed line). The observed increase in saturation magnetisation during cooling implies the possible production of more magnetite.

Petrographic analysis was undertaken to determine the opaque mineralogy for the eastern Main Zone. Reflected light microscopy on samples revealed a minor number of large lamellae of magnetite occurring in both pyroxene and plagioclase (Figure 4.25). During transmitted light microscopy, it was discovered that smaller lamellae (Figure 4.26 and Figure 4.27) are more abundant but due to their small size, they could not be accurately identified as magnetite. However, it was concluded that based on TMA and the appearance of larger lamellae the small lamellae are most likely magnetite. To a minor extent, discrete ilmenite and pyrrhotite grains were also found.

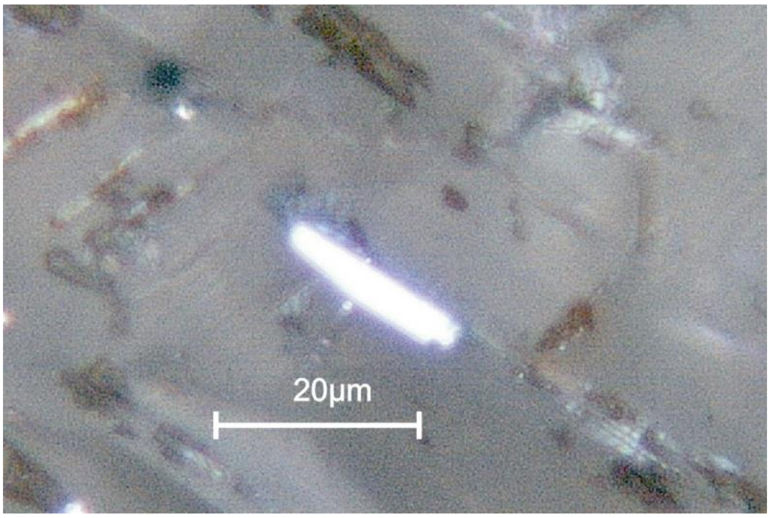

Figure 4.25 A "large" magnetite needle occurring in plagioclase grain from site 70, reflected light.

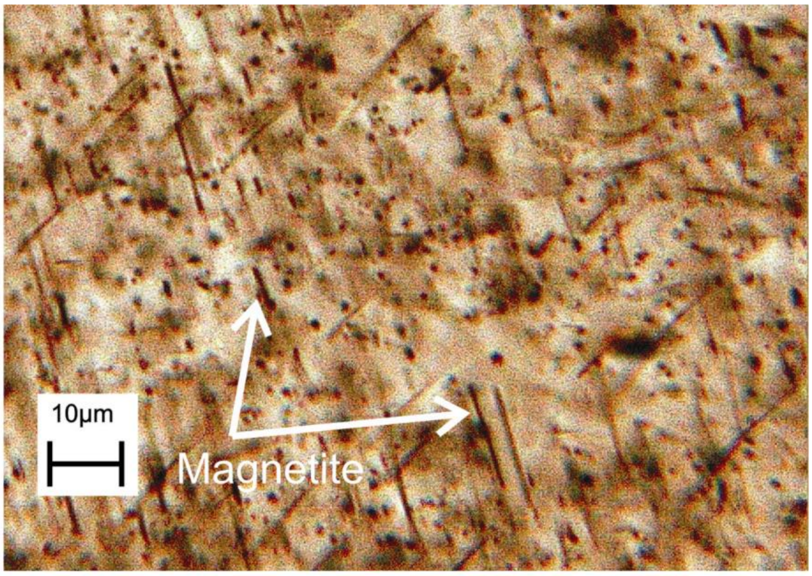

Figure 4.26 Magnetite occurring as needles in pyroxene from site 8, transmitted light.

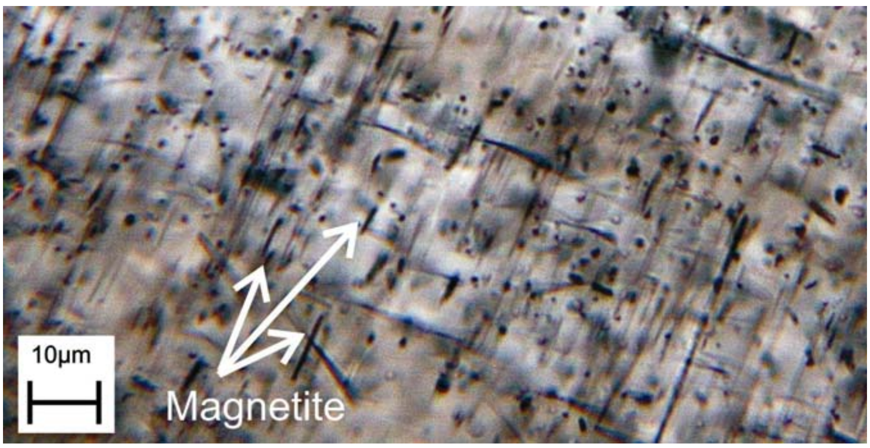

Figure 4.27 Magnetite occurring as needles in plagioclase grain from site 44, transmitted light.

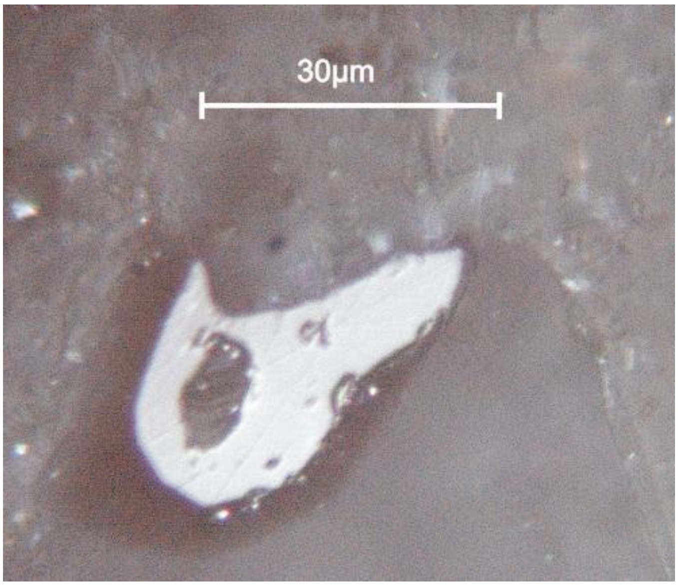

Figure 4.28 Discrete ilmenite grain from site 2, reflected light

4.2.5 Field stability tests.

Fold Test

Rocks from the Eastern Lobe outcrop in a crude "hook" shape, dipping towards the centre of the complex at angles of between 10 and 15°. This "hook" shape is produced initially from Belfast through to Steelpoort where rocks have a north-south trend and dip towards the west at angles of between 10 and 15°. Moving from Steelpoort further north rocks curve towards the west causing strikes approximately NW and dips inwards in a SW direction.

In an attempt to restore samples to a horizontal attitude, bedding corrections were applied to all HB components. The dips and strikes used are listed in Table 4.6. Upon stepwise unfolding a uniform increase in statistical precision parameter κ was observed from 47.7 to 83.2 (Figure 4.29,c). The resulting increase in κ, although not as drastic as encountered in the Western Lobe, has produced a positive fold test at the 95% confidence level according to the classic fold test of McElhinny (1964b).

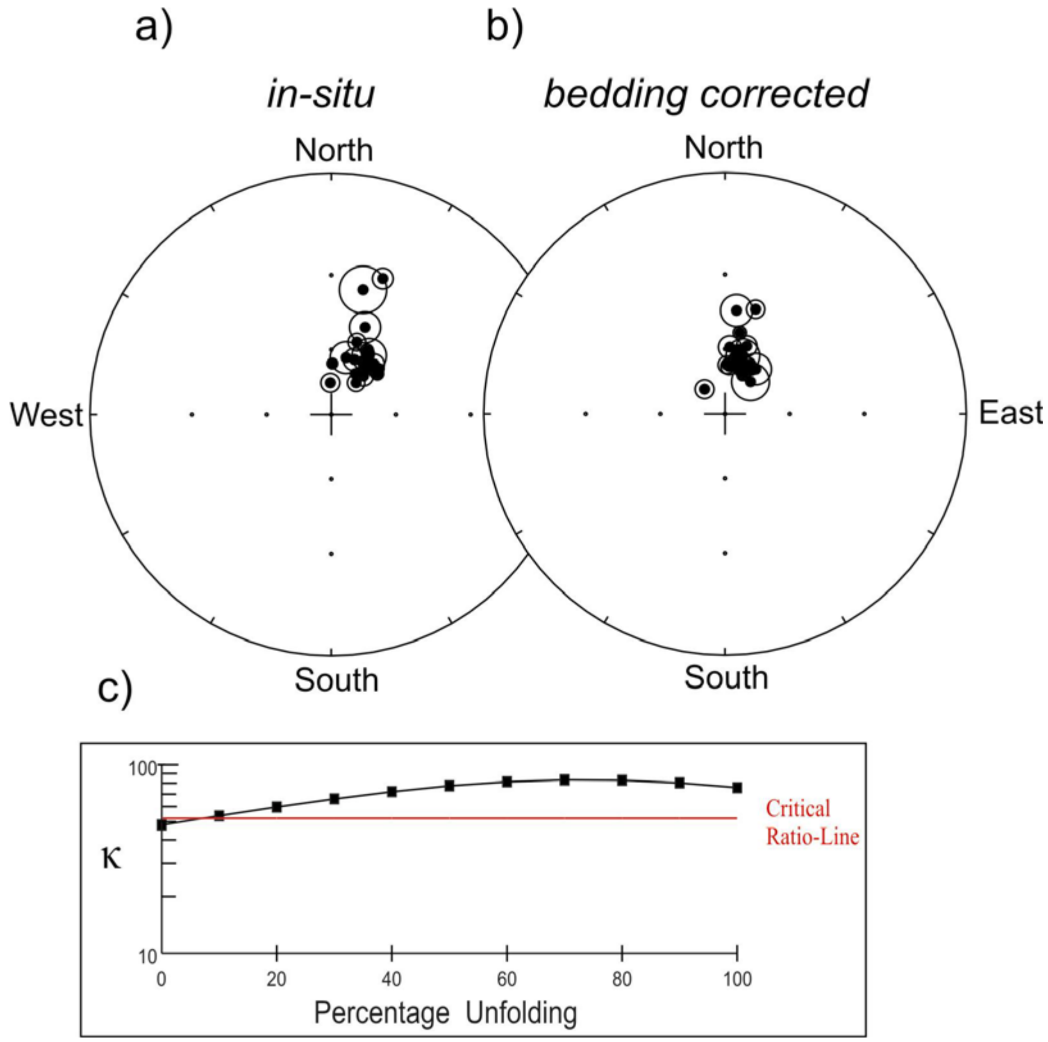

Figure 4.29 Site mean direction for Main Zone sites from the Eastern Lobe in both *in situ.,* sites with negative inclinations have been inverted to positive inclination (a), and bedding corrected co-ordinates (b). Closed symbols denote positive inclination, while open circles denote negative inclinations. c) Shows variation in precision parameter κ as a function of stepwise unfolding. The red line is the 'critical ratio-line' indicating the 95% statistically significant level.

Reversal Test

Samples from the eastern Main Zone possess magnetisation in both negative and positive directions. Two reversal tests were implemented in order to determine if the reversely magnetised samples were of similar age to the normally magnetised ones. It was found that the samples share a common mean at 95% confidence according to the method of McFadden and Lowes (1981). The other reversal test developed by McFadden & McElhinny (1990) indicated a positive reversal test with a "C" classification, $\gamma_{observed}$ = 5.39 and γ_{crit} = 10.35. Since the samples produced a positive reversal test, it is assumed that are related to the same magmatic event and that a reversal in the Earth's magnetic field was recorded.

4.2.6 Interpretation of palaeomagnetic data from the Eastern Lobe Main Zone

The majority of NRM directions from the Eastern Lobe display a scatter in directions, with the exceptions of sites obtained from dimension stone quarries. During component analysis it was revealed that the majority of samples possessed low temperature components that caused the scattering in NRM direction. Complete progressive demagnetisation successfully removed all minor low temperature components and allowed for the identification of well defined high temperature components, which produce extremely well clustered results.

During thermal demagnetization, it was revealed that samples had maximum unblocking temperatures at around 565-580°C, suggesting that titanium-poor titanomagnetite or nearly pure magnetite is the bulk remanence carrier. This finding was further strengthened by thermomagnetic analysis indicating a Curie temperature at ≈ 580°C and petrographic analysis revealing magnetite in the form of lamellae in plagioclase and pyroxene as the dominant opaque mineralogy.

The presence of both polarities and improved grouping after palaeo-horizontal corrections point toward a primary magnetisation being recorded by HB components. With this in mind, HB components were used to calculate a mean direction of magnetisation for the eastern Main Zone (with negative inclinations inverted) of declination = 14.7°, inclination = 63.8° (α_{95} = 3.3º, N =26 sites). The calculated pole position from this mean direction yielded a palaeolatitude of 18.3° and palaeolongitude of 40.5°, dp/dm = 4.2°/5.2°. This pole was calculated at mean sampling co-ordinates of 25°S and 29.7°E.

4.3 Critical Zone

Outcrops of the Critical Zone produced few viable palaeomagnetic drill sites. In total only four sites were obtained on surface: two from river beds and two from road exposures. The rather restricted number of suitable sites on surface led to samples being obtained from underground platinum mines, where another six sites were sampled. Four mines were visited: Hackney (2 sites- Eastern lobe), Royal Bafokeng resource (BRPM, 2 sites- Western Lobe), Amandelbult (Western Lobe) and Modikwa (Eastern Lobe) (Figure 4.30). Coverage of the Critical Zone is imperfect, with large sections not being sampled (Figure 4.31).

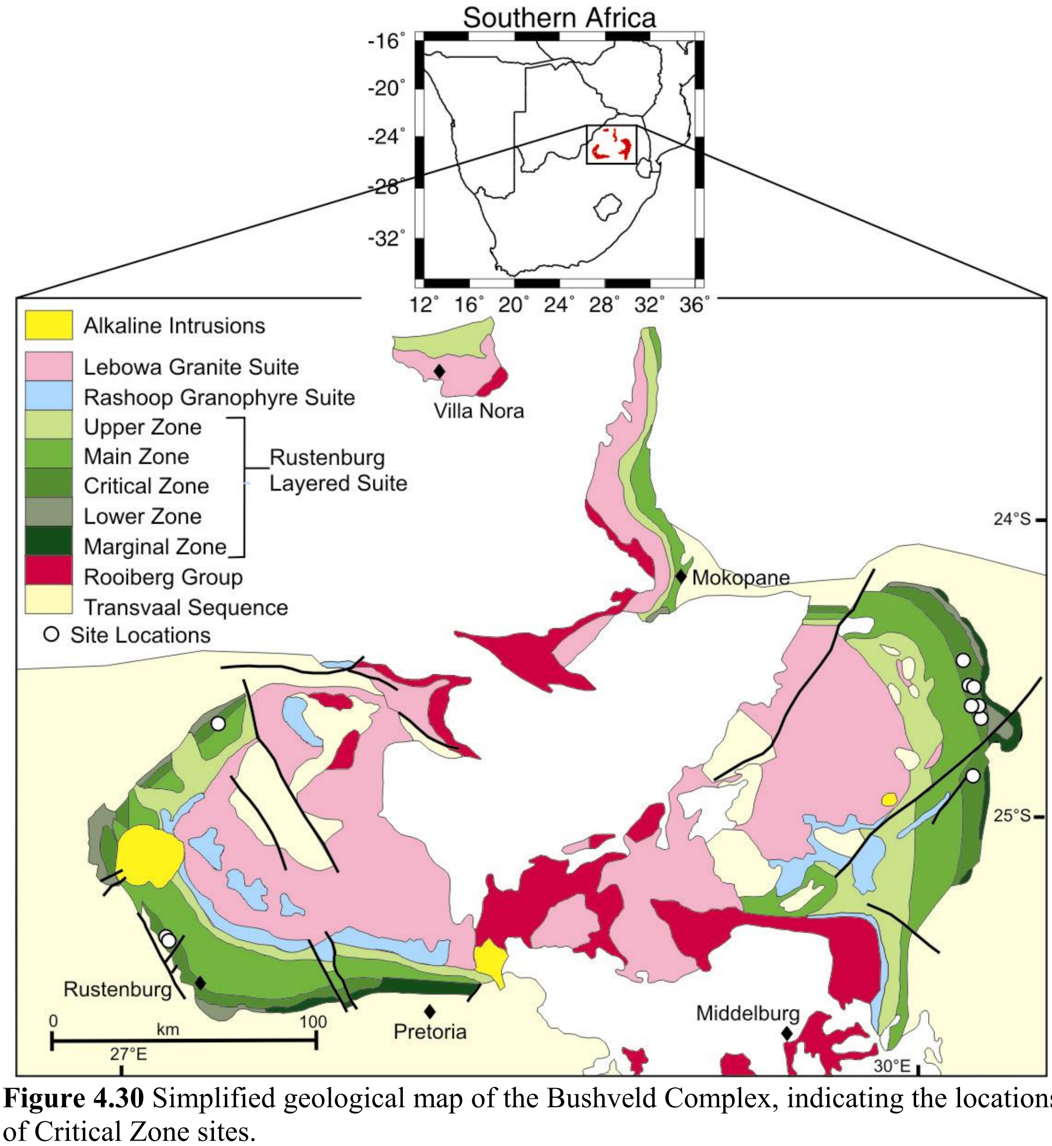

Figure 4.30 Simplified geological map of the Bushveld Complex, indicating the locations of Critical Zone sites.

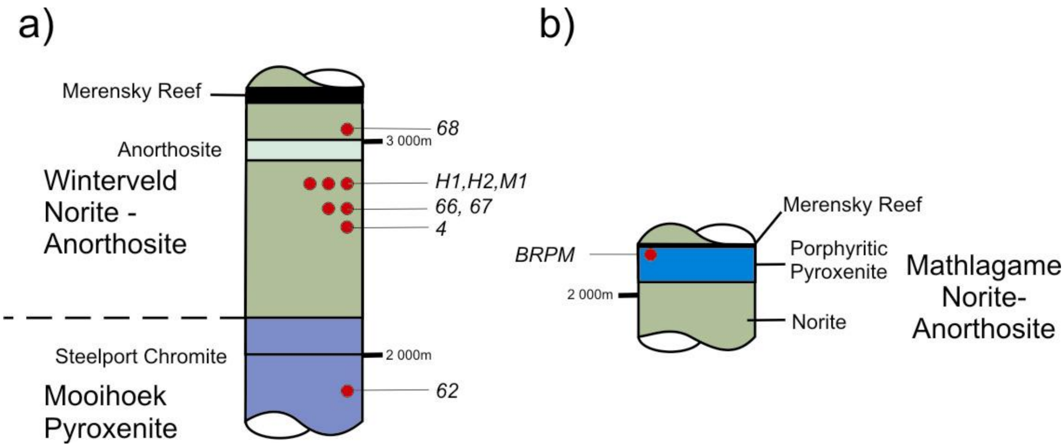

Figure 4.31 Simplified stratigraphic column of the Critical Zone for both the Eastern Lobe (a) and Western Lobe (b) with site locations. H1 and H2 are from Hackney Mine, while M1 is from Modikwa mine.

Figure 4.32 One of the rare surface outcrops of the Critical Zone in the Eastern Bushveld Complex, site 68.

In previous studies samples were orientated underground using a magnetic compass. This method of orientation is not very reliable, as the readings can easily be affected by a number of underground articles, namely infrastructure (electrical cables, cooling vents, and support pillars), equipment and highly magnetic rocks. Before samples could be obtained a reliable method of orientating had to be found.

To ameliorate the problem of orientating samples underground, an instrument was devised that could measure the angles from the strike of the rock to a survey pegs. The device is made up of a laser pointer and protractor mounted on a piece of Perspex with a straight edge (Figure 4.33). The device is then placed against the rock and the angle between the strike of the rock and the survey peg is measured. Angles were taken to two survey pegs as well as the distance from the pegs to the sample, and then by trigonometry the strike of the rock sample could be obtained. For a detailed description of the mathematics behind this, consult Appendix A. By measuring the angle to two survey pegs, the accuracy of the method could be determined and in general it was found that measurements were within 1-2° of each other. Other methods of orientating samples probably exist, but with limited help from mine surveyors this method provided to be extremely useful and reliable.

Figure 4.33 Orientation device used to accurately orientate samples underground. The flat end of the device is placed along the strike of the rock and the laser pointer is then pointed towards the survey peg, where the bearing is read off.

4.3.1 NRM

From the 10 sites, a total of 88 core samples were analysed initially for NRM and bulk susceptibility before demagnetisation was carried out. NRM intensities showed a wide range from 0.3 to 467 mA/m, with an average value of 124.6 mA, and susceptibility from 114 to 1016 $\times10^{-6}$ SI units, with an average of 382.3 $\times10^{-6}$ SI units. Variation in susceptibility and NRM intensity with stratigraphic location can be seen in Figure 4.34. The mean NRM values and bulk susceptibility values for all sites with errors are shown in Table 4.7. Samples from Amandelbult were not analysed as orientation marks on the hand samples wore off before cores could be extracted.

Table 4.7 Site mean NRM, mean bulk susceptibility and Q ratio of all sites. *Dec.* = declination, *Inc.* = inclination, α_{95} = 95 percent confidence circle around mean direction, N= number of samples, +/- = 1 σ error and Susc.= Susceptibility

Site	NRM Dec.	NRM Inc.	α_{95}	N	Intensity Average (A/m)	+/- (mA/m)	Susc. Average ($\times10^{-6}$ SI units)	+/- ($\times10^{-6}$)	Q Ratio
4	50.7	24.4	54.4	13	0.3	0.2	114.8	35.0	0.4
66	178.4	-51.9	10.6	8	15.5	5.8	230.6	81.6	0.8
67	175.1	-35.6	18.3	9	14.9	5.7	274.9	60.3	0.9
68	333.2	32.6	14.5	9	15.3	4.8	275.2	166.9	0.9
M	224.1	-73.5	2.8	11	467.3	41.3	379.1	29.4	1.3
B1	147.9	23.9	63.1	10	462.7	255.0	1016.8	556.0	3.4
B2	354.2	60.9	55	11	8.4	6.8	518.2	152.6	1.7
H2	67.5	11.8	3.4	10	96.5	25.8	385.7	72.7	1.3
H1	166.2	-41.5	9.4	7	40.4	6.3	245.2	27.0	0.8

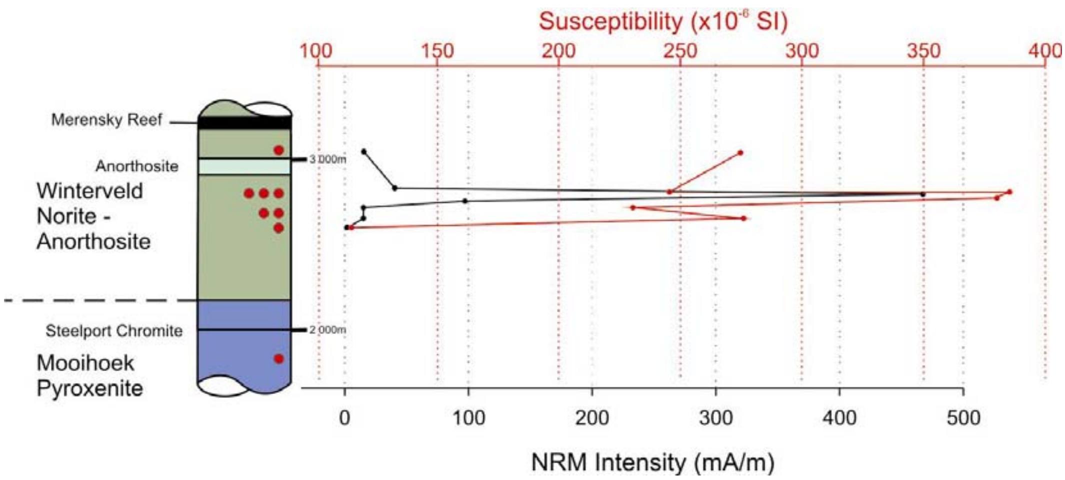

Figure 4.34 Variation in NRM intensity and susceptibility for the eastern Critical Zone

Mean NRM directions for the Critical Zone, with the exception of sites H2, 4 and B1, group in two clusters (Figure 4.35); the first has steep negative inclinations in a southerly direction, while the second is roughly anti-polar to the first with steep positive inclinations in a northerly direction. Sites show varying degrees of within-site grouping, a few sites show exceptional grouping, while others show poor grouping (Table 4.7).

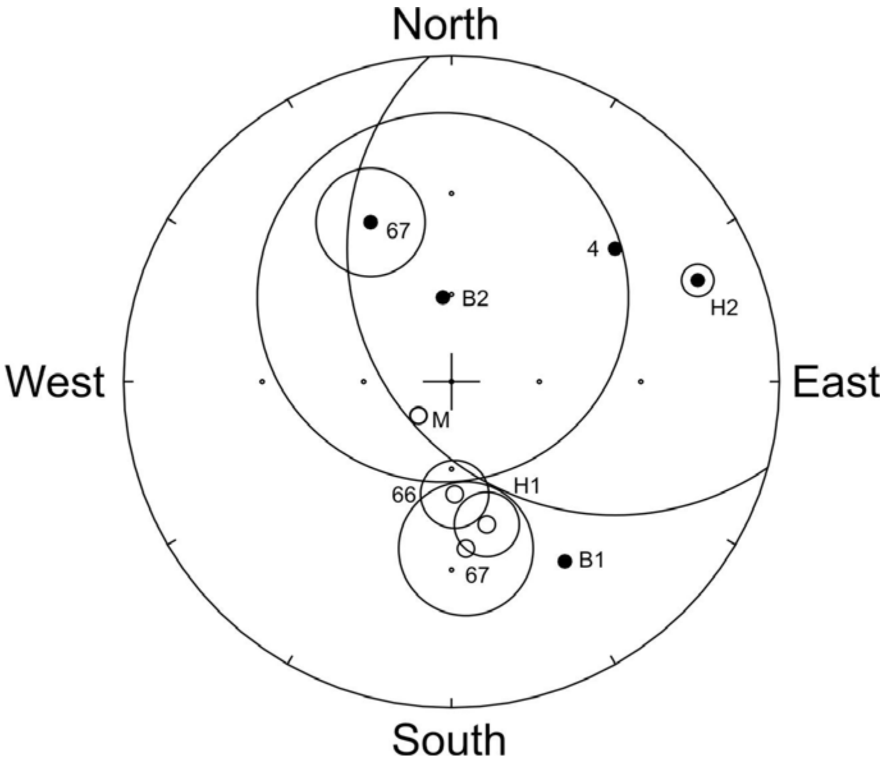

Figure 4.35 Site mean NRM directions from Critical Zone Sites with α_{95} circles. α_{95} for site B1 is too large to plot. M=Modikwa mine, H= Hackney mine, B =BRPM mine.

4.3.2 Demagnetisation

In an attempt to elucidate the magnetic history of the Critical Zone since formation, samples were subjected to AF (33) and thermal demagnetisation (55). Demagnetisation was carried out using between 10 and 16 steps up to 620° C (but generally 600°C) or 95mT (maximum level obtained from AF machine). Once demagnetisation was completed, data were plotted on Zijderveld diagrams and subjected to principal component analysis to determine the ChRM and low coercivity or low temperature blocking components (LB). Samples from BRPM2 and M2 (Modikwa mine) were unstable during demagnetisation and results were rejected from analysis.

4.3.3 Components of magnetisation

Samples behaved exceptionally well to both thermal and AF demagnetisation, and two magnetisation components have been readily identified. LB components are present in most samples, but they are mostly scattered at site-level (Figure 4.36 and Table 4.8). These low temperature components are typically removed at around 500ºC or 30-40mT. Their directions are not related to any significant geological meaning and are not considered further.

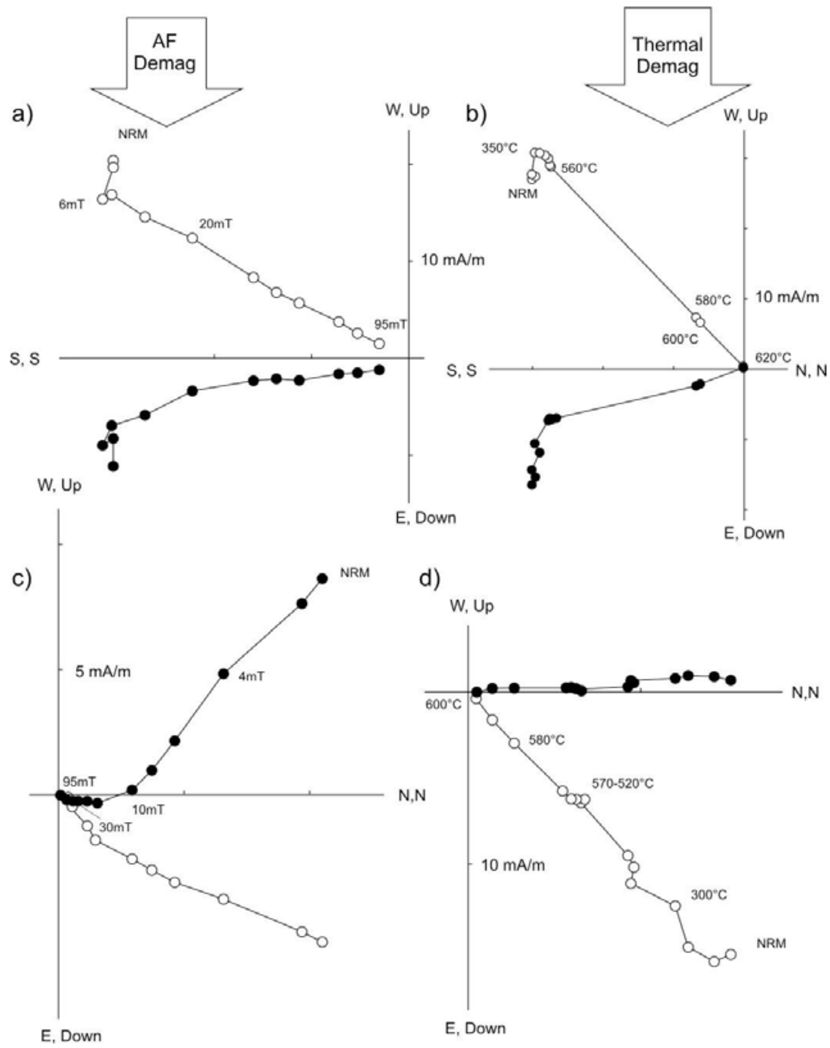

Figure 4.36 Typical Zijderveld diagrams from AF (a & c) and thermal demagnetisation (b & d) of samples from the Critical Zone. Open (solid) symbols represent projections onto the vertical (horizontal) planes, respectively.

Table 4.8 Site mean LB component directions. *Dec.* = declination, *Inc.* = inclination, α_{95} = 95 percent confidence circle around mean direction, N_o = original number of samples per site, N = number of samples analysed per site and κ = precision parameter.

Site	Dec	Inc	α_{95}	N_o/N	κ
4	27	-35.3	55.1	13/2	22.72
66	79.4	-17.7	20.6	8/4	20.85
67	336.4	-69.2	103.2	9/5	1.53
68	313.7	23.8	23.2	9/7	7.75
M	53.2	-54.1	180	11/3	1.04
B1	153.1	8.2	69.1	10/9	1.52
B2	60.2	9.2	108.8	11/6	1.35
H1	254.5	-55.8	95.5	7/3	2.78

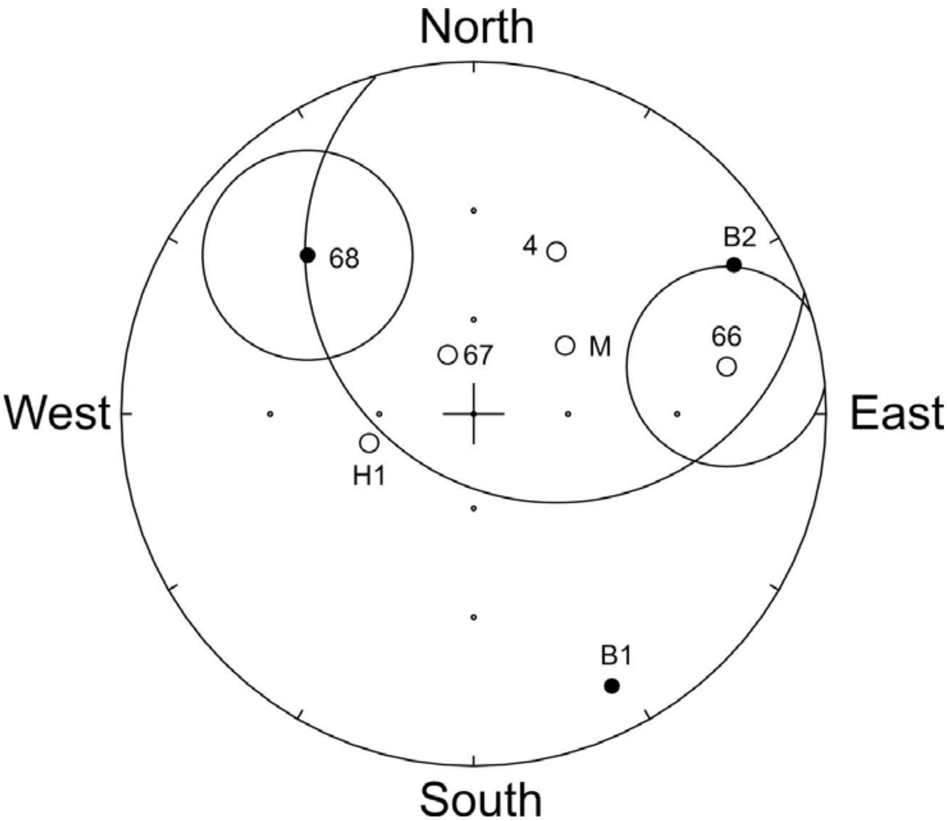

Figure 4.37 Site mean LB site components from Critical Zone rocks, α_{95} circles for site 4, 66 and 68 are show as the others are too large to plot (greater then 60°)

With the removal of low coercivity (or low temperature) remanence, one of two approximately anti-polar higher coercivity (or high temperature) remanence directions were isolated above 550°C or 50mT (Figure 4.36). HB components show reasonable grouping within-site (α_{95} around 6°), mean site directions plotting with a SSW declination and steep negative inclination or anti-polar to this (NNE declination and steep positive inclination). The resulting HB components are shown in Figure 4.38 and listed in Table 4.7.

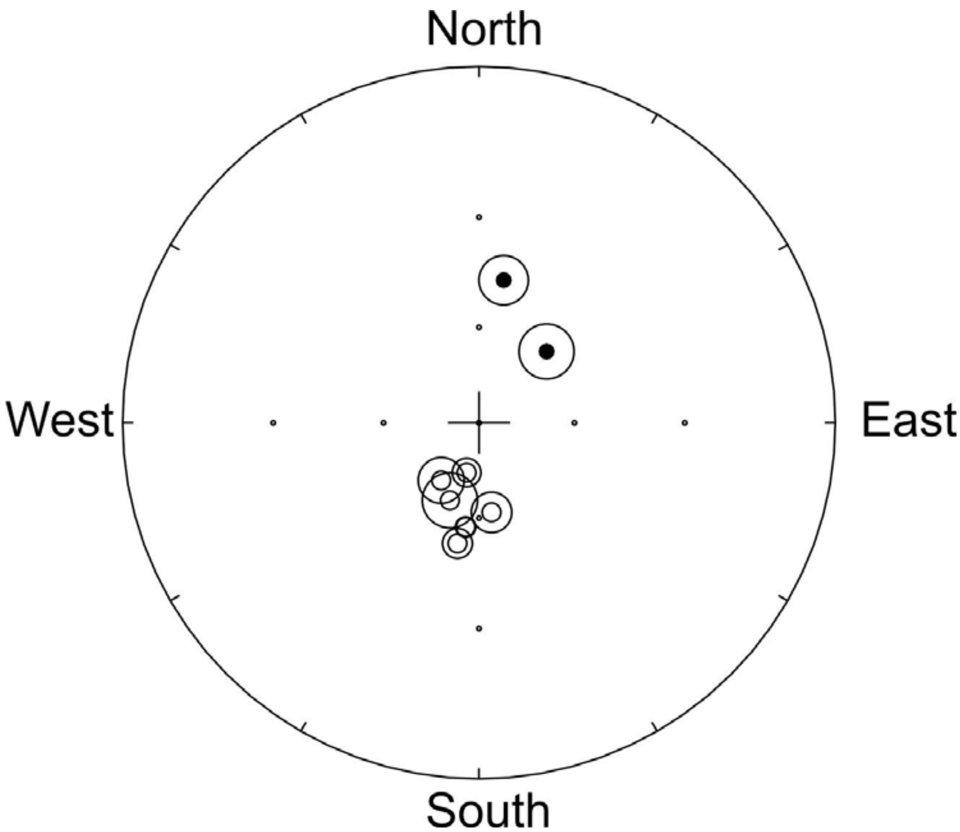

Figure 4.38 Site mean direction for Critical Zone *in situ.* Solid symbols indicate a positive inclination, while open symbols indicate a negative inclination

Table 4.9 Site mean HB component of magnetisation directions of each site *in situ*. N_o = original number of samples per site, N = number of samples analysed per site; α_{95} = 95 percent confidence circle around mean direction; κ = precision parameter.

Site	Dec	Inc	strike	Dip	N_o/N	α_{95}	κ
4	43.5	59.2	182	12	13/7	8.2	25.68
66	200.5	-63.8	184	10	8/7	8.4	53.02
67	213.2	-68.1	184	10	9/6	7.1	90
68	9.8	45.8	145	11	9/6	6.8	195
H2	187.3	-57.1	182	10	11/10	3	265.56
B	172	-61.5	330	14	10/10	6.1	63.05
M	194	-73.6	184	10	11/11	4.5	101.83
H1	190.1	-52	182	10	7/7	4.3	193030

4.3.4 Thermomagnetic and petrographic analysis

Thermomagnetic analysis (TMA) was carried out on a horizontal translation balance (Curie Balance) in order to determine the Curie temperature of samples and hence the carrier of magnetisation. TMA illustrated in Figure 4.39 indicates that samples have a Curie temperature of ≈ 580°C.

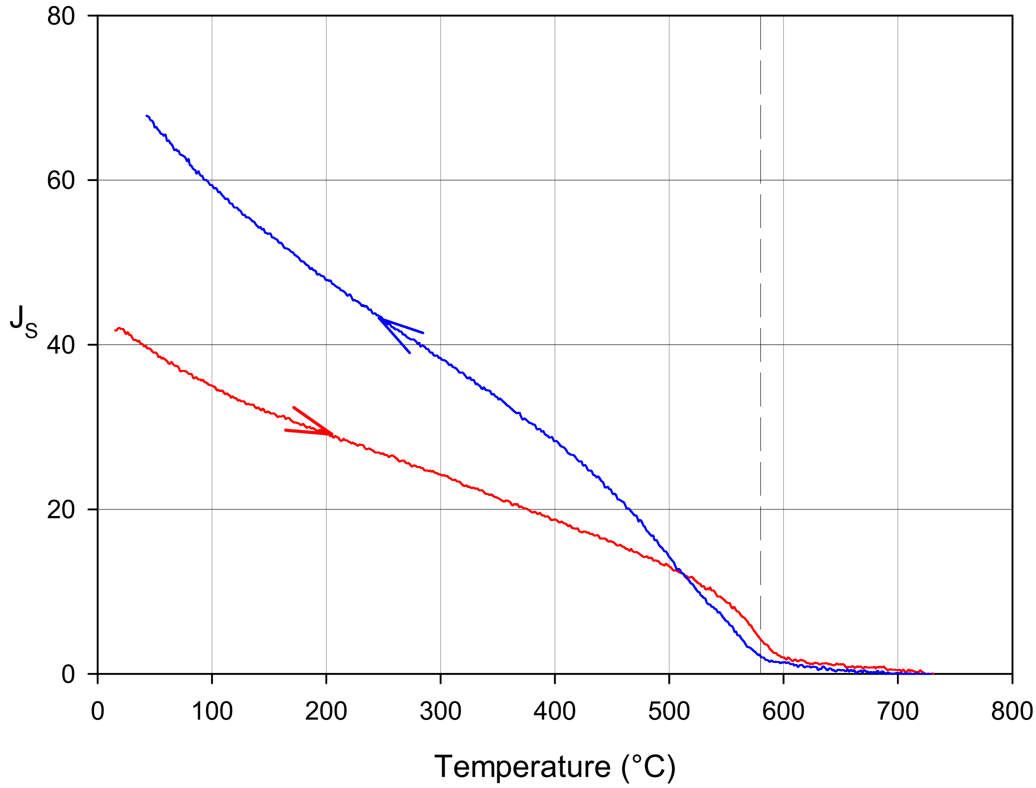

Figure 4.39 Typical thermomagnetic analysis response from Critical Zone, site 66 is illustrated above. Red line and arrow indicate heating phase while blue line and arrow indicates cooling phase. Curie temperature for magnetite at ≈ 580°C observed (dashed line). In this example there is a large observed increase in saturation magnetisation during cooling implies the possible production of more magnetite.

Thin section analysis revealed minor number of different sulphides (pyrrhotite being the majority). Petrographic analysis failed to identify magnetite in thin section. Magnetite might occur as needles or lamellae in both plagioclase and pyroxene; however grains were too small to identify. Due to TMA analysis having a Curie temperature of ≈ 580°C, it is assumed that the lamellae are magnetite as identified in all other zones.

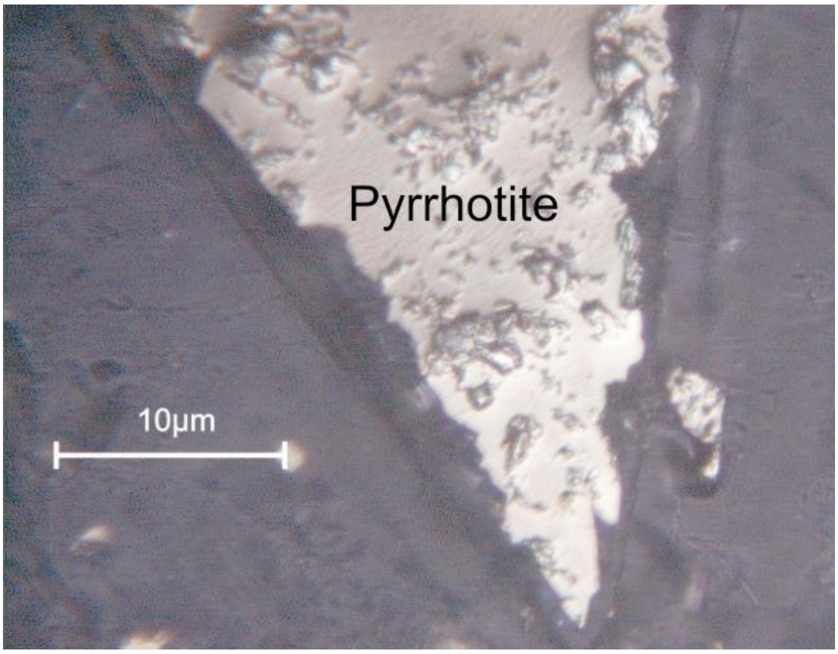

Figure 4.40 Petrographic analysis revealed pyrrhotite as the dominate sulphide mineral. Thin section obtained from site M.

4.3.5 Field stability tests.

Fold Test

Rocks of the Bushveld Complex and hence that of the Critical Zone all dip towards the centre of the Complex, with varying dip angles of between 10° and 18°. Bedding corrections were applied to all HB components to restore the layers to a horizontal attitude (dips and strikes used in the bedding correction are listed in Table 4.9). Upon uniform unfolding, site mean directions showed a minor increase in grouping (Figure 4.41) and precision parameter κ from 42.41 to 67.5 and a slight decrease in α_{95} value from 8.1 to 6.8. This minor improvement was not sufficient to produce a positive fold test of McElhinny (1964).

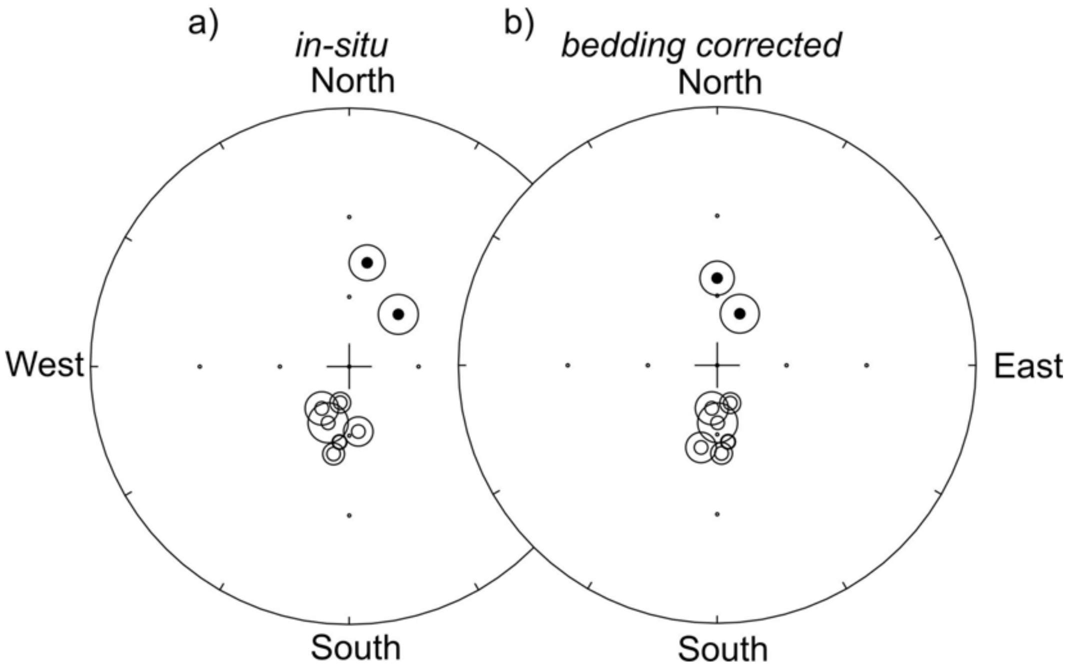

Figure 4.41 Site mean direction for Critical Zone sites *in situ* (a), and bedding corrected co-ordinates (b). Closed symbols denote positive inclination while open circles denotes negative inclinations.

Reversal Test

Two reversal tests were implemented in order to determine whether the reversely magnetised samples were of similar age to the normally magnetised ones. It was found that the samples shared a common mean at 95% confidence according to the method of McFadden and Lowes (1981). The other reversal test developed by McFadden & McElhinny (1990) indicated a positive reversal test with a "C" classification, $\gamma_{observed}$ = 5.71 and γ_{crit} = 16.11. Since the samples indicated a positive reversal test, it is assumed that are related to the same magmatic event and that a reversal in the Earth's magnetic field was recorded.

4.3.6 Interpretation of palaeomagnetic data from the Critical Zone

NRM directions from the Critical Zone show a reasonable grouping in two anti-polar groupings. During demagnetisation it was revealed that samples possess minor low unblocking components that have no correlation with any known remanence direction for the area. Remanent directions converge upon HB components as demagnetisation preferentially removed the less stable components, which displayed well clustered results.

HB components had maximum unblocking temperatures at around 565-580°C, suggesting that titanium-poor titanomagnetite or nearly pure magnetite was the bulk remanence carrier. This finding was further strengthened by thermomagnetic analysis indicating a Curie temperature at ≈ 580°C.

The presence of both polarities in samples, and the slight improvement in grouping produced after palaeo-horizontal corrections points toward a primary magnetisation being recorded by HB components. Although the Critical Zone was not significant at the 95% confidence level for the fold test of McElhinny (1964), the resulting pole position after bedding corrections plots closer in proximity to the other zones. Therefore, it is assumed that the zone acquired its magnetisation while the layer was in a near horizontal position.

The calculated mean direction of magnetisation for the Critical Zone with negative inclinations inverted, is declination = 1.7° , inclination = 61.7° (α_{95} = 6.8º, N =8 sites) and resulting in a pole position with palaeolatitude = 22.1° and palaeolongitude = 31°, dp/dm = 8.1°/10.5° (palaeopole calculated at mean sampling co-ordinates of 25°S and 29.7°E).

4.4 Upper Zone

Palaeomagnetic drill locations for the Upper Zone were extremely limited, with only eight sampling localities being obtained. This absence of suitable sampling sites is reflected in the scarce distribution of sites throughout the Upper Zone (Figure 4.42).

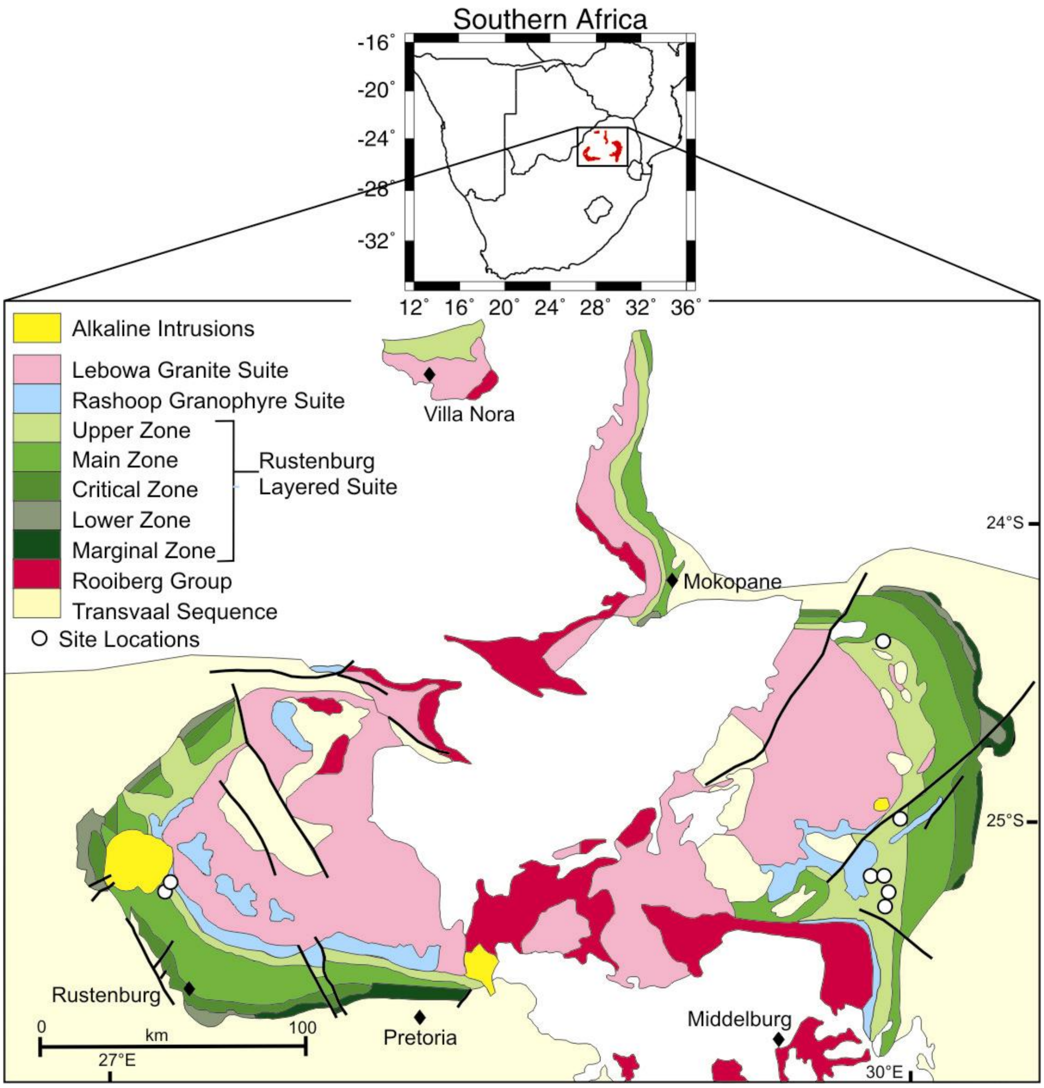

Figure 4.42 Simplified geological map of the Bushveld Complex, indicating the locations of sites.

From the eight sites attained from the Upper Zone, two were from the Western Lobe and the remaining six from the Eastern Lobe. Sites were located in river beds (5) and road cuttings (3). Unfortunately, due to the limit in suitable palaeomagnetic outcrop, coverage of the Upper Zone is rather poor (Figure 4.43).

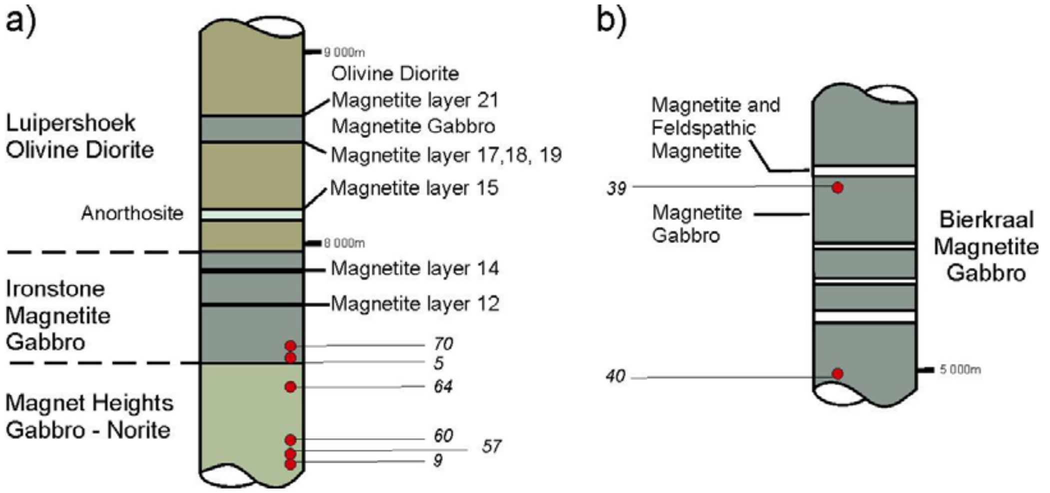

Figure 4.43 Simplified stratigraphic column of the Upper Zone indicating locations of sites for the Eastern Lobe (a) and Western Lobe (b).

Figure 4.44 Two river sites from the Upper Zone. Left picture is from the Western Lobe (site 39) while the right picture is from the Eastern Lobe (site 70).

4.4.1 NRM

A total of 91 cores were initially measured for NRM and bulk susceptibility before being subjected to progressive demagnetisation. NRM intensities showed a broad range in values from 0.322 A/m up to 42.24 A/m, with an average value of 14.7 A/m. Susceptibility values also exhibited a large variation in results from 750 up to 50,094 $\times 10^{-6}$ SI units with an average value of 18,139 $\times 10^{-6}$ SI units. Variations in susceptibility and NRM intensity for the Eastern Lobe are shown in Figure 4.45. The mean NRM and bulk susceptibility values for all sites with errors are shown in Table 4.10.

Table 4.10 Site mean NRM, mean bulk susceptibility and Q ratio of all sites. *Dec.* = declination, *Inc.* = inclination, α_{95} = 95 percent confidence circle around mean direction, N= number of samples, +/- = 1 σ error and Susc. = Susceptibility

Site	NRM Dec.	NRM Inc.	α_{95}	N	Intensity Average (A/m)	+/- (mA/m)	Susc. Average ($\times10^{-6}$ SI units)	+/- ($\times10^{-6}$)	Q Ratio
5	212.0	-62.0	6.7	13	4.8	1293.9	750.0	118.2	24
9	6.5	52.3	23.2	10	1.7	428.6	16191.9	1939.0	0.4
39	155.6	-77.6	28.5	13	5.1	647.3	50094.2	23916.0	0.4
40	130.1	-27.4	13.5	13	0.3	182.9	652.9	190.7	1.9
57	319.0	-21.2	16.9	13	28.9	19735.5	30083.0	7870.4	3.6
60	198.4	-6.4	29.5	10	30.7	13113.7	21980.1	10500.7	5.3
64	175.4	-60.9	41.0	9	3.5	345.5	7220.9	1381.3	1.8
70	342.0	-76.7	12.5	10	42.2	3886.15	n/a	n/a	0.6

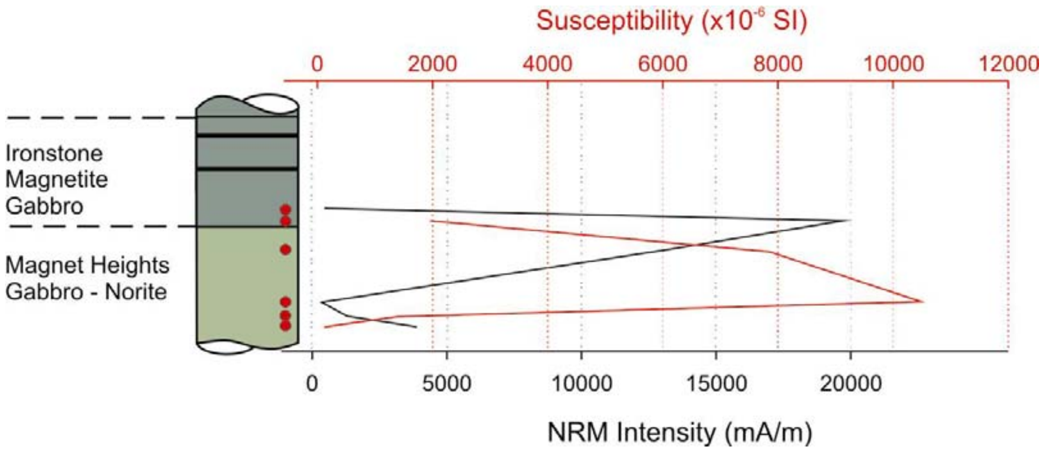

Figure 4.45 Variation in NRM intensity and susceptibility for the Upper Zone of the Eastern Lobe.

Samples within sites show poor grouping (illustrated by high α_{95} values in Table 4.10 and Figure 4.46) and the resulting mean NRM directions from sites show an extremely scattered distribution around a steep negative inclination with SSW declinations. Site 9 is roughly anti-polar in directions to the others.

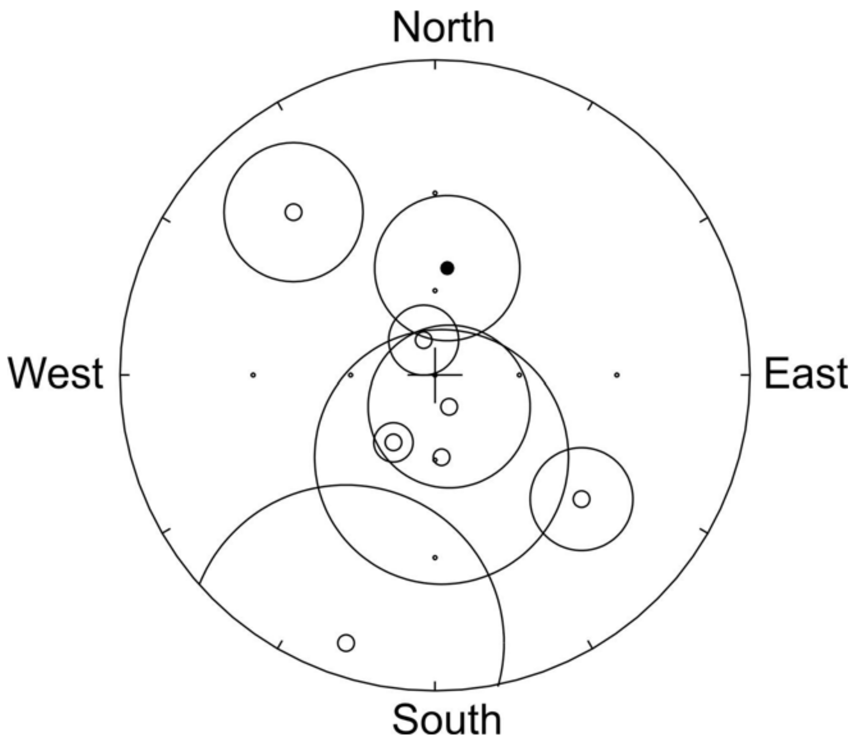

Figure 4.46 Site mean NRM results from the Upper Zone of the Bushveld Complex.

4.4.2 Demagnetisation

Samples were subjected to both AF (42 samples) and thermal demagnetisation (45 samples) to test for magnetic stability. The levels of demagnetisation for AF demagnetisation were: 2, 4, 6, 8, 10, 15, 20, 30, 40, 50, 70 and 95 mT, for thermal demagnetisation, the demagnetisation levels were: 100, 200, 300, 400, 450, 500, 520, 540, 560, 580 and 595°C. Some variations in the above levels occurred due to different levels of magnetisation being present in different samples. Once demagnetisation was completed, data were plotted on Zijderveld diagrams and subjected to principal component analysis to determine the ChRM and low temperature blocking components.

4.4.3 Components of magnetisation

Figure 4.47 includes a selection of orthogonal plots that show the demagnetisation characteristics of samples from the Upper Zone. Typically two components of magnetisation were identified by demagnetisation techniques and identified as LB and HB. In the case of sites 57 and 39, three components of magnetisation were seen. However due to their overlapping blocking temperature, the resulting curved Zijderveld diagram enabled only two components to be identified by the linefind process. They were also labelled LB and HB.

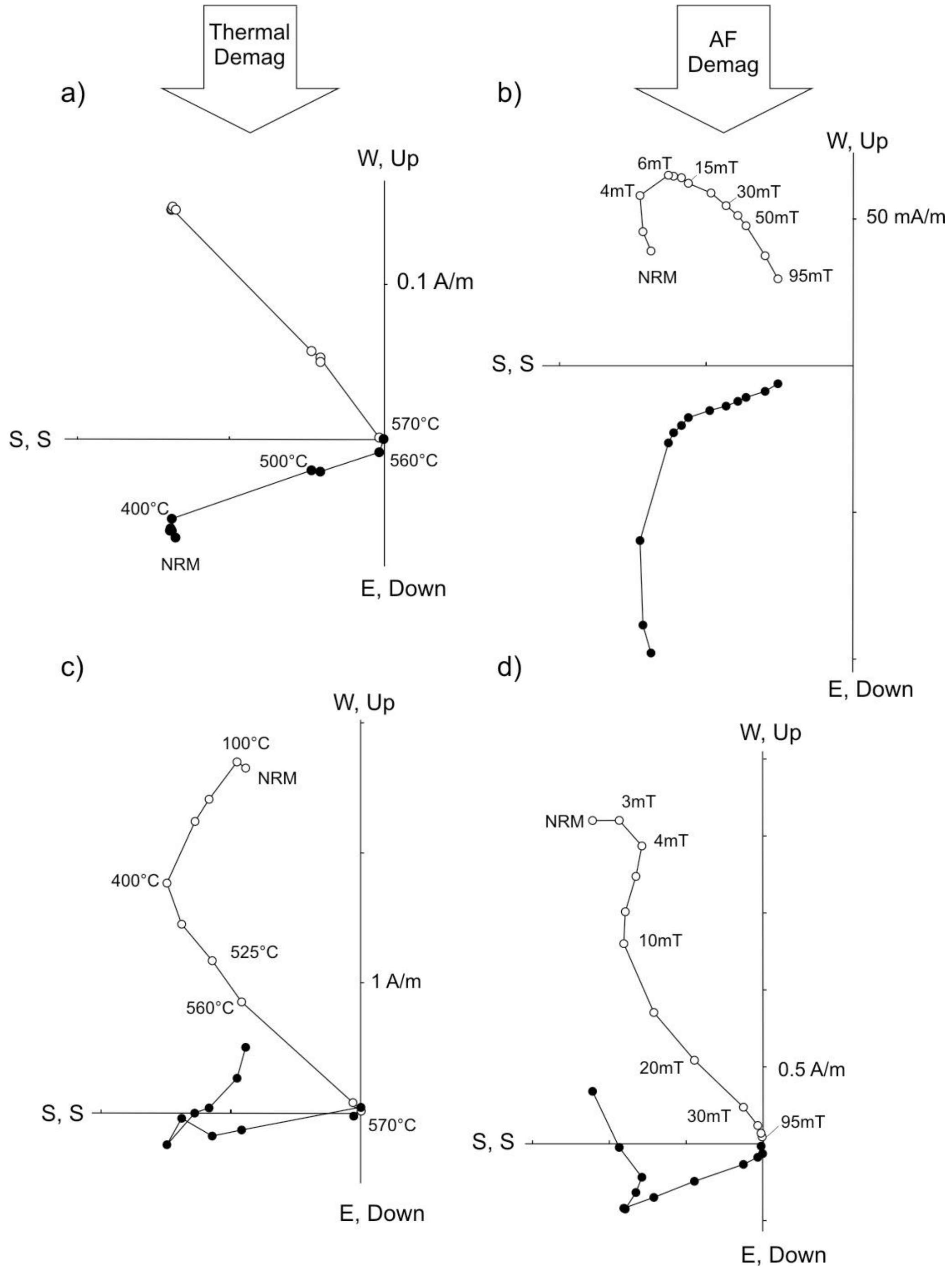

Figure 4.47 Typical Zijderveld plots for thermal (b & d) and AF (a & c) demagnetisation of Upper Zone rocks. Generally two components of magnetisation were identified as seen in (a) and (b). On the odd occasion three components were present in samples. However, due to the curved diagrams only two components were identified with certainty (c & d). Open (solid) symbols represent projections onto the vertical (horizontal) planes, respectively.

In general LB components are mostly scattered at site level (represented by high α_{95} values in Table 4.11). In-situ mean LB components from site 39 and 70 plot close to the present magnetic field observed in South Africa and probably represent a recent viscous overprint (Figure 4.48). Mean LB components from the other sites show no clear relationship to any known remanence direction for the region or that of the dipole field, and hence are not considered further.

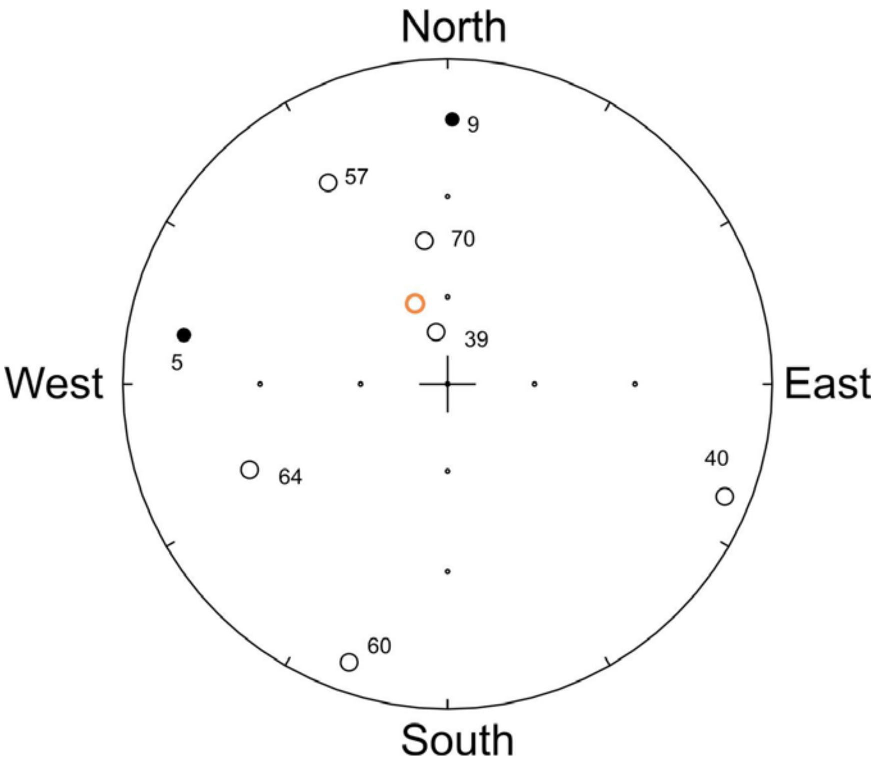

Figure 4.48 Site meas LB components from Upper Zone α_{95} are not shown as the majority of sites have values greater then 60°. The orange open circle in a NW steep direction represents the current magnetic direction in South Africa.

Table 4.11 Site mean LB component directions. *Dec.* = declination; *Inc.* = inclination; N_o = original number of samples per site, N = number of samples analysed per site; α_{95} = 95 percent confidence circle around mean direction; κ = precision parameter.

Site	Dec	Inc	α_{95}	N_o/N	κ
5	280.5	10.9	66.9	13/3	4.47
9	1	11.7	87.9	10/9	1.31
39	347.6	-71.4	24.9	13/8	5.91
40	112.1	-4.7	19.7	13/13	5.37
57	329.3	-18.5	18.1	13/13	6.2
60	199.5	-5.5	180	10/2	4.54
64	246.6	-22.8	180	9/4	0.93
70	350.8	-41.9	57.8	10/6	2.3

As AF and thermal demagnetisation preferentially remove LB components, remanent directions converge upon two anti-polar HB directions: those that are consistently removed between 560 and 580°C by thermal demagnetisation, and those above 50mT by AF demagnetisation. In situ site mean components show good clustering in a northerly declination, with steep negative inclinations or in anti-polar direction of southerly declination with a steep positive inclination. The resulting HB components are shown and listed in Figure 4.49 and Table 4.12.

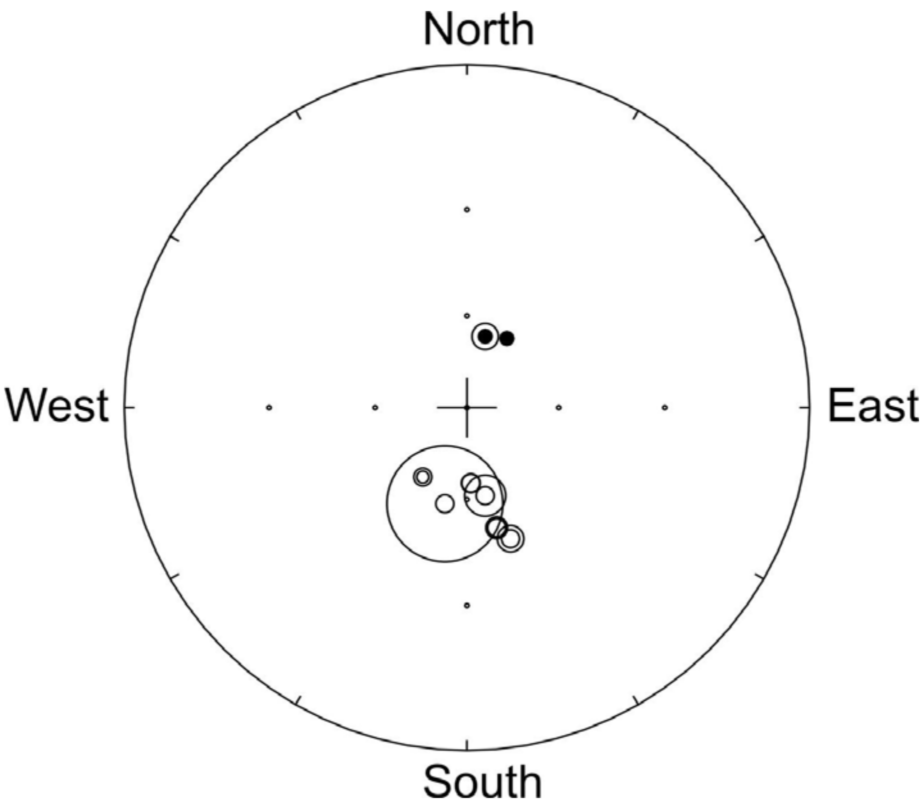

Figure 4.49 *In situ* site mean direction for Upper Zone Rocks, showing two distinctive polarities.

Table 4.12 Site mean HB component of magnetisation directions of each site *in situ*. N_o = original number of samples per site, N = number of samples analysed per site; α_{95} = 95 percent confidence circle around mean direction; κ = precision parameter.

Site	Dec	Inc	Strike	Dip	N_o/N	α_{95}	κ
5	212.5	-63	210	15	13/13	1.9	571.91
9	30	63.8	172	10	10/10	1.2	1897.72
39	161.6	-46.1	320	25	13/13	3.8	216.81
40	166.1	-50.3	320	25	13/12	3.2	304.18
57	14.4	65.8	156	10	13/10	4.2	175.44
60	192.9	-57.9	155	10	10/10	17.7	15.22
64	177.1	-65.1	134	8	9/8	3	287.94
70	168.3	-60.6	155	10	10/10	6.4	215.52

In the case of site 57, samples possessed exceptionally high NRM intensities (average 28.9A/m) and during AF demagnetisation intensities dropped drastically. By 15mT only 0.8% of the original NRM intensity was preserved (intensity around 0.5 A/m). This drastic decrease in intensity caused the Zijderveld diagram at first glance to be dominated by the secondary component. However on closer examination, the primary magnetisation was observed above 30 mT or 560°C (Figure 4.50). It is important to note that if demagnetisation was not carried out until NRM intensities were completely nullified, the overprint represented by the secondary component would have been assumed to have been primary and the true primary magnetisation would not have been detected.

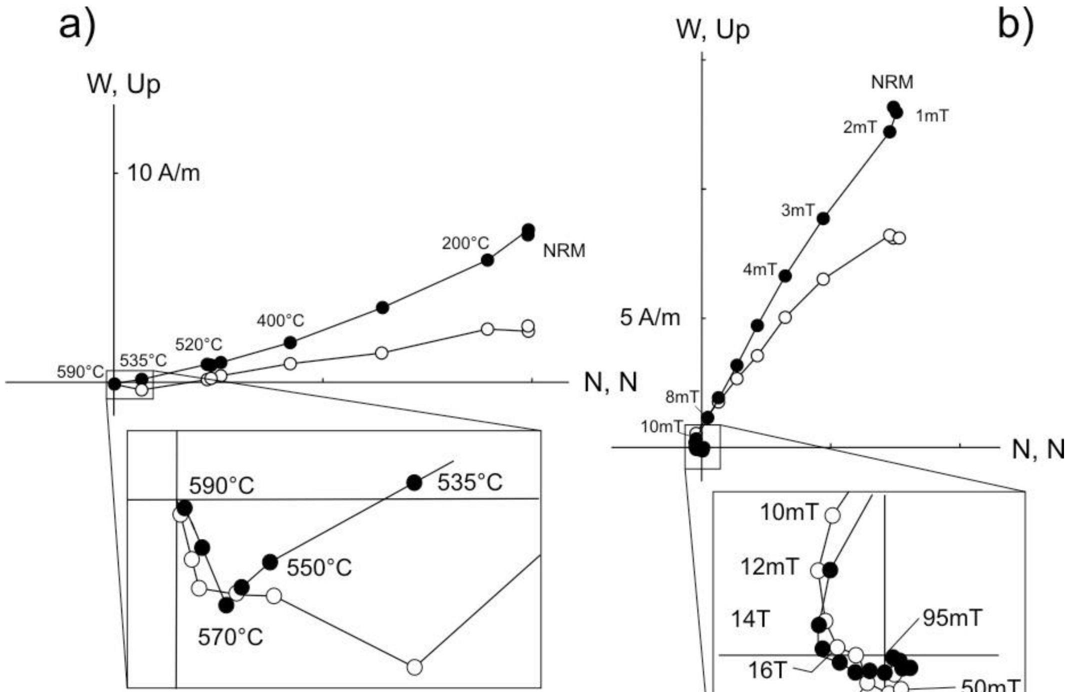

Figure 4.50 Examples of thermal (a) and AF demagnetisation (b) of samples from site 57. NRM intensities were extremely high and were removed rapidly with AF demagnetisation. HB components were identified after 30mT. Thermal demagnetisation (c) showed a more consistent decay during demagnetisation; however HB components still only represent a small percentage of the original intensity. Open (solid) symbols represent projections onto the vertical (horizontal) planes, respectively.

4.4.4 Thermomagnetic and petrographic analysis

TMA illustrated in Figure 4.51 indicates that samples have a Curie temperature of ≈ 580°C. The Curie curves indicate a decrease in saturation magnetization during cooling, implying that some oxidation probably occurred during heating and cooling.

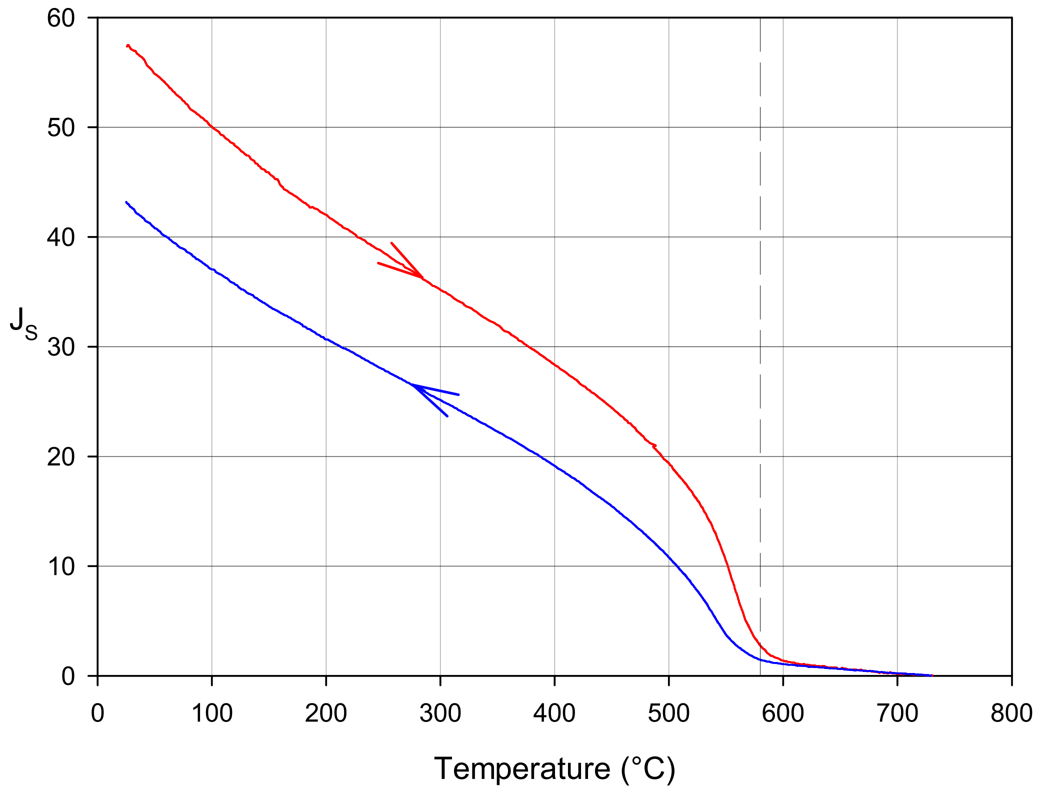

Figure 4.51 Typical thermomagnetic analysis response from Upper Zone sites, above sample taken from site 39. Red line and arrow indicate heating phase, while blue line and arrow indicates cooling phase. Curie temperature for magnetite at ≈ 580°C observed (dashed line). The observed decrease in saturation magnetisation during cooling indicates that some oxidation occurred during heating and cooling.

Petrographic analysis revealed the presence of discrete magnetite grains occurring in a variety of sizes from as small as 9 μm up to 90 μm. The occurrence of magnetite as exsolution lamellae in pyroxene and plagioclase is observed to a minor degree, but is not as abundant as experienced in the Main Zone. Ilmenite is also present as large discrete grains.

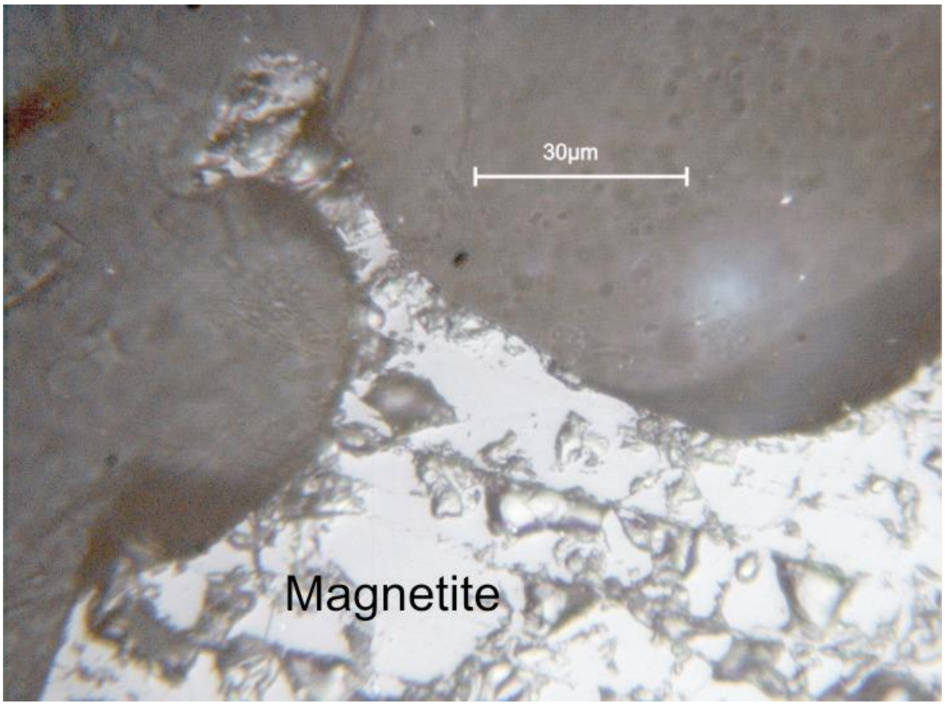

Figure 4.52 Thin section analysis revealed the occurrence of a magnetite in a variety of sizes above section obtained form site 57

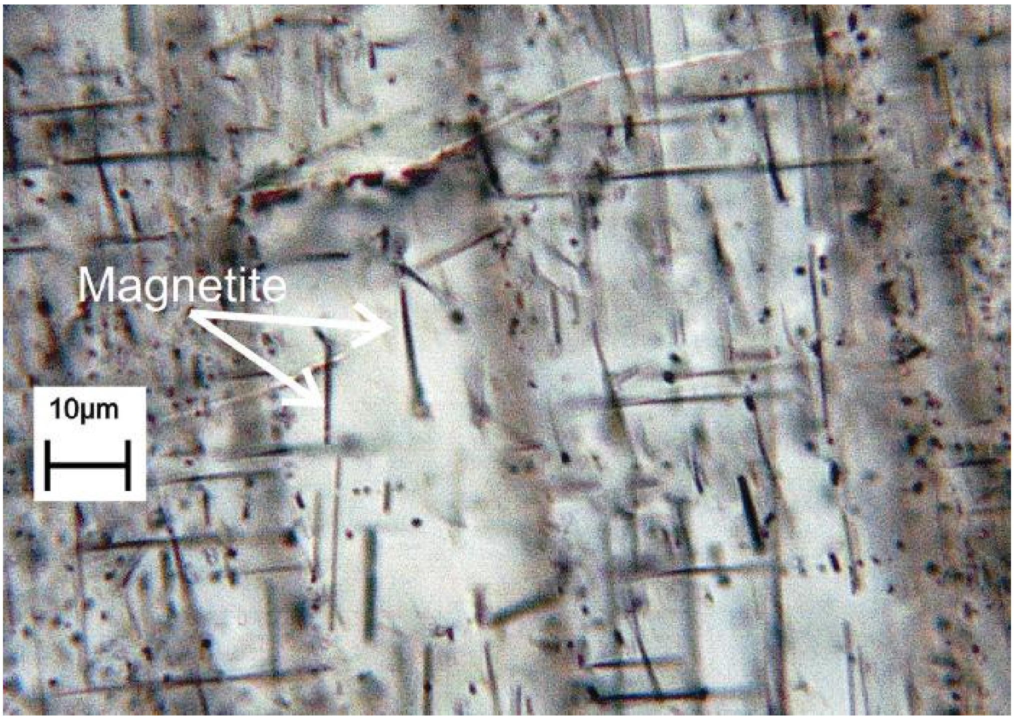

Figure 4.53 Petrographic analysis of plagioclase from the Upper Zone revealed lamellae of magnetite (transmitted light). Above thin section from site 39.

4.4.5 Field stability tests.

Fold Test

As with the rocks in the Critical Zone of the Bushveld Complex, the Upper Zone rocks all dip towards the centre of the complex, with varying angles of between 10° and 18°. Samples were restored to a horizontal attitude by applying bedding corrections to HB components. Dips and strikes used in restoration are listed in Table 4.12. Upon uniform unfolding, site mean directions showed a marginal increase in precision parameter κ from 42.41 to 51.21 and a slight decrease in α_{95} value from 8.6 to 7.8. This minor improvement was not sufficient to produce a positive fold test of McElhinny (1964).

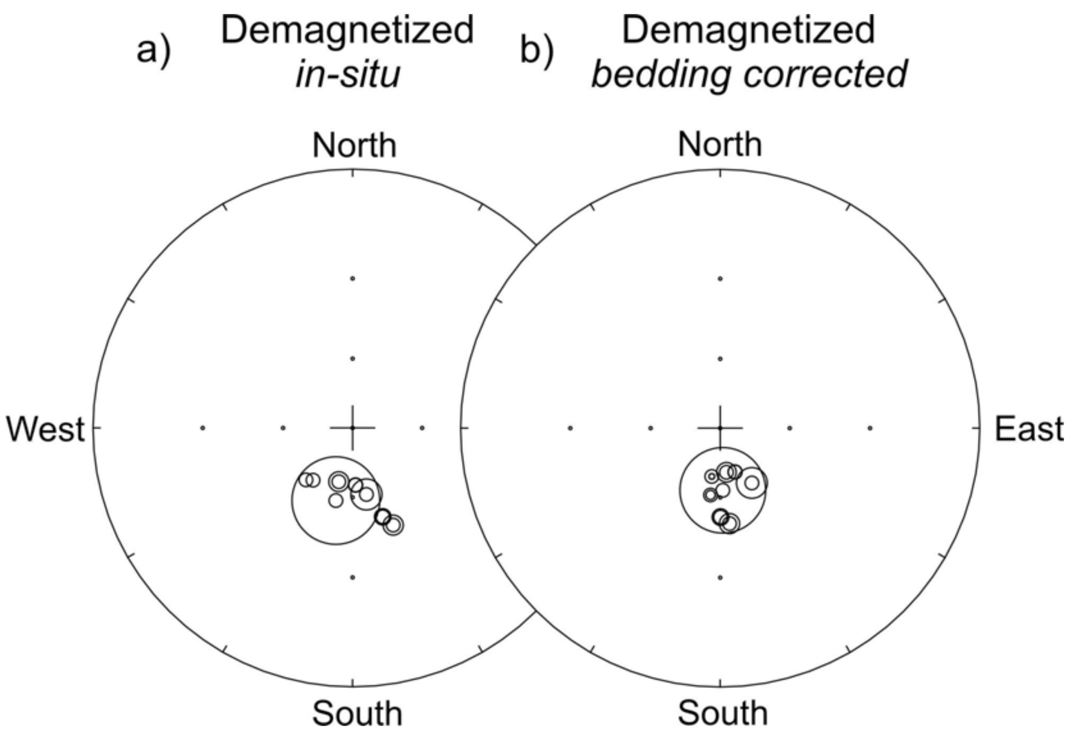

Figure 4.54 Site mean direction for Upper Zone rocks in both *in situ* (a) and bedding corrected co-ordinates (b). Closed symbols denote positive inclination.

Reversal Test

In order to determine whether the two polarities recorded represent similar ages of magnetisation, two reversal tests were implemented. The first of McFadden and Lowes (1981) found that the sites shared a common mean at 95% confidence. The second reversal test developed by McFadden & McElhinny (1990), indicated a positive reversal test with a "C" classification, $\gamma_{observed}$ = 6.94 and γ_{crit} = 14.88. Since the samples indicated a positive reversal test, it is assumed that are related to the same magmatic event and that a reversal in the Earth's magnetic field was recorded.

4.4.6 Interpretation of palaeomagnetic data from the Upper Zone

In general, samples from the Upper Zone contained low temperature components that were successfully removed during progressive demagnetisation to reveal the presence of high temperature components that produce extremely well clustered results for sites.

Both thermal demagnetisation spectra and thermomagnetic analysis suggest that Ti-poor magnetite or nearly pure magnetite (maximum unblocking temperatures at around 565-580°C and Curie temperatures at ≈ 580°C) is the bulk remanence carrier. This was further strengthened by petrographic analysis in which the opaque mineralogy of samples was discovered to be dominated by magnetite.

Two positive reversal tests indicate that the HB components are the primary magnetic signature and that all sites were emplaced over the same time span.

Bedding-corrected data, although showing better grouping, were not significant at the 95% confidence level during the application of the positive fold test. However, the resulting palaeopole position obtained from bedding-corrected data shows a better association with poles calculated from the other Zones of the Bushveld and have therefore concluded that the Upper Zone probably obtained its magnetization while the complex was horizontal.

The high-temperature components of all the samples inverted to the same polarity, yield a mean remanence direction with declination = 354.8° , inclination = 61.6° (α_{95} = 7.8º, N =8 sites) and a pole position with palaeolatitude =22.1° and palaeolongitude = 25.6°, dp/dm = 9.3°/12° (palaeopole calculated at mean sampling co-ordinates of 25°S and 29.7°E).

4.5 Northern Lobe Main Zone

The Northern Lobe of the Bushveld Complex is exposed over a 110 km in length, starting approximately 35 km to the southwest of Mokopane (formerly Potgietersrus) and extending north. Rock exposure in the area is very poor due to the topography being virtually flat and large areas being covered by a thick alluvial cover. However, a limited number of outcrops do occur in river sections and on the surrounding hills (referred to as the pyramid hills). These were the location of our palaeomagnetic drill sites. In total, 27 sites were obtained (Figure 4.55): 23 from the Main Zone located in the vicinity of Mokopane, and four from the Upper Zone near Villa Nora. As stated above, samples were derived from river sections (14), low lying hill outcrops (12) and one from a road cutting.

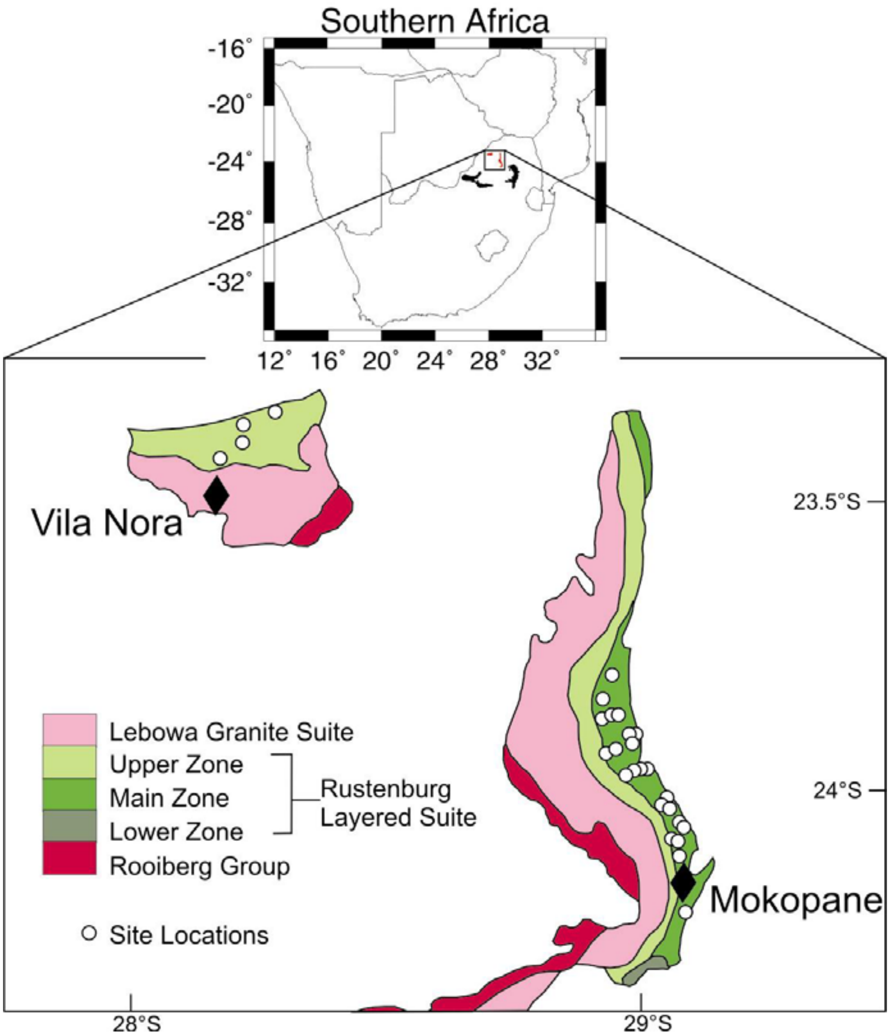

Figure 4.55 Simplified geological map of the Northern Lobe of the Bushveld Complex, indicating the locations of samples

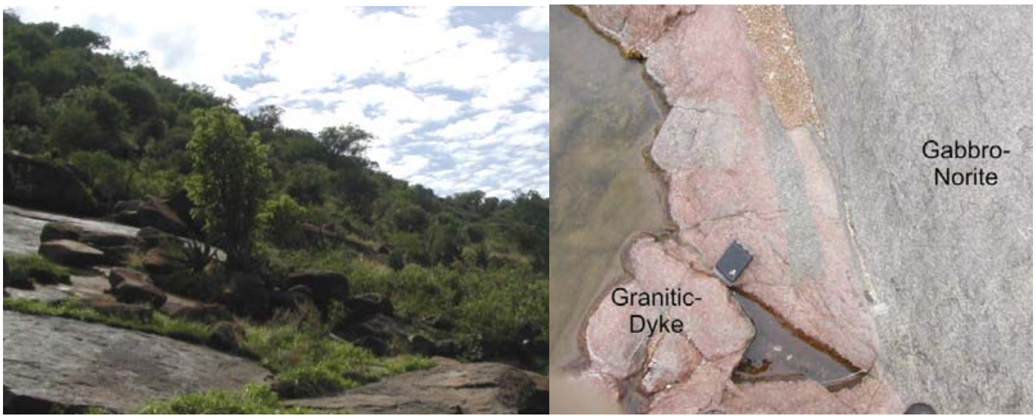

Figure 4.56 Examples of sampling locations in the Northern Main Zone. On the left is a typical low-lying hill exposure (site 3) and on the right is a river exposure (in this picture a granitic dyke occurred at the site, it is thought to be related to the intrusion of the Bushveld. Samples from the dyke did not reveal any coherent direction).

4.5.1 NRM

From the 27 sites, a total of 245 core samples were analysed initially for NRM and bulk susceptibility before demagnetisation was carried out. NRM intensities showed a wide range of variation from 5.7 to 5716 mA/m, with an average value of 1560 mA/m and susceptibility from 245 to 6986 $\times 10^{-6}$ SI units, with an average of 1000 $\times 10^{-6}$ SI units. A histogram plot of NRM intensities and susceptibilities is given in Figure 4.57. While mean NRM values and bulk susceptibility values for all sites with errors are shown in Table 4.13.

Table 4.13 Site mean NRM, mean bulk susceptibility and Q ratio of all sites. *Dec.* = declination, *Inc.* = inclination, α_{95} = 95 percent confidence circle around mean direction, N= number of samples, +/- = 1 σ error and Susc. = Susceptibility.

Site	NRM Dec.	NRM Inc.	α_{95}	N	Intensity Average (mA/m)	+/- (mA/m)	Susc. Average ($\times10^{-6}$ SI units)	+/- ($\times10^{-6}$)	Q Ratio
1	42.3	46.7	6.5	9	492.78	29.03	1114.3	142.8	19
2	247.9	78.6	59.6	9	1192.08	663.66	791.2	80.3	63
3	67.4	72.3	35.4	9	860.39	192.62	633.2	33.2	57
4	11.4	52.6	7.1	9	1530.70	662.59	818.3	239.9	78
5	9.3	52.1	39.5	8	4744.56	1441.80	1071.2	183.8	186
6	21	54.4	10.6	19	187.26	88.94	286.0	58.4	27
7	0.4	32.5	32.6	9	8.29	4.91	285.0	23.6	1
8	208.8	-48.1	17	9	14.57	4.45	545.0	33.7	1
9	323.7	51.1	5.7	10	5716.24	700.13	6986.5	2366.5	34
10	51.2	67.2	12.8	9	2319.47	1292.81	1752.3	1198.5	55
11	45	64	18	9	11.43	4.38	280.2	20.2	2
12	23.7	23.6	9.2	8	113.05	38.14	690.5	70.0	7
13	9.4	48.2	11.5	9	1094.96	527.80	526.9	50.9	87
14	21.9	63.4	36.9	9	110.14	15.68	838.5	142.8	6
15	183.3	-49	10.2	9	164.87	42.65	1878.9	648.0	4
16	281.6	70.3	40.1	9	1873.99	1082.47	1119.1	598.5	70
17	123.4	87.4	29.3	7	268.46	153.55	76.8	17.0	146
18	16.6	55.6	45.9	10	160.51	39.14	304.0	96.3	22
19	300.6	32.7	57	6	14620.15	1655.62	1843.6	778.6	332
20	114.4	77.6	24.4	10	763.43	310.62	301.4	129.4	106
21	56.3	61.8	17.6	11	817.03	354.41	564.6	143.3	61
22	41.2	62.7	3.5	9	1272.26	403.90	245.1	70.1	217
23	73.9	61	11.7	8	3126.01	434.20	2096.4	344.5	62
24	161	35.8	37.1	7	589.40	94.29	822.1	178.1	30
25	34.9	39.2	53.1	6	5.78	2.14	260.1	60.4	1
26	9.1	28.2	48.7	5	7.52	1.75	301.4	60.7	1
27	52.1	39.2	41	8	52.81	12.53	574.0	17.9	4

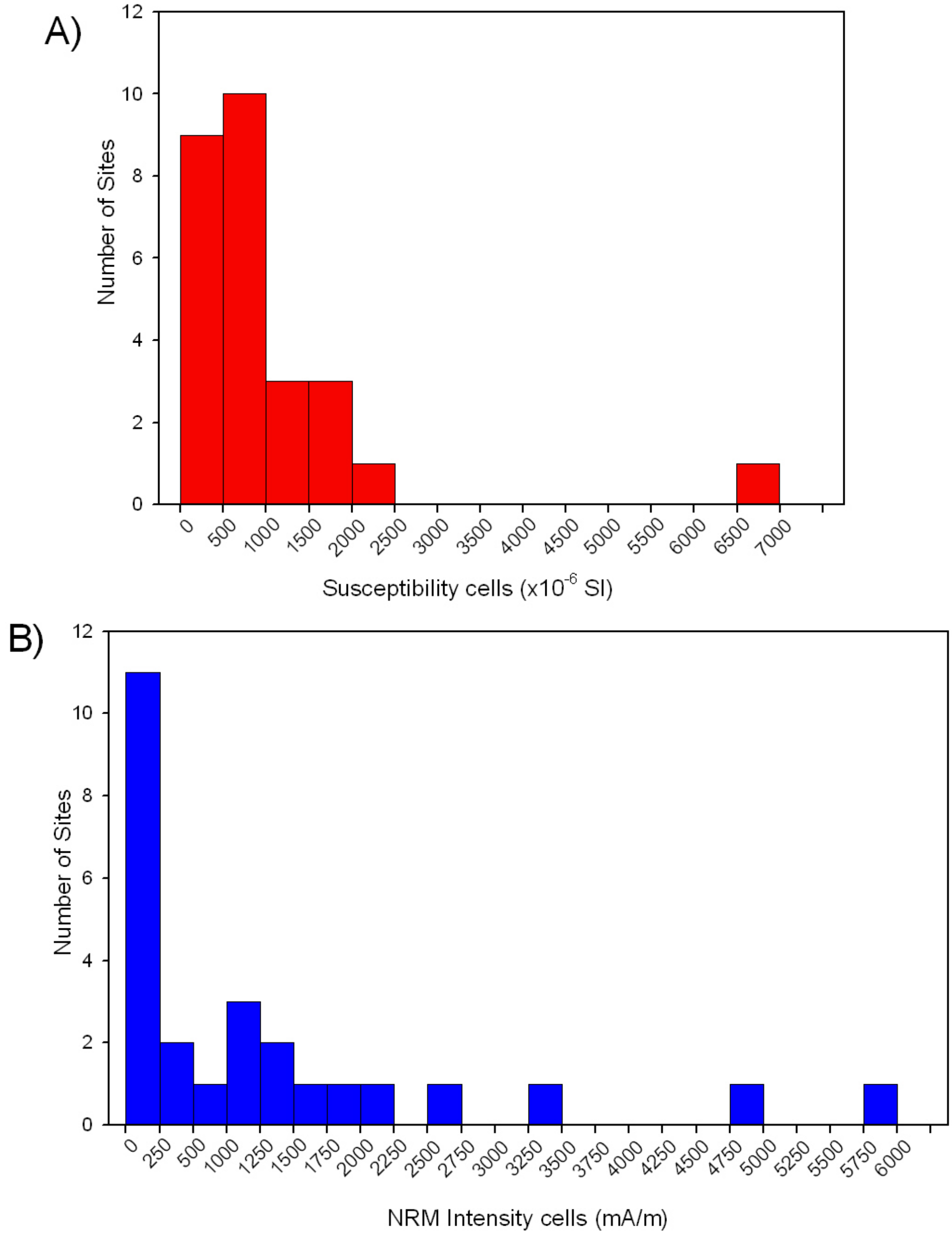

Figure 4.57 Histogram plot of site mean susceptibility (a) and site mean NRM intensity (b) of sites from the Main Zone of the Northern Lobe, with the exception of site 19 (14620.15A/m).

The majority of mean NRM directions show a scattered "shotgun pattern" around a northeasterly declination, and steep positive inclination (Figure 4.58), while two sites possess an anti-polar direction to this grouping. Samples within sites show extremely poor grouping, with average α_{95} values of 30° (listed in Table 4.13).

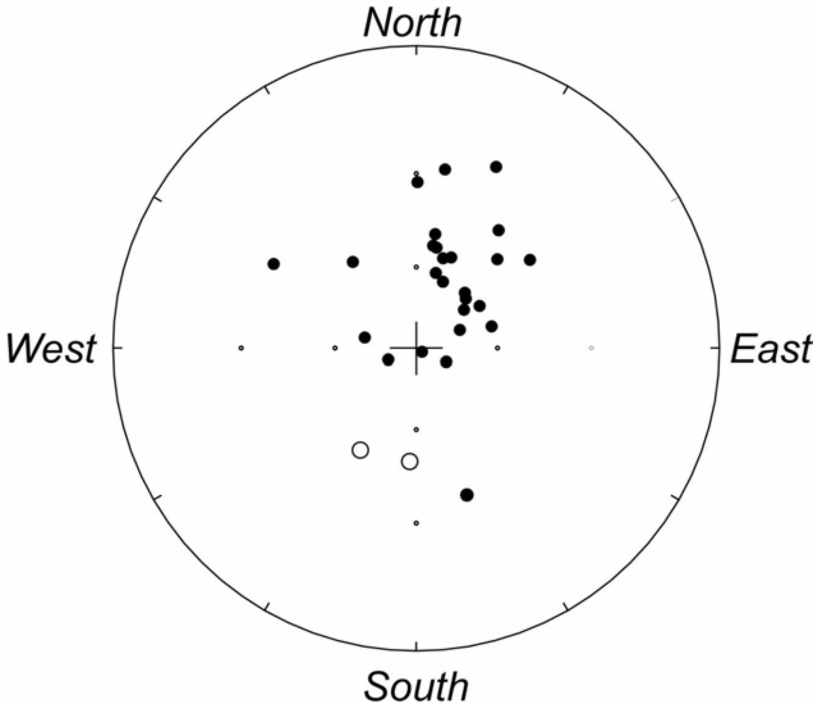

Figure 4.58 Site mean NRM directions from Main Zone rocks of the Northern Lobe, α_{95} circles are not shown as values are on average around 30°.

4.5.2 Demagnetisation

Samples were subjected to stepwise demagnetisation by both AF and thermal method in an attempt to determine the magnetic history of the rocks. AF treatment was conducted on 112 samples and thermal treatment on the remaining 133 samples. Demagnetisation was carried out using between 10 and 16 steps up to 620° C (but generally 600°C) or 95mT (maximum level obtained from AF machine). After demagnetisation, NRM directions were analyzed and interpreted with Zijderveld diagrams (Zijderveld, 1967) and principal component analysis was used to determine the directions of the various NRM components. Samples obtained from the Villa Nora section (sites 16-19) were unstable upon demagnetisation and did not reveal any coherent components of magnetisation, and have therefore not been included in the analysis of the Northern Lobe.

4.5.3 Components of magnetisation

NRM analysis of all rock samples showed the presence of two components of magnetisation (Figure 4.59). Samples behaved exceptionally well to both thermal and AF demagnetisation. Once again LB components identified in samples have directions that are all random within sites (Figure 4.60 and Table 4.14) and are typically removed at around 500ºC or 30-40mT. LB directions have no significant geological meaning and they are not considered further.

Table 4.14 Site mean LB component directions from the Main Zone of the Northern Lobe. *Dec.* = declination, *Inc.* = inclination, α_{95} = 95 percent confidence circle around mean direction, N_o = original number of samples per site, N = number of samples analysed per site.

Site	Dec	Inc	α_{95}	N_o/N	κ
1	40.2	49.2	64.8	9/8	1.69
2	3.6	-58.3	53.8	9/9	1.88
3	246.9	52.7	151.5	9/10	1.09
4	25.5	32.0	74.9	9/6	1.76
5	16.4	30.0	48.2	8/5	3.47
6	2.7	55.6	30.9	19/19	2.15
7	341.7	1.6	17.0	9/6	16.57
8	219.2	-48.4	38.0	9/5	5.00
9	194.7	35.4	99.1	10/5	1.57
10	171.1	23.1	28.6	9/8	4.71
11	28.8	75.6	17.4	9/9	9.68
12	12.6	-18.2	35.9	8/7	3.78
13	315.6	30.3	70.1	9/9	1.22
14	300.7	-56.8	87.3	9/8	1.37
15	174.1	-43.5	61.1	9/4	3.24
16	32.8	76.8	92.5	9/6	1.49
17	160.0	0.6	n/a	7/2	n/a
18	165.9	-16.7	145.7	10/3	1.93
19	40.9	84.3	180.0	6/3	1.51
20	177.7	19.7	64.1	10/8	1.70
21	32.5	22.4	26.5	11/8	5.33
22	3.4	-5.0	n/a	9/1	n/a
23	122.6	39.6	62.2	8/8	1.35
24	167.6	-0.6	61.0	7/8	1.78
25	187.6	-11.0	n/a	6/2	n/a
26	25.8	-53.4	20.3	5/3	38.04
27	51.3	4.5	32.5	8/8	2.74

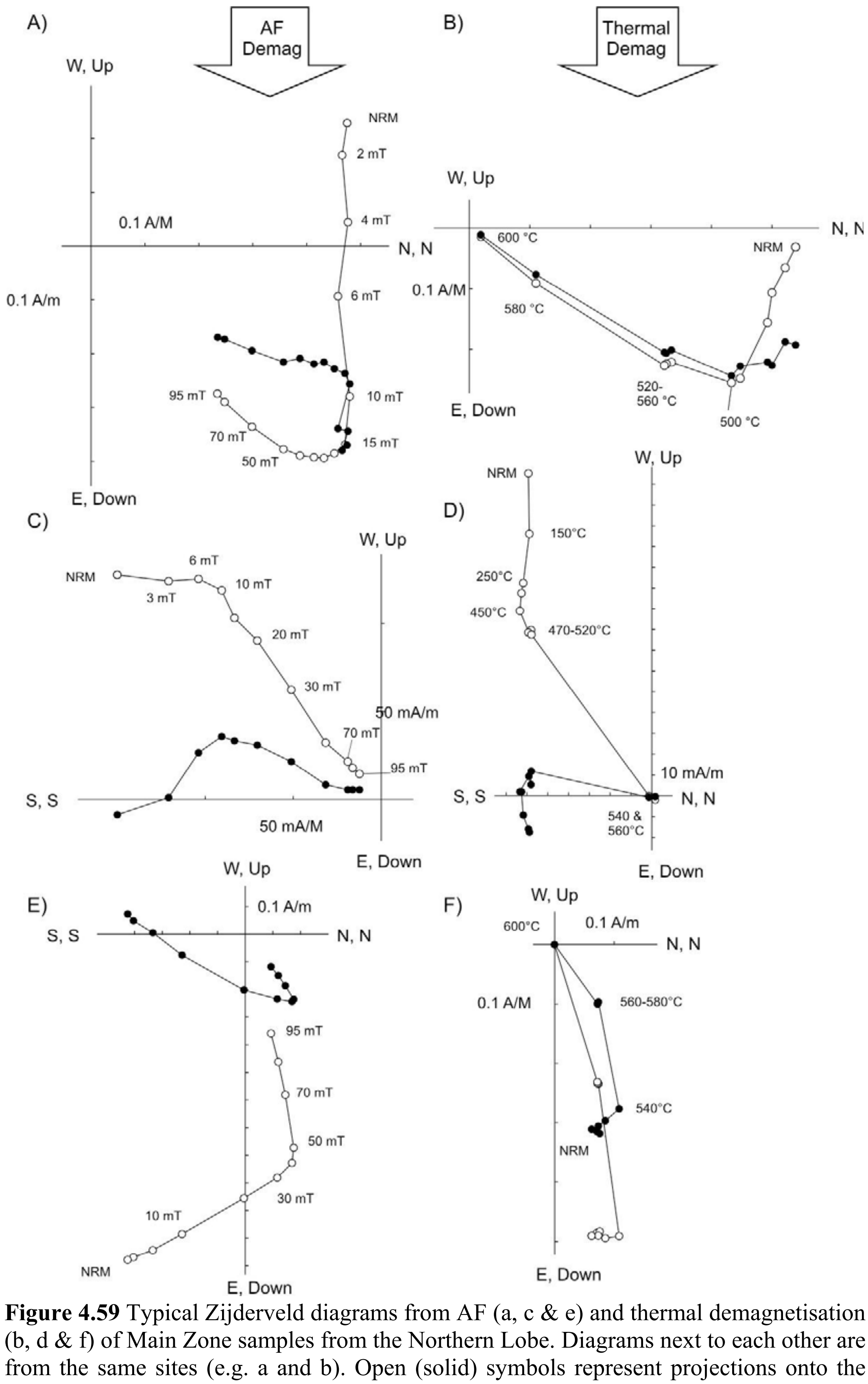

Figure 4.59 Typical Zijderveld diagrams from AF (a, c & e) and thermal demagnetisation (b, d & f) of Main Zone samples from the Northern Lobe. Diagrams next to each other are from the same sites (e.g. a and b). Open (solid) symbols represent projections onto the vertical (horizontal) planes, respectively.

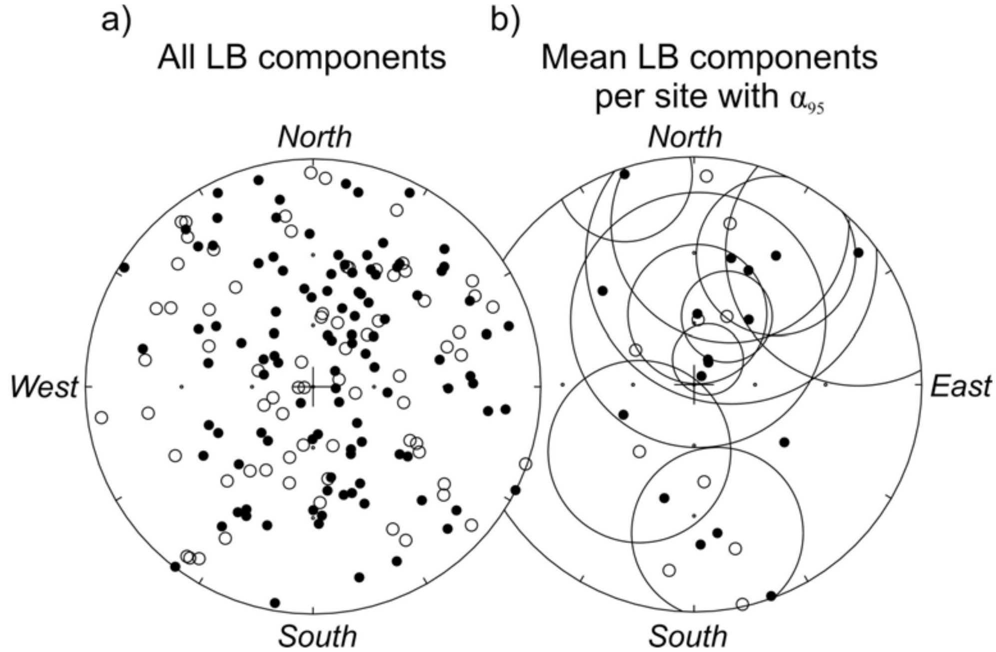

Figure 4.60 a) All LB site components from Northern Lobe Main Zone samples, b) Corresponding site mean LB components per site with α_{95} circles, some sites do not haveα_{95} circles plotted as they were greater then 60°.

With the removal of low coercivity (or low temperature) remanence, one of two approximately anti-polar higher coercivity remanence (or high temperature remanence) directions were isolated above 550°C or 50mT (Figure 4.59). HB components show reasonable grouping within-site (α_{95} around 6°). Mean site directions plot with SSW declination and steep negative inclination or anti-polar to this (NNE declination and steep positive inclination), resulting HB components are shown in Figure 4.61 and listed in Table 4.15.

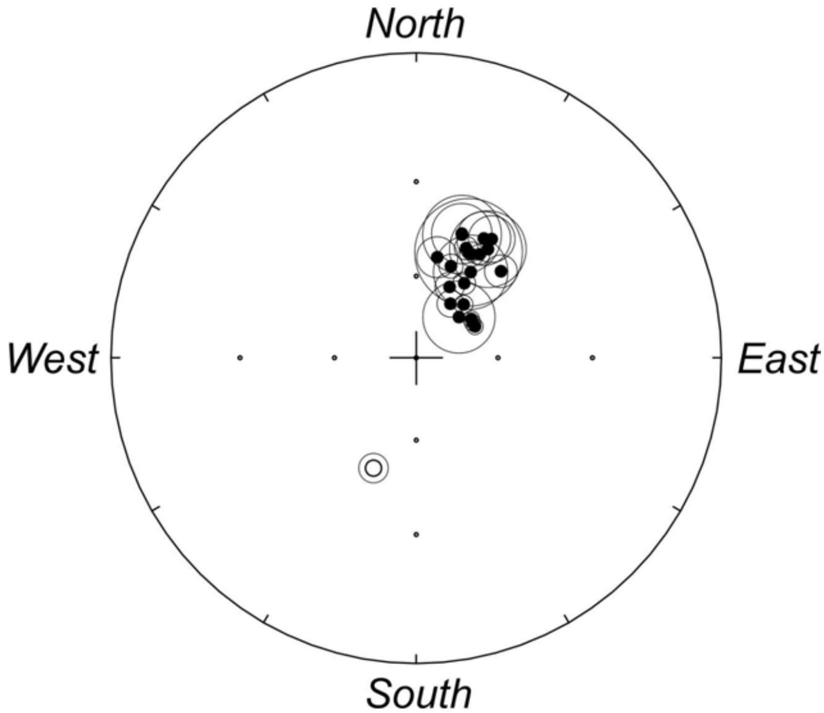

Figure 4.61 Site mean *in situ* direction for Main Zone samples from the Northern Lobe. Solid symbols indicate a positive inclination, while open symbols indicate a negative inclination

Table 4.15 Site mean HB component of magnetisation directions of each site *in situ*. N_o = original number of samples per site, N = number of samples analysed per site; α_{95} = 95 percent confidence circle around mean direction; κ = precision parameter.

Site	Dec	Inc	Strike	Dip	N_o/N	α_{95}	κ
1	44.4	46.7	202	15	9/9	5.3	94.89
2	32.4	40.5	146	27	9/7	7.2	71.12
3	29.5	41.6	156	25	9/4	8.4	120.17
4	26.4	47.8	156	25	9/3	17.4	51.32
5	11.8	52.8	135	15	8/9	6.9	56.98
6	24.4	46.9	160	20	19/9	3.8	180.27
7	31.5	46.6	146	22	9/6	3.3	420.14
8	33.4	43.8	159	25	9/4	12.1	58.23
10	25.2	61.2	146	22	9/9	5.1	101.88
11	32.8	57.6	146	22	9/9	3.9	176.18
12	20.1	43.1	146	22	8/5	9.5	66.32
13	20.7	54.4	170	23	9/9	4.1	155.63
14	28.1	47.9	141	25	9/6	4.0	274.81
15	201.3	-47.8	141	25	9/8	4.8	134.40
20	54.8	65.1	169	20	10/9	2.9	306.99
21	58.1	65.5	209	26	11/9	2.9	312.93
22	41.6	63.7	169	24	9/9	3.3	243.67
23	61.9	65.4	180	16	8/8	2.9	373.32
24	46.4	68.1	187	21	7/3	13.0	90.60
25	32.4	53.2	168	30	6/6	12.5	29.60
26	20.4	43.4	170	20	5/3	12.4	99.64
27	32.3	66.3	180	25	8/4	4.8	367.53

4.5.4 Thermomagnetic and petrographic analysis

TMA illustrated in Figure 4.62 indicates that samples have a Curie temperature of ≈ 580°C. In this case the Curie curves indicate an increase in saturation magnetization during cooling, implying production of secondary magnetite, probably from a non-magnetic phase.

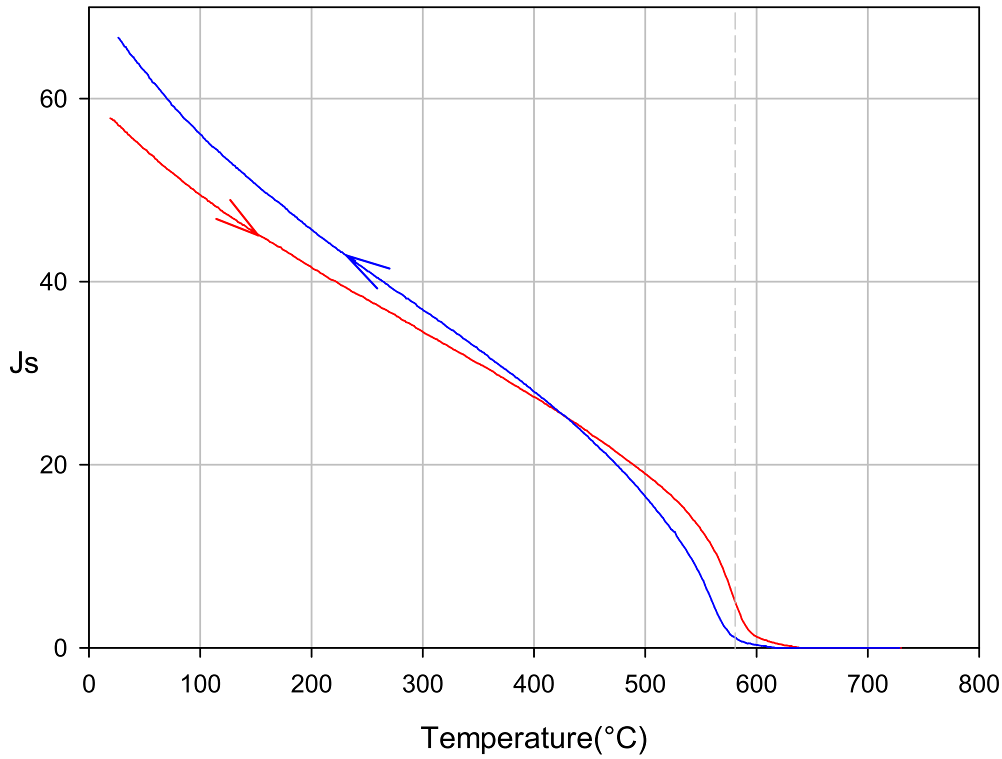

Figure 4.62 Thermomagnetic analysis of a Northern Lobe Main Zone sample from site 15. The red line indicates the heating phase while the blue line indicates the cooling phase. Curie temperature for magnetite is observed at ≈ 580°C (dashed line). Curves show almost reversible, a slight increase in saturation magnetisation is noted during cooling, implying the possible production of more magnetite.

Polished thin sections studied under a petrographic microscope revealed the presence of minor amounts of various sulphides (pyrrhotite being the majority) and ilmenite. Magnetite was identified as both discrete grains and as needles within plagioclase and pyroxene crystals.

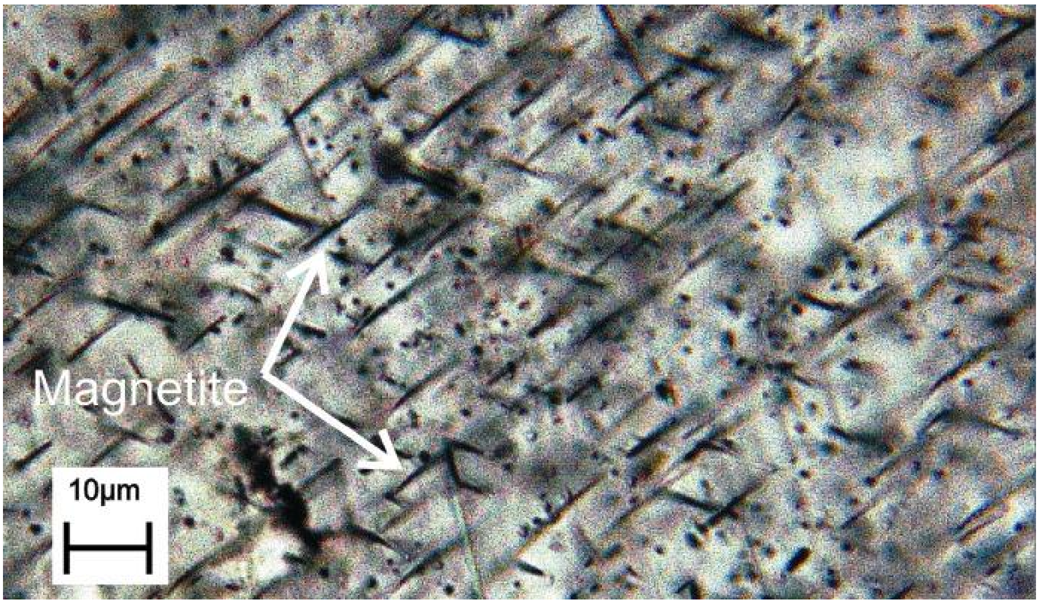

Figure 4.63 Polished then section from site 15 in the Main Zone of the Northern Lobe indicating magnetite lamellae occurring in plagioclase, transmitted light.

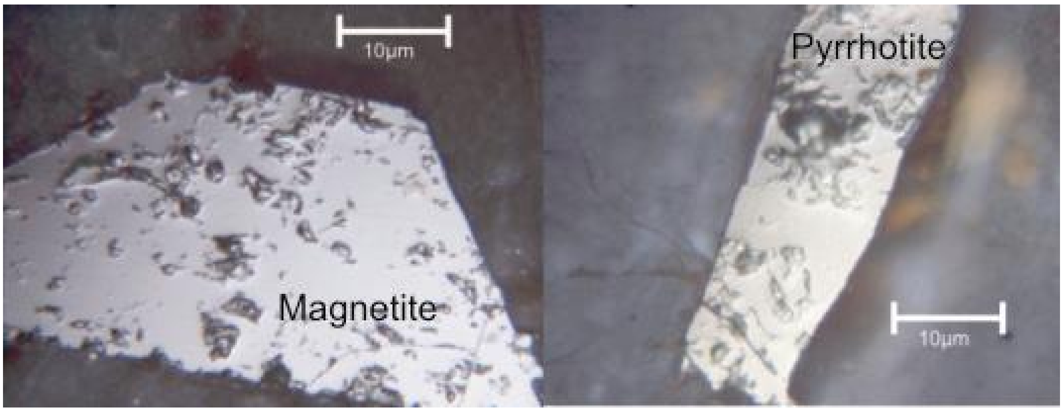

Figure 4.64 Polished then section from the Main Zone of the Northern Lobe. On the left is a large grain of magnetite from site 4 and on the right is a pyrrhotite grain from site 24, reflected light.

4.5.5 Field stability tests.

Fold Test

In the Northern Lobe, rocks to the south of Mokopane (Figure 4.55) strike northeast and dip at angles of 15 to 27° west. To the north, the strikes change towards the northwest and eventually to due north, with westward dips of 10 to 45° (van der Merwe, 1976).

Upon stepwise unfolding, a slight increase in statistical precision parameter κ was observed from 47.98 to 67.55 and minor decrease in α_{95} value from 4.5° to 3.8°

(Figure 4.65,c). The resulting increase in κ is not significant at the 95% confidence level according to the classic fold test of McElhinny (1964b).

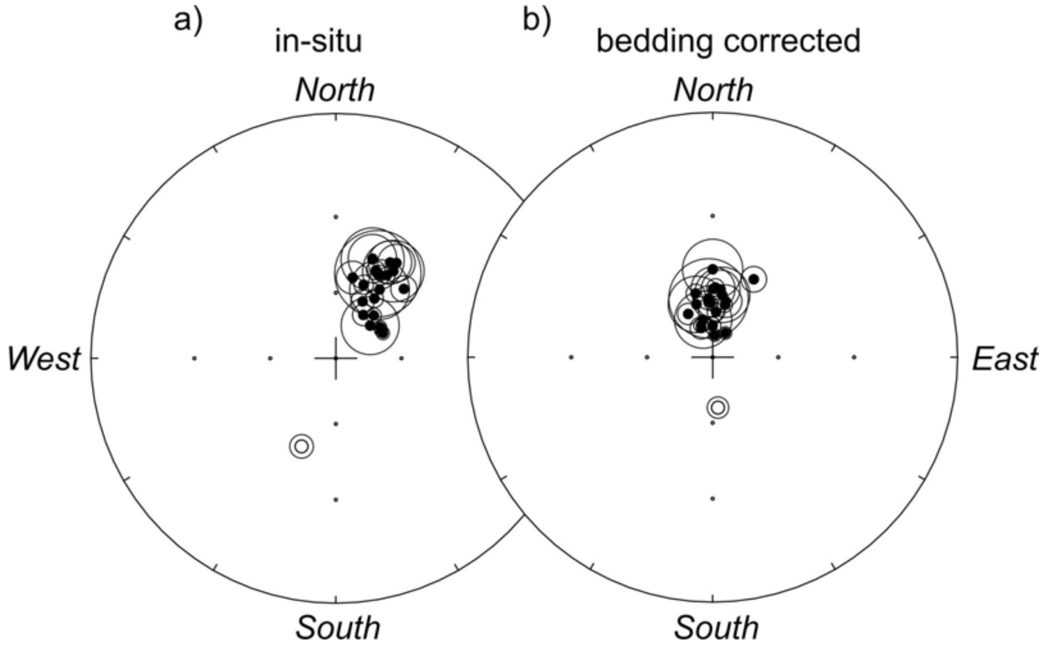

Figure 4.65 Site mean direction for Main Zone rocks from the Northern Lobe sites *in situ* (a), and bedding corrected co-ordinates (b). Closed symbols denote positive inclination while open circles denotes negative inclinations.

Reversal Test

Due to only one site possessing a negative inclination, only the reversal test of McFadden and Lowes (1981) could be applied to the data. It was found that the site shared a common mean at 95% confidence level; this leads to the belief that they are related to the same magmatic event and that a reversal in the Earth's magnetic field was recorded.

4.5.6 Interpretation of palaeomagnetic data from the Northern Main Zone

Resulting NRM directions show a scattered distribution around a northeasterly declination and steep positive inclination. Two sites possess directions that are anti-polar to the other sites. Both AF and thermal demagnetisation removed low coercivity remanence that were scattered at site-level and have no correlation with any geological event. On completion of demagnetisation remanent directions converge upon HB components that display well clustered results.

HB components had maximum unblocking temperatures at around 565-580°C, suggesting that Ti-poor magnetite or nearly pure magnetite is the bulk remanence carrier. This finding was further strengthened by thermomagnetic analysis indicating a Curie temperatures at ≈ 580°C and petrographic analysis revealing magnetite in the form of lamellae in plagioclase and pyroxene as the dominate opaque mineralogy.

Samples from the northern Main Zone contained both reversed and normal polarities. A reversal test conducted on samples indicated that the two polarites are of similar age, and argues for primary magnetisation.

A slight improvement in sample clustering was obtained after palaeo-horizontal corrections were implemented. Although the findings of the fold test of McElhinny (1964b) was not significant at the 95% confidence level, the resulting pole position plots closer in proximity to the other zones. Therefore, it is assumed that the zone acquired its magnetisation while the layer was in a near horizontal position.

The calculated mean direction of magnetisation for the Northern Lobe with negative inclinations inverted, is declination = 359.8° , inclination = 66.1° (α_{95} = 3.8º, N =22 sites) and resulting in a palaeopole position with palaeolatitude =17.5° and palaeolongitude = 28.8°, dp/dm = 5.1°/6.2° (palaeopole calculated at mean sampling co-ordinates of 24°S and 28.9°E).

CHAPTER 5: INTERPRETATION OF BUSHVELD RESULTS

The previous chapter gave a detailed account of all palaeomagnetic results obtained from the Bushveld Complex. The pages that follow tie all these results together to determine the palaeomagnetic history of the rocks.

5.1 Reconciliation of All New Data

Samples behaved exceptionally well to both thermal and AF demagnetisation, with two magnetisation components (LB and HB) having been readily identified. LB components, although present in the majority of samples, did not reveal any coherent directional pattern, and are typically removed below 300-400ºC or 30 mT. With the removal of low coercivity remanence, well-defined HB components are successfully revealed around 560-580°C and above 50 mT, indicating that the prime remanence carrier is possibly magnetite or Ti-poor magnetite (TM). This observation is further strengthened by Curie temperatures of ~ 580°C from thermomagnetic analysis, and the identification of magnetite occurring as needles or lamellae in pyroxene and plagioclase from petrographic analysis. The resulting HB components generate an extremely well grouped set of results for each zone as seen in Figure 5.1. Both normal and reversed polarities are present.

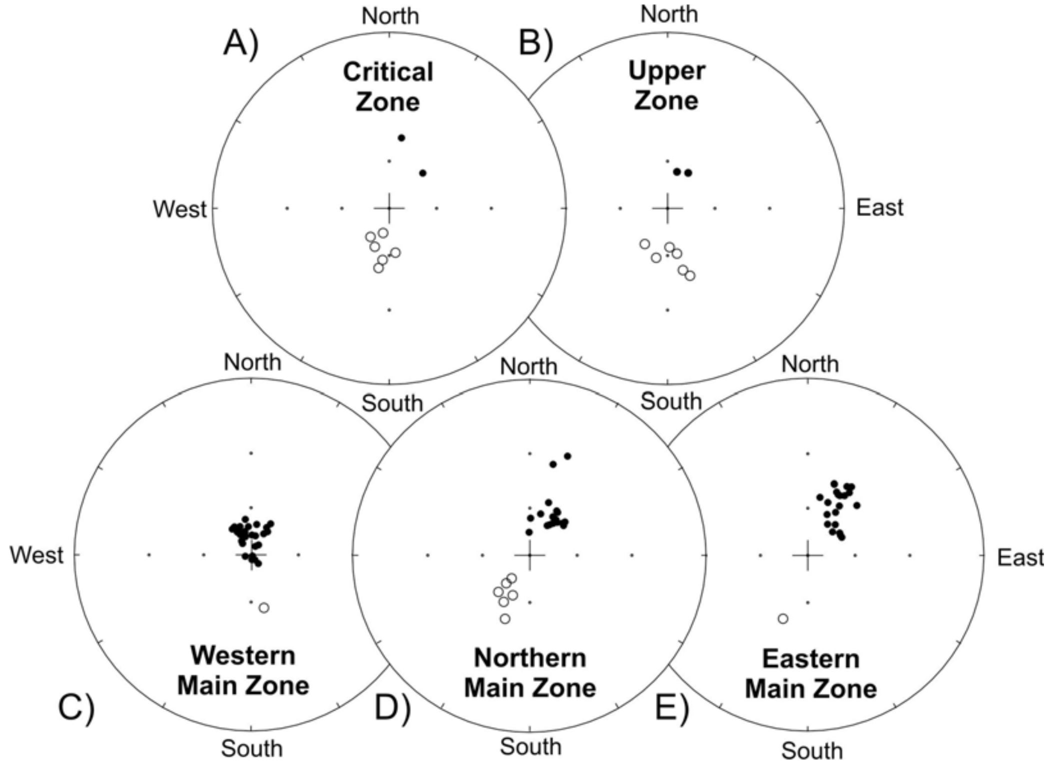

Figure 5.1 Mean *in-situ* site HB components from all zones of the Bushveld Complex. Upper Zone results are shown in A, Critical Zone in B, western Main Zone in C, northern Main Zone in D, and eastern Main Zone in E.

In an attempt to determine the relative timing of magnetisation with respect to the attitude of the Bushveld Complex, bedding corrections were applied to samples. All zones experienced an increase in precision parameter κ upon stepwise unfolding. The resulting bedding corrected site mean directions for all zones are listed in Table 5.1 and illustrated in Figure 5.2, where it can be seen that a vast improvement in grouping has occurred not only within zones, but also as a whole.

Table 5.1 Mean Zone statistics. N = number of sites per zone, α_{95} = 95 % confidence circle around mean direction; κ = precision parameter.

Zone	Declination	Inclination	N	α_{95}	κ
Western Main Zone	3.1	66.7	32	2	169.27
Eastern Main Zone	14.7	63.8	26	3.3	83.2
Critical Zone	1.7	61.7	8	6.8	67.5
Upper Zone	174.8	-61.6	8	7.8	51.21
Northern Main Zone	359.8	66.1	22	3.8	67.55

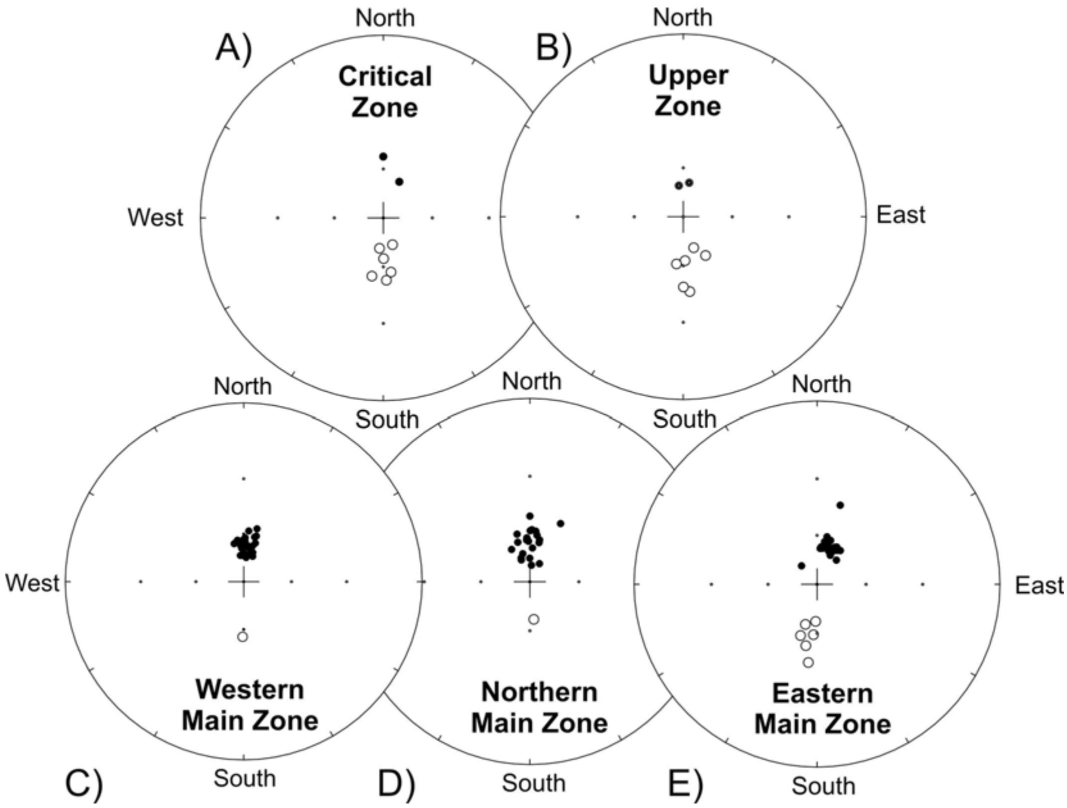

Figure 5.2 Mean bedding-corrected site HB components from all Zones of the Bushveld Complex. Upper Zone results are shown in A, Critical Zone in B, western Main Zone in C, northern Main Zone in D, and eastern Main Zone in E.

Despite these improvements, only two zones statistically passed the classic fold test at the 95% confidence level. These included the western and eastern Main Zones. A summary of fold test data can be found in Table 5.2.

Table 5.2 Summary of fold test results on all zones, with precision parameter (κ) before and after application of bedding corrections.

Zone	Fold Test Result	κ-before	κ-after
Western Main Zone	Significant at 95% confidence level	58.49	169.27
Eastern Main Zone	Significant at 95% confidence level	42.7	83.2
Critical Zone	Not significant at 95% confidence level	42.41	67.5
Upper Zone	Not significant at 95% confidence level	42.41	51.21
Northern Main Zone	Not significant at 95% confidence level	47.98	67.55

With only two zones passing the fold test of McElhinny (1964b), it cannot be confidently stated that all zones were formed in the near horizontal attitude. However, with the restoration of zones to the horizontal attitude there is a noticeable improvement in both site grouping and α_{95} values. A regional fold test applied to all samples revealed a positive result at the 95% confidence level, enriching the idea that emplacement was acquired in a near horizontal attitude, unfortunately this result is slightly biased towards the Main Zone results as the majority of samples were collected there. From these observations it is concluded that the Bushveld Complex was in a near-horizontal attitude when the temperature of magnetite (580°C) was reached.

The occurrence of igneous intrusions formed in a horizontal orientation before undergoing subsidence has been reported in a number of petrofabric and magnetic fabric studies: The Great Eucrite Gabbro intrusion of Ardnamurchan in NW Scotland has recently been interpreted by observations of magnetic fabric to have been emplaced in a horizontal orientation, and then at a later stage underwent considerable subsidence (O'Driscoll et al., 2006). Magnetic fabrics observed in the layered series of the Sonju Lake intrusion in northeastern Minnesota, suggests a horizontal emplacement (Maes et al., 2006). Petrofabric analyses carried out on the Great Dyke, revealed that pyroxenes from bronzitites exhibit well-developed linear lamination fabrics in the layering plane, with c-axes (longest axis) aligned parallel to the length of the Great Dyke. b-axes are dominated by a strong central maximum perpendicular to the layering plane (Wilson, 1992). Aligned elongate crystals are a characteristic feature of crescumulate type textures and have been interpreted to be diagnostic of in situ crystallization perpendicular to the floor of the magma chamber (Donaldson, 1974; Lofgren and Donaldson, 1975). The observed petrofabric findings suggest that the "Dyke" could have been emplaced in a horizontal orientation, before undergoing tilting.

Although petrofabric/magnetic fabric findings have not been established for the Bushveld Complex, the above examples illustrate that it is possible for an igneous intrusion to have been emplaced in a horizontal attitude before undergoing subsidence or tilting.

5.1.1 Recorded Reversals

During demagnetisation it was observed that a number of polarity changes had been recorded throughout the RLS (Figure 5.3).

Data from the Western Lobe (Figure 5.3) appear to demonstrate a clear-cut relationship between zones and polarity. Samples from both the Upper and Critical Zones are normally magnetised, while samples from the Main Zone are reversely magnetised with the exception of site 28b, a pyroxenite layer that is normally magnetized. However, gabbro-norite samples obtained directly above (± 5 cm) and below (± 3 cm) this pyroxenite layer possess reversed magnetisation and shows no sign of overprint. The distinctive zonal classification for the lobe is slightly misleading due to the unfortunate circumstance that few viable palaeomagnetic sites were available and therefore bad coverage was obtained in the Western Lobe. Upper Zone findings are based only on two sites and the Critical Zone from only one. Although the Main Zone has reasonable coverage it is still not perfect.

Magnetisation recorded in the Eastern Lobe is similar to that in the Western Lobe, although the relationship between zones and polarity is not as obvious. Within each zone several polarities are present (Figure 5.3), but overall the dominant magnetisation for each zone is the same as the Western Lobe with the Upper and Critical Zones possessing normal magnetisation and the Main Zone being dominated by reversed magnetisation.

In an effort to determine if the observed changes in polarity within zones were the result of recorded reversals in the Earth's magnetic field, two reversal tests were implemented on the data. The first one of McFadden and Lowes (1981) resulted in all zones sharing a common mean at 95% confidence level. The second reversal test of McFadden and McElhinny (1990) was only implemented on zones where more then one reversal was recoded. Zones obtained positive results with "C" classifications. The positive results generated from the reversal tests indicate that the BC had successfully recorded several reversals; the results of the two reversal tests are shown in Table 5.3.

Table 5.3 Summary of reversal tests. γ_o is the observed angle between the two polarities and γ_c is the critical angle between the two mean directions

Zone	**Reversal test of *McFadden and Lowes (1981)***	**Reversal test of *McFadden and McElhinny (1990)***		
Western Main Zone	Passed at 95 % confidence level	*N/A:* only one reversal		
Eastern Main Zone	Passed at 95 % confidence level	Passed: C	γ_o= 5.39	γ_c=10.35
Critical Zone	Passed at 95 % confidence level	Passed: C	γ_o=5.71	γ_c=16.11
Upper Zone	Passed at 95 % confidence level	Passed: C	γ_o=6.94	γ_c=14.88
Northern Zone	Passed at 95 % confidence level	*N/A*: only one reversal		

The two reversal tests were also implemented on all samples in determining a "regional" reversal test. The classical McFadden and Lowes (1981) test revealed that all samples share a common mean at 95% confidence, while the alternative test of McFadden and McElhinny (1990) indicates a positive reversal test with a "B"classification, $\gamma_{observed}$ = 5.63 and γ_{crit} = 7.28.

From the available palaeomagnetic data it appears that the rocks of the Upper and Critical Zones of the Bushveld Complex cooled below the Curie Temperature for magnetite (~580°C) while the Earth's magnetic field was in a normal polarity and the rocks from the Main Zone acquired their magnetisation during a reversed polarity. During the cooling of each zone, the Earth's magnetic field underwent two reversals in direction. The exact positions where polarity changed within zones are not well defined, due to the unfortunate circumstance that large gaps occur in the coverage.

It should be noted that the observed change in polarity recorded in the Eastern Lobe above the Pyroxenite Marker, could provide further proof in strengthen the isotopic findings of Kruger (1994) in indicating that a major magma influx occurred above the Pyroxenite Marker. Unfortunately, samples were not obtained directly above the Pyroxenite Marker but at a distance further up the stratigraphy, located above the Mottled Anorthosite layer (Figure 5.3). Therefore it is possible that the Pyroxenite Marker might in fact possess the same polarity as the rest of the Main Zone. Further sampling closer to the Marker is needed to accurately determine this. With the available data, there is not enough credible information in proving the occurrence of new magma influx; a more detailed and continuous study across the entire RLS is required to provide precise information.

Using the current data the only viable conclusions that can be inferred on the polarity findings is that during the cooling of the BC the rocks successfully recorded a number of reversals in the Earth's magnetic field. The exact location of these reversals are not well constrained.

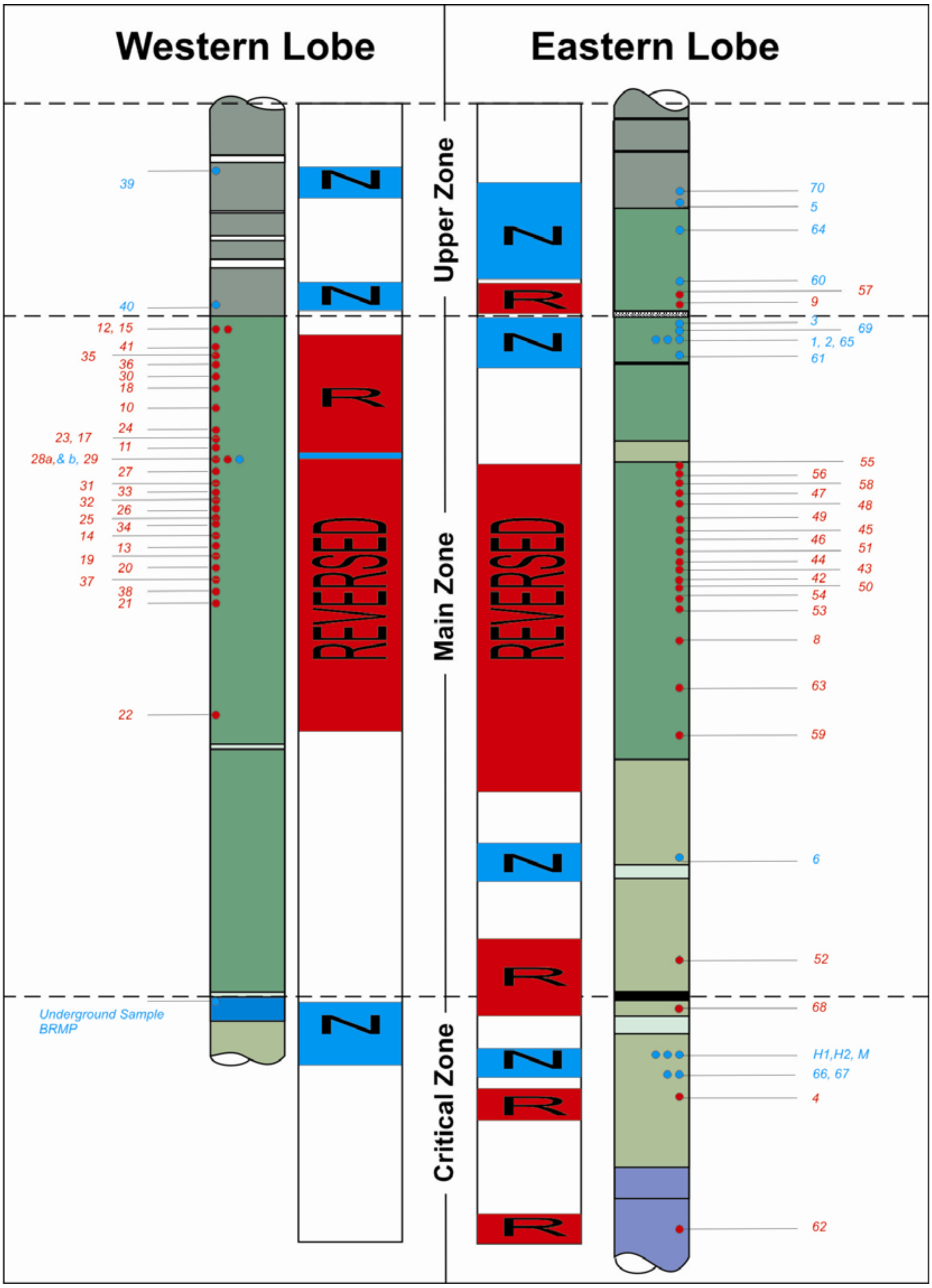

Figure 5.3 Simplified lithostratigraphic column of the Rustenburg Layered Suite in the Western Lobe and Eastern Lobe indicating the stratigraphic location and polarity of sampling sites. Red sites indicate a reversed polarity was recorded while blue represents a normal polarity. White areas in polarity the column indicate polarity is unknown.

5.1.2 Pole Positions

With reversed and normal polarity sites within each zone sharing a common mean at the 95 % confidence level, HB components were inverted to the same polarity and yielded a combined mean remanence direction, from which pole positions were calculated. Resulting directions and poles positions for each zone are given in Table 5.4 and shown in Figure 5.4 where they produce well clustered positions.

Table 5.4 Mean magnetisation directions and palaeomagnetic pole positions with associated errors dp and dm; Dec. = Declination, Inc. = Inclination, N = number of sites, α_{95} = 95 percent confidence circle around mean direction.

Zone	Dec.	Inc.	N	α_{95}	Pole Latitude	Pole Longitude	dp	dm
Main West Zone	1.1	66.9	32	2	15.5	28.2	2.7	3.3
Main East Zone	14.7	63.8	26	3.3	18.3	40.5	2.7	5.2
Critical Zone	1.7	61.7	8	6.8	22.1	31	8.1	10.5
Upper Zone	354.8	61.6	8	78	22.1	25.6	9.3	12
Northern Main Zone	359.8	66.1	22	3.8	17.5	28.8	5.1	6.2

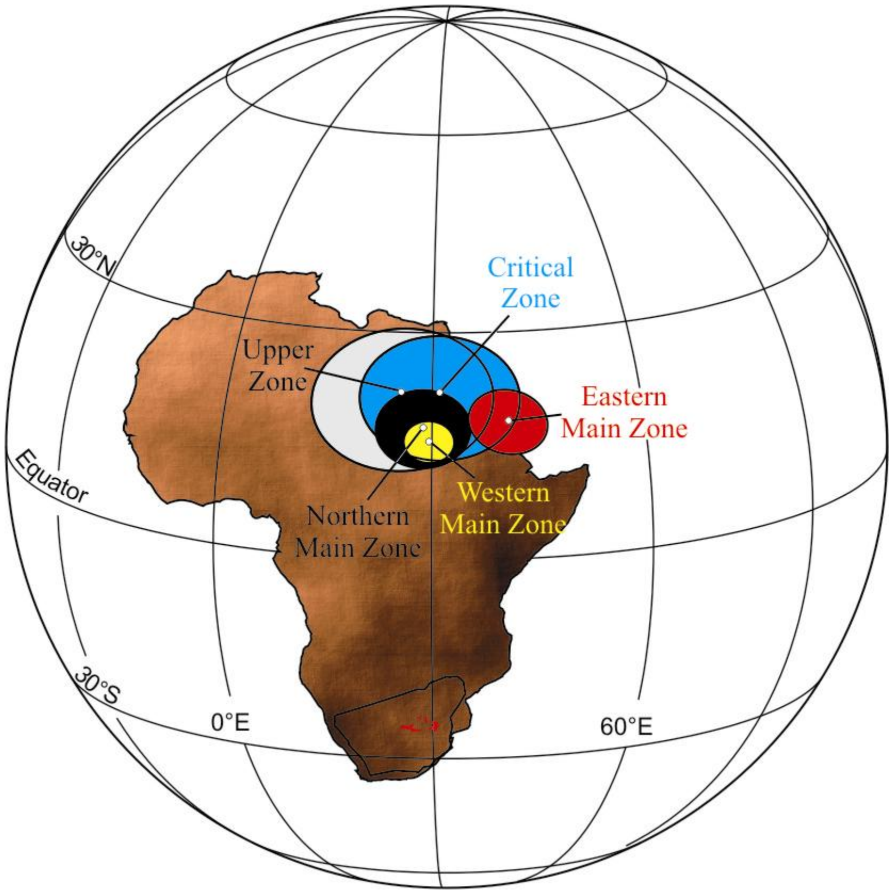

Figure 5.4 Equal-area projection of newly obtained pole positions for western Main Zone (yellow), eastern Main Zone (red), northern Main Zone (black), Critical Zone (blue) and Upper Zone (grey).

5.2 Comparison of Results with Previous Studies

NRM results from previous studies showed good agreement with results from this study. However, the primary magnetic component directions and hence pole positions presented here are generally of better quality and have produced results with smaller errors in confidences (Figure 5.5).

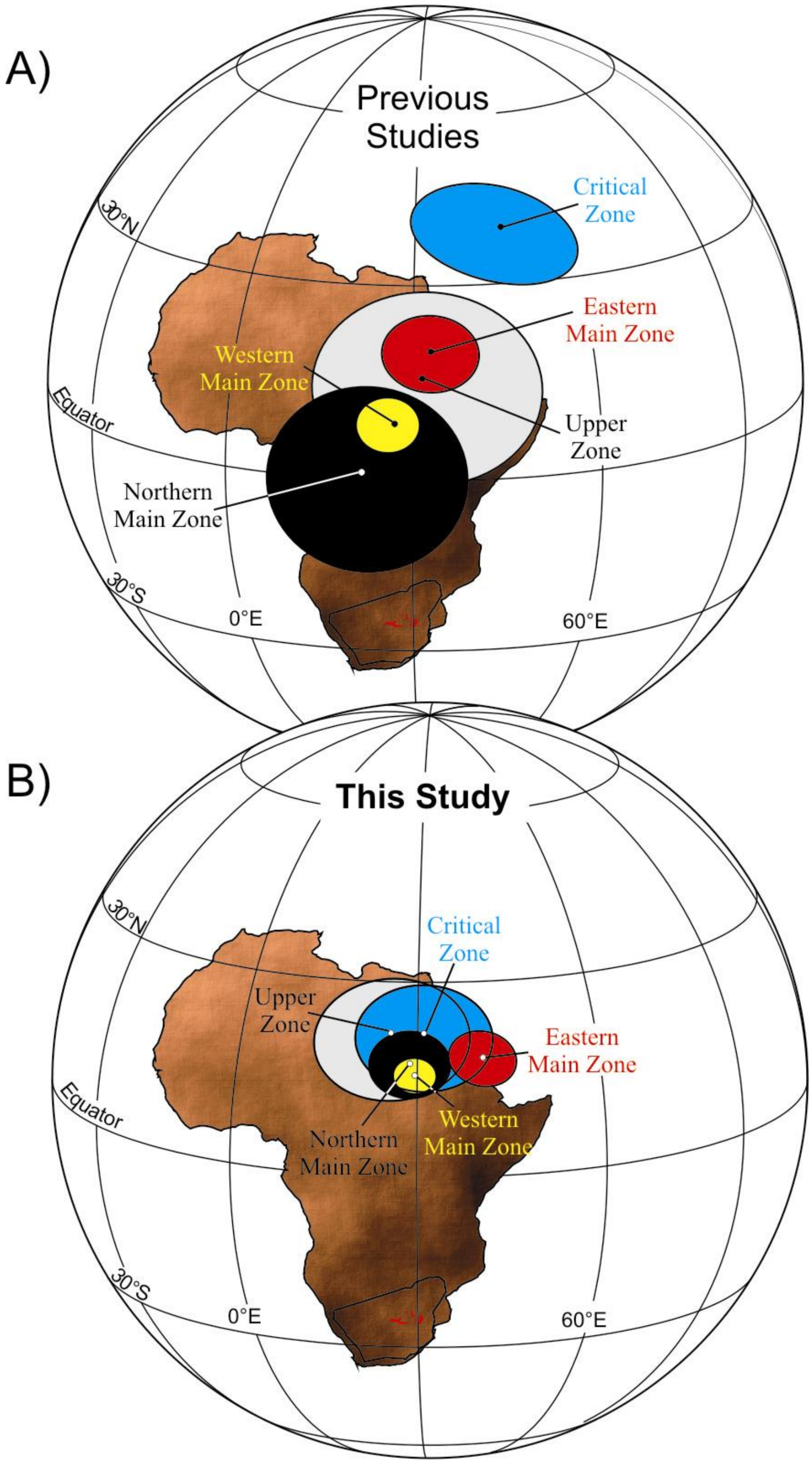

Figure 5.5 Comparison between old and new results for the Bushveld Complex. A) Pole positions obtained by Hattingh (1983), and Hattingh and Pauls (1994). B) Newly obtained pole positions from this study.

Upon examination of older data, it was discovered that the observed differences between the results can be linked to two possibilities:

- Possibility one:

  The first and possibly the most important finding was that Hattingh (1983) had used a method described by Briden (1972) to determine an "optimum" AF demagnetization value for each site (also referred to as the Briden S.I. Unit) in order to calculate the primary magnetisation component.

  The procedure of using a Briden S.I. unit to determine levels of magnetisation was widely used in the 1980s and when used correctly, it will determine when there is a change in direction of components. However during Hattingh's study, the Briden S.I. unit only identified where the secondary component was starting to be removed and as a result the final primary component was not successfully determined.

  On comparing the percentage of NRM intensity still preserved at the "optimum" demagnetisation level it was discovered that a large percentage of the original magnetisation was still preserved; the results are shown in Table 5.5

Table 5.5 Comparison of percentage of magnetisation still preserved (from this study) at "optimum" field (average value used) as determined by Hattingh (1983).

Zone	"Optimum" Field determined by Hattingh (1983)	Percentage of magnetisations still preserved
Western Main Zone	30 mT	88%
Eastern Main Zone	20 mT	90%
Critical Zone	30 mT	62%
Upper Zone	30 mT	72%

  Figure 5.6 represents a typical Zijderveld diagram for samples from the western Main Zone; the "optimum" demagnetisation level determined by Hattingh (1983) is represented by the red circle. It is clear that this represents the transition from the secondary to primary component. If demagnetisation is stopped at this "optimum" level, and principal component analysis is used to determine the primary magnetisation and the origin is not use as a point (therefore by definition, not determined

primary magnetisation), the resulting direction would be given by the red arrow. If the line is forced to pass through the origin, when only considering points up to 30mT the resulting magnetisation would be given by the green arrow. During this study all samples were completely demagnetised and the best-fitting line determined from principal component analysis naturally decays towards the origin (blue arrow in Figure 5.6). The difference between the results reported here and those by Hattingh (1983) are clearly shown by Figure 5.6,c.

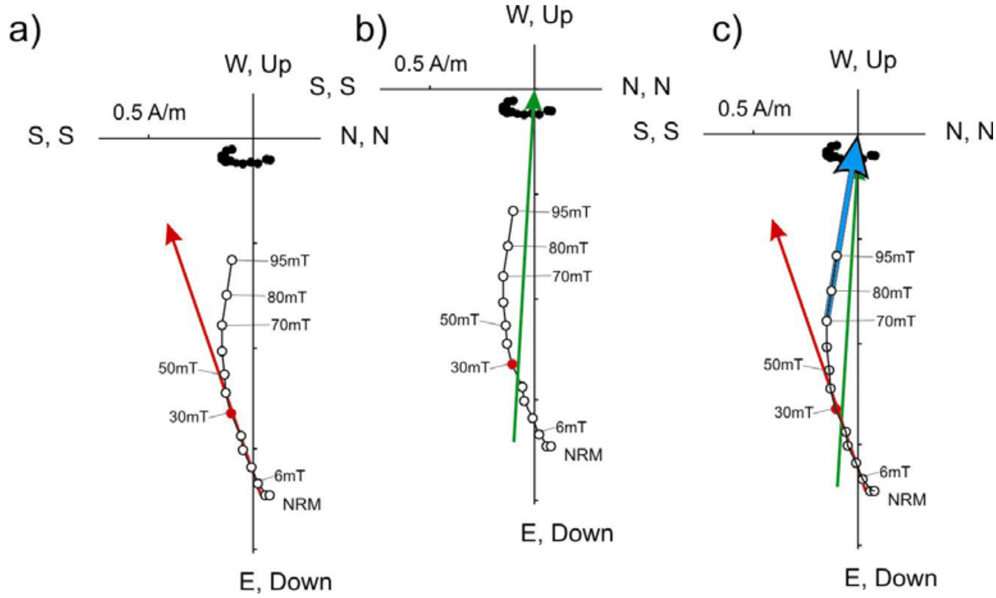

Figure 5.6 A typical Zijderveld diagram response from the western Main Zone the red circle is the "optimum" level for demagnetisation as determined by Hattingh (1983) a) The red arrow represents the best least-squared fit along a demagnetisation path without forcing the line through the origin. b) The green arrow represents the best least-squared fit along a demagnetisation path forcing the line through the origin, when only considering points up to 30mT. c) Blue arrow represents direction of magnetisation from this study when the sample was completely demagnetised, resulting in the best least-squared fit line through the origin. The other two arrows have been left on to illustrate the difference in directions determined from the previous study. Open (solid) symbols represent projections onto the vertical (horizontal) planes, respectively

- Possibility two:

  It was found that a number of sites presented in this study had not completely removed the secondary component during AF demagnetisation, and thermal treatment was further needed to determine the primary direction. In previous studies only AF demagnetisation was used and it is therefore likely that the same problems occurred resulting in primary components not being successfully determined.

Based on the two observations given above it is clear to see why there is a difference between these new results and those determined over 20 years ago by Hattingh (1983).

5.3 Conclusions

New palaeomagnetic data collected throughout the Bushveld Complex yielded palaeomagnetic poles that eliminated the spread in the apparent polar wander path as determined in earlier studies. The resulting better constrained/grouped palaeopoles positions are in agreement with precise age data, constraining the time period of emplacement of the BC.

Although only two zones yielded statistically positive results from fold tests, the resulting bedding corrected HB components from all zones produce better grouping, supporting a primary magnetic signature and indicates that the complex was intruded in a near horizontal position and that it underwent sagging only after it had cooled below ~580°C.

A number of magnetic reversals were identified throughout the complex; at this stage it is not possible to give an accurate description of the Earth's magnetic field during the emplacement of the complex due to the discontinuous coverage across stratgraphy. However, it is believed that in general the rocks of the Upper and Critical Zones cooled below the temperature of magnetite in a normal magnetic field while the Main Zone rocks cooled while the Earth's field was reversed. Within each zone the Earth's magnetic field switched a number of times allowing the cooling rocks to record the reversal, this is identified more readily in the Eastern Lobe were coverage is better. Positive reversal tests were obtained from each zone indicating that the two fields are anti-polar, thereby suggesting that a reversal in the Earth's magnetic field was successfully recorded.

Another important finding from this palaeomagnetic study is that sites have high Koenigsberger ratios (Q), on average 41, testifying to the importance of remanent magnetisation for magnetic modelling of the complex.

CHAPTER 6: PALAEOMAGNETIC STUDY OF THE PHALABORWA COMPLEX

6.1 General Geology of the Phalaborwa Complex

The Phalaborwa Complex outcrops in an elongated kidney-shape in the Limpopo Province in northern South Africa (Figure 6.1). The complex is chiefly composed of a vertical pipe-like body of pyroxenite, with an oval body of foskorite (texturally variable assemblage of coarse olivine, magnetite, apatite and phlogopite) and carbonatite in the centre (Harmer, 2000).

The complex was intruded into the Archaean basement gneisses at 2,060.6 ± 0.5 Ma (U-Pb on baddeleyite, Reischmann, 1995) in several alkaline cycles, which emplaced, in several successive stages, a suite of rocks ranging from ultramafic to peralkaline in character. The first phase was that of the massive ultramafic pipe-like body consisting mainly of pyroxenites. This was followed by an alkaline phase in which the surrounding syenite plug-like bodies were emplaced. At a later stage, foskorite and banded carbonatite of the central pegmatoid body were emplaced. The final phase saw the intrusive injection of the transgressive carbonatite (PMC, 1976).

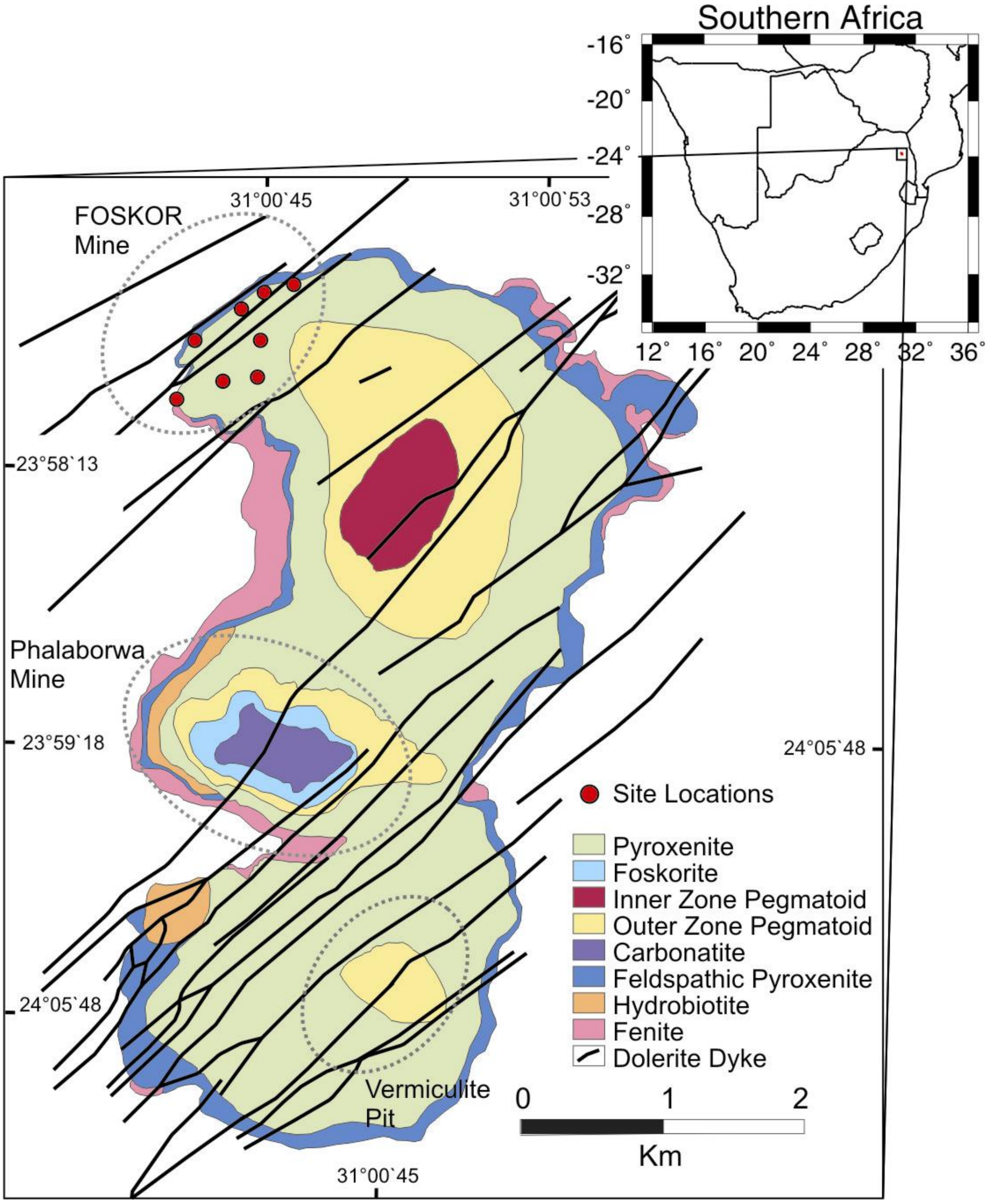

Figure 6.1 Simplified geological map of the Phalaborwa Complex with site locations obtained from the pyroxenites the three pits/mines are shown by dashed outline modified from Morgan and Briden (1981).

6.2 Sampling of the Phalaborwa Complex

Originally it was intended to sample pyroxenites throughout the entire complex. Unfortunately, the main Phalaborwa mine was unsafe to enter to obtain pyroxenite samples, due to side wall instability (Figure 6.2), while in other areas exposure was not adequate to obtain palaeomagnetic samples. In the end it was only possible to sample eight sites in the northern Foskor pit (Figure 6.1 and Figure 6.3). All samples were obtained with the use of a portable drill and orientated via sun and magnetic compasses.

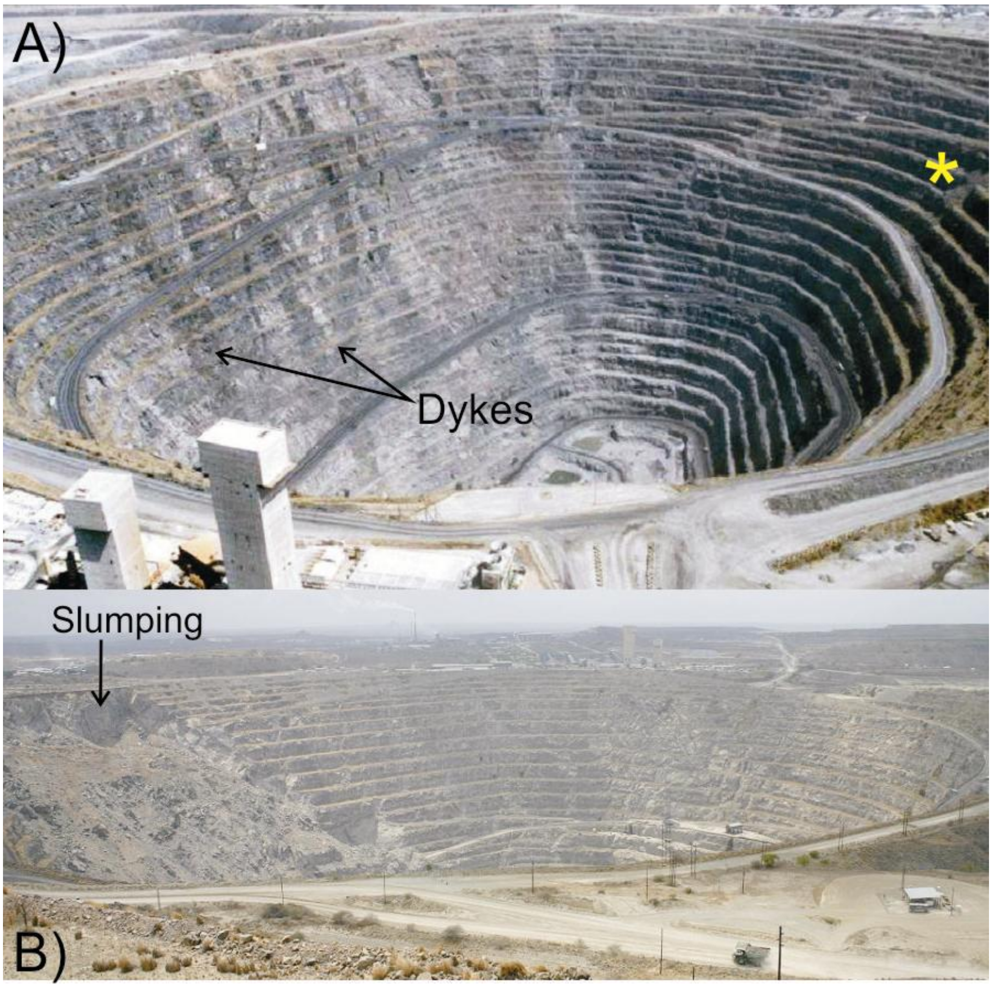

Figure 6.2 A) Oblique aerial photograph of the Phalaborwa open pit 10 years ago looking east (Garcia, 1996). The yellow star represents the slumped area shown in B. B) Phalaborwa open pit today looking west, with major sidewall stability problems.

Figure 6.3 View of the Phalaborwa Foskor pit from the north looking south, where all eight pyroxenite sites were obtained. The pit is composed mainly of pyroxenite. One of the dolerite dykes is visible in the picture.

6.2.1 Palaeomagnetic results

NRM

From the eight sites a total of 90 core samples were analysed initially for NRM and bulk susceptibility before demagnetisation was carried out. A wide range in NRM intensities was observed, ranging from 3.5 to 214.5mA/m, with the average value being 64.5mA/m. Susceptibility values, with the exception of site P-7 (4532×10^{-6} SI units), were more consistent, with values ranging from 214 to 327 $\times10^{-6}$ SI units, with an average of 248 $\times10^{-6}$ SI units. A histogram plot of NRM intensities and susceptibilities is given in Figure 6.4 a & b. Mean NRM values and bulk susceptibility values for all sites with errors are shown in Table 6.1.

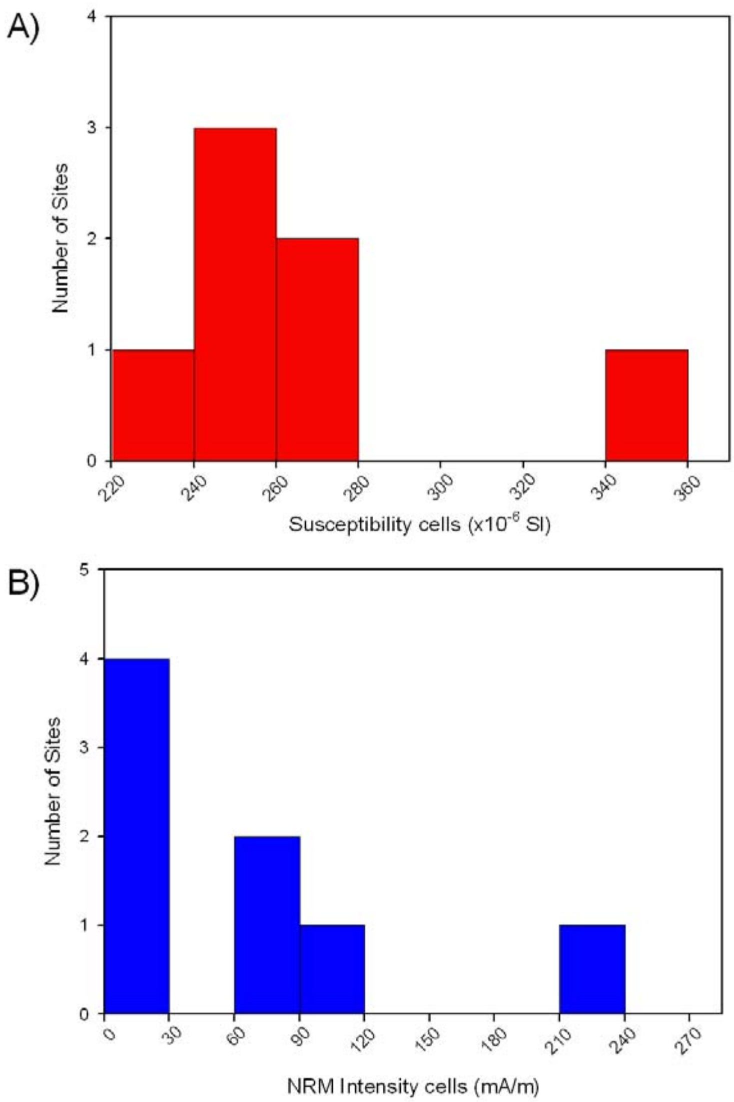

Figure 6.4 Histogram plot of site mean susceptibility with site P-7 excluded (4532×10^{-6} SI units) (a) and all site mean NRM intensity (b) from the Phalaborwa Complex.

Table 6.1 Site mean NRM and mean bulk susceptibility as well as Q ratio of all sites. *Dec.* = declination, *Inc.* = inclination, α_{95} = 95 percent confidence circle around mean direction, N= number of samples, +/- = 1 σ error.

Site	NRM Dec.	NRM Inc.	α_{95}	N	Intensity Average (A/m)	+/- (mA/m)	Susc. Average ($\times 10^{-6}$ SI units)	+/- ($\times 10^{-6}$)	Q Ratio
P-1	353.4	48.3	7.9	9	214.5	17.1	226.0	42.0	8.2
P-2	1.4	28.1	30.2	13	64.6	37.6	237.3	56.9	7.8
P-3	356.9	33.1	29.2	9	17.1	4.7	327.3	6.4	2.2
P-4	15.5	41.7	2.9	11	74.7	23.5	248.1	25.1	12.8
P-5	6	34.9	4.7	13	3.5	1.5	228.0	30.4	0.7
P-6	352.8	54.2	50.2	8	12.6	0.8	255.6	89.6	1.2
P-7	13.1	19.2	7.6	15	115.3	37.1	4531.7	1277.6	1.2
P-8	35.4	35.6	14.8	12	14.10	9.9	213.9	18.5	2.7

Individual samples from each site show variable clustering in direction. Four sites show good grouping, with α_{95} less then 8°, while the remaining four sites have exceptionally large α_{95} values (Table 6.1). The distribution of NRM directions illustrated in Figure 6.5 show a reasonable grouping in a moderate positive inclination with northerly declinations.

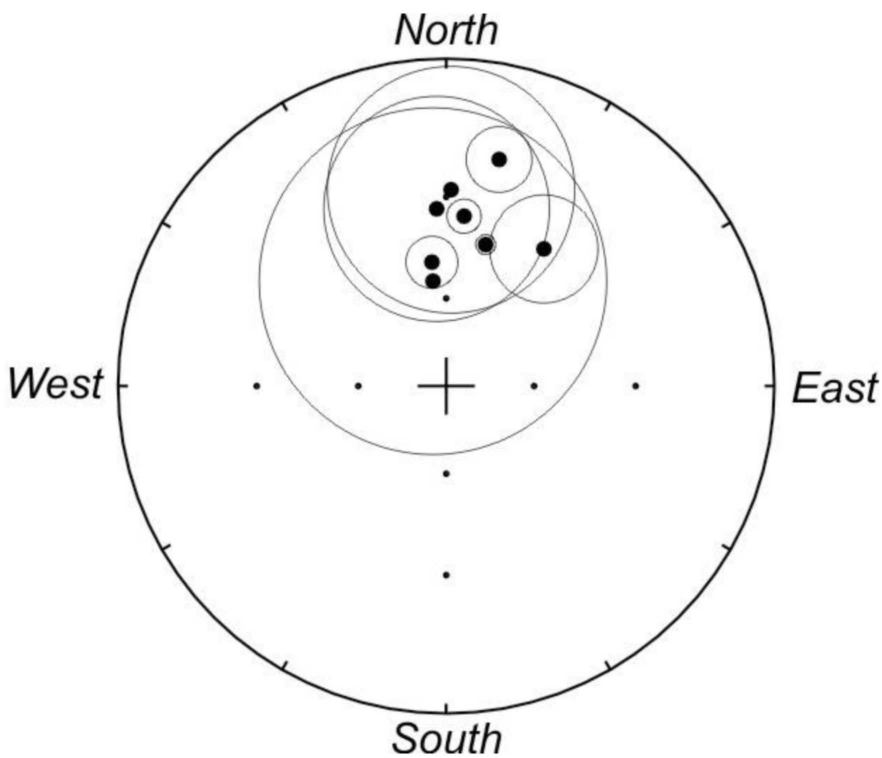

Figure 6.5 Site mean NRM directions from pyroxenites of the Phalaborwa Complex with α_{95} circles.

Demagnetisation

Samples were subjected to stepwise demagnetisation by both AF and thermal methods in an attempt to determine the magnetic history of the rocks. AF treatment was conducted on 45 samples and thermal treatment on the remaining 45 samples. Demagnetisation was carried out using between 10 and 16 steps up to 620° C (but generally 600°C) or 95 mT (maximum level obtained from AF instruments). After completion of demagnetisation, NRM directions were analyzed and interpreted with Zijderveld diagrams (Zijderveld, 1967), and principal component analysis was used to determine the directions of the various NRM components.

Components of magnetisation

Figure 6.6 illustrates a selection of orthogonal plots that show the demagnetisation characteristics of samples from the Phalaborwa Complex. A number of samples comprise two components of magnetisation: a low coercivity or low unblocking component, and a well defined high-stability or high temperature blocking component.

LB components (Figure 6.7), although present, are mostly scattered at site level (represented by exceptionally high α_{95} values in Table 6.2). Although they have very low statistics the mean direction is similar to that of the present day Earth's field and may be representative of a recent VRM. Samples presented here show the same characteristics as those obtained from dimension stone samples in the eastern and western Main Zone of the Bushveld Complex, in which LB components, although present, possess only a small percentage of the overall magnetisation.

Table 6.2 Site mean LB component directions for Phalaborwa samples. *Dec.* = declination, *Inc.* = inclination, α_{95} = 95 percent confidence circle around mean direction, N_o = original number of samples per site, N = number of samples analysed per site and κ = precision parameter.

Site	Dec	Inc	α_{95}	N_o/N	κ
P-1	304.9	-15.2	n/a	9/7	1.04
P-2	12.1	-23.1	n/a	13/7	1.08
P-3	45.1	-18.2	n/a	9/4	0.9
P-4	330.8	-37	76.9	11/5	1.95
P-5	19.8	-52.4	n/a	13/3	1.18
P-7	357.8	-31.4	17.2	15/15	3.4
P-8	130.9	29.7	52.6	12/3	6.55

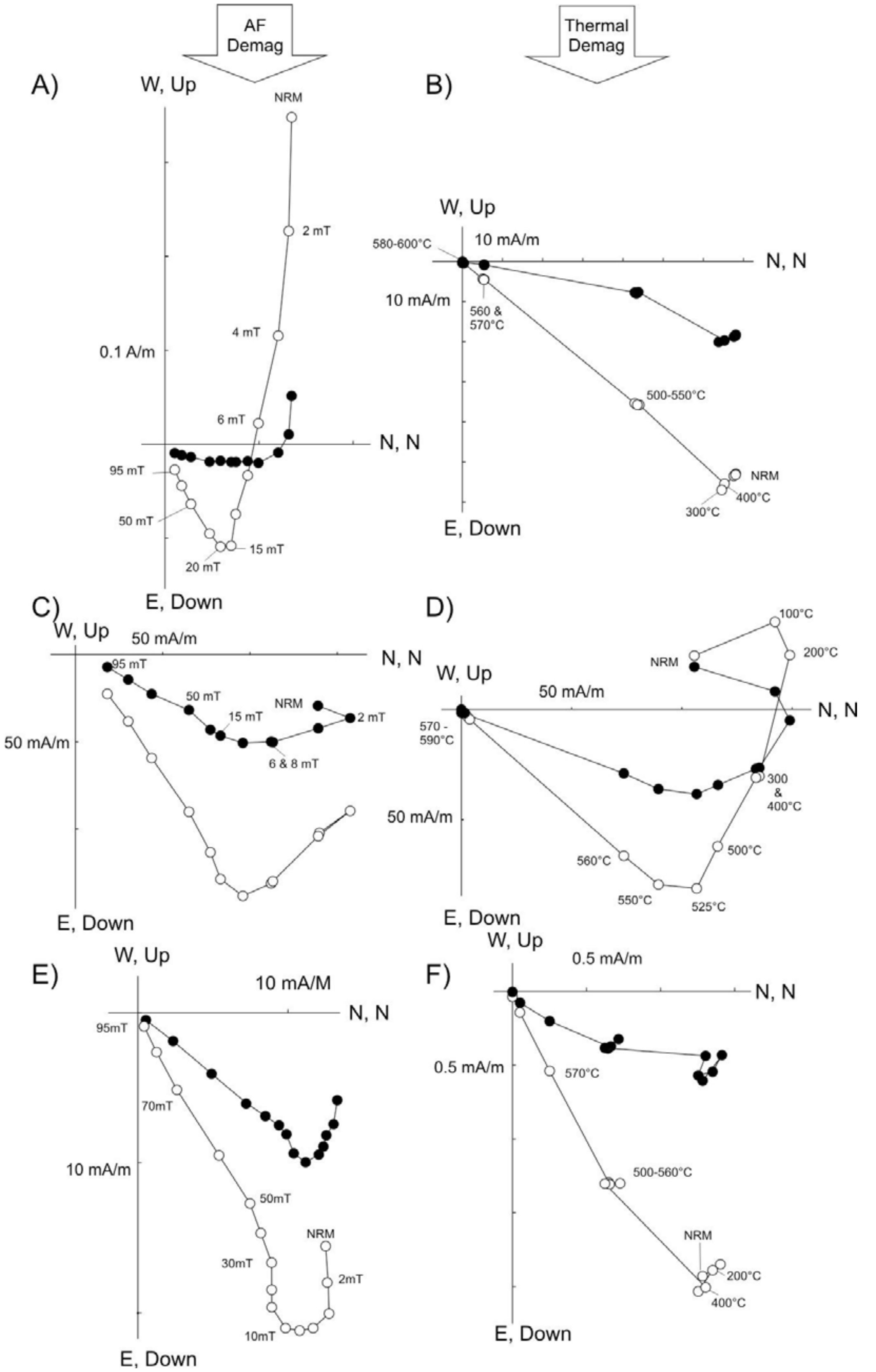

Figure 6.6 Characteristic examples of AF (a, c & e) and thermal (b, d & f) demagnetisation from Phalaborwa pyroxenite. Open (solid) symbols represent projections onto the vertical (horizontal) planes, respectively.

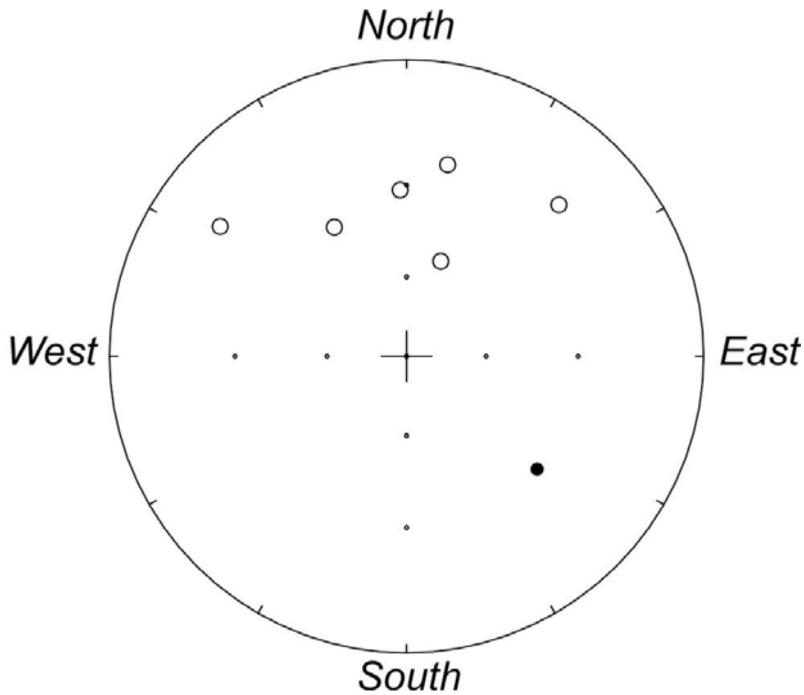

Figure 6.7 Site mean LB components from Phalaborwa sites, α_{95} circles are not shown as most values are greater then 90°.

Removal of low coercivity remanence isolates well-defined HB components that are identified above 550°C and 50mT. Both thermal and AF demagnetisation yielded similar directional results. HB components showed reasonable grouping within site (α_{95} on average 8°), while mean site directions have an improved grouping from those measured at NRM with mean directions in a northerly declination and steep positive inclination. The resulting HB components are shown in Figure 6.8 and listed in Table 6.3. Results from site P-6 were unstable upon demagnetisation and have not been included in the findings.

Table 6.3 Site mean HB component of magnetisation directions of each site *in situ*. N_o = original number of samples per site, N = number of samples analysed per site; α_{95} = 95 percent confidence circle around mean direction; κ = precision parameter.

Site	Dec	Inc	N_o/N	α_{95}	κ
P-1	359.8	61.2	9/9	10.7	74.96
P-2	1.8	48.9	13/13	14.1	43.34
P-3	354	52	9/9	8.2	127.82
P-4	7.5	56.3	11/11	3.6	454.69
P-5	0.3	59	13/13	6.9	122.73
P-7	19	61.2	15/15	3.4	168.04
P-8	16.5	60.4	12/12	12.2	30.61

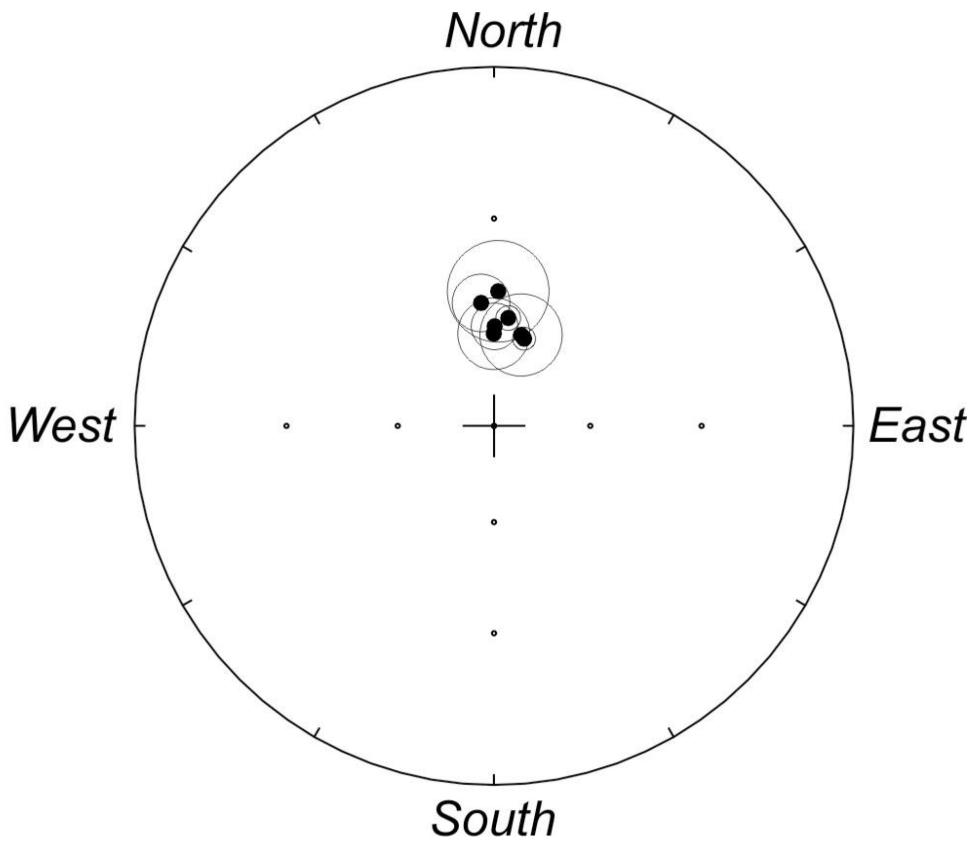

Figure 6.8 Site mean direction for Phalaborwa samples, *in situ.*

6.2.2 Thermomagnetic and petrographic analysis

In an attempt to determine the Curie temperature and hence the carrier of magnetisation of samples from the Phalaborwa Complex, thermomagnetic analysis (TMA) was carried out on a horizontal translation balance (Curie Balance). Typical response to TMA is shown in Figure 6.9, in which samples indicate a Curie temperature of ≈ 580°C.

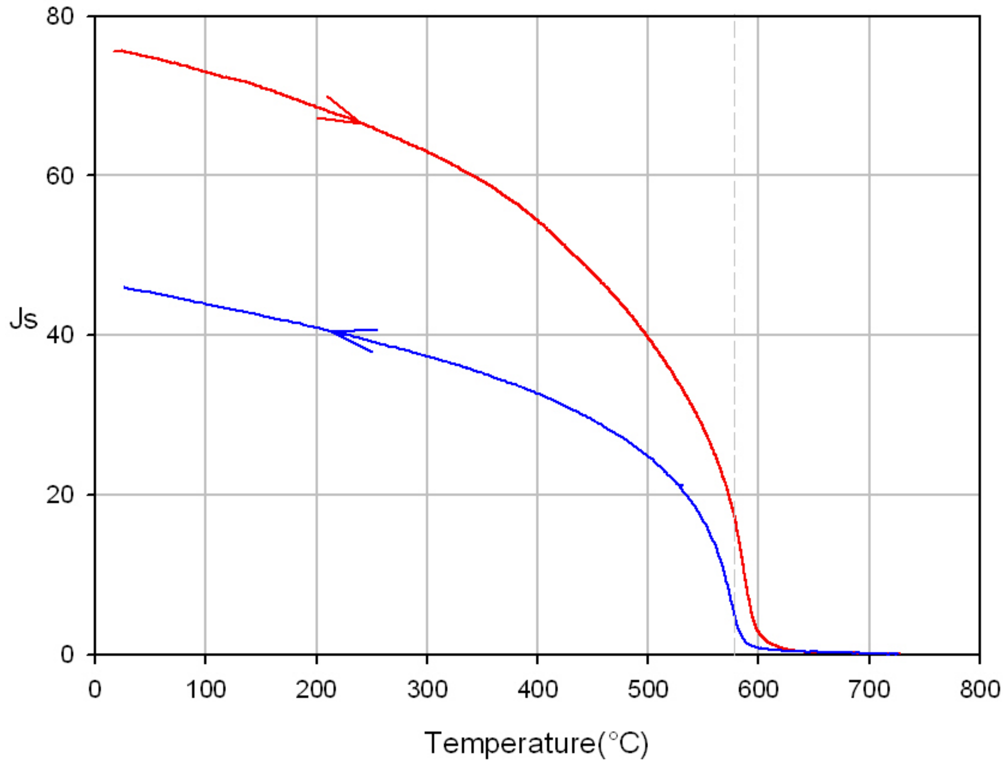

Figure 6.9 Typical thermomagnetic analysis response from Phalaborwa sites, above example is from site P-4. Red line and arrow indicate heating phase while blue line and arrow indicate cooling phase. Curie temperature for magnetite at ≈ 580°C observed (dashed line). The observed decrease in saturation magnetisation during cooling indicates that some oxidation occurred during heating and cooling.

Petrographic analysis was undertaken to determine the opaque mineralogy for the pyroxenites of the Phalaborwa Complex. On examination it was discovered that a number of minor sulphides were present, with pyrrhotite being the most common (overall percentage is low). Although magnetite was not present in large grains, on closer inspection it was revealed that magnetite occurred to a minor extent as small discrete grains. Based on the response from Curie temperature curves, it is believed that magnetite is the dominant carrier of magnetisation and may occur more abundantly as exceptionally small grains undetectable in thin section.

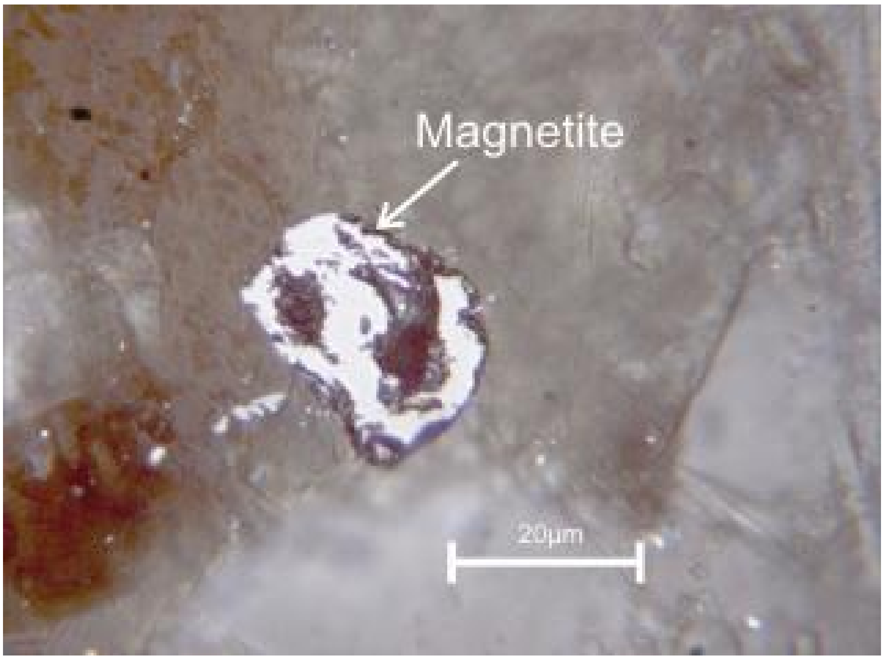

Figure 6.10 Discrete magnetite grain from site P-3, reflected light

6.2.3 Interpretation of palaeomagnetic data from the Phalaborwa Complex

The majority of samples analysed contained minor low temperature components, which were successfully removed during progressive demagnetisation, and allowed for the identification of well defined high temperature components, which produce extremely well clustered results.

Thermal demagnetisation spectra and thermomagnetic analysis suggest that Ti-poor magnetite or nearly pure magnetite (maximum unblocking temperatures of 565-580°C and Curie temperatures at ≈ 580°C) is the bulk remanence carrier. Petrographic analysis further strengthens these observations, revealing magnetite as an opaque mineral.

The high-temperature mean components of all sites yield a mean remanence direction with declination = 5° , inclination = 57.39° (α_{95} = 5.2º, N =7 sites) and a palaeopole position (Figure 6.11) with palaeolatitude =27.9° and palaeolongitude = 356°, dp/dm = 5.5°/7.6° (palaeopole calculated at mean sampling co-ordinates of 24°S and 31.1°E).

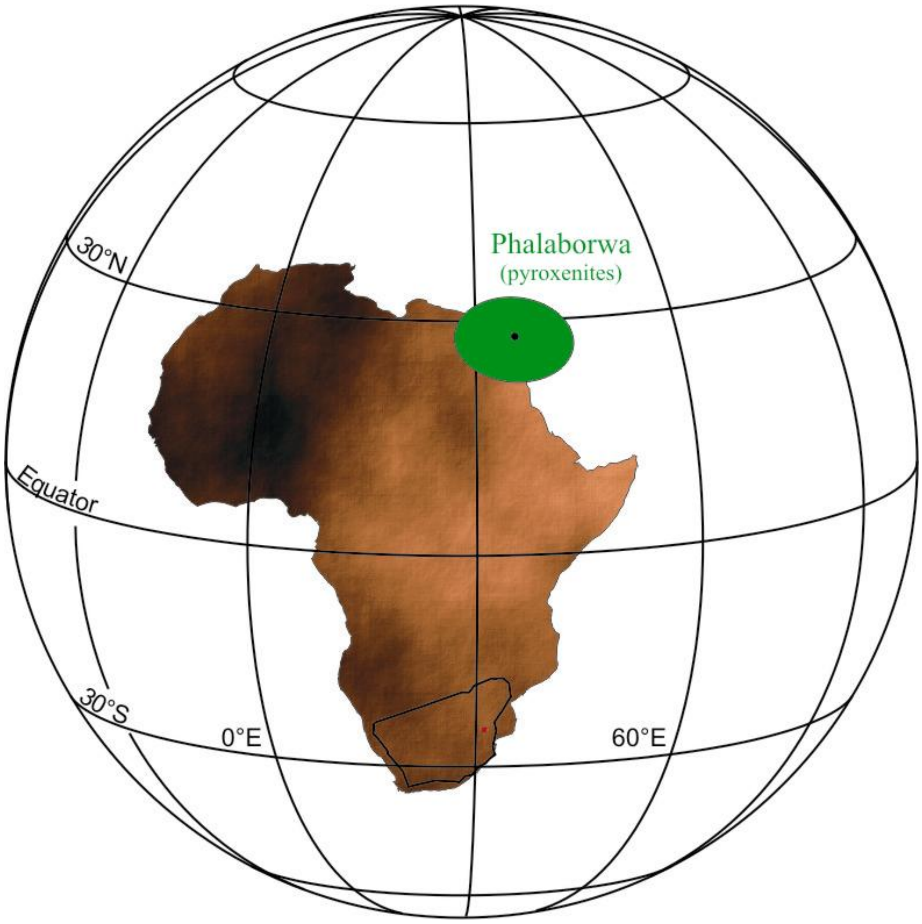

Figure 6.11 Resulting palaeopole position from the Phalaborwa pyroxenites.

6.3 Comparison of Results with Previous Studies

Palaeomagnetic data reported in this study show reasonable agreement with those presented by Morgan and Briden (1981). The difference in pole position is of the order of approximately 10°, with associated ellipse of confidence for each palaeopole overlapping (Figure 6.12). The observed variation between the two results is possibly due to the previous study determining primary components from a single demagnetised direction at around 400°C or 50 mT for each sample, and not by principal component analysis carried out on Zijderveld diagrams. It is also possible that with advancement in technology better magnetic cleaning was obtained during demagnetisation for this study. The newly obtained pole for the Phalaborwa pyroxenites now plots closer to those obtained for the coeval Rustenburg Layered Suite of the Bushveld Complex.

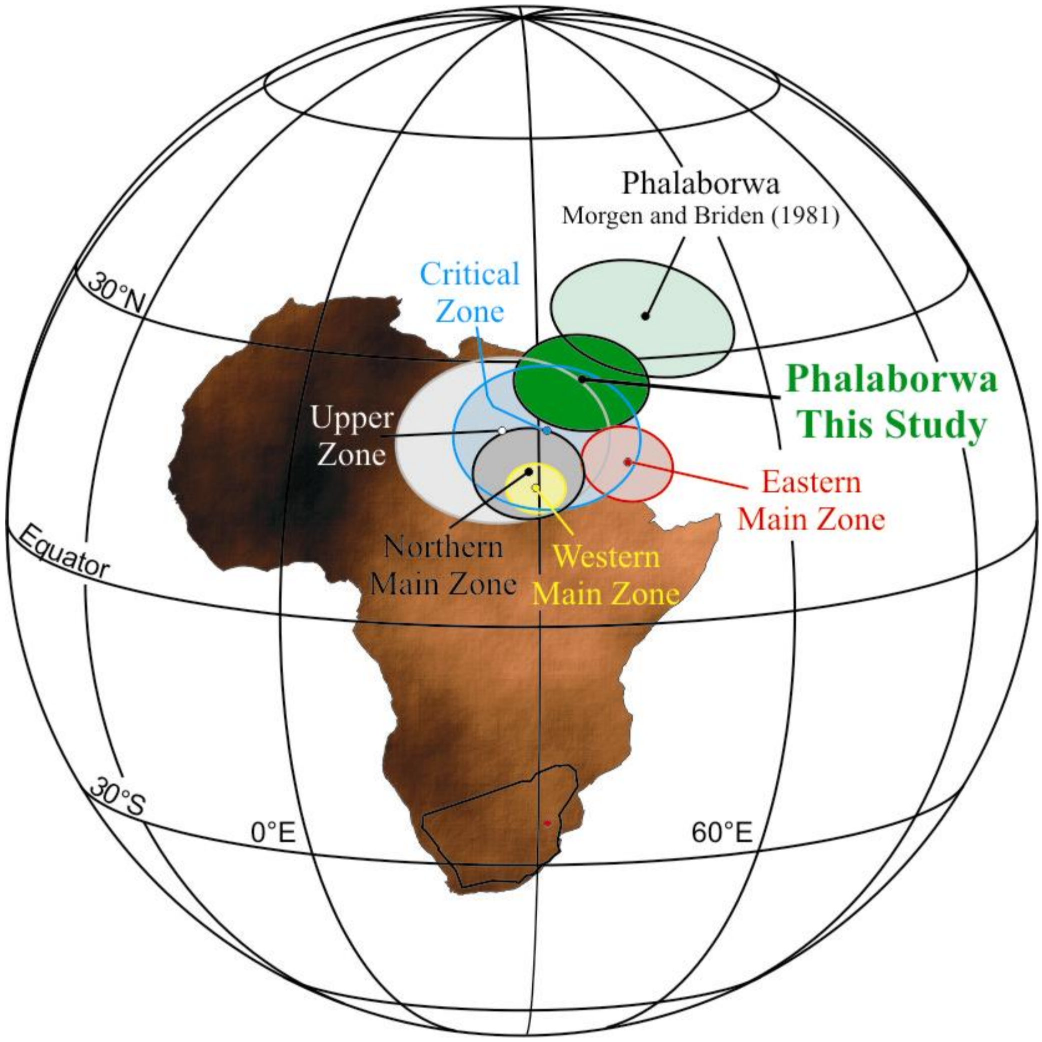

Figure 6.12 Pole positions from the Phalaborwa pyroxenites (this study-dark green) as well as the previous Phalaborwa study (light green) and poles from the Bushveld Rustenburg Layered suite (this study - different shades of grey).

6.4 Conclusion

Newly obtained palaeomagnetic data from the Phalaborwa pyroxenites are of excellent quality and the predominant magnetisation is in close approximation to that of previous palaeomagnetic studies. The newly determined results are believed to have successfully isolated minor secondary components to produce a better grouped primary signature. The resulting pole position for the Complex statistically overlaps pole positions from the marginally older Rustenburg Layered Suite from the Bushveld Complex.

CHAPTER 7: PALAEOMAGNETIC DATA FROM DOLERITE DYKES IN NORTHERN SOUTH AFRICA

Regional aeromagnetic data obtained from the South African government reveal that northern South Africa is riddled with dykes (Figure 7.1). Unfortunately, very little information is known about those occurring in the Bushveld and Phalaborwa Complexes. The following sections give an account of results obtained from palaeomagnetic analysis conducted on dyke samples collected from the Phalaborwa Complex and the Eastern Bushveld Complex.

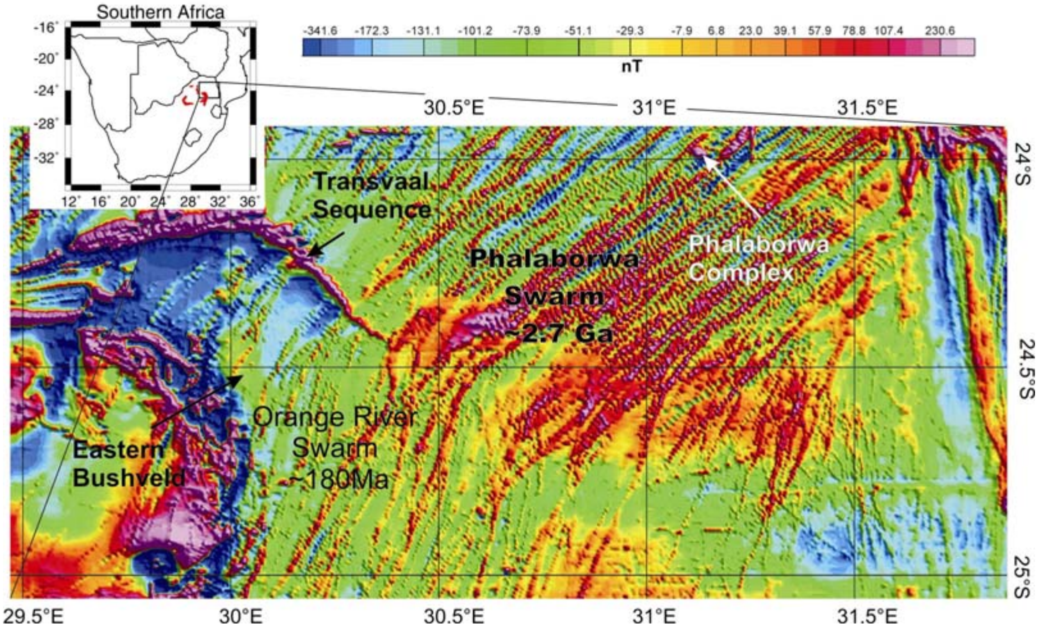

Figure 7.1 Regional aeromagnetic data over northern South Africa. The major geological bodies in the area are visible: Bushveld Complex, Phalaborwa Complex, Transvaal Sequence, as well as the Orange River and Phalaborwa dyke swarm. Regional aeromagnetic data provided by Council for Geoscience.

7.1 General Background

Examination of dyke swarms and their relationship to major mafic magmatic events in the Kaapvaal Craton reveals that dyke swarms have repeatedly exploited certain orientations (Uken and Watkeys, 1997). Three main trends have been identified in which dyke swarms were repeatedly emplaced: northeast, northwest and east-west. Ages and orientations of major dyke swarms for the entirety of southern Africa are summarized by Hunter and Reid (1987). For this study only the northeast swarm that intrudes the Bushveld and Phalaborwa Complexes were considered.

The northeast-trending dyke swarm consists of two main ages and compositions (Uken and Watkeys, 1997):

- Dykes that are thought to be related to the 2.7 Ga Ventersdorp rifting event.
- Dykes that have been assumed to be Karoo (Jurassic) in age based on a few dykes that reveal a post-Karoo date (approximately 180 Ma) (Hunter and Reid, 1987). These dykes have re-utilized the older fracture fabric of the earlier dolerite dykes.

An ITC database (Chavez Gomez, 2001) of mafic dykes in southern and eastern Africa, complied of digitizing dykes from aeromagnetic data in the area has classified the two dyke swarms as the Phalaborwa swarm (~2.7 Ga) and the Orange River Swarm (~180 Ma), as shown in Figure 7.2. The database reveals that the dykes present in the Bushveld Complex are only from the Orange River Swarm, i.e. Jurassic in age. However, a palaeomagnetic study conducted on a number of these dykes revealed that the resulting pole position clearly does not resemble any Karoo pole but instead overlaps with major geological events at around 2 Ga (Letts et al., 2005), indicating an intrusion age of ~1.9 Ga (based on palaeopole position).

Dykes occurring in the Phalaborwa Complex had also been previously assumed to be Karoo in age, until a palaeomagnetic study conducted on them in the late 1970s indicated that they are Precambrian in age and are possibly related to the 1,880 ± 25 Ma Mashonaland dolerites (Morgan and Briden, 1981).

During this study thirteen dykes that intruded the Phalaborwa Complex and Eastern Bushveld Complex were sampled.

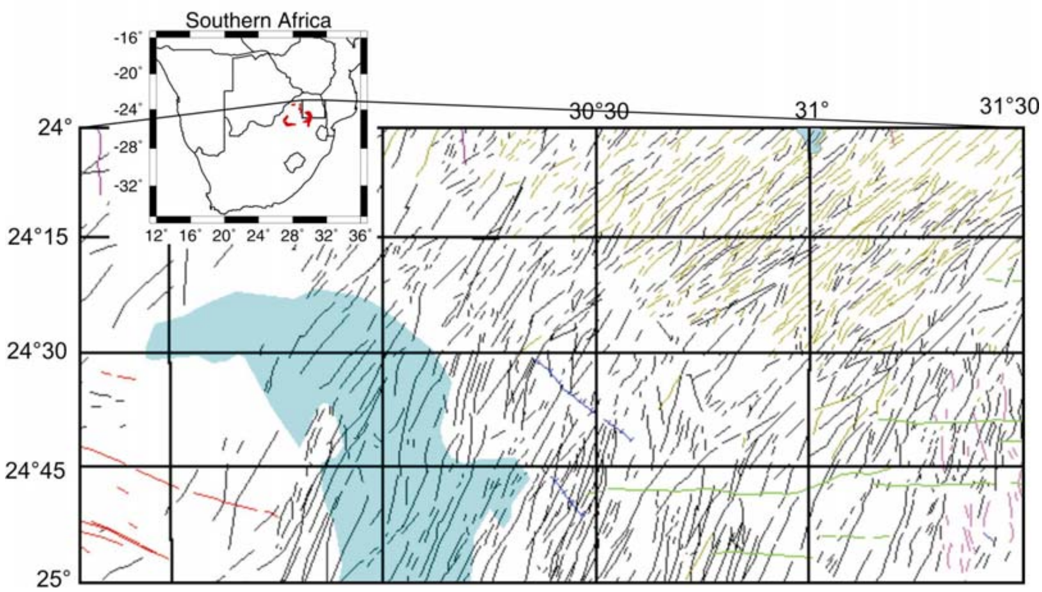

Figure 7.2 Map of the Eastern Bushveld and Phalaborwa Complexes (both in blue) with the different dyke swarms taken from the ITC database. The dyke swarms are as follows: Black = Orange River, Yellow = Phalaborwa (top right), Blue = Pongola, Red = NNW Striking Pongola, Green = Nelspruit, Purple (top left) = Buby-Crystal Springs and Pink (lower right) = Lebombo. The dyke swarm names are taken from the ITC dataset (Chavez Gomez, 2001).

7.2 Palaeomagnetic Results from Dolerite Dykes in the Phalaborwa Complex

A total of nine dykes were sampled in the complex: four in the Foskor pit, three in the main Phalaborwa Pit and two in the Vermiculite Pit. Sampling locations within the complex are shown in Figure 7.3.

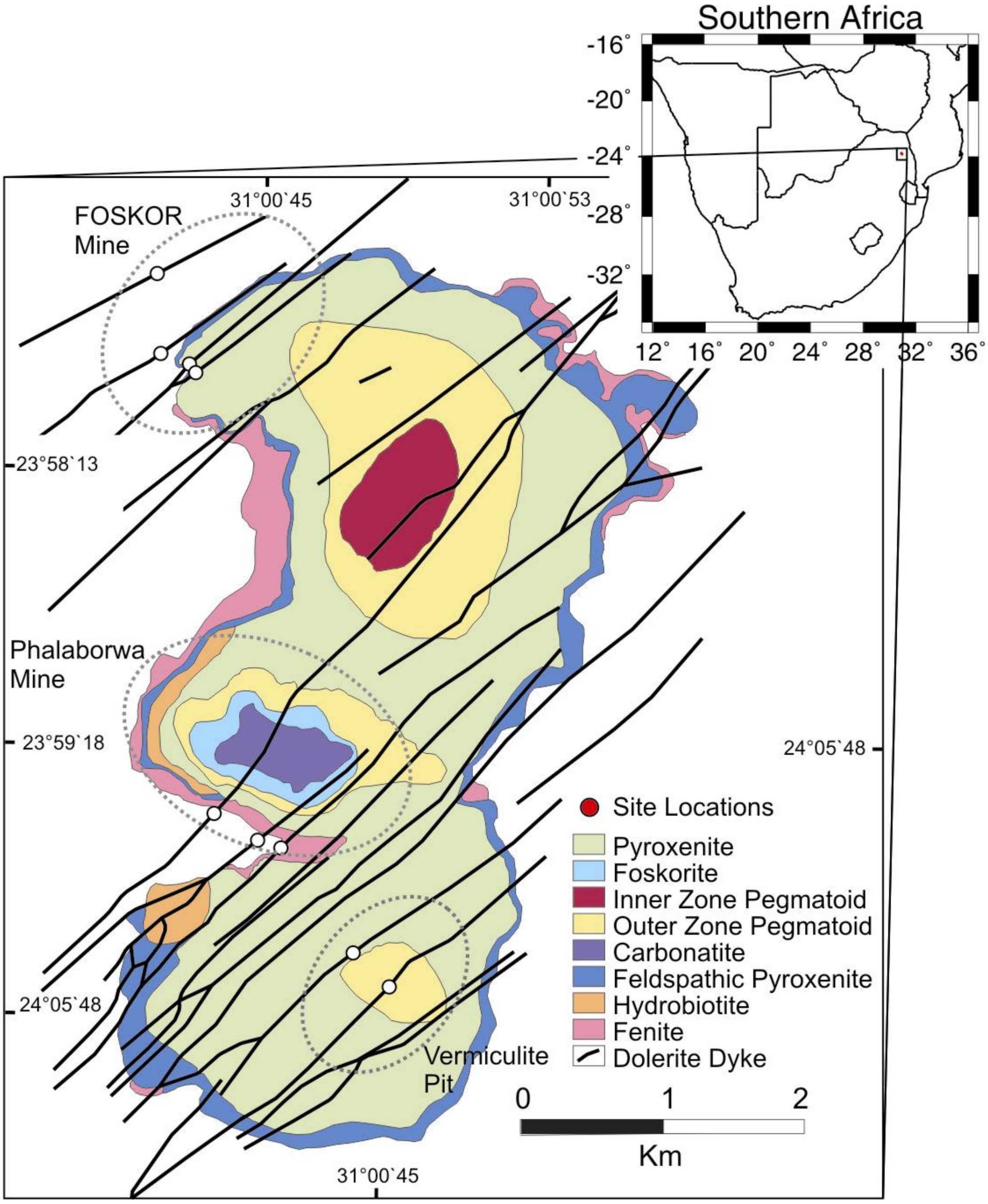

Figure 7.3 Simplified geological map of the Phalaborwa Complex, indicating the locations of dyke sites.

7.2.1 NRM

A total of 79 dolerite dyke cores were initially measured for NRM and bulk susceptibility before being subjected to progressive demagnetisation. NRM intensities showed a broad range in values from 1.38 A/m up to 30.83 A/m, with an average value of 9.04 A/m. Susceptibility values also exhibited a large variation in results from 15,907 to 49,172 $\times 10^{-6}$ SI units, with an average value of

32,561 $\times 10^{-6}$ SI units. Histograms of susceptibility and intensity are shown in Figure 7.4. The mean NRM and bulk susceptibility values for all sites with errors are shown in Table 7.1.

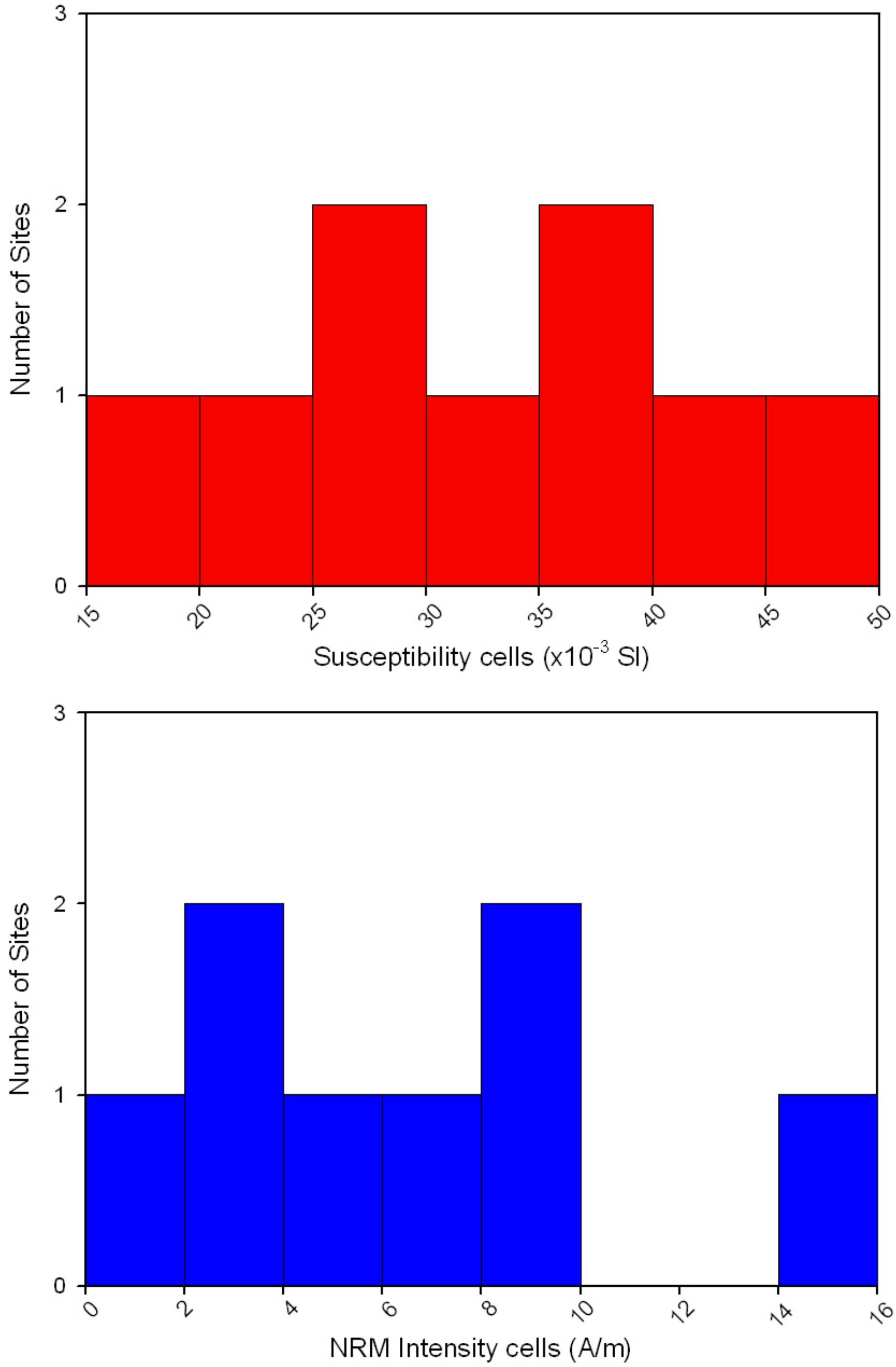

Figure 7.4 Histogram plot of site mean susceptibility in 10 $^{-3}$ SI units (A) and site mean NRM intensity in A/m excluding P-2 (30A/m) (B) of sites from dykes.

Table 7.1 Site mean NRM, mean bulk susceptibility and Q ratio of all sites. *Dec.* = declination, *Inc.* = inclination, α_{95} = 95 percent confidence circle around mean direction, N= number of samples, +/- = 1 σ error and Susc.= Susceptibilty. Site names represent sample location: F = FOSKOR pit, P= Phalaborwa pit, V= vermiculite pit.

Site	NRM Dec.	NRM Inc.	α_{95}	N	Intensity Average (A/m)	+/- (A/m)	Susc. Average ($\times 10^{-6}$ SI units)	+/- ($\times 10^{-6}$)	Q Ratio
F-1	11.8	50.9	6.3	7	3.15	3.8	28750.2	351.8	4.5
F-2	121.3	-63.9	1.3	10	8.48	3.2	33458.3	628.0	10.6
F-3	129.6	-68.7	3.6	10	8.76	11.7	35131.99	3779.7	10.4
F-4	158.7	-66.8	5.3	10	6.79	19.0	29177.5	837.4	9.7
P-1	167.1	-78.9	3.4	10	15.70	5.7	49172.5	772.5	13.3
P-2	317.3	69.7	20	5	30.83	20.4	15907.4	42325	81.2
P-3	20.6	35.1	73.9	11	1.38	3.3	40557.1	473.2	1.4
V-1	328.3	4.6	29.4	9	2.29	28.5	39453.6	1131.04	2.4
V-2	354.6	54.9	49.6	7	4.00	7.4	21442.0	1169.4	7.8

NRM results show two anti-polar groupings. Four sites posses a southeasterly to southwesterly declination with a steep negative inclination, while the remaining 5 sites have a more dispersed direction around a northerly declination and steep positive inclination (Figure 7.5). On the whole, sites show good grouping with α_{95} varying from 1.3° to 6.3°, with the exception of sites P-3, V-1 and V-2, where grouping is extremely poor (α_{95} listed in Table 7.1).

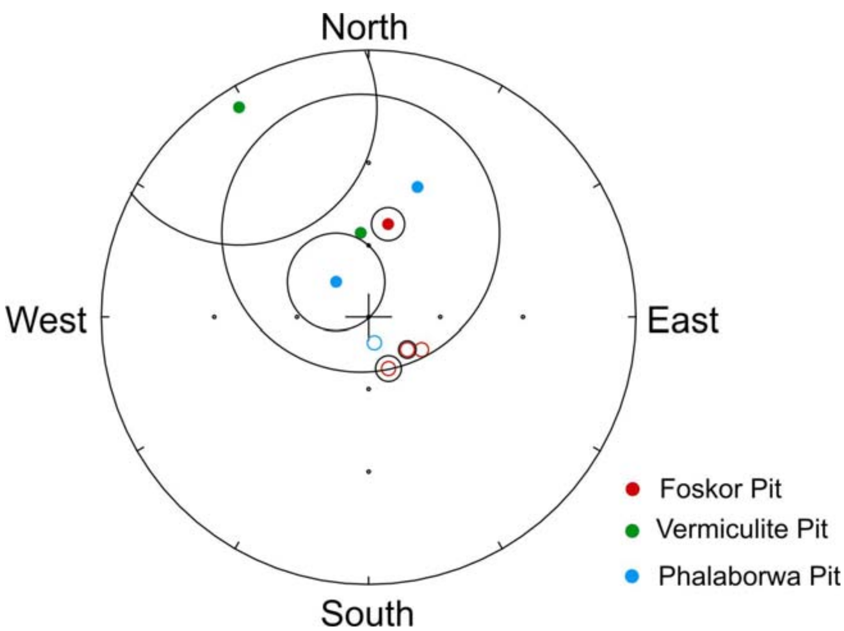

Figure 7.5 Site mean NRM directions from Phalaborwa dyke samples, the different colours represent sampling locality: red = Foskor Pit, green = vermiculite pit and Blue = main Phalaborwa pit.

7.2.2 Demagnetisation

In order to determine the primary magnetisation of the intruded dykes, samples were subjected to progressive demagnetisation. Demagnetisation was completed with the use of thermal demagnetisation on 43 samples, and AF demagnetisation on the remaining 36 samples. The levels of demagnetisation for AF demagnetisation were: 2, 4, 6, 8, 10, 15, 20, 30, 40, 50, 70 and 95 mT. For thermal demagnetisation, the levels were: 100, 200, 300, 400, 450, 500, 520, 540, 560, 580 and 595°C. Some variations in the above levels occurred due to different levels of magnetisation being present in different samples. Once demagnetisation was completed, data were plotted on Zijderveld diagrams and subjected to principal component analysis to determine low temperature blocking components and high-stability component of NRM.

7.2.3 Components of magnetisation

Figure 7.6 includes a selection of orthogonal plots typifying the behaviour of dyke samples. Samples behaved exceptionally well to both thermal and AF demagnetisation, showing the presence of two components of magnetisation. Once again, LB components identified in samples have directions that are all random within sites and are typically removed at around 500ºC or 30-40 mT. LB directions are not related to any significant geological meaning and are not considered further. Dyke samples that have a negative inclination generally had very small overprints, which did not severely alter the primary magnetisation direction.

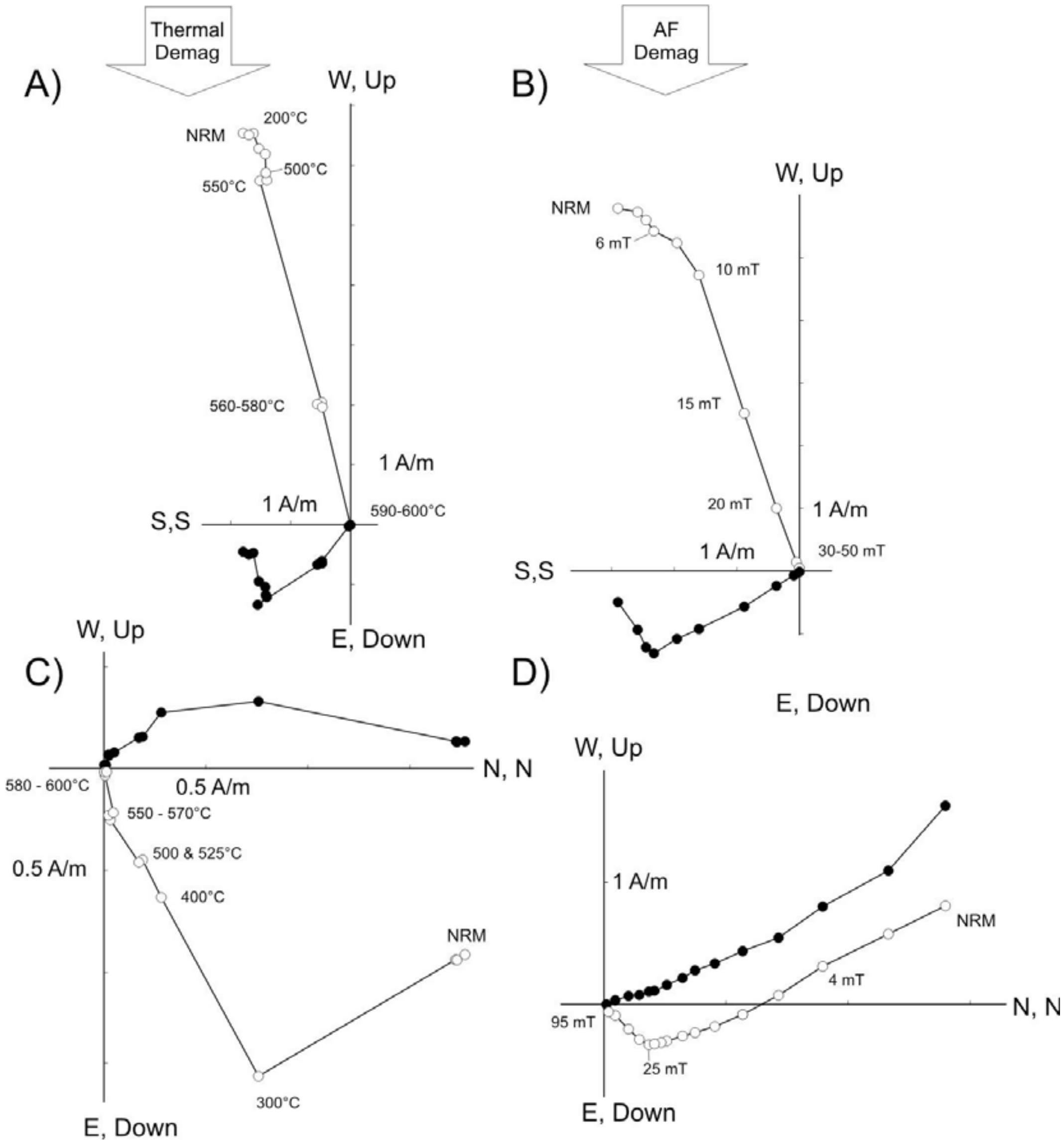

Figure 7.6 Typical Zijderveld diagrams from thermal (A & C) and AF demagnetisation (B & D). Diagrams a and b are from Foskor site 4 (F-4) and diagrams c and d are from Vermiculite site 1 (V-1).Open (solid) symbols represent projections onto the vertical (horizontal) planes, respectively.

With the removal of low coercivity (or low temperature) remanence, one of two approximately anti-polar higher coercivity remanence (or high temperature remanence) directions were isolated above 550°C or 50mT (Figure 7.6). HB components show reasonable grouping within site (α_{95} around 5°). Mean site directions plot with southerly to southeasterly declination and very steep negative inclination or anti-polar to this (northerly to north-westerly declination and very steep positive inclination). Resulting HB components are shown in Figure 7.7 and listed in Table 7.2.

Table 7.2 Site mean HB component directions for all dyke samples. *Dec.* = declination, *Inc.* = inclination, α_{95} = 95 percent confidence circle around mean direction, N_o = original number of samples per site, N = number of samples analysed per site; κ = precision parameter. Site names represent sample location: F = FOSKOR pit, P= Phalaborwa pit, V= Vermiculite Pit.

Site	Dec	Inc	α_{95}	N_o/N	κ
F-1	14.8	52.8	4.4	7/7	158.1
F-2	121	-62.9	1.7	10/9	959.5
F-3	132.3	-66.6	3	10/11	234.7
F-4	141.4	-66.9	3.2	10/10	230.2
P-1	168.1	-77.9	3.2	10/10	232.0
P-2	342.4	74.8	6.2	5/5	401.1
P-3	321.2	70.5	3.8	11/10	159.9
V-1	314.2	61.3	8	9/7	93.3
V-2	315.7	72.7	21	7/7	14.3

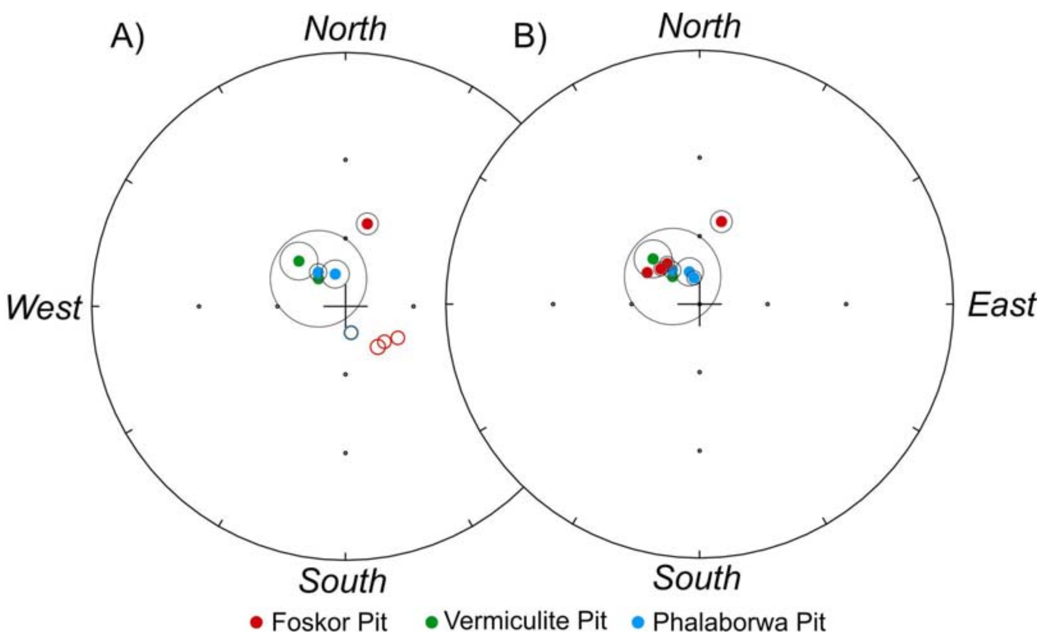

Figure 7.7 Site mean *in situ* direction (a), (b) sites inverted to positive inclination. Solid symbols indicate a positive inclination, while open symbols indicate a negative inclination**.**

7.2.4 Field stability tests

Reversal Test

Two reversal tests were implemented in order to determine whether the reversely polarized dykes were of similar age to the normally polarized dykes. It was found that the dykes shared a common mean at 95% confidence according to the method of McFadden & Lowes (1981). The reversal test of McFadden & McElhinny

(1990) also indicated a positive reversal test with a "C" classification (i.e. the angle between the reversals is between 170° and 160°; critical angle = 16.58°; observed angle = 7.58°). Since the samples produced a positive reversal test, it is assumed that they are related to the same magmatic event, and that a reversal in the Earth's magnetic field was recorded.

7.2.5 Thermomagnetic and petrographic analysis

Thermomagnetic analysis (TMA) was carried out on a horizontal translation balance (Curie Balance) in order to determine the Curie temperature of samples and hence the carrier of magnetisation. TMA illustrated in Figure 7.8 indicates that samples have a Curie temperature at ≈ 580°C. Analysis of site V-2 revealed that upon heating, the saturation magnetization first increased at 150-170°C and then followed a normal decay for a Curie temperature at ~580°C. The kink at 150-170°C is a typical low-temperature titanomagnetite (maghemitization) phenomenon (Ade-Hall et al., 1971), possibly related to hydrothermal alteration.

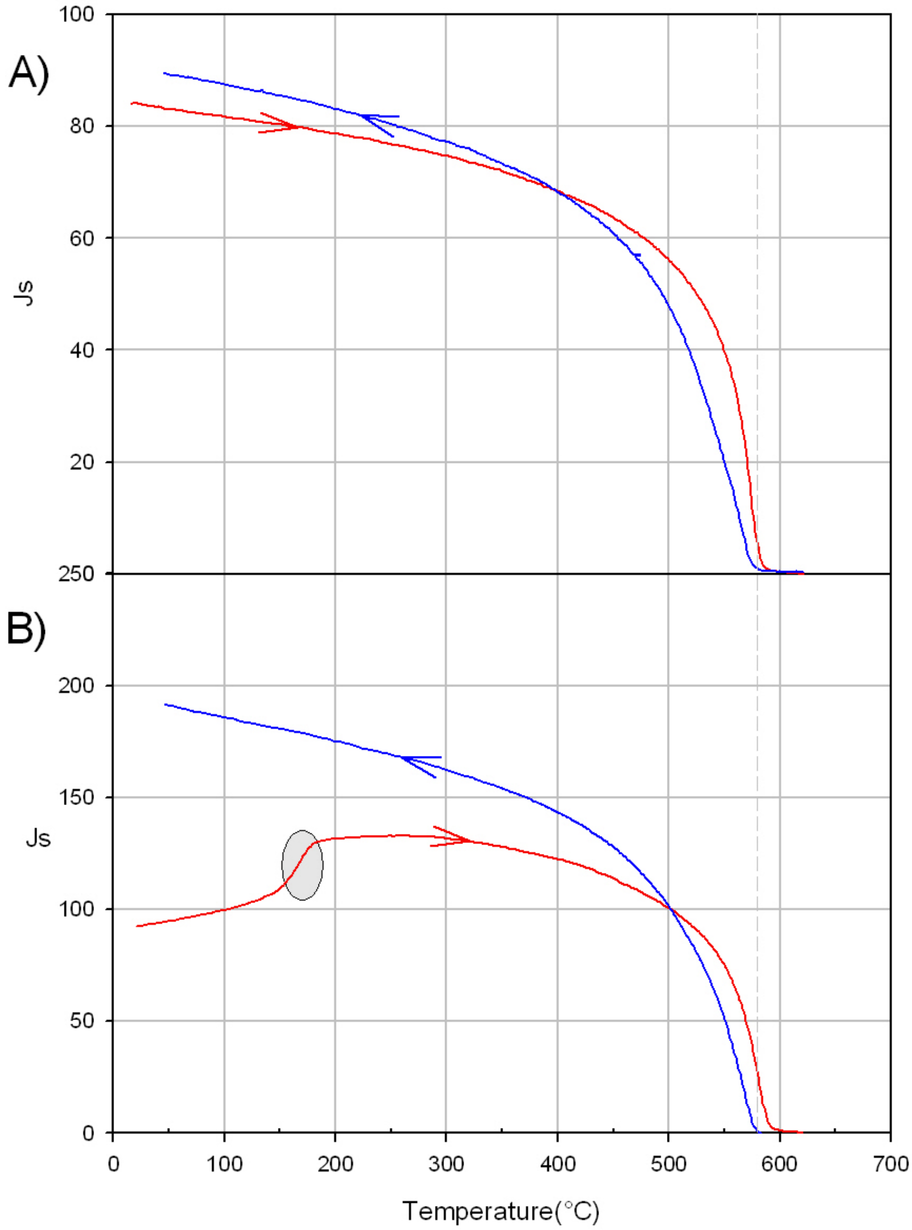

Figure 7.8 Thermomagnetic analysis of two dyke samples, A is from site F-3 while B is from site V-2. The majority of samples typically display Curie curves such as the one illustrated in A, in which a small increase in saturation magnetisation is seen during cooling, implying the possible production of more magnetite. In “B” there is irreversible creation of a magnetic phase with higher saturation magnetization at 150– 180°, indicated by grey ellipse. The red line indicates the heating phase while the blue line indicates the cooling phase. Curie temperature for magnetite is observed at ≈ 580°C (dashed line).

In an effort to further characterise the properties of the dykes a petrographic study was conducted. The majority of samples were dominated by pure magnetite with a number of grains showing skeletal textures indicative of rapid cooling (Figure 7.9). A minor number of magnetite grains had lamellae of ilmenite (Figure 7.10).

Samples from V-2 site showed minor alteration of magnetite that could not be identified due to grain sizes being smaller then the optical resolution (Figure 7.11). Petrographic observations of the opaque mineralogy are in agreement with the findings obtained by thermomagnetic analysis, i.e. that magnetite is the dominant carrier of magnetisation.

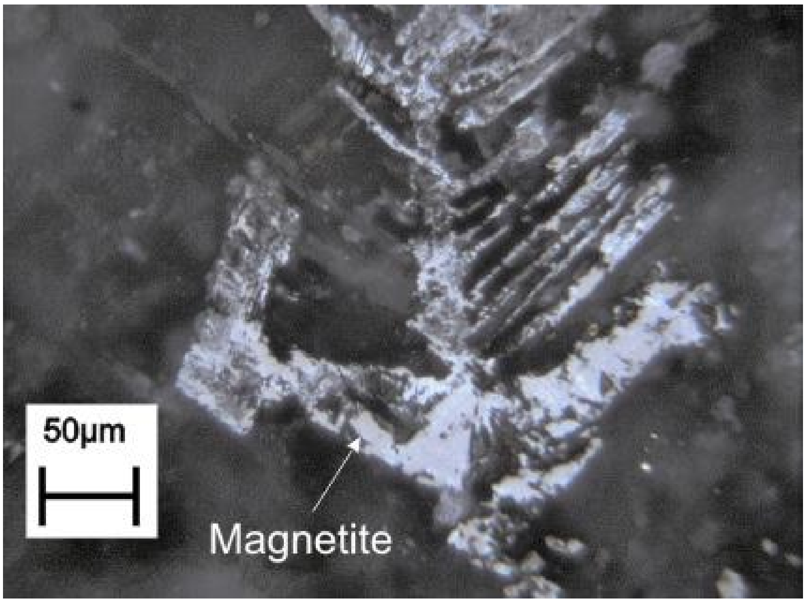

Figure 7.9 A polished thin section showing a magnetite grain with a quenched texture from site F-3, reflected light.

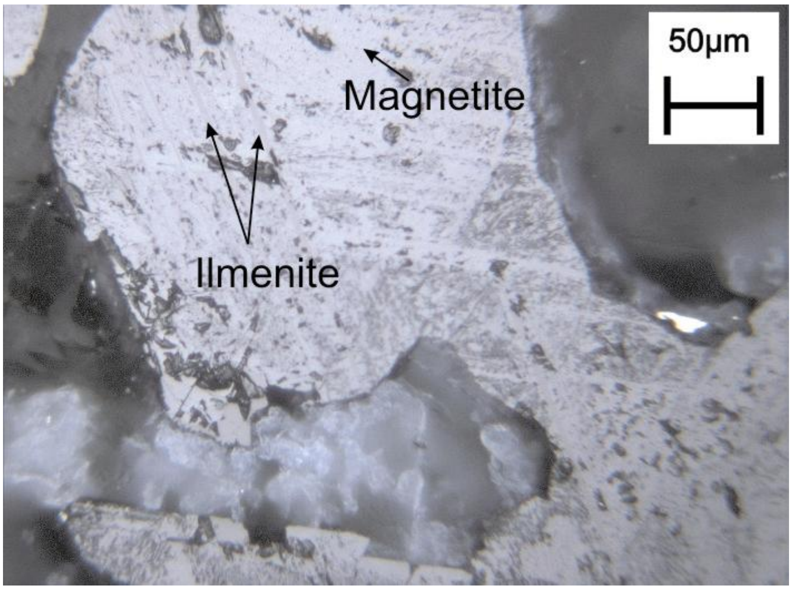

Figure 7.10 A polished thin section showing a magnetite grain with lamellae of ilmenite, from sire P-1.

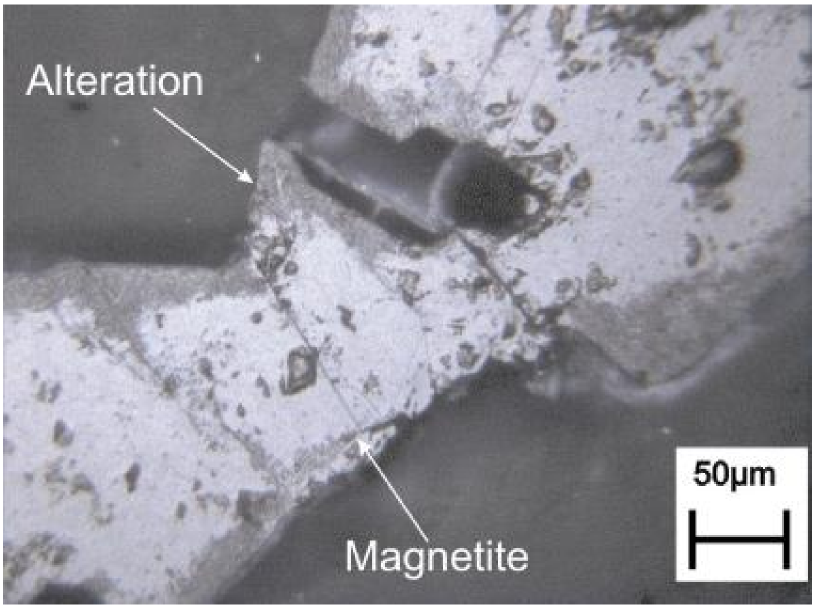

Figure 7.11 A polished thin section showing a magnetite grain with some type of alteration (too small to identify) sample from V-2 site, reflected light.

7.3 Palaeomagnetic Results from Bushveld Dykes

Four underground dyke sites were sampled from the Eastern Bushveld Complex: two from Hackney mine and two from Modikwa mine. The results from the these sites were combined with five additional sites sampled in 2003 as part of the author's M.Sc. dissertation (Letts, 2004). Results have been combined to produce a better palaeomagnetic result for the intruded dykes. The locations of the nine sites are indicated in Figure 7.12, where they are plotted on high-resolution and regional aeromagnetic data over the Bushveld Complex (aeromagnetic data courtesy of Anglo-Platinum).

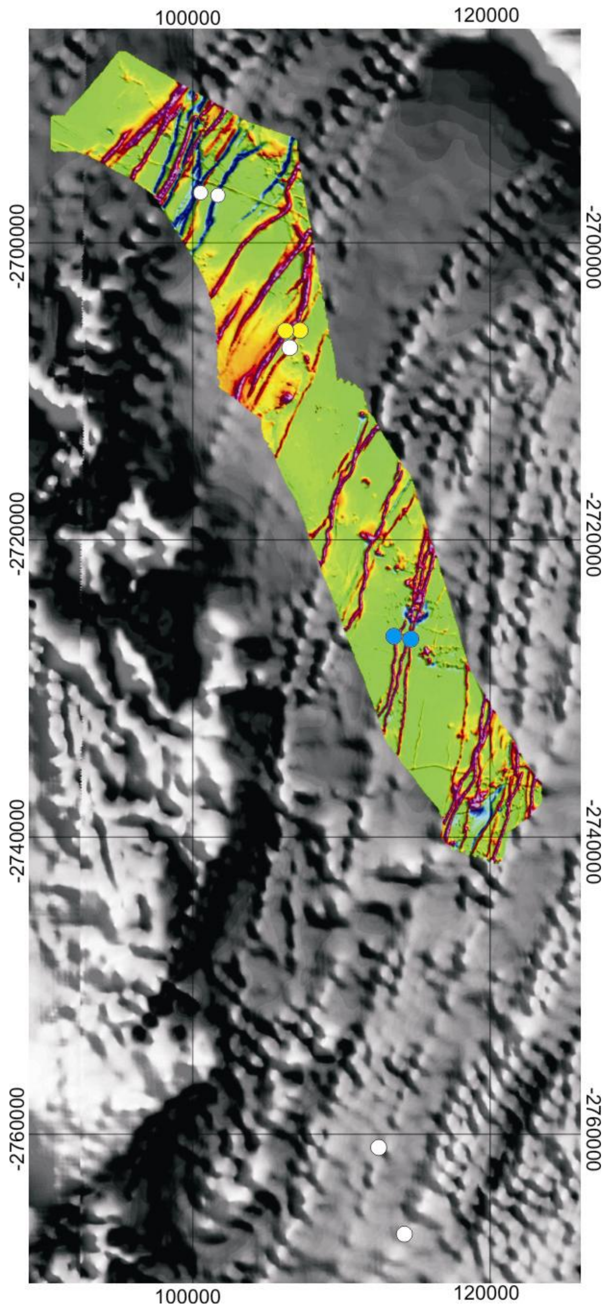

Figure 7.12 The position of dyke samples collected from the Eastern Bushveld Complex: four sites from this study (yellow-Hackney mine and blue–Modikwa mine) and five sites (white) from the author's previous study (Letts, 2004), plotted on high-resolution aeromagnetic data draped on top of regional aeromagnetic data courtesy of Anglo Platinum. Coordinates are in WGS84 (LO 31).

NRM

From the nine sites, a total of 67 core samples were analysed initially for NRM and bulk susceptibility before demagnetisation was carried out. Sites showed two groupings based on NRM intensities: the first consisting of sites T-1&2 and B-1 to 4, in which values ranging from 0.43 A/m up to 4.28 A/m with an average value of 2.57 A/m. The second group consisted of sites M1&2 and B-5 in which intensity values were considerably higher: 10.96, 12.47 and 22.1 A/m respectively. Susceptibility values showed more consistent results within sites with values ranging from 10,473 up to 30,942 $\times 10^{-6}$ SI units, with an average value of 25,576 $\times 10^{-6}$ SI units. Histograms of susceptibility and intensity are shown in Figure 7.13. The mean NRM and bulk susceptibility values for all sites with errors are shown in Table 7.3.

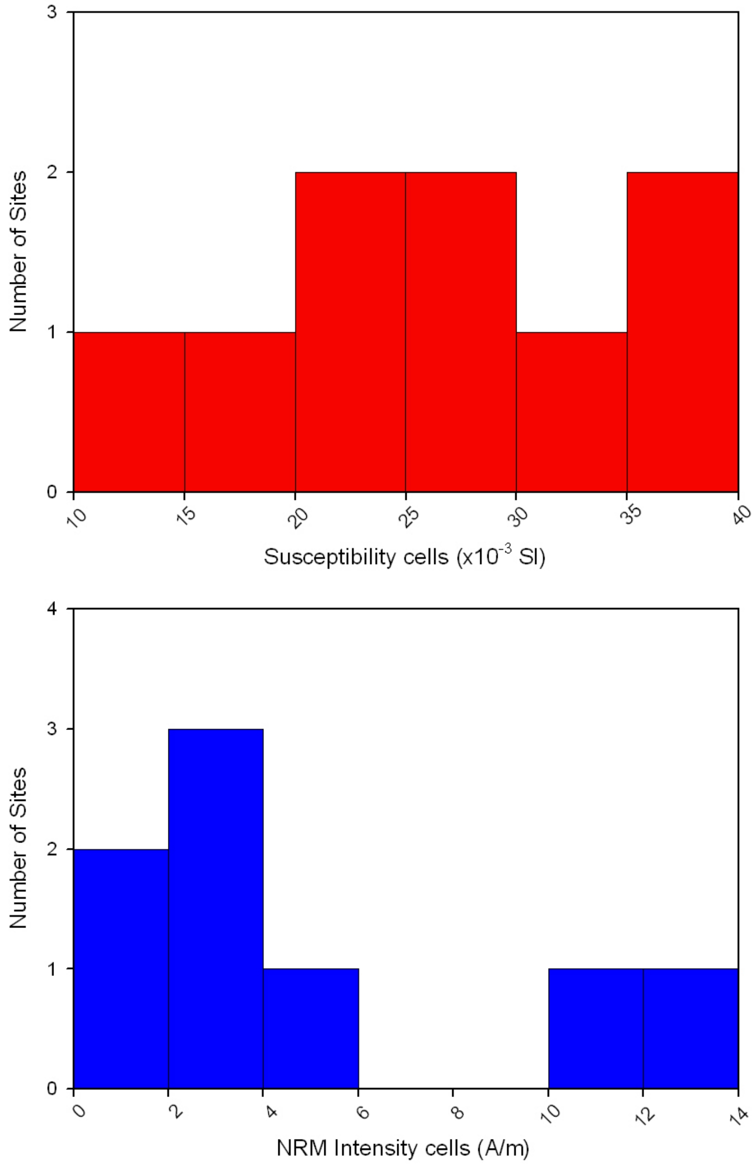

Figure 7.13 Histogram plot of site mean susceptibility in 10^{-3} SI units (A) and site mean NRM intensity in A/m excluding B-5 (22A/m) (B) of sites from dykes occurring in the Eastern Bushveld Complex.

Table 7.3 Site mean NRM, mean bulk susceptibility and Q ratio of all sites. *Dec.* = declination, *Inc.* = inclination, α_{95} = 95 percent confidence circle around mean direction, N = number of samples, +/- = 1 σ error. Site names represent sample location: M = Modikwa Mine, H = Hackney Mine and B = samples Letts et al (2005).

Site	NRM Dec.	NRM Inc.	α_{95}	N	Intensity Average (A/m)	+/- (mA/m)	Susc. Average ($\times10^{-6}$ SI units)	+/- ($\times10^{-6}$)	Q Ratio
M-1	170.4	-62.8	4.6	9	10.96	2130.7	36942	662.6	12.4
M-2	178.3	-63.5	4	10	12.47	13204.1	35449	1896.5	14.7
H-2	186.7	-67.9	6.1	10	3.35	529.4	23159	225.3	6
H-1	211.6	-65.4	12.4	7	3.27	253.7	25422	750	5.3
B-1	212	-73	6.2	8	3.387	1225	17288	9502	9.6
B-2	138	-71	3.8	9	4.282	447	30184	1507	6.4
B-3	6	-79	19.1	5	0.69	31	10473	5988	3.6
B-4	343	84	19.1	3	0.43	18	24154	1523	0.7
B-5	12	65	13.6	6	22.1	1041	27114	6297	36.8

Within sites NRM directions from dykes are reasonably clustered and show dual polarity (Table 7.3 and Figure 7.14). The majority of sites (six) possess a southerly declination with very steep negative inclination. The seventh negative site plotted with a northerly declination; however its α_{95} is large enough to place it with the other sites. The remaining two sites plot anti-polar to them in a northerly declination and with very steep positive inclination.

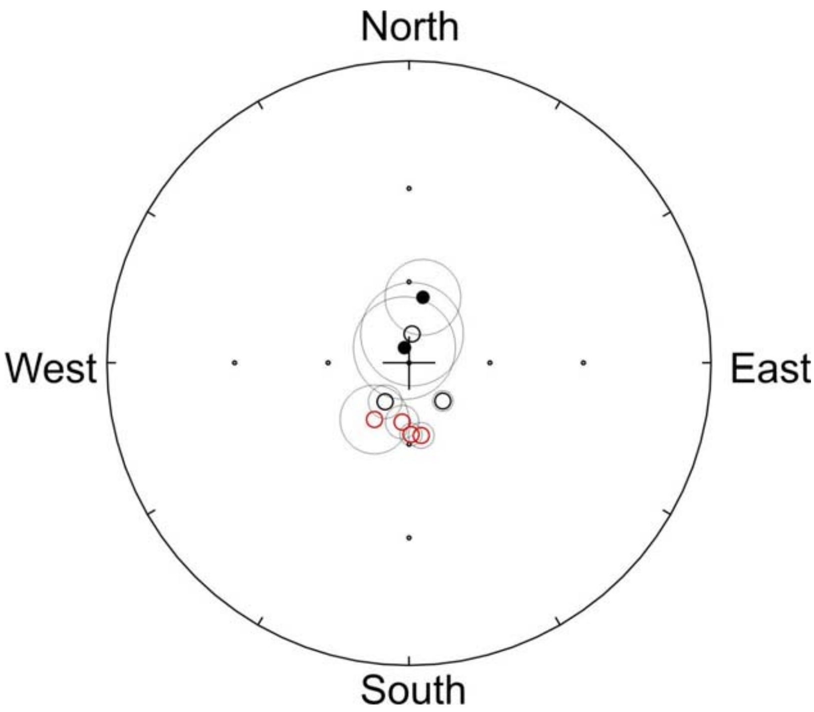

Figure 7.14 Site mean NRM directions from Bushveld dyke samples. Red samples represent new sites while black samples indicate results from Letts et al (2005).

7.3.1 Demagnetisation

In an attempt to elucidate the magnetic history of the dykes since formation, samples were subjected to AF (28) and thermal demagnetisation (37). Demagnetisation was carried out using between 10 and 16 steps up to 600°C or 95 mT (maximum level obtained from AF machine). Some variations in the above levels occurred due to different levels of magnetisation being present in different samples. Once demagnetisation was completed, data were plotted on Zijderveld diagrams and subjected to principal component analysis to determine low temperature blocking components and high-stability component of NRM.

7.3.2 Components of magnetisation

Typical examples of thermal and AF demagnetisation behaviour are given in Figure 7.15. Samples behaved exceptionally well to both thermal and AF demagnetisation, showing the presence of two components of magnetisation. LB components identified in samples have directions that are all random within sites and are typically removed at around 500ºC or 30-40mT. Samples obtained from surface have stronger LB components relative to those obtained underground. Once again LB directions present in samples are not related to any significant geological event and are therefore not considered further.

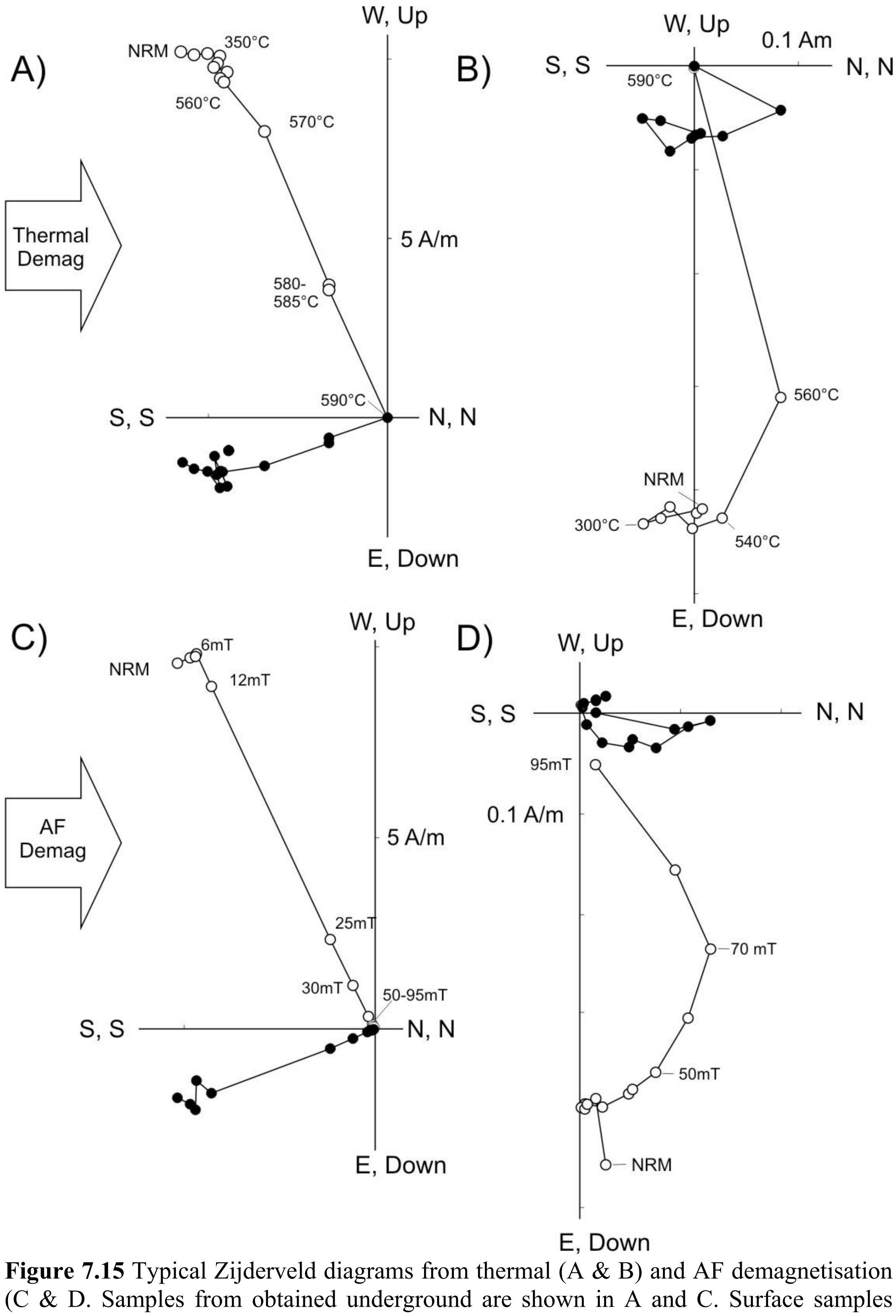

Figure 7.15 Typical Zijderveld diagrams from thermal (A & B) and AF demagnetisation (C & D. Samples from obtained underground are shown in A and C. Surface samples obtained from the authors M.Sc. dissertation (Letts, 2004) are reflected in B and D. Open (solid) symbols represent projections onto the vertical (horizontal) planes, respectively.

On completion of demagnetisation, one of two anti-polar higher coercivity remanence directions were isolated above 550°C or 50mT (Figure 7.15). The majority of the sites produced directions in a very steep negative inclination with south to southeasterly declination. The remaining two sites were opposite in directions with northerly declination and very steep positive inclinations. With the exception of sites B3, B4 and B5 sites showed exceptionally good grouping with within-site directions α_{95} around 3°. Resulting HB components are shown in Figure 7.16 and listed in Table 7.4.

Table 7.4 Site mean HB component directions for all dyke samples. *Dec.* = declination, *Inc.* = inclination, α_{95} = 95 percent confidence circle around mean direction, N_o = original number of samples per site, N = number of samples analysed per site; κ = precision parameter. Site names represent sample location: H-Hackney mine, M- Modikwa mine and B- M.Sc results.

Site	Dec	Inc	α_{95}	N_o/N	κ
H-1	185.4	-70.4	2.8	9/5	1885.7
H-2	180.5	-65.2	3.4	10/10	201.2
M-1	167.2	-64.3	2.6	10/9	401.6
M-2	172.9	-60.2	3.3	7/7	215.4
B-1	185	-73	3.2	8/8	298.54
B-2	137	-68	3.5	9/9	220.51
B-3	110.1	-78.9	20.1	5/5	21.84
B-4	359.9	62.2	18	3/3	48.12
B-5	10	65.6	12.8	6/6	28.19

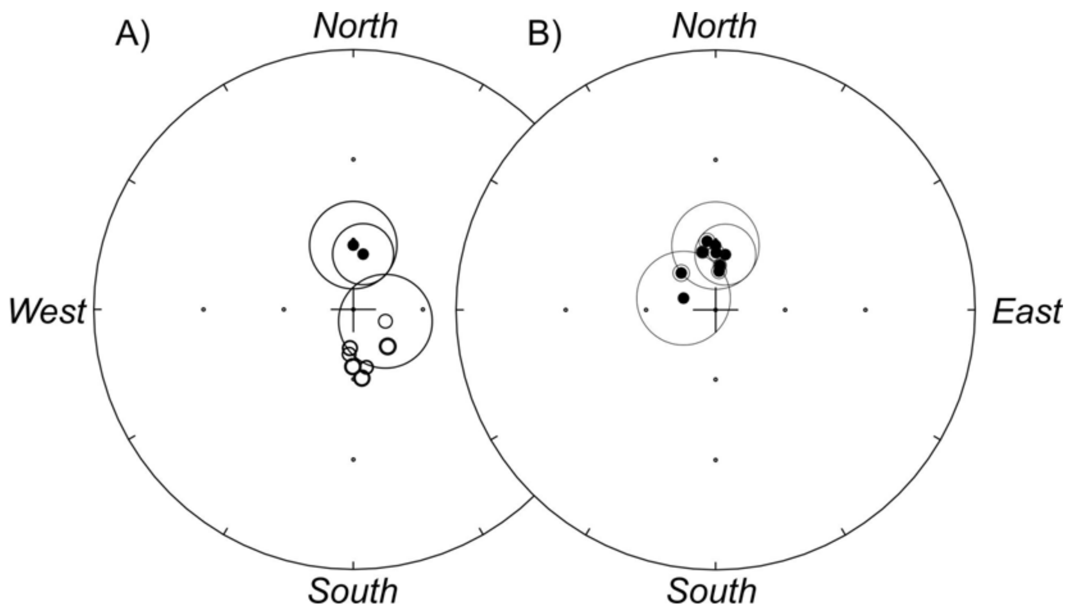

Figure 7.16 Site mean *in situ* direction (a), b) sites inverted to positive inclination. Solid symbols indicate a positive inclination, while open symbols indicate a negative inclination**.**

7.3.3 Field stability tests

Reversal Test

In order to reveal if the reversed polarity recorded by the dykes is related to the same magmatic event, two reversal tests were implemented. It was found that the dykes shared a common mean at 95 % confidence according to the method of McFadden & Lowes (1981). The reversal test of McFadden & McElhinny (1990) produced a positive reversal test, with a "C" classification (critical angle = 15.08°; observed angle = 9.33°). With the production of a positive reversal test, it is assumed that the reversely polarized dykes are of similar age to the normally polarized dykes and that a reversal in the Earth's magnetic field was recorded.

7.3.4 Thermomagnetic and petrographic analysis

TMA displayed in Figure 7.17 indicates that samples have a Curie temperature at ≈ 580°C, suggesting magnetite or Ti-poor magnetite as the prime remanence carrier. The majority of samples showed almost reversible Curie curves upon cooling and heating, except for a small increase in saturation magnetization during cooling. This increase probably indicates secondary production of magnetite. TMA on sample B-3 produced a distinctively different curve to those experienced in other sites. Upon heating, the saturation magnetisation first increased at 150-170°C, followed by a distinctive decrease at ~350°C. The kink at 150-170°C is a typical low-temperature titanomagnetite alteration (maghemitization) phenomenon (Ade-Hall et al., 1971), possibly related to hydrothermal alteration, while the decrease at 350°C is probably related to the inversion of maghemite.

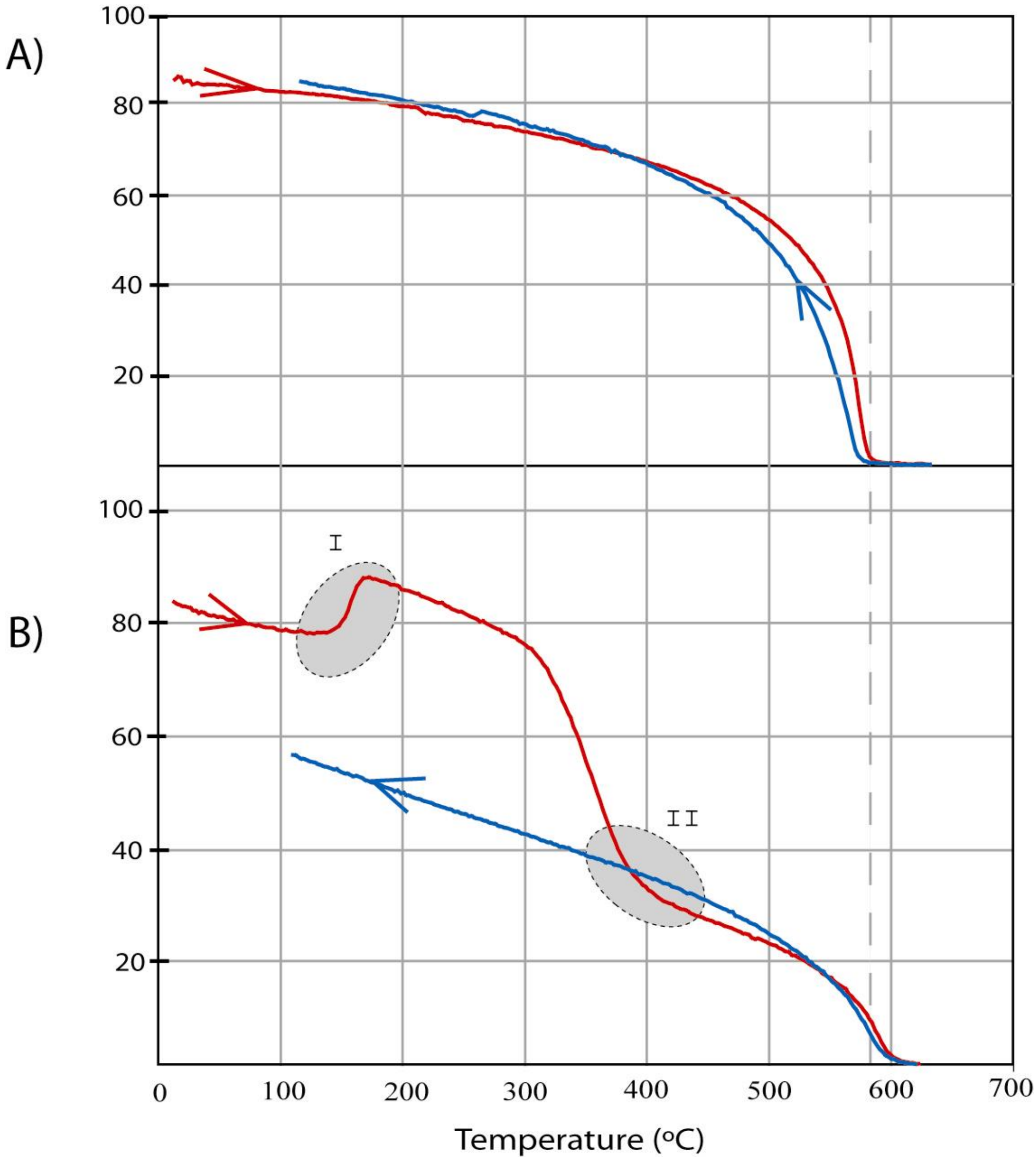

Figure 7.17 Thermomagnetic analysis of two dyke samples, A is from site M-1 and B is from site B-3. The majority of samples typically display Curie curves such as the one illustrated in "A", in which a small increase in saturation magnetisation is seen during cooling, implying the possible production of more magnetite. In "B" there is irreversible creation of a magnetic phase with higher saturation magnetization at 150– 180° (indicated by grey ellipse I) followed by inversion of maghemite to a weaker magnetic phase around 350°C (indicated by grey ellipse II). The red line indicates the heating phase while the blue line indicates the cooling phase. Curie temperature for magnetite is observed at ≈ 580°C (dashed line).

Petrographic analysis was undertaken to further characterise the dykes in terms of opaque mineralogy. In general, samples revealed quenched magnetite grains, (indicating rapid cooling) as the dominant opaque mineralogy (Figure 7.18). A number of magnetite grains contain lamellae of ilmenite, possibly due to high-temperature deuteric oxidation during late stage crystallisation of the dyke (Figure 7.19). Samples from site B-3 are dominated by highly altered magnetite - the majority of the alteration mineral could not be determined due to grain sizes being smaller then the optical resolution. However, some alteration has been identified as hematite (Figure 7.20). Petrographical findings of the opaque mineralogy are in agreement with the findings obtained by thermomagnetic analysis, i.e. that magnetite is the dominant carrier of magnetisation.

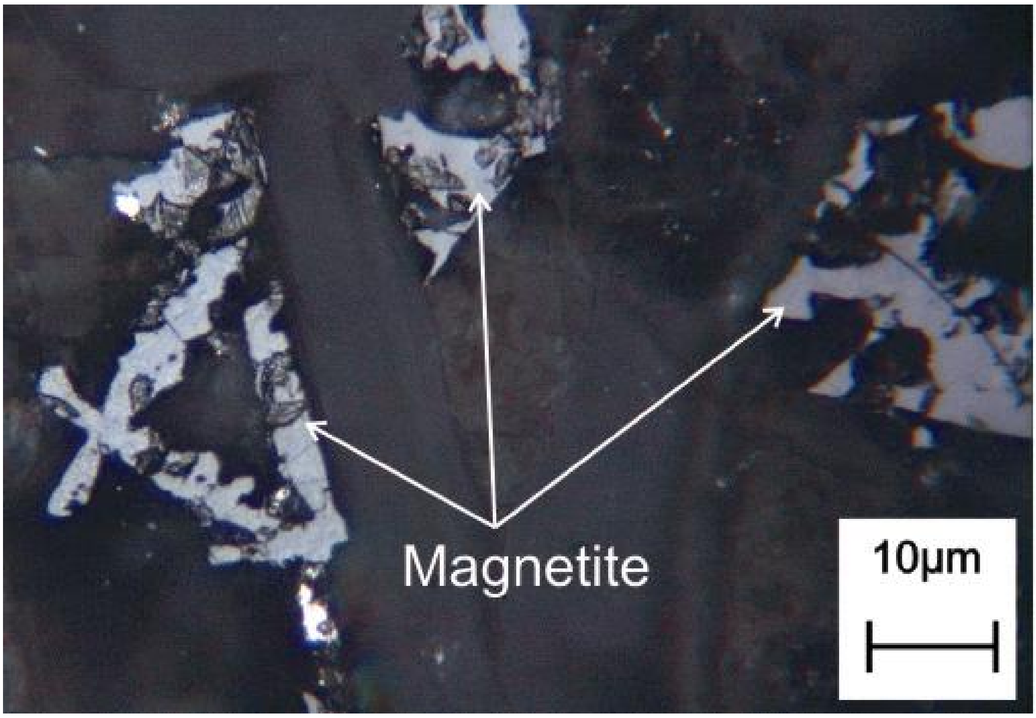

Figure 7.18 A polished thin section showing a magnetite grain with a quenched texture from site M-1, reflected light.

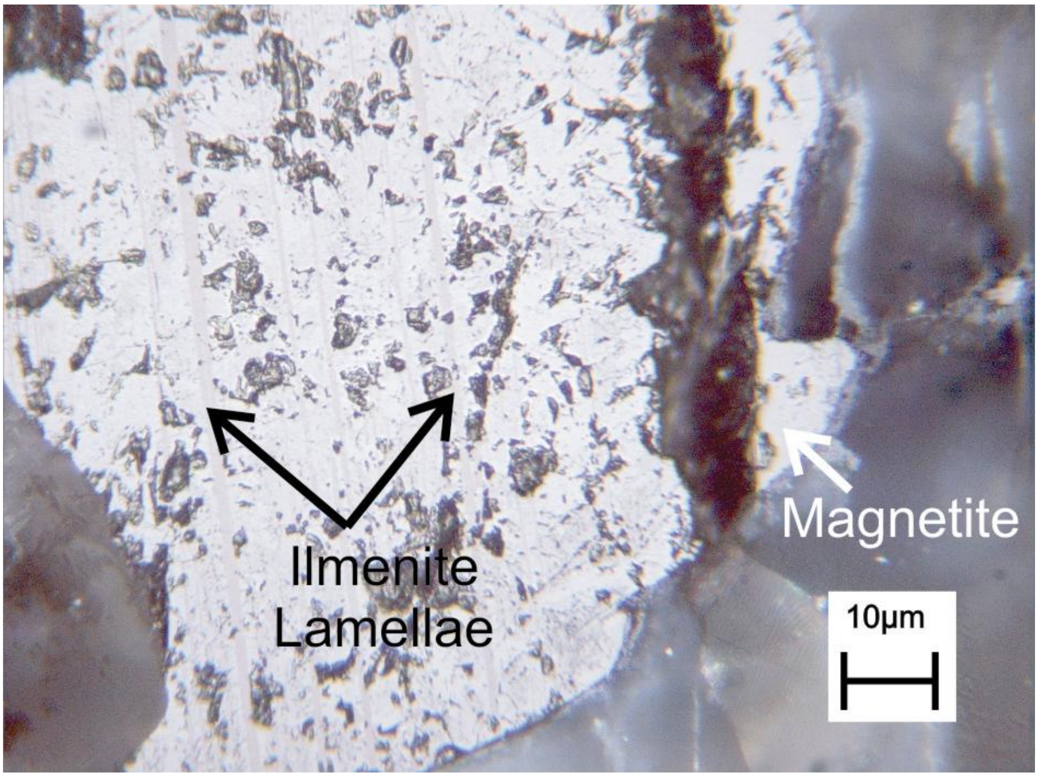

Figure 7.19 A polished thin section showing a magnetite grain with lamellae of ilmenite, from site H-2.

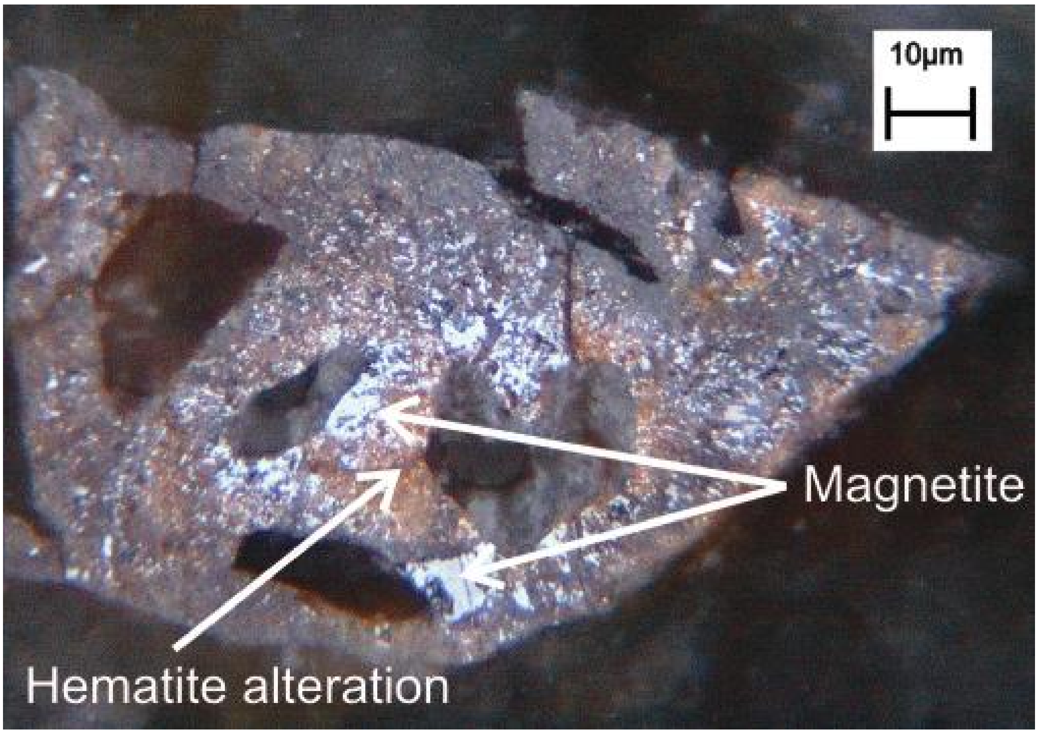

Figure 7.20 A polished thin section showing an extremely altered grain of magnetite with quenched texture, from site B-3. The majority of the grain has been altered to some other mineral which could not be determined, due to grain sizes being smaller then the optical resolution. However, some of the alteration has been determined as hematite, reflected light.

7.4 Reconciliation of Palaeomagnetic Data from Dykes

Palaeomagnetic data from dyke samples obtained in both the Phalaborwa and Bushveld Complexes are of excellent quality, with normal and reversed polarities being recorded. Polarities from both complexes were found to share a common mean at the 95 % confidence level.

With positive reversal tests being obtained, HB components isolated from Phalaborwa dykes were inverted to the same polarity, yielding a combined mean remanence direction with a declination of 328° and inclination of 69.2° (α_{95} 7.9), and a palaeopole position with palaeolatitude of 8.3° and palaeolongitude of 12.2° (dp/dm = 11.5°/13.5°). Repeating the same procedure on Bushveld dykes resulted in a mean remanence direction with a declination of 350.7° and inclination of 68.6° (α_{95} 6.5) and a palaeopole position with palaeolatitude of 8.3° and palaeolongitude of 24.1° (dp/dm = 9.3°/11°). The resulting palaeopole positions are depicted in Figure 7.21.

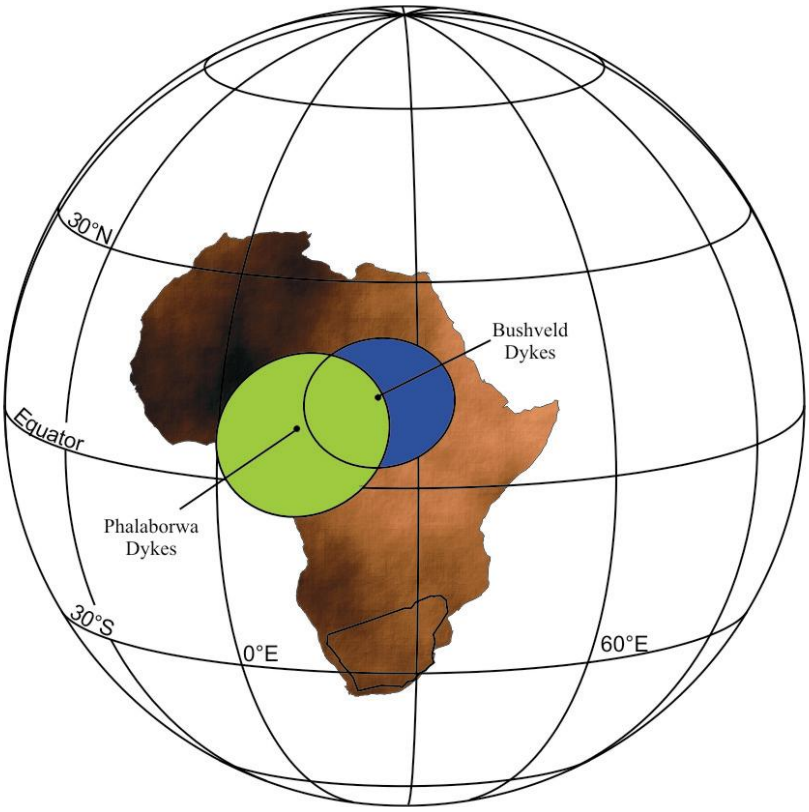

Figure 7.21 Palaeomagnetic palaeopole positions generated from dykes in the Phalaborwa complex and the Bushveld Complex. The two palaeopoles have considerable overlap and are therefore assumed to be part of the same magmatic event.

Based on positive reversal tests from each complex and the statistical overlap in uncertainty levels from the two palaeopole positions as depicted in Figure 7.21, it is plausible that the dykes are related to the same magmatic event. With this information at hand, the results from the two complexes have been combined together.

Repeating the reversal test on the combined group indicates that the dual polarities share a common mean at 95% confidence level and the reversal test of McFadden and McElhinny (1990) produced a positive reversal test, with a "C" classification (critical angle = 10.49°; observed angle = 4.72). Converting sites to the same polarity yielded a mean direction with a declination of 339.5° and inclination of 69.3° (α_{95} = 5), and a palaeopole position with palaeolatitude of 10.8° and palaeolongitude of 18.1° (dp/dm = 7.3°/8.5°).

7.5 Comparison of results with previous studies

Dykes from the Phalaborwa and Bushveld have both been previously studied. The Phalaborwa dykes were initially studied by Morgan and Briden (1981) in which they determined a pole position for the intruded dykes and older syenite hills of the Phalaborwa complex, while the Bushveld dykes were initially studied as part of the author's M.Sc. dissertation (Letts et al., 2005) but have been combined in this study with newly obtained samples from the area.

A comparison between new and old palaeomagnetic data is shown in Figure 7.22. Although Phalaborwa results obtained from this study (dark green) and those from the previous study of Morgan and Briden (light green) overlap, the older results plot more to the west and do not overlap with those of the Bushveld Complex. A possible reason for the difference between the results might be due to the fact that Morgan and Briden had combined the dolerite dykes with the older syenite bodies from the Phalaborwa Complex. Another probable reason for the difference could lie in the fact that primary components were not determined by principal component analysis.

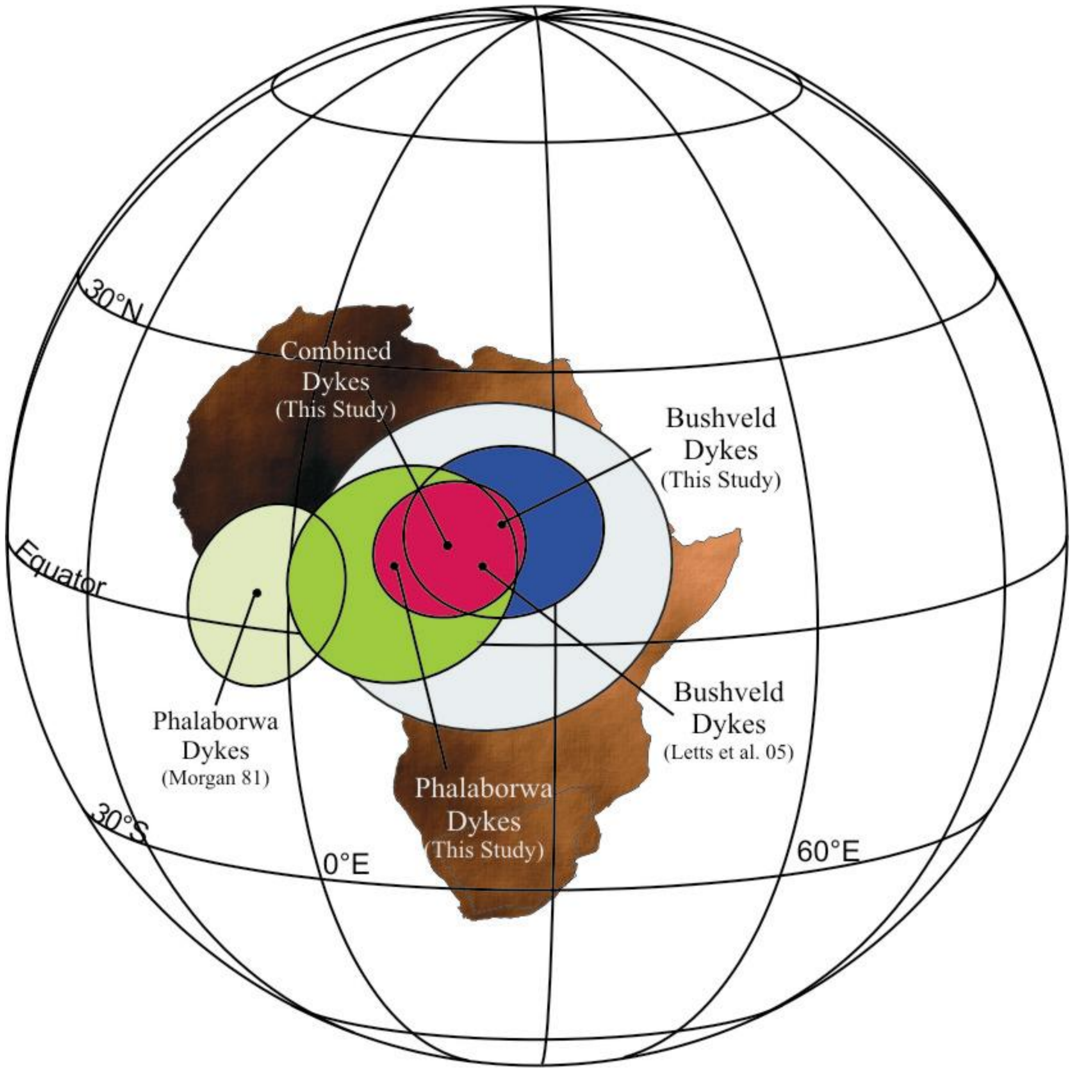

Figure 7.22 Palaeopole positions with their 95% confidence limits for dykes reported in this study occurring in the Phalaborwa Complex (dark green), Bushveld Complex (dark blue) and combined (red), as well as previous studies on the dykes. The pole obtained by Morgan and Briden (1981) from the Phalaborwa Complex consisted of dykes and older syenite bodies (light green).

Combined dyke samples from the Phalaborwa and Bushveld Complex have produced a well defined pole position. When compared with relevant poles from southern Africa, the new pole obtained from this study statistically overlaps with the ~1.9 Ga post-Waterberg dolerites (Hanson et al., 2004) and the 1,876 ± 68 Ma (Barton, 1979) Sand River Dykes obtained by Morgan (1985) (Figure 7.23).

As mentioned above, the new pole position shows good correlation with ~1.9 Ga dykes with the exception of the Hartley Lava pole (Evans et al., 2002).

Petrographic analysis on the Hartley lavas indicated that the rocks were subjected to later low-grade metamorphism (Cornell et al., 1998) and the recorded pole possibly represents this remagnetization event.

Based on the pole position, it is suggested that the dykes occurring in both the Phalaborwa and Bushveld Complex are the result of the same magmatic event at ca. 1.9 to 2.0 Ga. An $^{40}Ar/^{39}Ar$ plagioclase age of 1,649 ± 10 Ma had previously been determined on one of the dykes occurring in the Bushveld Complex (Letts et al., 2005). However, it is believed that this age represents a thermal resetting event and not the age of emplacement. Additional Ar-Ar age analyses are currently being conducted on the dykes at the Norwegian Geological Survey.

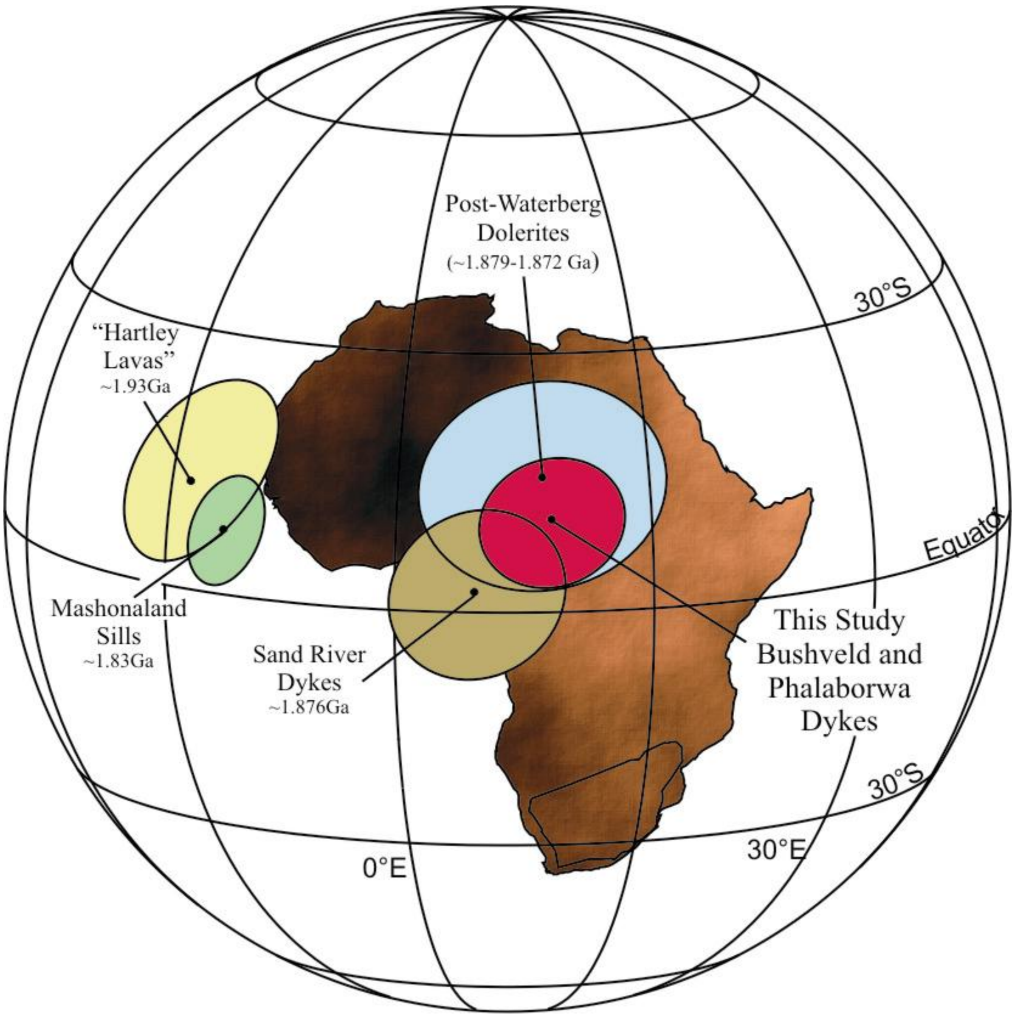

Figure 7.23 Palaeomagnetic pole positions from this study as well as relevant poles from southern Africa: post-Waterberg dolerites (Hanson et al., 2004), Sand River dykes (Morgan, 1985), Mashonaland sills (Bates and Jones, 1996) and Hartley lavas (Evans et al., 2002).

CHAPTER 8: APPLICATIONS TO PALEOGEOGRAPHY

Palaeomagnetic investigations not only provide valuable information on the past magnetic field of the Earth, but also important information relating to the way in which parts of the Earth's crust have moved apart or come together during the Earth history. The palaeomagnetic data obtained during this study will be applied below to paleogeographic continental reconstruction of the Kaapvaal and the postulated continent of Vaalbara and supercontinent Columbia around 2.0 Ga.

8.1 Apparent Polar Wander Path for the Kaapvaal Craton over the time period 2.2 to 1.8 Ga

Based on palaeomagnetic information it is possible to plot the movement of a continent by plotting successive positions of palaeomagnetic poles of varying geological age on the present latitude-longitude grid. This path, relative to the present day continents, traced out by the palaeomagnetic pole, is called the apparent polar wander (APW) path for that region, and is a convenient way of summarizing palaeomagnetic data for a continent, instead of producing palaeogeographical maps at each geological period (McElhinny and McFadden, 2000).

8.1.1 Overview of South African palaeomagnetic results used in the APW path construction

In an attempt to trace the movement of the Kaapvaal Craton between ca. 2.2 and 1.8 Ga, newly obtained palaeomagnetic data from this study, together with other reliable data with well constrained geological ages for the craton were compiled. A brief overview of palaeomagnetic poles used is given below and is also summarized in Table 8.1.

Table 8.1 Palaeomagnetic pole positions and associated errors dp and dm, used in the construction of the APW path for the Kaapvaal Craton from 2.2 - 1.8 Ga. Corresponding references for pole positions and ages can be found in overview text poles marked with * indicate results from this study.

Group and Lithology	Pole Latitude	Pole Longitude	dp	dm	Age (Ma)
Ongeluk Lavas (Evans, 1997)	0.5°N	280.7°E	5.3°	5.3°	2,222 ± 13
Gamagara Formation (Evans et al , 2002)	2.2°N	81.9°E	7.2°	11.5°	2,142 ± 81
Phalaborwa Complex *	27.9°N	35.6°E	5.5°	7.6°	2,060.6 ± 0.5
Combined Bushveld Complex *	15.6°N	27°E	4.8°	6.1°	2,054.4 ± 1.8
Vredefort Impact (Carporzen, 2006)	21.8°N	44.5°E	11.3°	15.4°	2,023 ± 4
Sand River Dykes (Morgan, 1985)	3°N	9°E	10°	11°	1,878 ± 86
Post-Waterberg Sills (Hanson et al., 2004).	15.6°N	17.1°E	8.9°	8.9°	1,874.6 ± 3.9
Mashonaland dykes (Evans et al., 2002)	7.6°N	338.2°E	5.1°	5.1°	~1,860
Phalaborwa and Bushveld Dykes *	10.8°N	18.1°E	7.3°	8.5°	~1,880

Combined Bushveld Complex Pole

To simplify the APW path for the Kaapvaal Craton, the five results obtained for the Bushveld Complex in this study have been grouped together to produce a single pole of 15.6°N, 27°E and dp/dm = 4.8°/6.1° with an emplacement age of 2,054.4 ± 1.8 Ma (Walraven and Hattingh, 1993b).

Post Waterberg Dolerites

A number of dolerites occurring as sills, irregular bodies and dykes have intruded the Waterberg group in northern South Africa. The intrusive event has been reported to have occurred around ~1.88 to ~1.87 Ga based on U-Pb baddeleyite ages (Hanson et al., 2004). Palaeomagnetic analysis conducted on samples (Figure 8.1) located at or near localities from geochronological samples produced well grouped anti-polar directions with a site mean pole at 15.6°N and 17.1°E, A95 = 8.9° (Hanson et al., 2004).

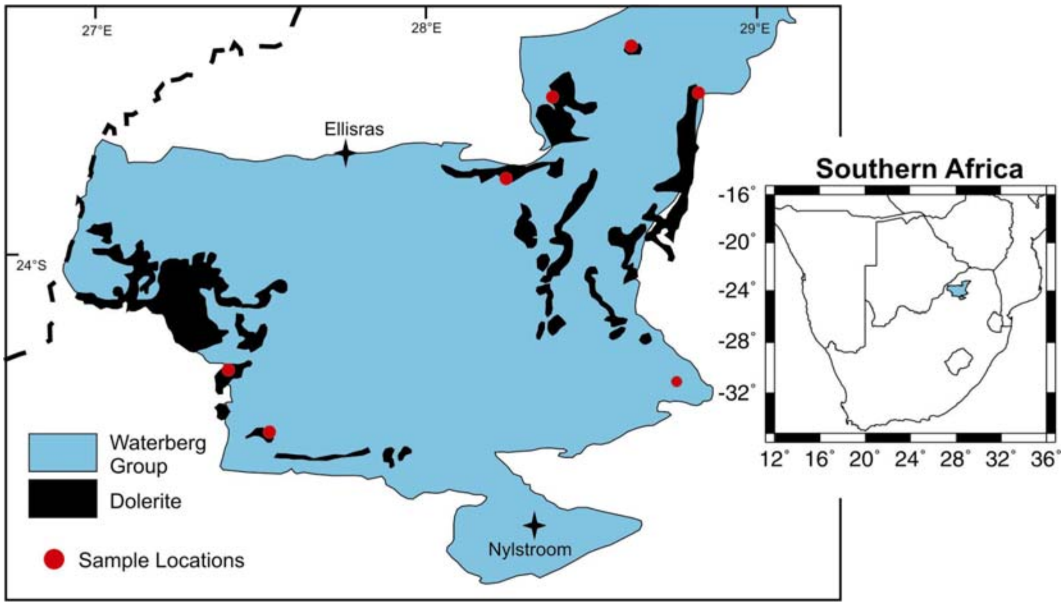

Figure 8.1 Simplified geological map of the Waterberg Group, showing palaeomagnetic locations of dolerite samples, modified from Hanson et al. (2004).

Vredefort Impact Structure

The 2,023 ± 4 Ma, (Kamo et al., 1996) Vredefort impact structure has been the subject of three palaeomagnetic studies. An initial study conducted by Hargraves (1970) sampled a range of lithologies within the central core and outer overturned collar rocks. A later study by Hart et al. (1995) obtained palaeomagnetic data from 16 sites within the central granitic basement of the structure. The most recent study conducted by Carporzen (2006) concentrated on the pseudotachylites and granophyre dykes (Figure 8.2) that are directly related to the impact event and obtained two paleopoles; 19.9°N, 47.7°E and dp/dm = 6.3°/8.6° for the pseudotachylites and 23.6°N, 41.3°E and dp/dm= 3.6°/4.9° for the granophyre dykes. For the purpose of reconstructing the APW path, the pseudotachylites and granophyre results were grouped together to produce a single pole for the impact at 21.8°N, 44.5°E and dp/dm= 11.3°/15.4°.

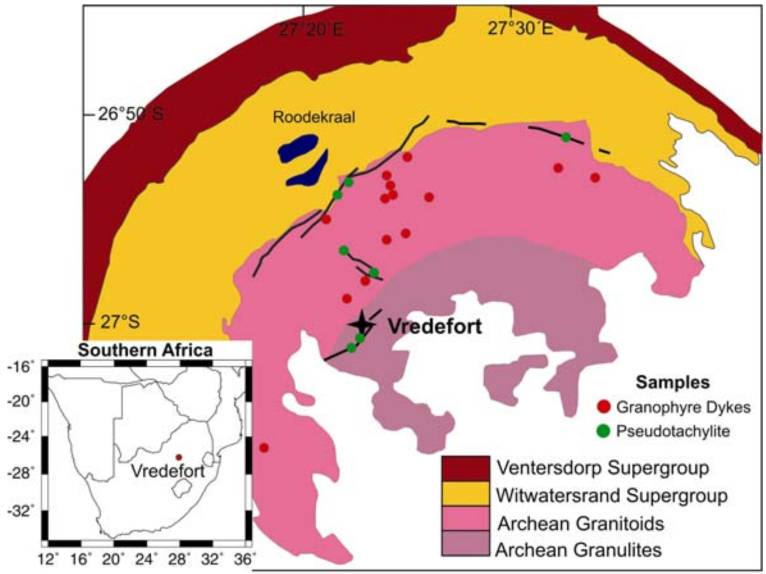

Figure 8.2 Geological map of the Vredefort area, showing the location of palaeomagnetic sites of pseudotachylites and granophyre, modified from Carporzen (2006).

Ongeluk Lavas

The Ongeluk lavas form part of the Griqualand West Sequence in the central-northern section of South Africa (Figure 8.3). They occur as a thick shallow-marine volcanic sequence of pillow lavas, massive basaltic andesite lavas and hyaloclastites and have been dated by Pb/Pb geochronology at 2,222 ± 13 Ma (Cornell et al., 1996). A palaeomagnetic investigation conducted by Evans (1997) sampled 20 flow-units from the Ongeluk basaltic-andesite to produce a reliable palaeopole position of 0.5° N and 79.3°W dp/dm = 5.3°/5.3°.

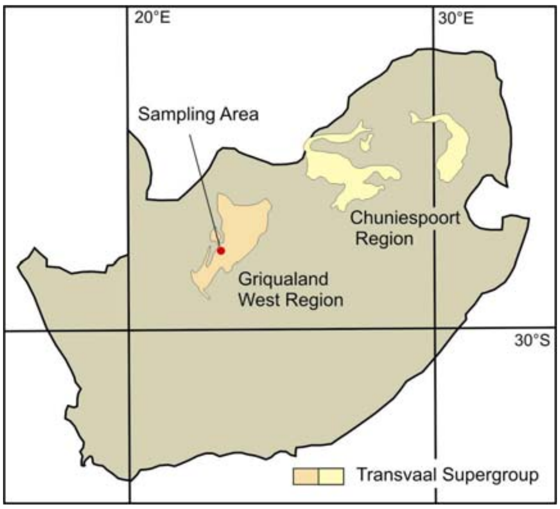

Figure 8.3 Regional map of South Africa, showing the extent of the Transvaal Supergroup with sampling area of the Ongeluk lavas modified from Evans et al. (1997).

Gamagara Formation

The basal Gamagara (or Mapedi) Formation of the Olifantshoek group in central South Africa consists of exceptionally well preserved Paleoproterozoic red beds and was the subject of a palaeomagnetic study (Figure 8.4) conducted by Evans et al. (2002). Dual-polarity palaeomagnetic data yielded a palaeopole position of 2.2° N and 81.9°E, dp/dm = 7.2°/11.5°. Unfortunately, no precise geochronogical data are available for the formation and an age bracket of 2,060 - 2,222 Ma has been determined from stratigraphic constraints (Evans et al., 2002). Although the age of the formation is questionable, the pole position obtained fits between that of the Bushveld and the Ongeluk lavas that were used to bracket the Gamagra Formation.

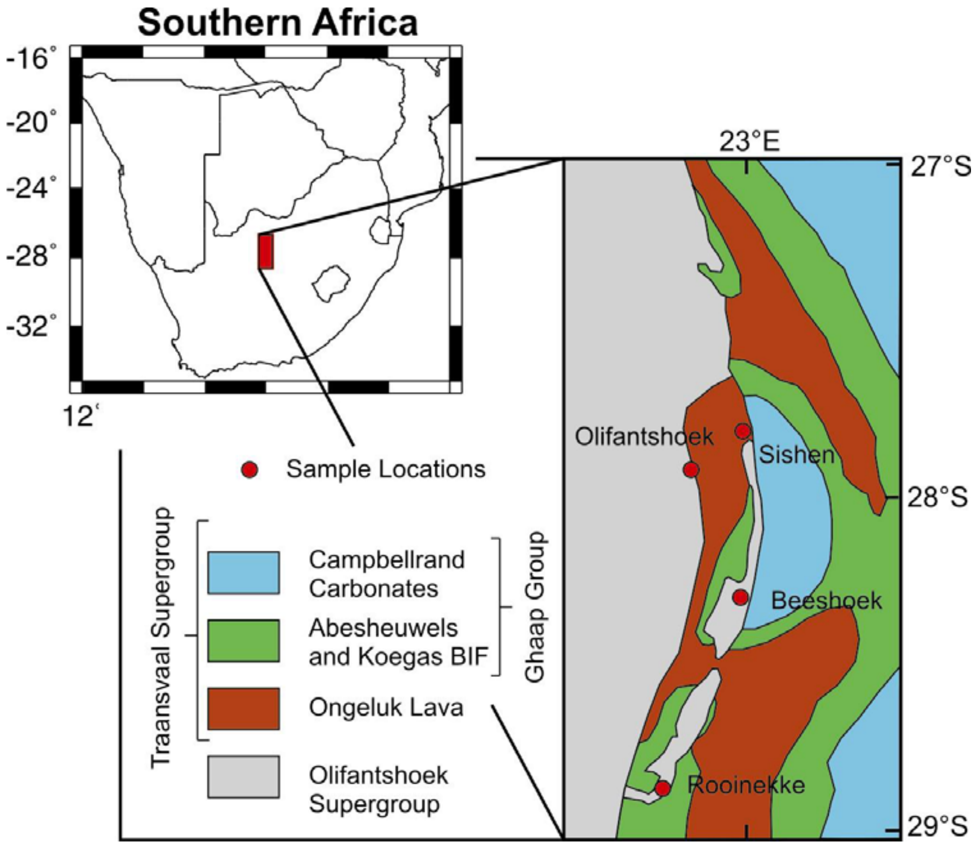

Figure 8.4 Simplified geological map of Griqualand West after Evans et al. (2002), showing palaeomagnetic localities of Gamagara formation samples.

Sand River Dykes

Samples from undeformed and unmetamorphosed tholeiitic dykes within the Southern Marginal Zone of the Limpopo Belt (Figure 8.5) yield a stable magnetisation direction, with a palaeomagnetic pole of 3°N, 9°E, dp/dm= 10°/11°

(Morgan, 1985). Whole rock Rb-Sr analyses conducted on four of the parallel dykes yielded an age of 1,876 ± 86 Ma (Barton, 1979).

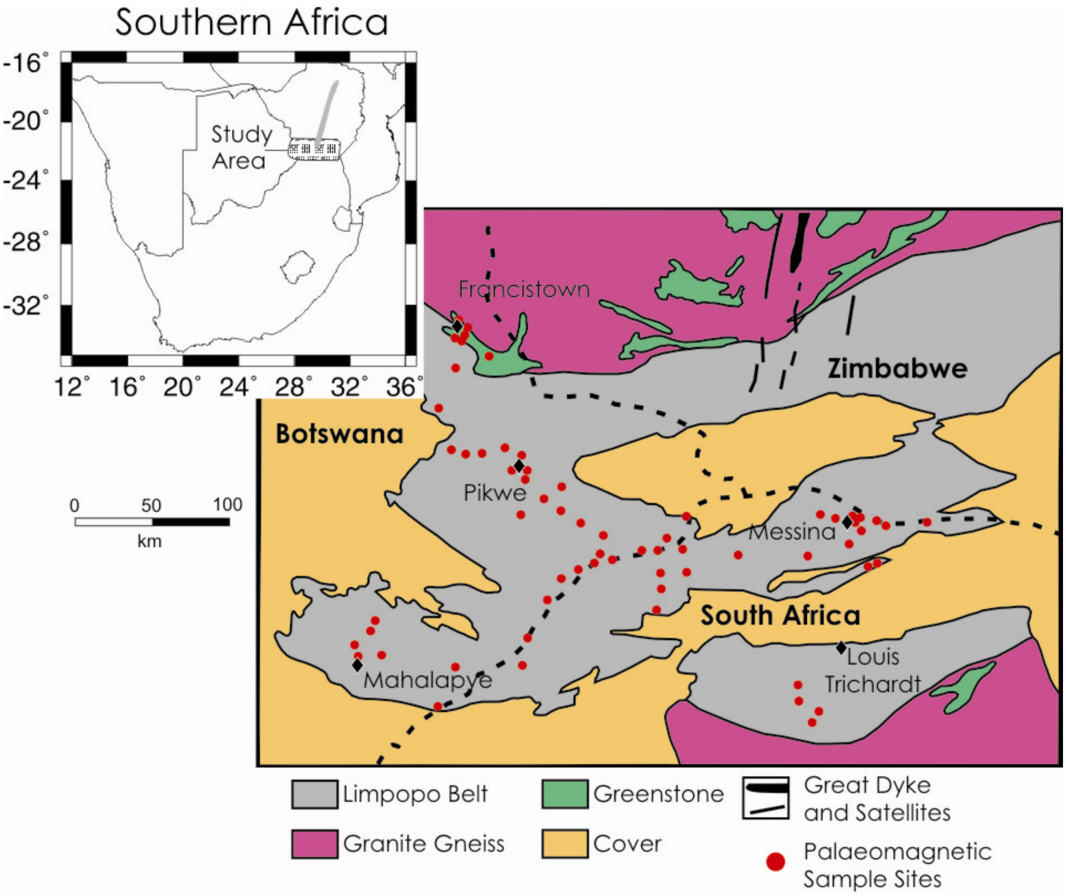

Figure 8.5 Geological map of the Sand River Dykes, showing the location of palaeomagnetic sites (Morgan, 1985).

Mashonaland Sills

The Mashonaland sills occur as a suite of early Proterozoic intrusive dolerites that crop out in the northeastern section of the Archean Zimbabwe craton (Figure 8.6). A recalculated paleopole for the Mashonaland sills of 7.6°N and 21.8°W, dp/dm 5.1°/5.1° was determined by Evans et al. (2002), where they combined the dual-polarity results obtained by McElhinny and Opdyke (1964) and Bates and Jones (1996). The sills are imprecisely dated using whole rock Rb-Sr analysis at 1,830 ± 230 Ma (Compston and McElhinny, 1975). However, an unpublished precise SHRIMP U-Pb baddeleyite ^{207}Pb/ ^{206}Pb age of 1,860 Ma (Wingate 2004; quoted by Dorland, 2004) has lead to the inclusion of this pole in the APW path.

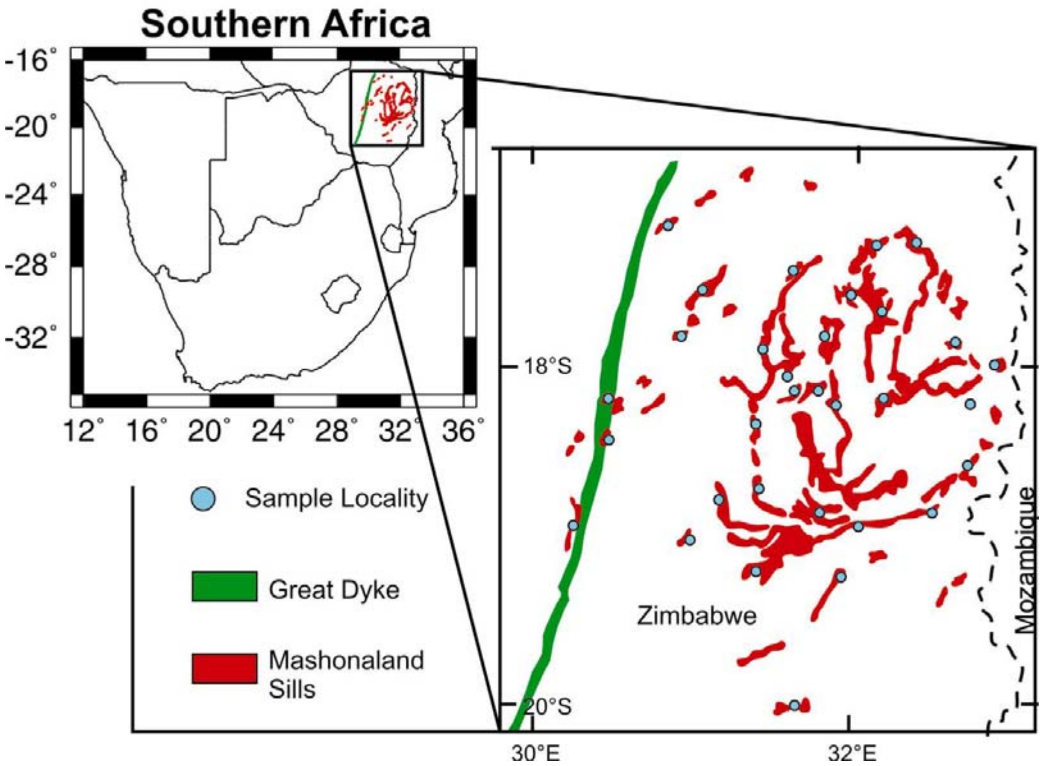

Figure 8.6 Simplified geological map of the Mashonaland sills over eastern Zimbabwe, showing palaeomagnetic localities, after Bates and Jones (1996).

8.1.2 Possible apparent polar wander path for the Kaapvaal Craton.

From the above mentioned palaeomagnetic poles and those obtained during this study, a proposed apparent polar wander path for the Kaapvaal Craton was constructed by running a smoothed (200) spherical spline (weighted via A_{95} values) through each pole. The resulting APW path produced a simple, single sinuous path that was drawn through the data, without violation of age information (Figure 8.7).

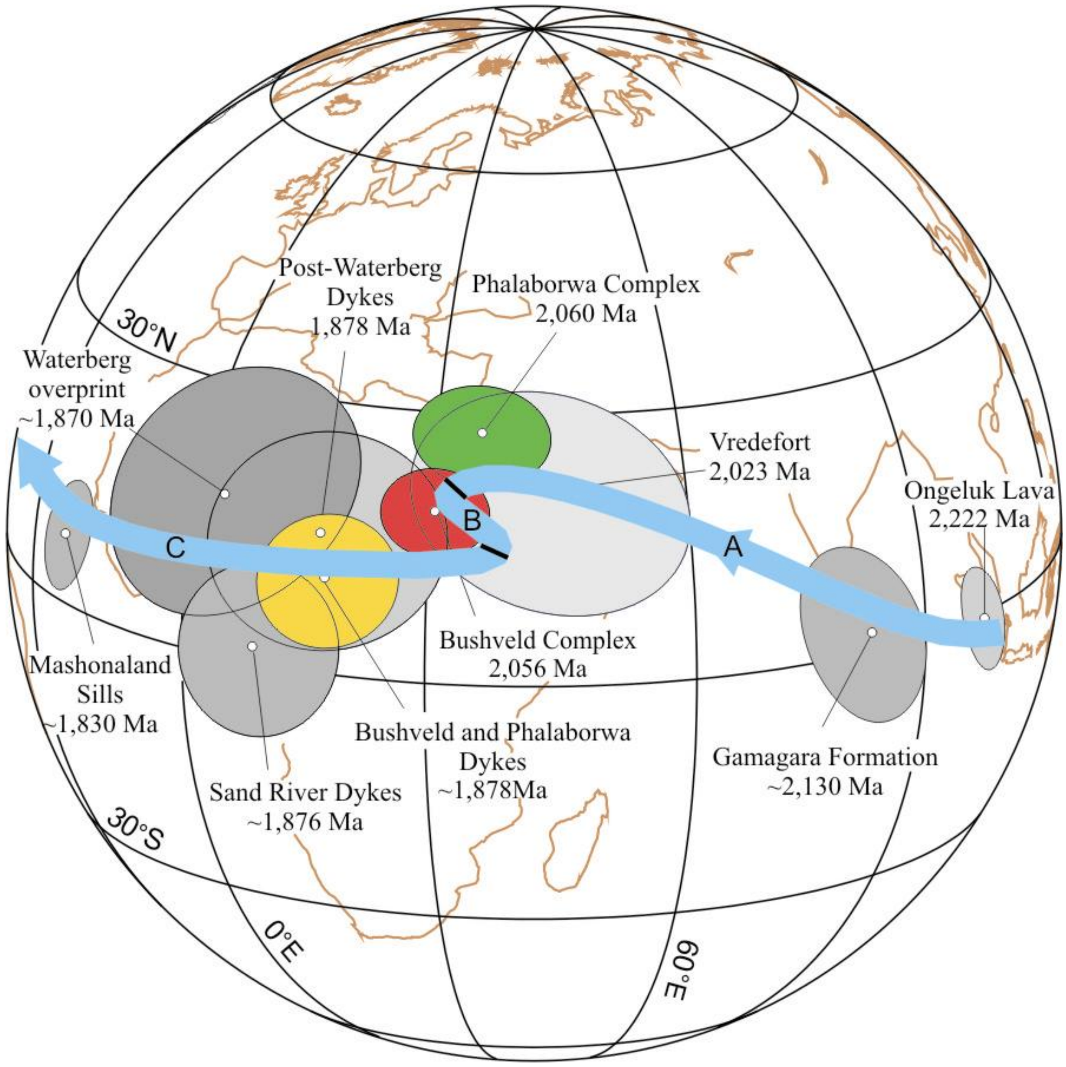

Figure 8.7 Orthogonal projection of the apparent polar wander (APW) path for the Kaapvaal craton from ca. 2222 to ca. 1830 Ma. Pole positions from this study are shown in colour, while results from previous studies are shown in different shades of grey. All ages, with the exception of those from the Gamagara formation, Mashonaland sills and Bushveld and Phalaborwa dykes are well constrained. The letters on the APW path represent three intervals: A= 2,222-2,053 Ma, B= 2,053-1,950 Ma (not well constrained) and C= 1,950-1,830 Ma.

The path starts with the 2,222 Ma Ongeluk lavas pole located over Indonesia (present day coordinates), and moves in a northwesterly direction towards the current location of Saudi Arabia where the 2,065 Ma Phalaborwa pole is located. The path then sweeps southeasterly to pass through the Bushveld (2,056 Ma) and Vredefort (2,023 Ma) poles, after which the path continues along a westerly direction through the remaining poles of the post-Waterberg dykes (1,878 Ma), Bushveld and Phalaborwa dykes (~1880 Ma) and Mashonaland sills (1,830 Ma).

On examination, the APW path was broken into three time periods in which it was possible to fit small circles to the poles and calculate the velocity of the craton. The first time interval A was from 2,222 to 2,053 Ma, in which the Kaapvaal Craton moved in a northwesterly direction along a small circle located at 66°N, 175°E with a radius of 85° at 4.8 cm/yr. During the second interval B 2,053 to 1,950 Ma, the craton experienced very little movement along a small circle located at 39°N, 321°E with a radius of 90° at a velocity of 0.9 cm/yr in a southeasterly direction. It should be noted that the B time interval is not well constrained by palaeomagnetic data. During the third interval C 1,950 to 1,830 Ma, the velocity increased to 5.3 cm/yr, with a westerly motion along a small circle located at 82°N, 11°E and radius of 71°.

The observed velocities for the time intervals A and C are within typical continental drift velocities, i.e. below 8 cm/yr. The decreased velocity and observed change in plate motion in the time interval B is a possible indication that a collision occurred during this period. It should be noted that palaeomagnetic information on its own is not sufficient to determine if a collision occurred as only the latitude and the amount of angular rotation can be determined.

8.2 Reconstruction of Continental Bodies Around 2 Ga Relative to the Kaapvaal Craton.

The formation and break-up of supercontinents is the most spectacular demonstration of the extremely dynamic nature of our planet and some evidence points to a periodicity in supercontinent formation during Earth's history (McCulloch and Bennett, 1994; Torsvik, 2003). Palaeomagnetism, which provides the latitude and rotation for a continent, is the quantitative reconstruction tool used to examine the time of growth and dispersal of supercontinents. In the pages that follow, the hypothesis of a supercontinent around the time of formation of the Bushveld and Phalaborwa Complexes will be tested in terms of palaeomagnetic information.

8.2.1 Previous supercontinents

Pangaea, the most recent and well constrained supercontinent on Earth, formed during the Carboniferous and Permian periods and was at its maximum extent in the Late Permian (Figure 8.8). The southern segment of Pangaea, known as Gondwana (Figure 8.8), formed at around 500-550 Ma and was composed of the Amazonia-Rio Plata cratons (South America), West Africa-Congo-Kalahari Cratons (Africa) and Madagascar – Seychelles – India - East Antarctica - Australia (referred to as East Gondwana). Not all continents combined simultaneously to form Pangea; some were added along its margins whilst others rifted off during the supercontinent cycle (Torsvik, 2003). Pangea ultimately ruptured during the Jurassic period (ca. 175 Ma), preceded by and associated with widespread magmatic activity, including the Karoo flood basalts and dyke swarms in South Africa (Le Gall et al., 2002).

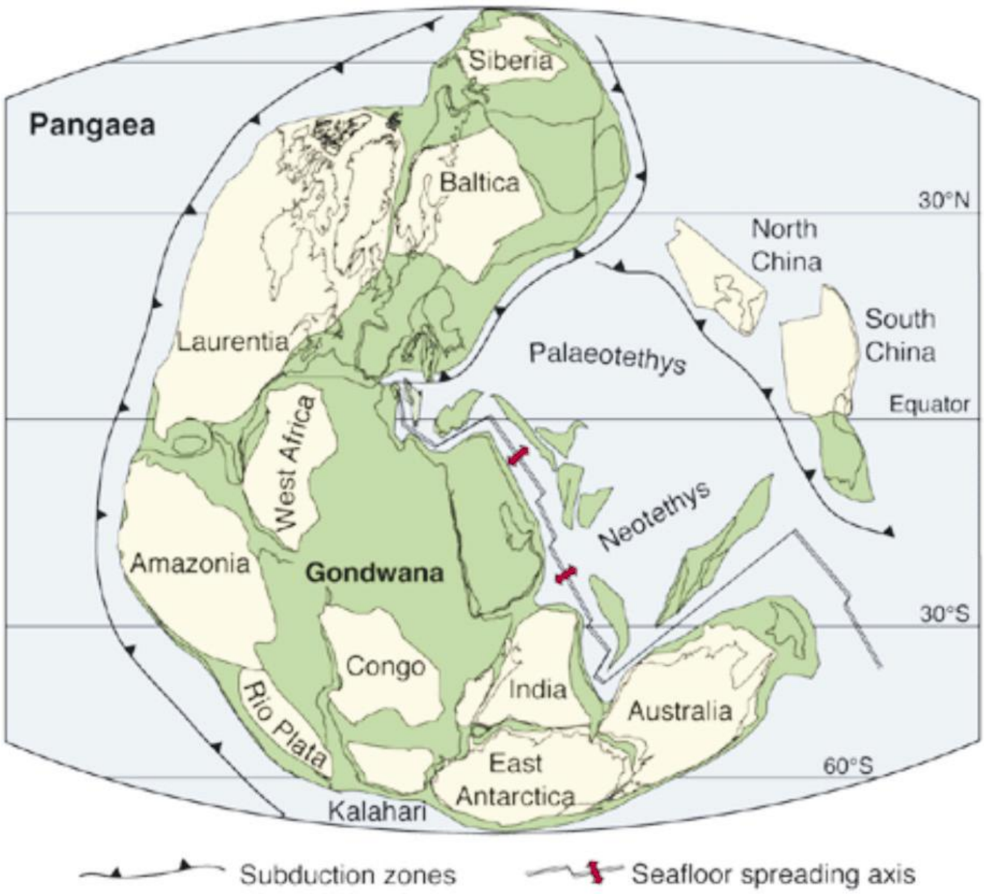

Figure 8.8 Pangaea supercontinent during the Late Permian period (Torsvik 2003). Precambrian terrains or continents that are commonly discussed in Rodinia (Figure 8.9) or Columbia reconstructions, but at very different locations, are highlighted in yellow.

The existence of a Precambrian supercontinent was theorized in the 1970s as many geologists noted a number of 1300-1000 Ma mountain belts presently located on different continents (Dewey and Burke, 1973), and in the early 1990s the name Rodinia was adopted for this supercontinent (Dalziel, 1992; Hoffman, 1991). Early palaeomagnetic studies of the Rodinia configuration were broadly supportive of the idea (Powell et al., 1993; Torsvik et al., 1996; Weil et al., 1998), but the quality of the data was insufficient to provide rigorous tests. This was partly due to the fact that many of these early palaeomagnetic studies were not tied to precise radiometric ages. Recent Rodinia models reveal a more dynamic planet at 750 Ma than previously realized (Figure 8.9). If Rodinia formed at 1100-1000 Ma, the breakup of the supercontinent probably occurred before 750 Ma and disruption commenced with the opening of an ocean between western Laurentia and Australia-East Antarctica. These relatively young cycles of supercontinent assembly and break up are now setting the stage for understanding the older cycles.

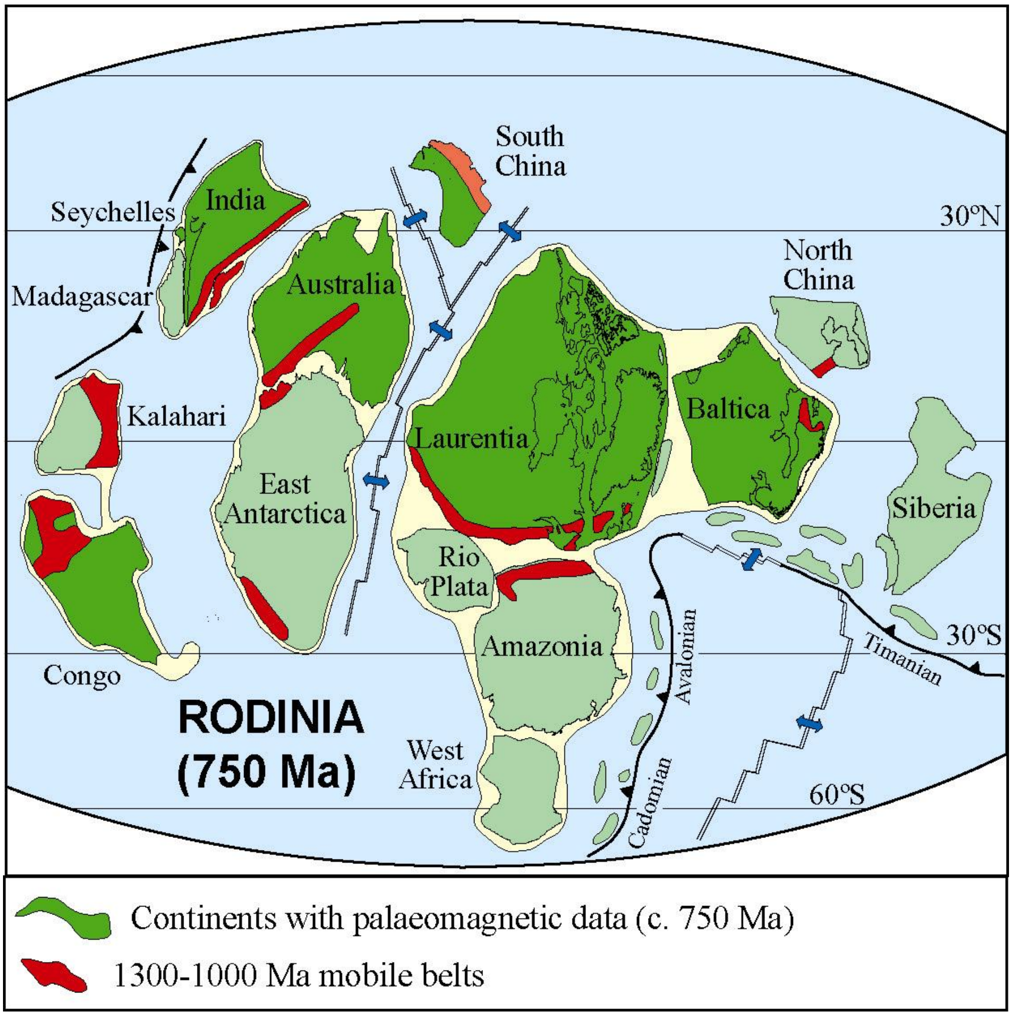

Figure 8.9 750 Ma reconstruction of Rodinia (Torsvik, 2003).

8.2.2 Proposed Palaeoproterozoic supercontinent Columbia

A hypothesised supercontinent called Columbia is believed to have formed prior to ~1.5 Ga. Its configuration (Figure 8.10) was based both on evidence of rifting and orogenic activity (Rogers and Santosh, 2002). A later review of 2.1 – 1.8 Ga orogens formed from the collision of Achaean and Palaeoproterozoic terrains around the world, together with lithostratigraphic, tectonothermal, geochronological and to a lesser extent palaeomagnetic data, prompted Zhao et al. (2002) to propose a new Columbia configuration (Figure 8.11). A detailed description on the rationale and motivation for the placement of Cratons in the ~2.0 Ga Columbia supercontinent can be found in Zhao et al. (2002).

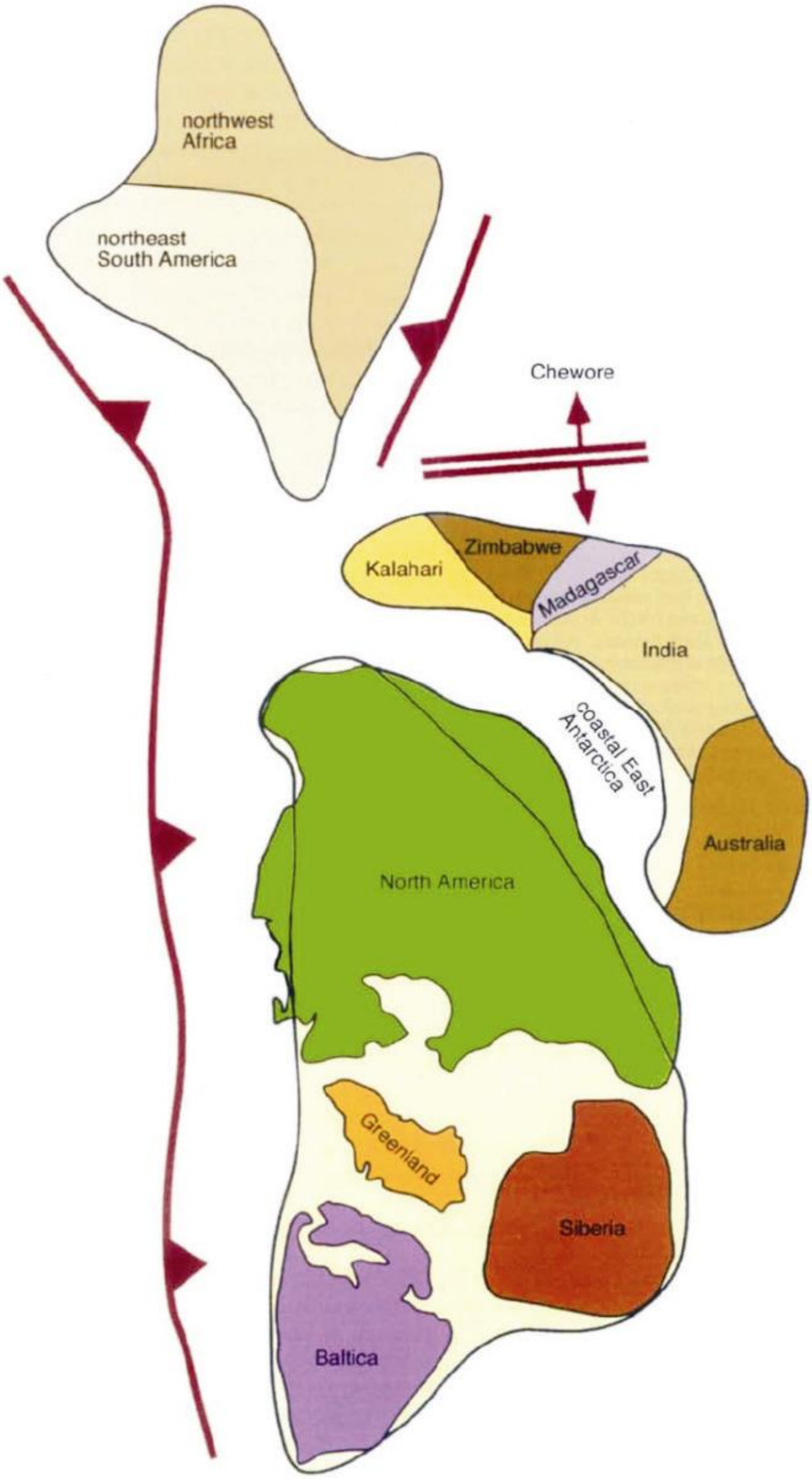

Figure 8.10 Proposed configuration of Columbia at ~1.5 Ga based on evidence of rifting and orogenic activity (Rogers and Santosh, 2002).

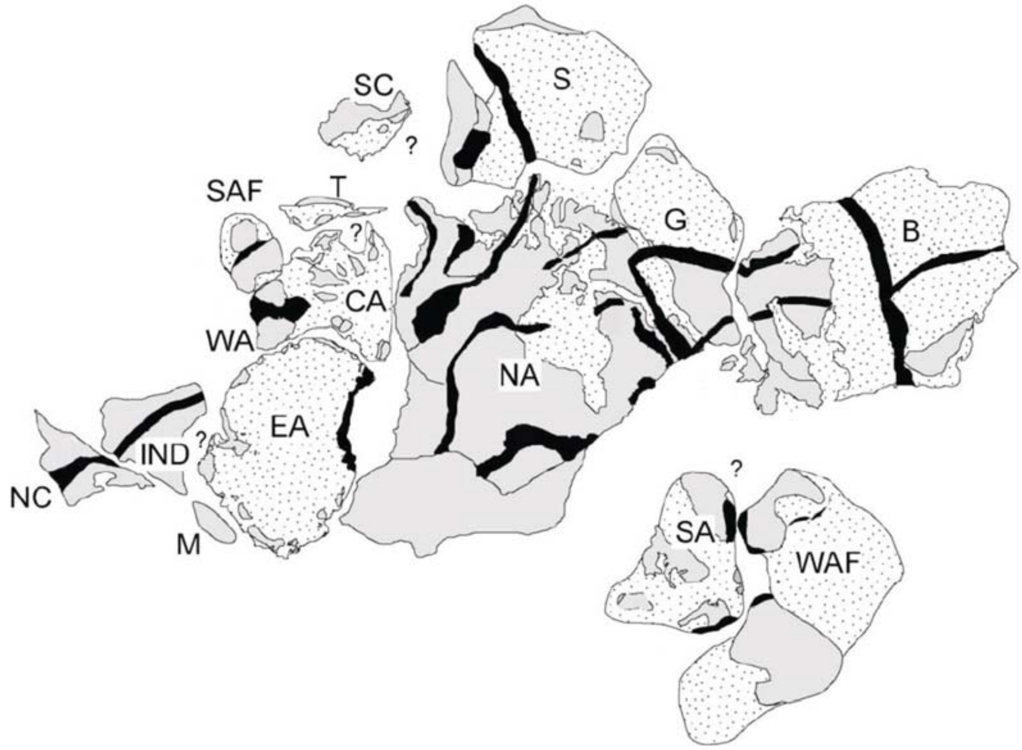

Figure 8.11 Reconstruction of the postulated Columbia Supercontinent (Zhao et al. 2002), essentially based on correlation of 2.1-1.8 Ga orogens and very few palaeomagnetic results. Symbols: B-Baltica (including Eastern Europe); CA-Central Australia; EA-East Antarctica; G-Greenland; IND-India; M-Madagascar; NA-North America; NC-North China; S-Siberia; SA-South America; SAF-South Africa; SC-South China; T-Tarim; WA-West Australia; WAF-West Africa. "?" indicates loose reconstruction connection, details of which can be found in Zhao et al. (2002).

According to Zhao's configuration for Columbia at ca 2 Ga, Vaalbara forms an integral part in the reconstruction with respect to the Kaapvaal Craton. The proposed "Vaalbara" continent, which is composed of the Kaapvaal and Pilbara Cratons (Figure 8.12), has been linked together based on the comparison of sequence stratigraphy and U-Pb geochronology and also some palaeomagnetic data between 2.8 and 2.1 Ga (Cheney et al., 1988).

Although Vaalbara was theorized to have been in existence between 2.8 and 2.1 Ga, Zhao et al. (2002) believed that the continent was still intact and was the site of two orogenic events with other cratonic bodies during the time interval 2.0 and 1.8 Ga. The first orogenic event is that of the Limpopo mobile belt (between 2.0 and 1.9 Ga), which formed as a result of the collision between the Kaapvaal and Zimbabwe cratons (Holzer et al., 1998). The second orogenic event resulted in the formation of the Capricorn Orogen in which the Pilbara and Yilgarn cratons were sutured around 2.0-1.8 Ga (Myers et al., 1996). These two orogens, together with other orogens at the same time period are believed by Zhao et al. (2002) to be the result of a world-wide amalgamation of cratonic blocks to form the supercontinent of Columbia.

In general, the amalgamation history and continental makeup of Columbia is essentially unknown and is hampered by the fact that only the latitudes for very few continents are known in terms of palaeomagnetic data.

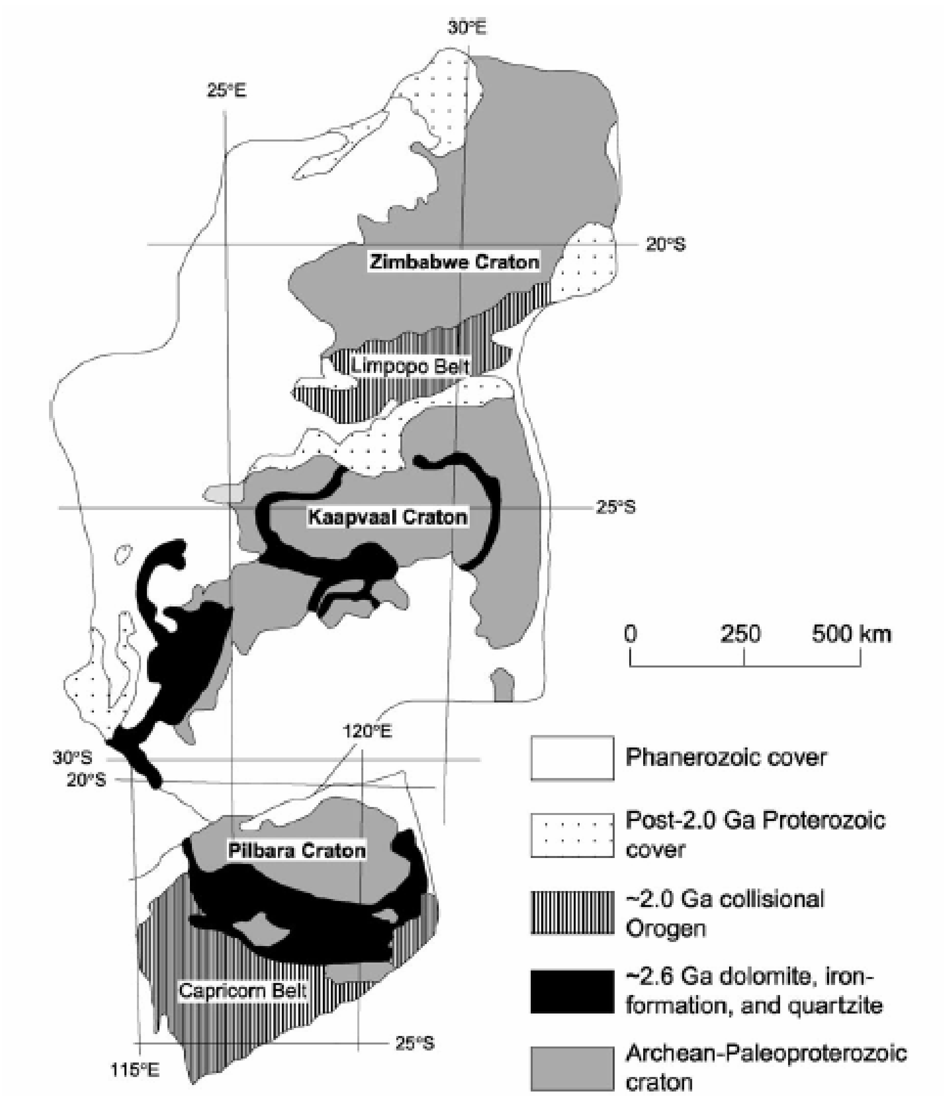

Figure 8.12 Proposed Vaalbara continent, showing connection between Kaapvaal and Pilbara cratons (Cheney, 1996).

8.2.3 Reconstruction of a Palaeoproterozoic supercontinent.

In order to test the hypothesis of the proposed supercontinent Columbia, palaeomagnetic and geochronological information from the Kaapvaal craton as well as other cratons involved in the assembly of Columbia were used to reconstruct the supercontinent at ca. 2 Ga. Before examining the Columbia configuration in its entirety at ca. 2.0 Ga, the proposed connection between the Kaapvaal and Pilbara cratons involved in the formation of the Vaalbara continent was first evaluated.

Proposed Vaalbara Continent.

Vaalbara forms an integral part in constructing the supercontinent of Columbia with respect to the positions of Southern African and Western Australian cratons. In order to test the Vaalbara hypothesis at ca. 2.0 Ga, two mean palaeomagnetic poles for each craton were required for the reconstruction.

At ca. 2.0 Ga the Kaapvaal craton possesses nine palaeomagnetic poles, they are: the Bushveld Complex (five poles, obtained in this study), the Phalaborwa Complex (this study), Vredefort granophyres and pseudotachylites (Carporzen, 2006) and the Witwatersrand Overprint (Layer et al., 1988). A brief description of each of the poles not obtained in this study can be found in the beginning pf this chapter. The above mentioned ca. 2 Ga poles were combined together to produce a new mean ca. 2.0 Ga Kaapvaal pole at 20.9° N and 36.2° E and A_{95}= 5.3° (Figure 8.13).

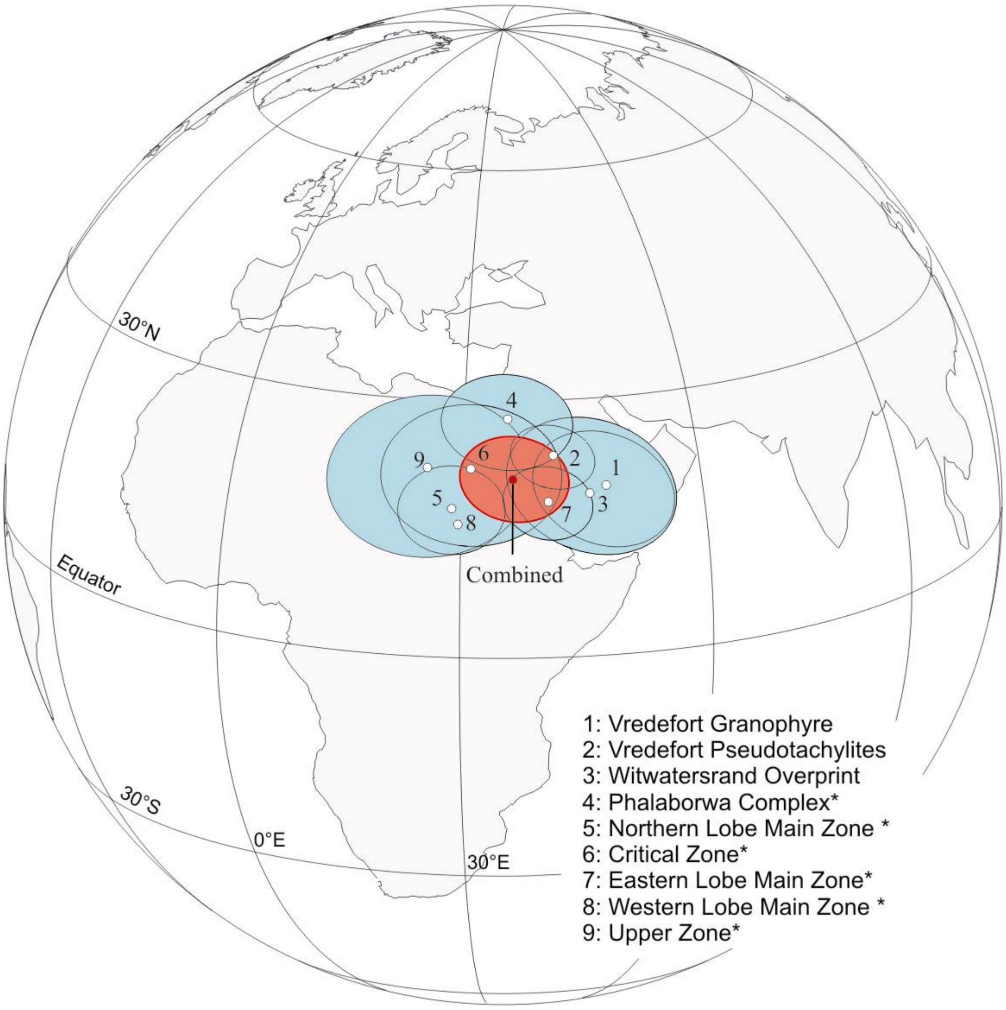

Figure 8.13 Palaeomagnetic poles at ca. 2 Ga. for the Kaapvaal craton. The combined mean palaeomagnetic pole is shown in red. A detailed description of the poles used in the illustrations can be found in the beginning of this Chapter; poles marked with * indicate poles obtained from this study.

The Pilbara craton in Western Australia possesses only one palaeomagnetic pole at ca. 2.0 Ga and that is of the Mount Tom Price banded iron ore formation in Western Australia (Schmidt and Clark, 1994), whose pole position is 37.4° S and 139.7° W, dp/dm=5.7°/11.3°. Unfortunately no precise geochronological data are available for the pole and an age of 2,000 ± 100 Ma has been estimated from stratigraphic relationships (Schmidt and Clark, 1994). No palaeomagnetic data are available for the Yilgarn Craton in Western Australia and this has therefore been left out of the reconstruction.

The two above-mentioned poles were used to plot the ancient latitudes and azimuthal orientations of each craton as defined by the palaeomagnetic software GMAP (Torsvik and Smethurst, 1999). The resulting reconstruction of the Kaapvaal and Pilbara Cratons at ca. 2.0 Ga is shown in Figure 8.14. Two possibilities are shown for the Pilbara Craton: one with the Capricorn Orogen facing the East (south polarity used), and the other rotated by 180° opposed. These alternative positions arise because of ambiguity in the choice of palaeopole polarity.

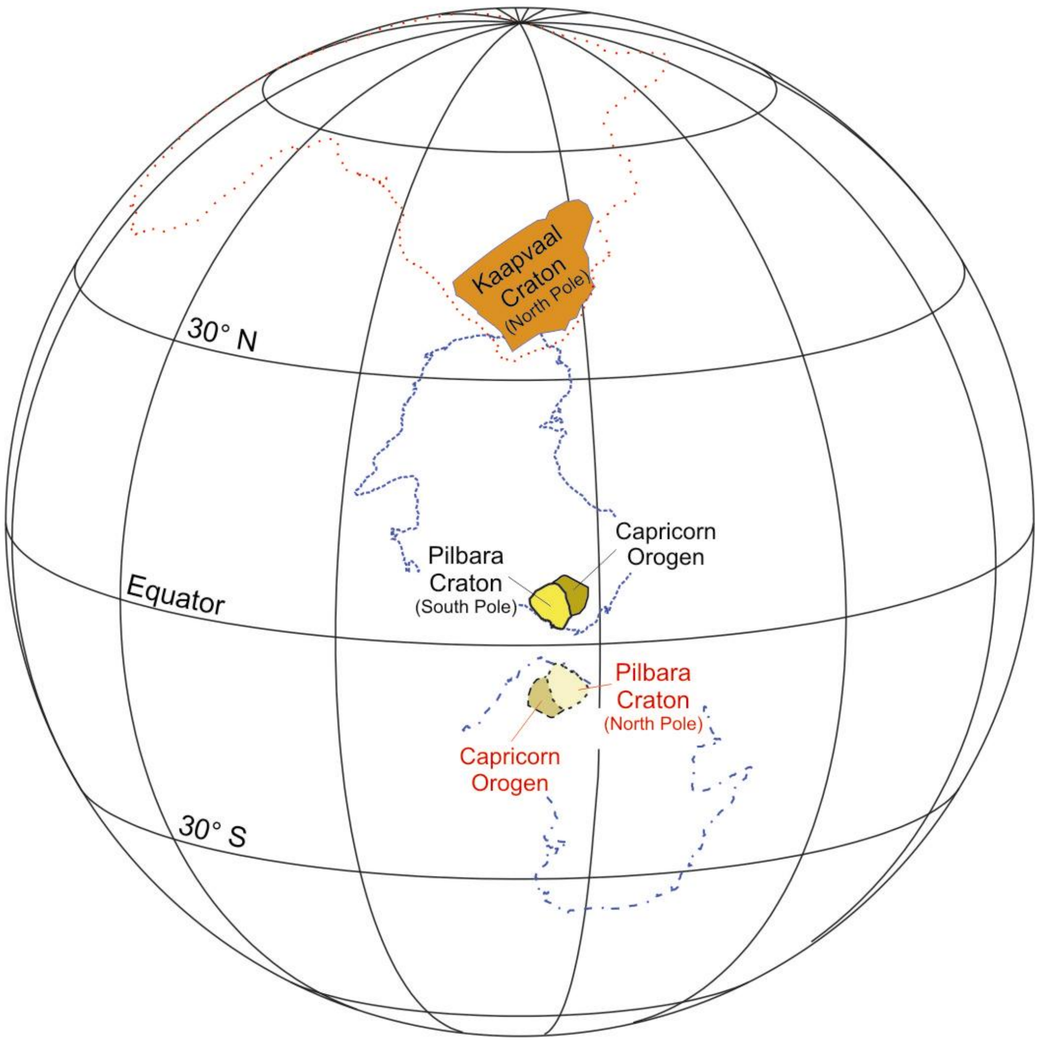

Figure 8.14 Reconstruction of the Kaapvaal and Pilbara Cratons based on a combined Kaapvaal pole at ca. 2 Ga and a pole from the Mount Tom Price banded iron ore formation in western Australia. The north and south polarity poles of the Pilbara Craton are shown to indicate that at ca. 2.0 Ga there was a large separation between the Kaapvaal and Pilbara Cratons and the existence of Vaalbara at ca. 2.0 Ga is very unlikely.

If the Pilbara and the mean Kaapvaal palaeopoles are matched precisely, there is a latitude gap of ~27º (ca. 3000 km) between the northern margins of the Kaapvaal craton and the southern polarity pole of the Pilbara Craton. However, with this polarity the Pilbara craton is positioned upside down, in terms of the Vaalbara reconstruction of Cheney (1996). Using a more realistic position of the Pilbara Craton (northern pole) the separation between the two Cratons has increased to ~ 3,900 km, thereby making the joint assembly of the two Cratons less likely.

Although the above findings show that the two cratons were unlikely to have been combined as a single entity at ca. 2.0 Ga, previous palaeomagnetic studies have found that the Vaalbara reconstruction may have existed between 3.1 Ga and 2.7 Ga (Zegers et al., 1998) and also at ca. 2.78 - 2.77 Ga (Strik et al., 2003).

Proposed Columbia Supercontinent

The Columbia supercontinent as proposed by Zhao (2002) in Figure 8.11 involves the assembly of 15 Archean cratons, namely: East Antarctica, Baltica, Central Australia, North China, South China, Greenland, India, Madagascar, North America (Superior, Hearne, Rae, Slave and Wyoming cratons), Siberia, South America (Guiana and Central Brazil cratons), Southern Africa (Kaapvaal and Zimbabwe), West Africa, Tarim, West Australia (Pilbara and Yilgarn cratons). Unfortunately, very little palaeomagnetic data are available for these terrains at ca. 2.0 Ga, and if available the age determination of the samples are not very precise. A summary of the poles obtained for the reconstruction can be found in Table 8.2. Regrettably, no palaeomagnetic results at ca. 2 Ga were found for Tarim, North China, South China, Greenland, East Antarctica or Madagascar, and therefore they were excluded from the reconstruction.

Table 8.2 Palaeomagnetic poles used for reconstruction of Columbia at ~ 2 Ga. *Dec.* = declination, *Inc.* = inclination, α_{95} = 95 percent confidence circle around mean direction. Pole Lat. = Palaeomagnetic Pole Latitude, Pole Long. = Palaeomagnetic Pole Longitude, Pole polarity = polarity used in reconstruction. # indicates reference: [1] Schmidt and Clark, 1994 , [2] Buchan et al., 1996, [3] Mikhailova, 1989 , [4] Onstott et al., 1984 , [5] Onstott and Dorbor, 1987, [6] Radhakrishna and Joseph, 1996 .

Terrain	Rock Formation	Dec.	Inc.	α 95	Pole Lat.	Pole Long	Age (Ma)	Pole Polarity
Western Australia [1]	Mt. Tom Price	308.8	-9.3	11.3	-37.4	220.3	2,000 ± 100	North
Kaapvaal	Combined	9.9	61.6	5.3	20.9	36.2	~ 2,046	South
Laurentia [2]	Marathon (Fort Frances)	133.5	-50.7	6.8	51.2	174.7	2,076 ± 5	North
Baltica	Combined	351.9	44.5	11.3	53.2	218.9	~ 2,000	North
Siberia [3]	Aldan Anorthosites	80	-7	15	2.7	233	~ 2,050 ± 50	South
Amozonia [4]	La Encrucijada	324	-7	4	55	188	2,065 ± 67	North
Western Africa [5]	Liberia Metamorphic	286.6	18.4	13	17.5	269.1	2,050 ± 6	North
India [6]	Agali-Anaikatti Dykes	13.9	27	26.1	75.7	153.2	2,000 ± 20	North

The combined mean pole for the Kaapvaal craton mentioned in Table 8.2 is the same as that used in the Columbia reconstruction (see Section 9.3.1 for more detail). The Baltica mean pole (Figure 8.15) is a combined pole from ten palaeomagnetic poles at ca 2.0 Ga, namely: Nilsia dykes (Finland), Iisalmi Intrusion (Finland), Iisalmi diabase dykes (Finland), Svecokarelin Gabbro

(Finland and Sweden), Tammela Intrusion (Finland), West Karelia Metadolerites (Russia), Karelia intrusion (Russia), Tulos Lake Metadolerites (Russia), Tsokkaoivi Gabbro (Finland) and Nordingra – Ornskolvik dykes (Sweden). The above mentioned poles for Baltica were obtained from the Global Palaeomagnetic Data Base. (McElhinny and Lock, 1996; http://www.ngu.no/dragon/Palmag/paleomag.htm).

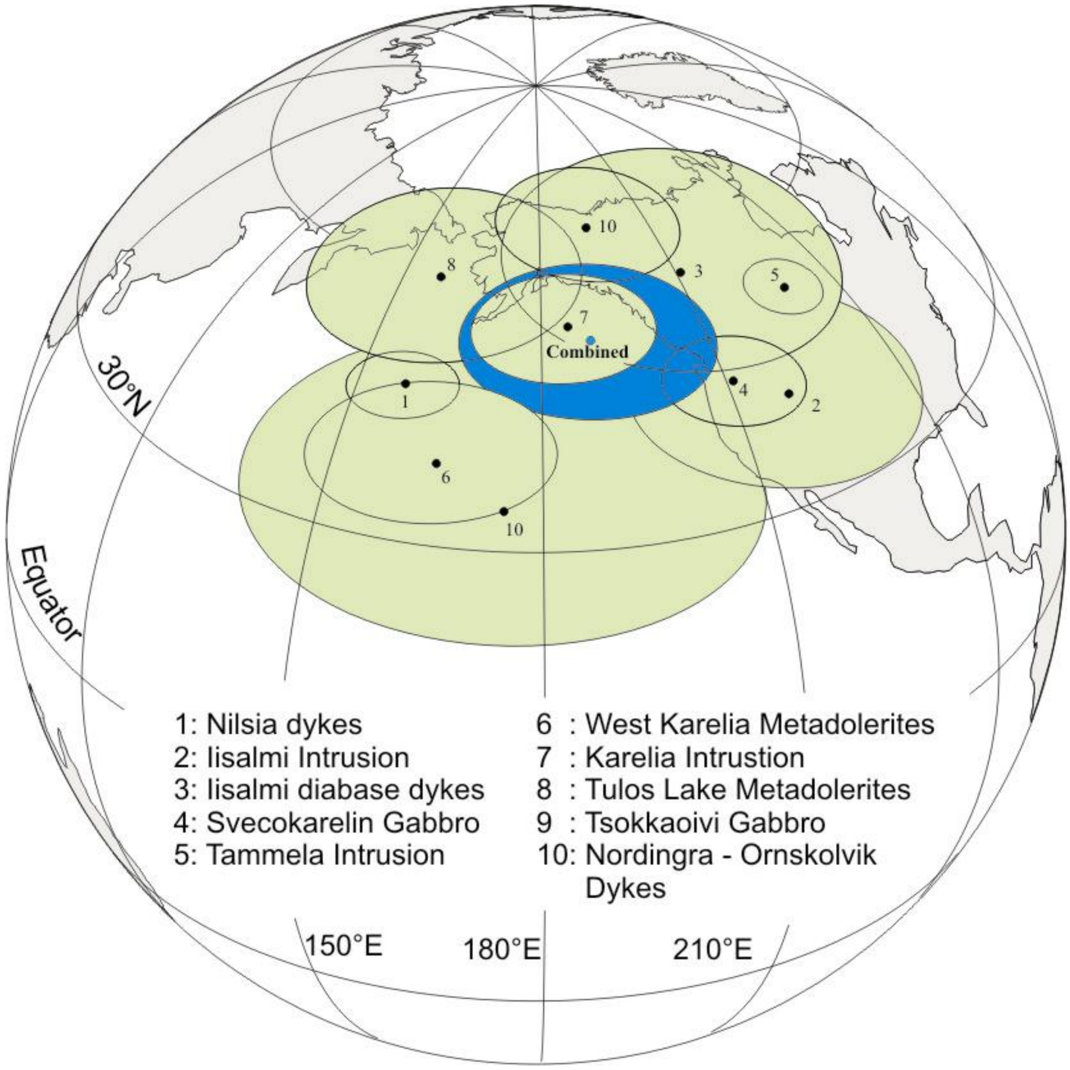

Figure 8.15 Palaeomagnetic poles for Baltica at ca. 2.0 Ga. The combined mean pole used for Baltica during this reconstruction is shown as the blue pole. Poles were obtained from the Global Palaeomagnetic Data Base (McElhinny and Lock, 1996) http://www.ngu.no/dragon/Palmag/paleomag.htm.

Using the listed poles and polarities in Table 8.2, an attempt at reconstructing the possible position and orientations of cratons in relation to each other was undertaken to test the hypothesis of the Columbia supercontinent (Figure 8.16).

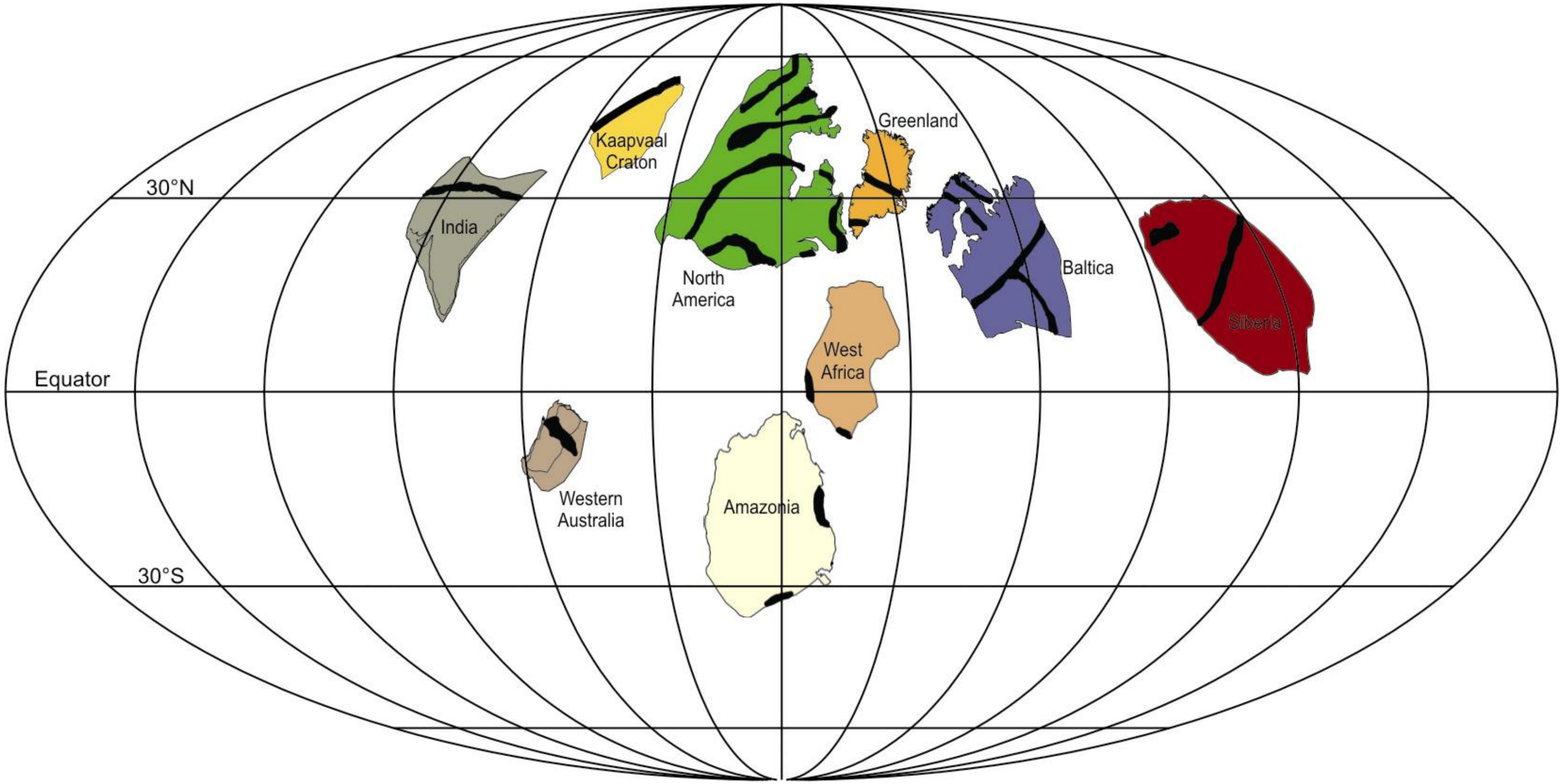

Figure 8.16 Reconstruction of the proposed supercontinent of Columbia at ca. 2.0 Ga, using palaeomagnetic data found in Table 8.2 (polarity of poles used are also listed). Cratons (especially Western Australia, India, Kaapvaal) have been plotted separately from other cratons as no obvious geologic reasons are available for putting them together with adjacent cratons. Black lines across cratons represent 2.1- 1.8 Ga orogens adapted from Zhao et al. (2002).

The positions of the various cratons were chosen so as to closely resemble that of the proposed Columbia supercontinent at ca. 2.0 Ga (Figure 8.11). The above reconstruction, based purely on palaeomagnetic data, is in reasonable agreement with that of Zhao et al. (2002). However, there are a number of similarities and differences observed. In both reconstructions, Laurentia and Baltica can be linked together; Western Africa and South America (Amazonia) are in close agreement and could possibly be connected; the position of the Kaapvaal craton and India are similar in both reconstructions, although they have been plotted separately from other cratons as no obvious geologic reasons are available for putting them together with adjacent cratons. The first major difference between reconstructions is the position of Siberia and Western Australia. According to Zhao et al. (2002) Siberia should be located above Laurentia, and Western Australia should be joined to the Kaapvaal Craton and located to the east of Laurentia. Another major difference is that a large section of the proposed supercontinent is missing in the above reconstruction, this is due to the lack of palaeomagnetic data from China (North and South), Tarim, East Antarctica and Madagascar.

8.3 Conclusion

The combination of palaeopoles with well constrained geochronological ages from the Kaapvaal Craton has produced a new robust mean palaeomagnetic pole for the craton at ca. 2.0 Ga. Comparing this pole with that of an equivalent aged pole from the Pilbara Craton in Western Australia provided a vital test in disproving the existence of the Vaalbara continent at 2.0 Ga. The finding does not disprove the existence of Vaalbara altogether, only that the two cratons were no longer amalgamated at 2.0 Ga.

Zhao's (2002) depiction of the Columbia supercontinent at ca. 2.0 Ga has some support from available palaeomagnetic data, although it is insufficient in providing a rigorous test. From the reconstruction it appears that some form of the supercontinent could have been in existence. In order to produce precise evidence for the existence of the supercontinent one needs to have not only well-constrained palaeomagnetic data, but also precise information on the age of magnetic remanence acquisition.

CHAPTER 9: CONCLUSIONS AND SUGGESTIONS FOR FURTHER WORK

Newly conducted palaeomagnetic studies on the Bushveld Complex, the Phalaborwa Complex and a number of dolerite dykes that intrude both complexes have yielded palaeomagnetic data that are of excellent quality and resulted in reliable palaeopole positions. The resulting poles were combined with similar aged Kaapvaal poles and in conjunction with other well-defined poles were then utilized to test the hypothesis of the proposed continental assemblage of the Columbia supercontinent and the Vaalbara continent.

Results determined from the Bushveld Complex have successfully removed the spread in palaeopole positions previously determined for the different zones of the complex. The initial spread reported in previous studies was discovered to be due to incorrect primary magnetisation directions being determined and was not due to a 50 my emplacement period, or unresolved structural complexities, or the result of post-crystallization to remagnetization by widespread thermal disturbance/fluid migration occurring during the emplacement of the ~1.88 post-Waterberg dolerite.

One of the striking features of the Bushveld palaeomagnetic data is the observed pattern of normal and reversed polarities. Although the data presented here appears to resemble a direct link between zones and polarity, the exact polarity changes in the sequence can only be regarded as approximate at this stage. More continuous sampling is required throughout the complex, especially at zone boundaries and around the observed polarity changes discovered in this study. Although the Earth's magnetic history is not well constrained during the cooling of the Bushveld Complex, each zone was considered separately when dealing with field stability tests. Dual polarities recorded within each zone were found to share a common mean at the 95 % confidence level, thereby indicating that they were related to the same magmatic event and had successfully recorded one of the oldest known reversals in the Earth's field, only predated by the 2.77 Ga reversal recorded in the Nullagine Synclinorium of the East Pilbara Basin in Western Australia. Fold tests implemented on zonal data revealed that only two zones yielded statistically positive results. However, the resulting bedding corrected HB components from all zones produced better groupings, thereby supporting a primary magnetic signature and indicating that the complex was intruded in a near horizontal position. The exact time and cause of sagging still remains unknown; the resulting palaeomagentic data only indicate that sagging took place once the complex had cooled below the Curie temperature for magnetite ~ 580°C.

Palaeomagnetic analysis conducted on pyroxenites from the Phalaborwa Complex successfully isolated minor secondary components to produce a better grouped primary signature. The resulting palaeopole position for the complex is in close proximity to those obtained from the coeval Bushveld Complex.

Dual polarity palaeomagnetic data obtained from dykes located in the Phalaborwa and Eastern Lobe of the Bushveld Complex produced two well defined palaeopole positions in which their uncertainty levels statistically overlapped, indicating a possible geological correlation. Based on the overlapping pole position, dyke samples were combined to produce a single palaeopole that when compared with relevant intrusive poles from southern Africa, suggested that the dykes occurring in both the Phalaborwa and Bushveld Complex have an emplacement age of ~1.9 Ga.

The palaeolatitude and orientation of the Kaapvaal Craton determined by this study around 2.0 Ga, when compared with the Pilbara Craton of Western Australia, suggest that the palaeogeographic reconstruction of the proposed “Vaalbara” Craton at ca 2.0 Ga is unlikely. However, the data tentatively appear to support the hypothesis of the Columbia Supercontinent as depicted by Zhao 2002 at 2.0 Ga.

Many of the original research questions initially proposed in this thesis relating to inconsistencies reported in previous palaeomagnetic studies have been successfully addressed. Although this study has obtained a robust and reliable palaeopole for the Kaapvaal Craton around 2.0 Ga, the cratonic configuration during the formation of the Bushveld Complex with emphasis on the postulated Columbia supercontinent still remains unclear. In order to accurately test the hypotheses of supercontinents and the cratonic configuration during the emplacement of the Bushveld Complex, more well-defined world-wide continental poles around 2.0 Ga are required.

Based on the “zonal” polarity results in the Bushveld Complex, an intriguing question has arisen in terms of the history of the Earth’s magnetic field during the formation of the Complex. Due to the limited number of suitable outcrops in the Bushveld Complex, a continuous succession of samples across the entire complex was impossible to obtain during this study. To solve this, an intended research project is planned to obtain continuous samples from boreholes using newly developed gyroscopic techniques to accurately orientated core. This will allow thorough coverage to be obtained throughout the complex and allow samples to be acquired across all zones and hopefully provide insight into the polarity variations.

REFERENCES:

Ade-Hall, J.M., Palmer, H.C. and Hubbar, T.P., 1971. The magnetic and opaque petrological response of basalt to regional hydrothermal alteration. The Geophysical Journal of the Royal Astronomical Society, 24: 137-174.

Barton, J.M., 1979. The chemical composition, Rb-Sr isotopic systematic and tectonic setting of certain post-kinematic mafic igneous rocks, Limpopo Mobile belt, Southern Africa. Precambrian Research, 9: 57-80.

Bates, M.P. and Jones, D.L., 1996. A palaeomagnetic investigation of the Mashonaland dolerites, north-east Zimbabwe. Geophysical Journal International, 126: 513-524.

Briden, J.C., 1972. A Stability Index of Remanent Magnetism. Journal of Geophysical Research, 77(8): 1401-1405.

Buchan, K.L., Halls, H.C. and Martensen, J.K., 1996. Palaeomagnetism, U-Pb geochronology and geochemistry of Marathon dykes, Superior Province, and comparison with Fort Frances swarms. Canadian Journal of Earth Science, 33: 1583-1595.

Buchanan, P.C., Reimold, W.U., Koeberl, C. and Kruger, F.J., 2002. Geochemistry of intermediate to siliceous volcanic rocks of the Rooiberg Group Bushveld Magmatic Province South Africa. Contrib Mineral Petrol, 144: 131-143.

Buick, I.S., Mass, R. and Gibson, R., 2001. Precise U-Pb titanite age constraints on the Bushveld Complex, South Africa. Journal of the Geological Society, London, 158: 3-6.

Butler, R.F., 1992. Paleomagnetism: magnetic domains to geologic terrains. Blackwell Scientific, Boston, 238 pp.

Cairncross, B. and Dixon, R., 1995. Minerals of South Africa. Geological Society of South Africa, Johannesburg, 290 pp.

Carporzen, L., 2006. Thesis: Meteorite impact crater magnetism in Vredefort (South Africa) and Rochechouart (France), Université Paris VII Denis Diderot, Paris, France, 288 pp.

Cawthorn, R.G. and Walraven, F., 1998. Emplacement and crystallization time for the Bushveld Complex. Journal of Petrology, 39(9): 1669-1687.

Chavez Gomez, S., 2001. A catalogue of dykes from aeromagnetic surveys in eastern and southern Africa. ITC (The International Institute for Aerospace and Earth Sciences, Enschede, 70 pp.

Cheney, E.S., 1996. Sequence stratigraphy and plate tectonic significance of Transvaal succession of southern Africa and its equivalent in Western Australia. Precambrian Research, 79: 3-24.

Cheney, E.S., Roering, C. and Stettler, E., 1988. Vaalbara, Geological Society of South Africa Geocongress '88, pp. Extended Abstracts: 85-88.

Compston, W. and McElhinny, M.W., 1975. The Rb-Sr age of the Mashonaland dolerites of Rhodesia and its significance for palaeomagnetic correlation in southern Africa. Precambrian Research, 2: 305-315.

Cornell, D.H., Armstrong, R.A. and Walraven, F., 1998. Geochronology of the Proterozoic Hartley Basalt Formation, South Africa: constraints on the Kheis tectogenesis and the Kaapvaal Craton's earliest Wilson Cycle. Journal of African Earth Sciences, 26: 5-27.

Cornell, D.H., Schutter, S.S. and Eglington, B.L., 1996. The Ongeluk basaltic andesite formation in Griqualand West, South Africa: submarine alteration in the 2222 Ma Proterozoic Era. Precambrian Research, 79: 101-123.

Dalziel, I.W.D., 1992. On the organization of American plates in the neoproterozoic and the breakout of Lauretia. GSA Today, 2: 237-241.

Dewey, J.F. and Burke, K., 1973. Tibetan, Variscan and Precambrian basement reactivation: products of continental collision. Journal of Geology, 81: 683-692.

Donaldson, C.H., 1974. Olivine crystal types in harrisitic rocks of the Rhum pluton and Archean spinifex. Geological Society of America Bulletin, 85: 1721-1726.

Dorland, H.C., 2004. Provenance ages and timing of sedimentation of selected Neoarchean and Paleoproterozoic successions on the Kaapvaal Craton., University of Johannesburg, Johannesburg, 326 pp.

Dunlop, D.J., 1979. On the use of Zijderveld vector diagrams in multi-component palaeomagneric studies. Physics of the Earth and Planetary Interiors, 26: 1-26

Evans, D.A., Beukes, N.J. and Kirschvink, J.L., 1997. Low-Latitude glaciation in the Palaeoproterzoic Era. Nature, 386: 262-266.

Evans, D.A.D., Beukes, N.J. and Kirschvink, J.L., 2002. Paleomagnetism of a lateritic paleoweathering horizon and overlying Paleoproterozoic red beds from South Africa: Implications for the Kaapvaal apparent polar wander path and a confirmation of atmospheric oxygen enrichment. Journal of Geophysical Research, 107: 12, 2326, doi:10.1029/2001JB000432.

Fisher, R.A., 1953. Dispersion on a sphere. Proc. Roy. Soc. London, A217: 295-305.

Frick, C., 1973. The Sill phase and chill zone of the Bushveld Igneous Complex. transactions Geological Society of South Africa, 76: 7-14.

Garcia, F., 1996. Palabora open pit. Available from: www.Mindat.org. Assessed on 15 October 2005.

Glatzmaier, G.A., 1997. Core Convection and the Geodynamo. Los Almos National Laboratory. Available from: http://ees5-www.lanl.gov/ IGPP/ Geodynamo.html. Assessed on 28 January 2003.

Glatzmaier, G.A. and Roberts, P.H., 1995a. A three-dimensional convective dynamo solution with rotating and finitely conducting inner core and mantle. Physics of the Earth and Planetary Interiors, 91: 63-75.

Glatzmaier, G.A. and Roberts, P.H., 1995b. A three-dimensional self-consistent computer simulation of a geomagnetic field reversal. Nature, 377: 203-209.

Gough, D.J. and Van Niekerk, C.B., 1959. A study of the palaeomagnetism of the Bushveld gabbro. Philos. Mag., 14: 126-134.

Groeneveld, D., 1970. The structural features and the petrography of the Bushveld Complex in the vicinity of Stoffberg, Eastern Transvaal. Geological Society of South Africa, Special Publication., 1: 36-46.

Hanson, R.E. et al., 2004. Paleoproterozoic intraplate magmatism and basin development on the Kaapvaal Craton: Age, paleomagnetism and geochemistry of ~1.93 to ~1.87 Ga post-Waterberg dolerites. South African Journal of Geology, 107: 233-254.

Hargraves, R.B., 1970. Palaeomagnetic evidence relevant to the origin of the Vredefort Ring. Journal of Geology, 78: 253-263.

Harmer, R.E., 2000. Mineralisation of the Phalaborwa Complex and the carbonatite connection in iron oxide-Cu-Au-U-REE deposits. In: T.M. Porter (Editor), Hydrothermal Iron Oxide Copper-Gold & Related Deposits: A Global Perspective. Australian Mineral Foundation, Adelaide, pp. 331-340.

Hart, R.J., Hargraves, R.B., Andreoli, A.G., Tredoux, M. and Doucoure, C.M., 1995. Magnetic anomaly near the centre of the Vredefort structure; Implications for impact-related magnetic signatures. Geology, 23: 277-280.

Hattingh, P.J., 1983. Thesis: A palaeomagnetic investigation of the Layered mafic sequence of the Bushveld Complex, University of Pretoria, Pretoria.

Hattingh, P.J., 1986a. The palaeomagnetism of the main zone in the western Bushveld Complex. Earth and Planetary Science Letters, 79: 441-452.

Hattingh, P.J., 1986b. The palaeomagnetism of the main zone of the eastern Bushveld Complex. Tectonophysics, 124: 271-295.

Hattingh, P.J., 1986c. The Palaeomagnetism of the Merensky Reef footwall rocks of the Bushveld complex. Transactions Geological Society of South Africa, 89: 1-8.

Hattingh, P.J., 1989. Palaeomagnetism of the Upper Zone of the Bushveld Complex. Tectonophysics, 165: 131-142.

Hattingh, P.J., 1995. Palaeomagnetic constraints on the emplacement of the Bushveld Complex. Journal of African Earth Sciences, 21(4): 549-551.

Hattingh, P.J., 1998. The Bushveld Complex and Palaeomagnetism. In: R.J. Durrheim and S.J. Webb (Editors), Southern African Geophysical Review, 2. South African Geophysical Association, pp. 75-77.

Hattingh, P.J. and Pauls, N.D., 1994. New Palaeomagnetic results from the Northern Bushveld Complex of South Africa. Precambrian Research, 69: 229-240.

Hatton, C.J. and Von Gruenewaldt, G., 1987. The geological setting and petrogenesis of the Bushveld chromitite layers. In: C.W. Stowe (Editor), Evolution of chromium ore fields. Van Nostr and Reinhold, New York, pp. 109-43.

Hoffman, P.F., 1991. Did the breakout of Laurentia turn Gondwana inside out? Science, 252: 1409-1411.

Holzer, L., Frei, R., Barton, J.M.J. and Kramers, J.D., 1998. Unravelling the record of successive high grade events in the Central Zone of the Limpopo Belt using Pb single phase dating of metamorphic minerals. Precambrian Research, 87(1-2): 87-115.

Hunter, D.R. and Reid, D.L., 1987. Mafic dyke swarms in Southern Africa. In: H.C. Halls and W.F. Fahrig (Editors), Mafic Dyke Swarms. Geological Association of Canada Special Paper 34, Toronto, Canada, pp. 445-456.

Irving, E., 1964. Paleomagnetism and its application to geological and geophysical problems. John Wiley & Sons, Inc., New York, 399 pp.

Kamo, S.L., Reimold, W.U., Krogh, T.E. and Colliston, W.P., 1996. A 2.023 Ga age for the Vredefort impact event and a first reports of shock metamorphosed zircons in pseudotachylitic breccias and granophyre. Earth And Planetary Science Letters, 144: 369-387.

Kruger, F.J., 1994. The Sr-isotopic stratigraphy of the western Bushveld Complex. South African Journal of Geology, 97(4): 393-398.

Kruger, J.F., 1990. The stratigraphy of the Bushveld Complex: a reappraisal and the relocation of the Main Zone boundaries. South African Journal of Geology, 93: 376-381.

Kruger, J.F., 2005. Filling the Bushveld Complex magma chamber: lateral expansion, roof and floor interaction, magmatic unconformities, and the formation of giant chromitite, PGE and Ti-V-magnetitite deposits. Mineralium Deposita, 40: 451-472.

Layer, P.W., Kroner, A., McWilliams, M. and Clauer, N., 1988. Regional magnetic overprinting of Witwatersrand Supergroup sediments, South Africa. Journal of Geophysical Research, 93: 2191-2200.

Le Gall, B. et al., 2002. $^{40}Ar/^{39}Ar$ geochronology and structural data from the giant Okavango and related mafic dyke swarms, Karoo igneous province, northern Botswana. Earth And Planetary Science Letters, 202: 595-606.

Lee, C.A., 1996. A review of the mineralization in the Bushveld Complex and some other layered mafic intrusions. In: R.G. Cawthorn (Editor), Layered Intrusions. Developments in Petrology. Elsevier, Amsterdam, pp. 103-145.

Letts, S.A., 2004. The development of aeromagnetic mapping and dyke interpretation methodologies with application to a high resolution aeromagnetic survey in the eastern Bushveld Complex. , The University of the Witwatersrand, Johannesburg, 217 pp.

Letts, S.A. et al., 2005. Palaeomagnetism and $^{40}AR/^{39}Ar$ geochronology of mafic dykes from the Eastern Bushveld Complex (South Africa). Geophysical Journal International, 162: 36-48.

Lofgren, G.E. and Donaldson, C.H., 1975. Curved, branching crystals and differentiation in comb-layered ricks. Contrib. Mineral. Petrol., 49: 309-319.

Maes, S.M., Miller, J.D., Miller, T.D., Brown, P.E. and Tikoff, B., 2006. Magnetic Fabric if the Sonju Lake Intrusion, Northeastern Minnesota: Evidence for Internal Structure and Emplacement Dynamics, Philadelphia Annual Meeting (22–25 October 2006), Philadelphia, Pennsylvania.

McCulloch, M.T. and Bennett, V.C., 1994. Progressive Growth of the Earths Continental - Crust and Depleted Mantle - Geochemical Constraints. Geochimica Et Cosmochimica Acta, 58: 4717 - 4738.

McElhinny, M.W., 1964a. An improved method for demagnetising rocks in alternating magnetic fields. Geophysical Journal of The Royal Astronomical Society, 10: 369-374.

McElhinny, M.W., 1964b. Statistical significance of the fold test in palaeomagnetism. Geophysical Journal Of The Royal Astronomical Society, 8: 338-340.

McElhinny, M.W., 1973. Palaeomagnetism and plate tectonics. Cambridge University Press, London, 358 pp.

McElhinny, M.W. and Lock, N.P., 1996. IAGA paleomagnetic databases with Access. Surveys in Geophysics, 17: 575-591.

McElhinny, M.W. and McFadden, P.L., 2000. Paleomagnetism Continents and Oceans. International Geophysics Series, 73. Academic Press, San Francisco, 386 pp.

McElhinny, M.W. and Opdyke, N.D., 1964. The paleomagnetism of the Precambrian dolerites of eastern Southern Rhodesia, an example of geological correlation by rock magnetism. Journal of Geophysical Resource, 69: 2465-2475.

McFadden, P.L. and Jones, D.L., 1981. The fold test in palaeomagnetism. Geophysical Journal Of The Royal Astronomical Society, 67: 53-58.

McFadden, P.L. and Lowes, F.J., 1981. The discrimination of mean directions drawn from Fisher distributions. Geophysical Journal Of The Royal Astronomical Society, 67: 19-33.

McFadden, P.L. and McElhinny, M.W., 1990. Classification of the reversal test in palaeomagnetism. Geophysical Journal International., 103: 725-729.

Merrill, R.T., McElhinny, M.W. and McFadden, P.L., 1983. The Magnetic Field of the Earth Paleomagnetism, the Core, and the Deep Mantle. International Geophysics Series, 63. Academic Press, San Diego, 365 pp.

Mikhailova, N.P., 1989. Paleomagnetic directions and pole positions: Data for the USSR - Issue 7. Soviet Geophysical Committee: World Data Center-B (Moscow): catalogue.

Mitchell, A.A. and Scoon, R.N., 1991. Discussion and reply on 'The stratigraphy of the Bushveld Complex: a reappraisal and relocation of the Main Zone boundaries' by Kruger, F. J. South African Journal of Geology, 93: 183-190.

Morgan, G.E., 1985. The palaeomanetism and cooling history of metamorphic and igneous rocks from the Limpopo Mobile Belt, southern Africa. Geological Society of America Bulletin, 96: 663-672.

Morgan, G.E. and Briden, J.C., 1981. Aspects of Precambrian palaeomagnetism, with new data from the Limpopo mobile belt and Kaapvaal Craton in Southern Africa. Physics of the Earth and Planetary Interiors, 24: 142-168.

Myers, J.S., Shaw, R.D. and Tyler, I.M., 1996. Tectonic evolution of Proterozoic Australia. Tectonics, 15: 1431-1446.

Nomade, S., Renne, P.R. and Merkle, R.W., 2004. $^{40}Ar/^{39}Ar$ age constraints on ore deposition and cooling of teh Bushveld Complex. South Africa. Journal of the Geological Society, London, 161: 411-420.

O'Driscoll, B., Troll, V.R., Reavy, R.J. and Turner, P., 2006. The Great Eucrite intrusion of Ardnamurchan, Scotland: re-evaluating the ring-dyke concept. Geology, 34: 189-192.

Onstott, T.C. and Dorbor, J., 1987. $^{40}Ar/^{39}Ar$ and paleomagnetic results from Liberia and the Precambrian APW data base for the West African Shield. Journal of African Earth Science, 6: 537-552.

Onstott, T.C., R.B., H., York, D. and Hall, C., 1984. Constaints on the motion of South America and African Shields during the Proterozoic, $^{40}Ar/^{39}Ar$ and paleomagnetic correlation between Venezela and Liberia Geological Society of America Bulletin, 95: 1045-1054.

Palabora, Mining Company Limited Mine Geological and Mineralogical Staff, 1976. The Geology and the Economic Deposits of Copper, Iron, and Vermiculite in the Palabora Igneous Complex: A Brief Review. Economic Geology, 71: 177-192.

Parker, E.N., 1955. Hydromagnetic dynamo models. Astrophysics Journal, 122: 239-314.

Powell, C.M., Li, Z.X., McElhinny, M.W., Meert, J.G. and Park, J.K., 1993. Paleomagnetic constraints on timing the Neoproterozoic break-up of Rodinia and the Cambrian formation of Gondwana. Geology, 21: 889-892.

Radhakrishna, T. and Joseph, M., 1996. Proterozoic palaeomagnetism of the mafic dyke swarm in the high grade region of Southern India. Precambrian Research, 76: 31-46.

Reischmann, T., 1995. Precise U/Pb age determination with baddeleyite (ZrO_2), a case study from the Phalaborwa Igneous Complex, South Africa. South African Journal of Geology, 98: 1-4.

Rogers, J.J.W. and Santosh, M., 2002. Configuration of Columbia, a Mesoproterozoic Supercontinent. Gondwana Research, 5(1): 5-22.

SACS, 1980. Bushveld Complex. In: K.L. E. (Editor), The stratigraphy of South Africa, Part I, Lithostratigraphy of the Republic of South Africa, South

West Africa/Namibia and the Republics of Bophuthatswana, Transkei and Venda. Geological Survey of South Africa, pp. 223-231.

Scharlau, T.A., 1972. Petrographische und petrologische Untersuchungen in der Haupt-Zon des ostlichen Bushvled-Komplexes, Distrct Groblersdal/Transvaal, Universitat zu frnakfurt am Main.

Schmidt, P.W. and Clark, D.A., 1994. Palaeomagnetism and magnetic anistropy of Proterozoic banded-iron formations and iron ores of the Hamersley Basin, Western Australia. Precambrian Research, 69(133-155).

Sharpe, M.R., 1981. Evolution of the Bushveld magma chambers, University of Pretoria, Research Report. 36.

Song, X. and Richards, P., 1996. Seismological evidence for differential rotation of the Earth's inner core. Nature, 382: 221-224.

Stacey, F.D. and Banerjee, S.K., 1974. The physical Principles of Rock Magnetism. Elsevier, Amsterdam, 195 pp.

Strik, G., Blake, T.S., Zegers, T.E., White, S.H. and Langereis, C.G., 2003. Palaeomagnetism of flood basalts in the Pilbara Craton, Western Australia: Late Archean continental drift and the oldest known reversal of the geomagnetic field. Journal of Geophysical Resource, 108: 2-21.

Su, W., Dziewonski, A.M. and Jeanloz, R., 1996. Planet within a planet: Rotation of the inner core of the Earth. Science, 274: 1883-1887.

Tankard, A.J. et al., 1982. The Bushveld Complex: A Unique layered intrusion. The Vredefort Dome: Astrobleme or gravity-driven Diapir?, Crustal evolution of Southern Africa, pp. 175-199.

Torsvik, T.H., 2003. The Rodinia Jigsaw Puzzle. Science, 300(5624): 1379-1381.

Torsvik, T.H. and Smethurst, M.A., 1999. Plate tectonic modelling: virtual reality with GMAP. Computers and Geosciences, 25: 395-402.

Torsvik, T.H. et al., 1996. Continental break-up and collision in the Neoprototozoic and Palaeozoic: A tale of Baltica and Laurentia. Earth Science Reviews, 40: 229-258.

Toshihiko, I., 2007. World Data Centre for Geomagnetism, Kyoto. Data Analysis Centre for Geomagnetism and Space MagnetismGraduate School of

Science, Kyoto University. Available from: http://swdcwww.kugi.kyoto-u.ac.jp/igrf/index.html. Assessed on 10 January 2007.

Uken, R. and Watkeys, M.K., 1997. An interpretation of mafic dyke swarms and their relationship with major mafic magmatic events on the Kaapvaal Craton and Limpopo Belt. South African Journal of Geology, 100(4): 341-348.

van der Merwe, M.J., 1976. The layered sequence of the Potgietersrus limb of the Bushveld Complex. Econ. Geol., 71: 1337-1351.

Wallace, W.M., 2002. Spinner Magnetometer JR5A / JR5. User's Manual. Instrument for measuring remanent magnetization., Advanced Geoscience Instruments Co. Brno, Czech Republic, pp. 43.

Walraven, F., 1985. Genetic aspects of the granophyric rocks of the Bushveld Complex. Economic Geology, 80: 1166-1180.

Walraven, F., 1997. Geochronology of the Rooiberg Group, Transvaal Supergroup, South Africa, Economic Geology Research Unit, University of the Witwatersrand, Johannesburg, South Africa, Information Circular, pp. 21.

Walraven, F. and Hattingh, E., 1993a. Geochronolgy of the Nebo Granite, Bushveld Complex. South African Journal of Geology, 96: 31-41.

Walraven, F. and Hattingh, E., 1993b. Geochronology of the Nebo Granite Bushveld Complex. South African Journal of Geology, 96: 31-41.

Weil, A.B., Van der Voo, R., MacNiocaill, C. and Meert, J.G., 1998. The Proterozoic supercontinent Rodinia: Paleomagnetically derived reconstructions for 1100 to 800 Ma. Earth and Planetary Science Letters, 154: 13 - 24.

Wilson, A., 1992. The Geology of the Great Dyke, Zimbabwe: Crystallization, Layering and Cumulate Formation in the P1 pyroxenite of Cyclic Unit 1 of the Darwendale Subchamber. Journal of Petrology, 33: 611-663.

Zegers, T.E., de Wit, M.J., Dann, J. and White, S.H., 1998. Vaalbara, Earth's oldest assembled continent? A combined structural, geochronological, and palaeomagnetic test. Terra Nova, 10: 250-259.

Zhao, G., Cawood, P.A., Wilde, S.A. and Sun, M., 2002. Review of global 2.1-1.8 Ga orogene: implications for a pre-Rodinia Supercontinent. Earth-Science Review, 59: 125-162.

Zijderveld, J.D.A., 1967. A.C. demagnetisation of rocks: Analysis of results. In: D.W. Collinson, K.M. Creer and S.K. Runcorn (Editors), Methods in Palaeomagnetism. Elsevier, Amsterdam, pp. 254-286.

APPENDIX A

Surface locations of Bushveld Complex sites.

Site	Zone	Area	Limb	Latitude (S)	Longitude (E)
Site 1	Main	Steelport	East	24°52.28	30°02.65
Site 2	Main	Steelport	East	24°52.36	30°02.66
Site 3	Main	Steelport	East	24°57.25	29°57.93
Site 4	Critical	Steelport	East	24°53.21	30°07.63
Site 5	Upper	Steelport	East	25°06.53	29°53.11
Site 8	Main	Rossenekal	East	25°13.50	30°00.46
Site 9	Upper	Rossenekal	East	25°22.26	29°51.28
Site 10	Main	Pretoria	West	25°37.62	28°12.89
Site 11	Main	Pretoria	West	25°36.43	28°03.03
Site 12	Main	Brits	West	25°34.62	27°40.05
Site 13	Main	Brits	West	25°36.58	27°39.43
Site 14	Main	Brits	West	25°36.54	27°37.28
Site 15	Main	Brits	West	25°34.66	27°38.26
Site 16	Main	Brits	West	25°34.79	27°38.16
Site 17	Main	Pretoria	West	25°36.43	28°04.55
Site 18	Main	Pretoria	West	25°37.06	28°11.97
Site 19	Main	Brits	West	25°36.28	27°41.66
Site 20	Main	Brits	West	25°37.06	27°34.81
Site 21	Main	Brits	West	25°35.99	27°52.45
Site 22	Main	Brits	West	25°37.15	27°48.04
Site 23	Main	Rustenburg West	West	25°30.86	27°18.44
Site 24	Main	Rustenburg West	West	25°31.17	27°19.12
Site 25	Main	Rustenburg West	West	25°32.57	27°20.06
Site 26	Main	Rustenburg West	West	25°32.86	27°19.91
Site 27	Main	Rustenburg West	West	25°32.78	27°21.26
Site 28	Main	Rustenburg West	West	25°32.15	27°20.55
Site 29	Main	Rustenburg West	West	25°32.00	27°20.36
Site 30	Main	Rustenburg West	West	25°31.52	27°19.71
Site 31	Main	Rustenburg East	West	25°33.03	27°21.97
Site 32	Main	Rustenburg East	West	25°33.49	27°22.32
Site 33	Main	Rustenburg East	West	25°34.01	27°22.26
Site 34	Main	Rustenburg East	West	25°34.51	27°23.37
Site 35	Main	Rustenburg East	West	25°32.88	27°25.74
Site 36	Main	Rustenburg West	West	25°31.82	27°22.05
Site 37	Main	Rustenburg East	West	25°36.42	27°30.06
Site 38	Main	Rustenburg East	West	25°36.06	27°32.49
Site 39	Upper	Sun City	West	25°20.85	27°12.43
Site 40	Upper	Sun City	West	25°22.55	27°12.43
Site 41	Main	Rustenburg East	West	25°32.86	27°26.04
Site 42	Main	Blefast	East	25°35.84	29°55.53
Site 43	Main	Blefast	East	25°35.88	29°55.32
Site 44	Main	Blefast	East	25°36.03	29°55.31
Site 45	Main	Blefast	East	25°41.01	29°55.04
Site 46	Main	Blefast	East	25°40.92	29°55.01
Site 47	Main	Blefast	East	25°40.82	29°54.73

Site	Zone	Area	Limb	Latitude (S)	Longitude (E)
Site 48	Main	Blefast	East	25°41.34	29°54.84
Site 49	Main	Blefast	East	25°41.16	29°55.04
Site 50	Main	Blefast	East	25°36.98	29°55.58
Site 51	Main	Blefast	East	25°36.75	29°55.23
Site 52	Main	Central East	East	25°20.31	29°22.77
Site 53	Main	Central East	East	25°15.85	29°37.57
Site 54	Main	Central East	East	25°15.94	29°37.48
Site 55	Main	Rossenekal	East	25°12.01	29°55.86
Site 56	Main	Rossenekal	East	25°11.87	29°56.08
Site 57	Upper	Rossenekal	East	25°22.89	29°50.31
Site 58	Main	Rossenekal	East	25°12.08	29°58.00
Site 59	Main	Rossenekal	East	25°13.17	30°00.89
Site 60	Upper	Rossenekal	East	25°11.54	29°53.78
Site 61	Main	Steelport	East	24°57.68	29°57.39
Site 63	Main	Top East	East	24°20.12	29°45.9
Site 64	Upper	Top East	East	24°24.92	29°47.35
Site 65	Main	Top East	East	24°22.61	29°46.88
Site 66	Critical	THP	East	24°38.04	30°8.32
Site 67	Critical	THP	East	24°38.42	30°08.04
Site 68	Critical	THP	East	24°24.07	30°00.83
Site 69	Main	Steelport	East	24°56.31	29°53.17
Site 70	Upper	Rossenekal	East	25°10.06	29°50.08
Northern Site 1	Main	Mokopane	Northern	24°13.64	29°02.07
Northern Site 2	Main	Mokopane	Northern	24°09.55	28°58.07
Northern Site 3	Main	Mokopane	Northern	24°09.01	28°57.78
Northern Site 4	Main	Mokopane	Northern	24°09.21	28°57.87
Northern Site 5	Main	Mokopane	Northern	24°08.39	28°58.64
Northern Site 6	Main	Mokopane	Northern	24°08.42	28°58.53
Northern Site 7	Main	Mokopane	Northern	24°02.09	28°54.09
Northern Site 8	Main	Mokopane	Northern	24°00.31	28°52.33
Northern Site 9	Main	Mokopane	Northern	24°01.09	28°51.75
Northern Site 10	Main	Mokopane	Northern	24°02.05	28°54.14
Northern Site 11	Main	Mokopane	Northern	24°02.45	28°54.16
Northern Site 12	Main	Mokopane	Northern	24°02.75	28°54.13
Northern Site 13	Main	Mokopane	Northern	24°03.95	28°58.09
Northern Site 14	Main	Mokopane	Northern	24°03.75	28°58.08
Northern Site 15	Main	Mokopane	Northern	24°03.85	28°58.18
Northern Site 16	Upper	Villa Nora	Northern	23°29.83	28°10.23
Northern Site 17	Upper	Villa Nora	Northern	23°27.27	28°09.92
Northern Site 18	Upper	Villa Nora	Northern	23°26.00	28°12.00
Northern Site 19	Upper	Villa Nora	Northern	23°31.00	28°07.05
Northern Site 20	Main	Mokopane	Northern	23°56.83	28°50.52
Northern Site 21	Main	Mokopane	Northern	23°56.72	28°50.64
Northern Site 22	Main	Mokopane	Northern	23°56.09	28°50.42
Northern Site 23	Main	Mokopane	Northern	23°55.14	28°49.25
Northern Site 24	Main	Mokopane	Northern	23°52.81	28°49.35
Northern Site 25	Main	Mokopane	Northern	23°59.31	28°53.89
Northern Site 26	Main	Mokopane	Northern	23°59.21	28°53.93
Northern Site 27	Main	Mokopane	Northern	23°59.03	28°54.25

Phalaborwa Complex and dyke locations

Site	Mine	Lithology	Latitude (S)	Longitude (E)
S-1	Outside Mine	Complex/ syenite	23°0.942	31°0.113
S-2	Outside Mine	Complex/ syenite	23°0.928	31°0.083
D-1	FOSKOR Mine	Dyke	23°0.928	31°0.096
D-2	FOSKOR Mine	Dyke	23°0.965	31°0.121
D-3	FOSKOR Mine	Dyke	23°0.967	31°0.122
D-4	FOSKOR Mine	Dyke	23°0.967	31°0.122
P-1	FOSKOR Mine	Complex/ pyroxenite	23°0.962	31°0.129
P-2	FOSKOR Mine	Complex/ pyroxenite	23°0.962	31°0.127
P-3	FOSKOR Mine	Complex/ pyroxenite	23°0.969	31°0.121
P-4	FOSKOR Mine	Complex/ pyroxenite	23°0.966	31°0.122
P-5	FOSKOR Mine	Complex/ pyroxenite	23°0.968	31°0.127
P-7	FOSKOR Mine	Complex/ pyroxenite	23°0.965	31°0.123
P-8	FOSKOR Mine	Complex/ pyroxenite	23°0.963	31°0.125
PMCd-1	Phalaborwa Mine	Dyke	23°0.997	31°0.124
PMCd-2	Phalaborwa Mine	Dyke	23°0.998	31°0.128
PMCd-3	Phalaborwa Mine	Dyke	23°0.998	31°0.128
Vd-1	Phalaborwa Mine / Vermiculite Pit	Dyke	24°0.004	31°0.135
Vd-2	Phalaborwa Mine / Vermiculite Pit	Dyke	24°0.007	31°0.136

Locations of dykes located in Bushveld Complex

Site	Latitude (S)	Longitude (E)
Dyke 1	24°27.70	30°03.08
Dyke 2	24°56.95	30°09.10
Dyke 3	24°52.95	30°07.00
Dyke 4	24°24.83	29°59.83
Dyke 5	24°22.25	30°00.05

APPENDIX B

Orientation of palaeomagnetic samples in underground mines.

The orientation of palaeomagnetic samples from underground mines has previously been conducted by using a magnetic compass. Unfortunately in a mining area this method is not very reliable as a number of artefacts can easily deflect the readings.

To ameliorate the problem of orientating samples, an instrument was devised that could measure the angles from the strike of the rock to a survey pegs, and then through simple geometry the strike of the sample is determined. The device is made up of a laser pointer and protractor mounted on a piece of Perspex. In order to determine the strike of the sample, the angle from the strike of the rock to two survey pegs is required (angles $\hat{T}$ and $\hat{A}$) and the distance to one of the survey pegs (the distance to both pegs was recorded in this study to check results, distances b and c). The geometry of the underground sampling is shown in the diagram below.

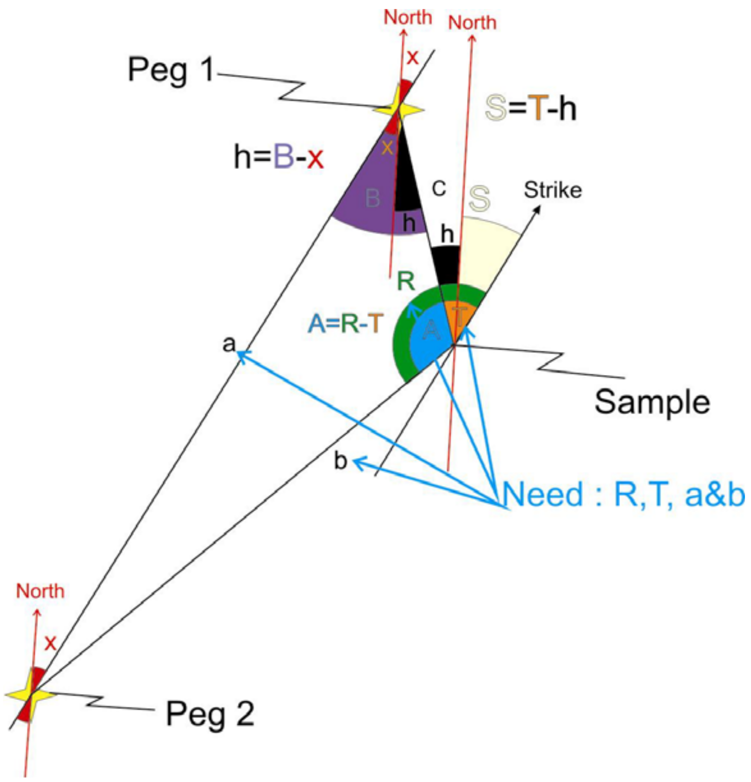

The exact coordinates of the survey pegs are also required (these were obtained from the mine). From the coordinates, the angle between true north and the azimuth of line connecting the two pegs is determined (angle $\hat{x}$) as well as the distance between the two pegs (distance a).

From the measured angles $\hat{R}$ and $\hat{T}$, the internal angle $\hat{A}$, is determined by

$$\hat{A} = \hat{R} - \hat{T}$$

If the distance b was measured then the angel $\hat{B}$ is calculated by use of the Sine Rule,

$$\hat{B} = arcsin(b \sin \frac{\hat{A}}{a})$$

Once $\hat{B}$ had been calculated the angel $\hat{h}$ is determined by

$$\hat{h} = \left| \hat{B} - \hat{x} \right|$$

and finally the strike of the sample S is calculated by

$$\hat{S} = \left| \hat{T} - \hat{h} \right|$$

or simply by placing all equations together

$$\hat{S} = \left| \hat{T} - \left(\left| \left[arcsin\left(b \sin \frac{\hat{A}}{a} \right) \right] - x \right| \right) \right|$$

if the distance c was measured then the strike can be determined using the following equation:

$$\hat{S} = \left| \hat{T} - \left(\left| \left[arcsin\left(c \sin \frac{\hat{A}}{a} \right) \right] - x \right| \right) \right|$$